JOHANNES GUTENBERG UNIVERSITÄT MAINZ

Electrochemically generated bromine for direct and mediated organic synthesis

Dissertation for attaining the academic degree of
“Doctor rerum naturalium” (Dr. rer. nat.) in Chemistry

FB 09 – Faculty of Chemistry, Pharmaceutical Sciences, Geography and Geosciences

Department of Chemistry

LILLA GABRIELLA GOMBOS

born in Budapest, Hungary

Mainz, September 2023

Dean:	Prof. Dr. Eva Rentschler
First reviewer:	Prof. Dr. Siegfried R. Waldvogel
Second reviewer:	Personal data.
Chair of audit:	Personal data.
Date of defense:	28.06.2024

A Családomnak

Declaration

The experimental and written work of this thesis has been carried out from September 2018 to September 2023 at the Department of Chemistry (FB09, Johannes Gutenberg University of Mainz) under the supervision of Prof. Dr. Siegfried R. Waldvogel.

I declare that I wrote this dissertation without any unauthorized external assistance and used only sources acknowledged in this work. All textual passages which are appropriated verbatim or paraphrased from published and unpublished texts as well as all information obtained from oral sources are indicated and listed in accordance with bibliographical rules.

Mainz, September 2023

_____

Lilla G. Gombos

Acknowledgement

Personal data.

Köszönetnyilvanítás

Personal data.

Abstract

This Ph.D. work focused on the development of new synthetic approaches in direct electrochemical bromination and bromine-mediated synthesis. The superiority of electrochemical bromination over the traditional methods was demonstrated using a safe and inexpensive alternative, sodium bromide, as an in-situ-generated bromine surrogate and supporting electrolyte in a dual role. A more sustainable and greener electrochemical dibromination method was successfully developed, focusing on naturally derived alkenes as precursors. The applicability of a terpene-based organobromine was demonstrated via a subsequent functionalization to an α,β-unsaturated nitrile for the first time. These results encouraged further studies for the bromocyclization of alkenoic acids and the selective α-bromination of electron-deficient enones. Finally, a possible bromine-mediated electrochemical Hofmann rearrangement of urea derivatives to hydrazines was investigated, furnishing the unexpected azobenzene products.

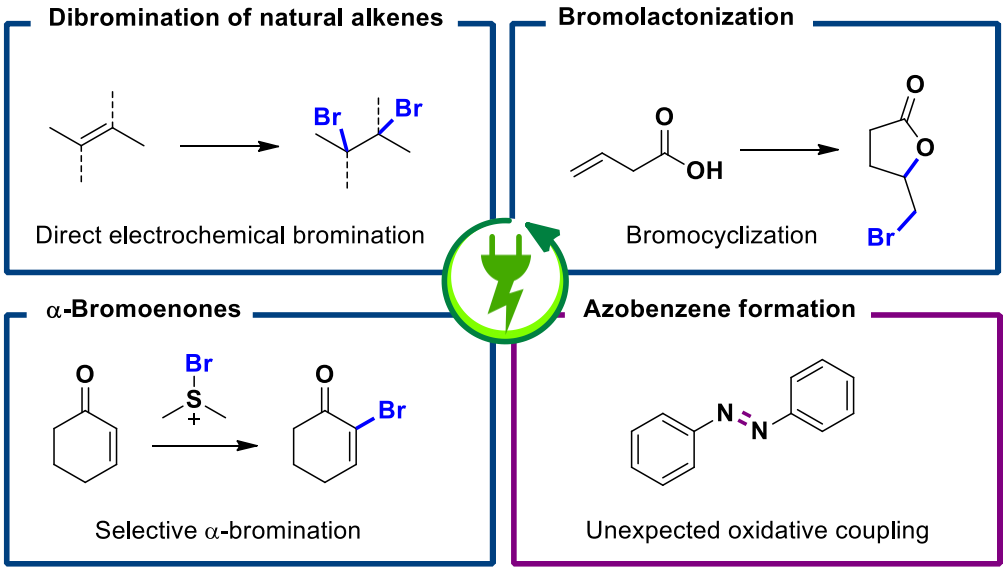

“Legnagyobb cél pedig, itt, e földi létben,

Ember lenni mindég, minden körülményben.”

Arany János

Content

1. Introduction and Overview

Halogenation reactions represent a fundamental part of today´s chemical industry, and the forming organohalides have been a center of attention as commercially important compounds. Among all the halogens, organochlorides and -bromides emerged as industrially significant entities. The highly versatile organobromides are widely used as synthetic intermediates in natural compounds[1] and pharmaceuticals.[2] Especially, 1,2-dibromides are crucial intermediates in the synthesis of fine chemicals and trivial patterns in fire retardants.[1] While the latter has been gradually outspelled due to their toxicity and biopersistance, bromination reactions remain the center of attention.

Most bromination reactions are conducted with toxic and corrosive elemental bromine. Besides creating hazardous reagent waste, these reactions are considered low atom economic as the maximum of bromine incorporation barely exceeds 50%.

Due to its pitfalls, the scientific community is urged to research economically and environmentally greener alternatives to elemental bromine as a brominating agent and to provide synthetic routes to more sustainable methodologies.

1.1 Bromine and its applications

Bromine is a dark brown-red, noxious, and high-density liquid at room temperature with a high vapor pressure of 0.30 atm (228 mmHg) at 25 °C. It is the third lightest element of halogens (group 17) in the periodic table, and its name originates from the Greek *βρῶμος* (bromos) word meaning “stench” referring to its pungent and unpleasant smell. Bromine was first discovered by Carl J. Löwig[3,4] and Antoine J. Balard[5] independently in 1825 and 1826. The highly reactive halogen is mainly found as its alkali salts and minerals in brines, Earth´s crust, and seawater. One of the richest sources is the Dead Sea, with an overall bromide concentration of 5.2 g/L, placing the Jordan Valley and the Middle East as one of the economically most significant bromine providers.[6] Currently, the global bromine market volume is estimated to be 962 thousand metric tons, and it is predicted to rise consistently.[7]

1.1.1. Industrial production of bromine

The industrial production and utilization of bromine can be divided into the production of elemental bromine and bromine compounds.[8] Elemental bromine is manufactured via brine or seawater oxidation with chlorine gas (Equation 1).

$$Cl_{2(g)} + 2\ Br^-_{(aq)} \rightarrow Br_{2(g)} + 2\ Cl^-_{(aq)} \quad \textbf{(1)}$$

Bromine can also be recovered from the quench water of waste incinerators and industrial by-products. In terms of the industrially established techniques, air blow-out (Figure 1A) and steaming out (Figure 1B) techniques are the most significant.[9,10] A simplified schematic representation of the processes is presented in Figure 1.

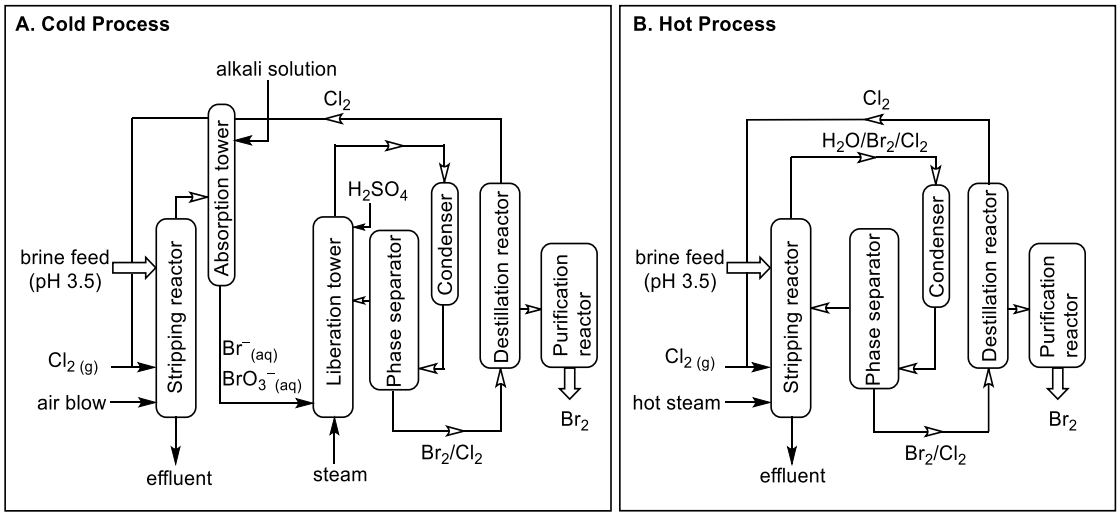

Figure 1. Schematic representation of industrial bromine production: cold or air blow-out process (A) and hot or steaming-out process (B).[11]

Acidified brine is led into the stripping reactor and treated with dry chlorine gas and low-pressure air to liberate elemental bromine. Then it is carried into the absorption tower, where the bromine content is enriched by reducing bromine to bromide and bromate accordingly. The resulting solution mixture is then acidified back to bromine in the liberation tower, which is subsequently condensed and separated from the aqueous solution. The remaining chlorine is distilled off and supplied back to the stripping tower. Finally, bromine is purified by treating it with concentrated sulfuric acid. In the steaming out or hot process, the bromine carrier is the hot steam, directly leading to the condenser and phase separator without the bromine enriching step (Figure 1B).

Other recovery techniques, such as ion-exchange resins,[9,12] gas[13] or liquid emulsion membranes,[14] selective electrochemical oxidation,[15–17] and high-gravity air stripping[9,18] also exist. However, due to their limitations, they have not progressed into industrially established techniques yet.

1.1.2. Synthetic utility and reactivity of bromine compounds

Elemental bromine is the starting point of a wide range of bromine compounds that are extensively utilized from flame retardants,[19,20] agricultural products,[20–22] through biocides,[1,20] as well as chemical commodities (Figure 2).[1,20]

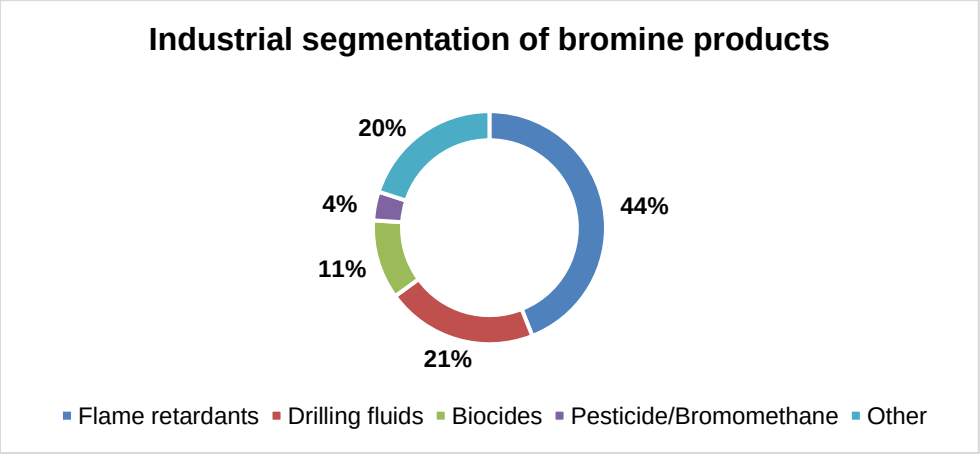

Figure 2. Global bromine market represented according to industrial applications.[23]

Compared to the more available and low-cost alkyl chloride derivatives, alkyl bromides show enhanced selectivity and reactivity as intermediates, contributing to increased sustainable utilization with reduced waste and environmental impact.[20] These preferential properties are allocated to the different bond enthalpies between the haloalkyl compounds, with the carbon-bromine (C–Br) bond being significantly weaker, and therefore, more reactive than the carbon-chlorine (C–Cl) bond (Figure 3).[24]

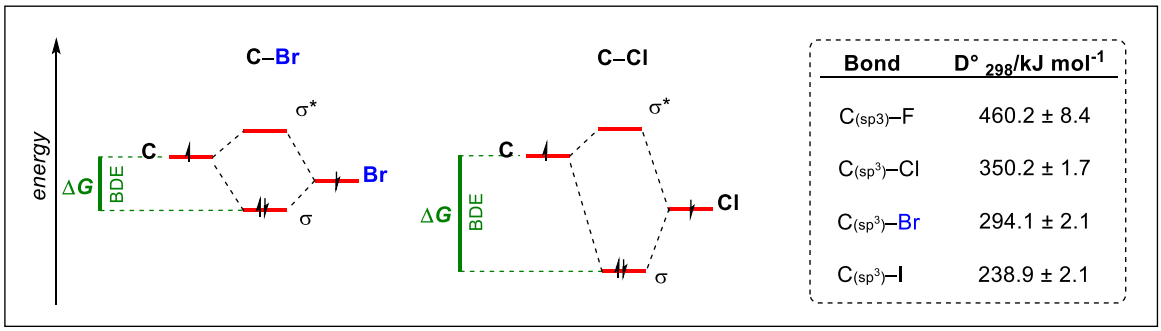

Figure 3. Representative molecular energy diagram of the carbon-bromine (left) and carbon-chlorine (middle) bonds. BDE = bond dissociated energy (D°). The corresponding carbon-halogen bond dissociation energies are included on the right (298 K).[24]

As a result of that, C(sp^3)–Br bromides readily undergo displacement reactions by other nucleophiles or metals to form the corresponding C–C, C–N, C–O, C–S, C–X (iodine or fluorine) and C–M (magnesium or lithium) bonds or elimination reactions (E_1 or E_2) to form alkenes and alkynes respectively. Scheme 1 represents the diversity of the obtainable products from a simple alkyl bromide.

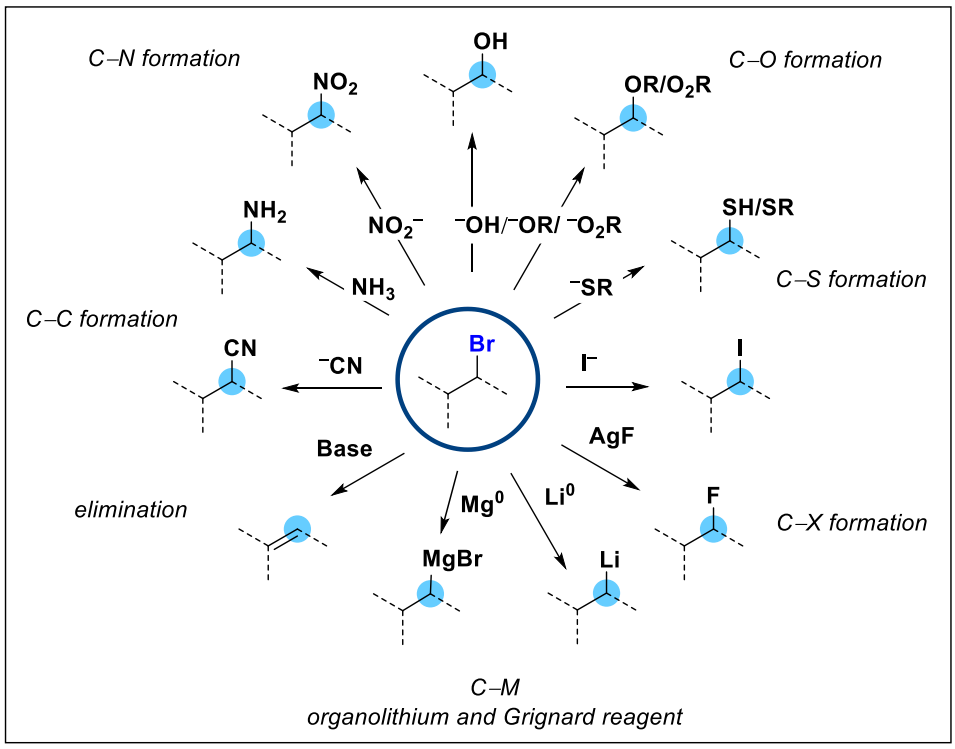

Scheme 1. Versatility of the C–Br bond functionalization. Respective carbon atom is labelled in blue. X = iodine, fluorine. M = metal.[20]

Substitution of C(sp^2)–Br is also feasible in the presence of a metal catalyst or a reactive metal (Cu, Fe, Li).[25–27] In addition to that, the efficient C–C bond formation

ability of aryl bromide species has been established via transition-metal catalyzed coupling reactions.[28]

In the light of their broad applicability and chemistry, the synthetic production of organobromine compounds has been the center of attention in recent decades. The two most established synthetic routes for forming alkyl bromide compounds are conducted via substitution or addition reactions.

1.2 Bromination of olefins via addition reactions

The saturation of alkenes proceeds readily with elemental bromine. Depending on the reaction conditions, dibromination, bromofunctionalization, and hydrobromination products can be obtained (Figure 4).

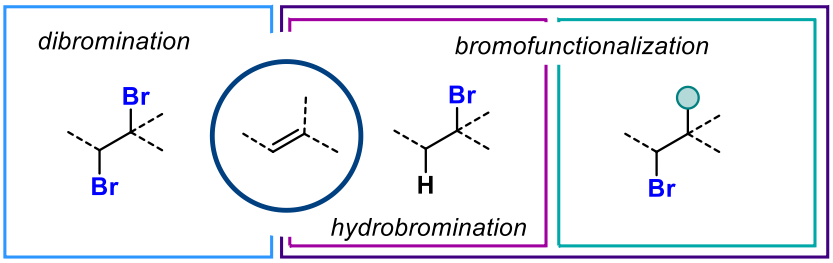

Figure 4. Dibromination, bromofunctionalization and hydrobromination of alkenes. The blue circle represents the co-nucleophile in the form of solvents or nucleophilic functional groups.

The addition of bromine to the alkene is a conjugated process. A nucleophilic attack on the polarized bromine molecule leads to the bromonium intermediate, which is subsequently opened by the bromide ion forming an anti-product.[29] Figure 5 shows the overall reaction coordinate for the formation of dibrominated product.

In terms of selectivity, the nucleophilic attack of the alkene can happen on both sides leading to the top- or the bottom-face bromonium ion intermediate.[30] The nucleophilic attack will take place on the opposite side, in case of an asymmetric alkene at the most hindered carbon that best stabilize the intermediate, leading to a racemic product mixture.[30]

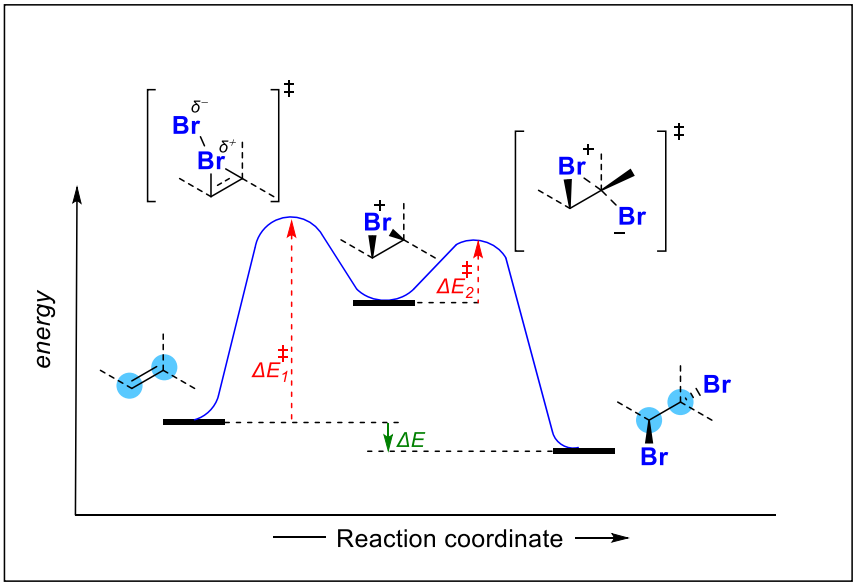

Figure 5. Reaction coordinate of the dibromination of alkene.[31]

In the presence of a nucleophilic solvent such as water, alcohols, or dimethyl sulfoxide, the solvent can compete in a nucleophilic attack leading to the bromofunctionalized product (Figure 5).[30] The same reactivity pattern is observed, where the molecular structural features allow inductive intramolecular cyclization forming more complex entities.[32] A great example is the well-established early 20th century halolactonization method using alkenoic acids and elemental iodine or bromine.[33] Interestingly, bromine is less frequently used, as the olefin saturation reaction competes with the cyclization, reducing chemoselectivity.[34] Nevertheless, the corresponding bromolactone products are commonly used in total synthesis of pharmaceuticals[35] and the lactone moieties are regular motifs in natural products.[36]

Selective bromination of electron-deficient olefins has also attracted significant attention.[37–40] For example, the selective bromination of α,β-unsaturated carbonyls allow the formation of synthetically useful α-bromoenones that are commonly utilized in the total synthesis of natural compounds[41,42] or cross-coupling reactions (Figure 6).[43,44] Moreover, they are existing moieties in APIs that are currently under experimental testing.[45] Nevertheless, formation of those regularly require harsh conditions or toxic phenylselenium halides.[37–40]

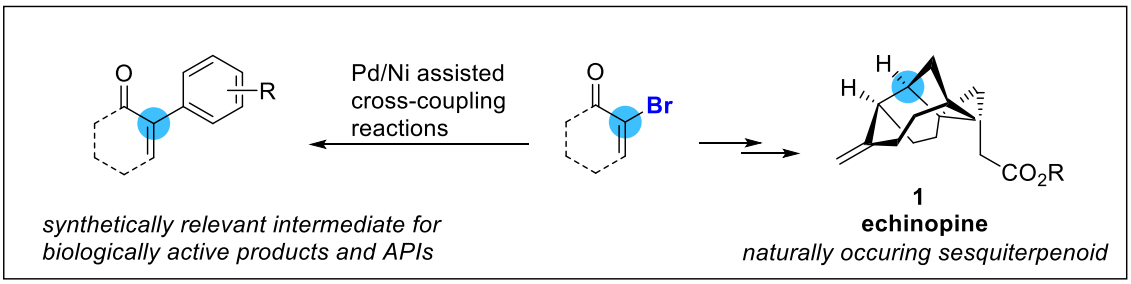

Figure 6. Synthetic importance of α-bromoenones.[41,44] Blue colour indicates the (former) C–Br bond.

Hydrobromination reactions of alkenes can proceed via an electrophilic addition or a free-radical addition of HBr to the olefin.[30,46,47] The electrophilic addition of HBr follows the Markovnikov´s rule with bromine attached to the most substituted carbon.[30] In the case of free-radical addition, the initiation step forms the bromine radical, which attacks the alkene and forms the most stabilized radical intermediate leading to the least-substituted organobromine product (Figure 7).[46,47]

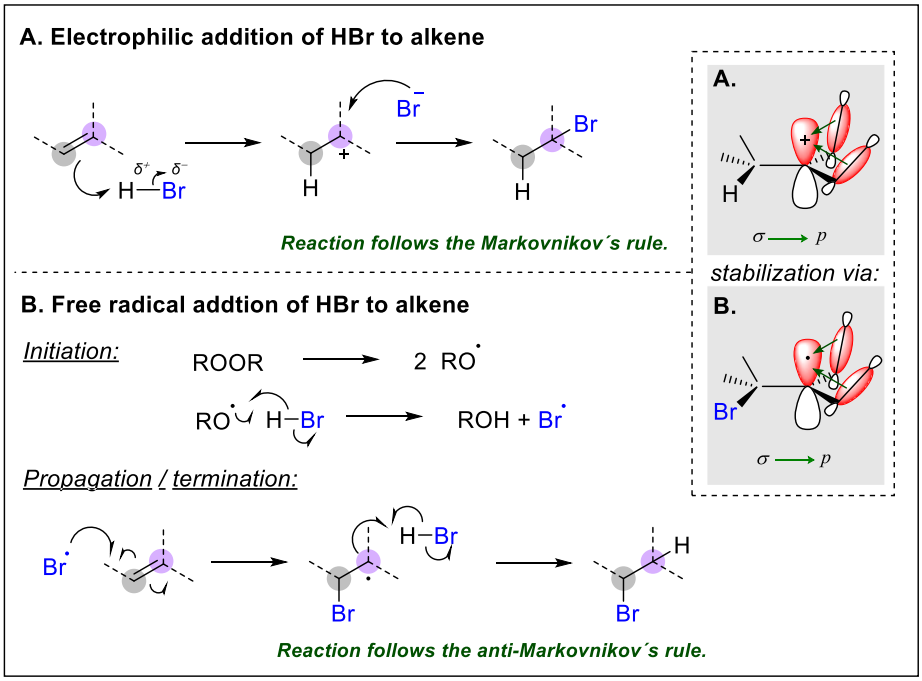

Figure 7. Representative reaction mechanism for the electrophilic (A) and free-radical addition (B) of HBr to alkene. Interacting orbitals are labeled in red. General carbon back-bone structure was labeled with grey and purple for clarity.[46,47]

The electrophilic addition to alkenes shows excellent selectivity. The outcome of the reaction is predictable, furnishing highly functional organobromine products.[2,20,22]

While the synthesis of these is relatively straightforward, in terms of its sustainable aspects there is still a lot to improve.

1.3 Bromine-mediated rearrangement reactions

In some cases, bromine is used as a mediator for profitable synthetic methodologies, which has a catalytic effect to induce and accompany the reaction. The bromine-mediated Hofmann rearrangement allows the formation of primary amine from a primary amide in the presence of bromine and aqueous sodium hydroxide.[48,49] The reaction is well-known and is a profound synthetic step in the total synthesis of several bioactive agents[50–54] such as (–)-cepharamine (**2**)[54] and (–)-oxycodone (**3**, Figure 8).[50]

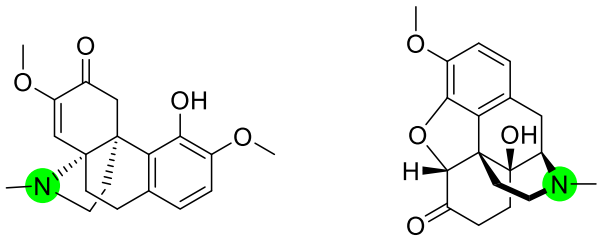

2

(–)-cepharamine
hasubanan alkaloid

3

(–)-oxycodone
μ-opioid receptor agonist

Figure 8. Naturally derived (–)-cepharamine (**2**) and synthetic alkaloid (–)-oxycodone (**3**). Participating nitrogens are labelled in green.[50,54]

The reaction proceeds via the oxidation of the primary amide **4** nitrogen to the *N*-bromo amide **I** when treated with bromine and sodium hydroxide (Scheme 2). Upon subsequent deprotonation, the migration of the carbon atom results in the formation of the isocyanate intermediate **II**, which is scavenged by water to form the corresponding unstable carbamic acid **III**. Thermal degradation of **III** via the liberation of carbon dioxide affords the desired amine product **5**.

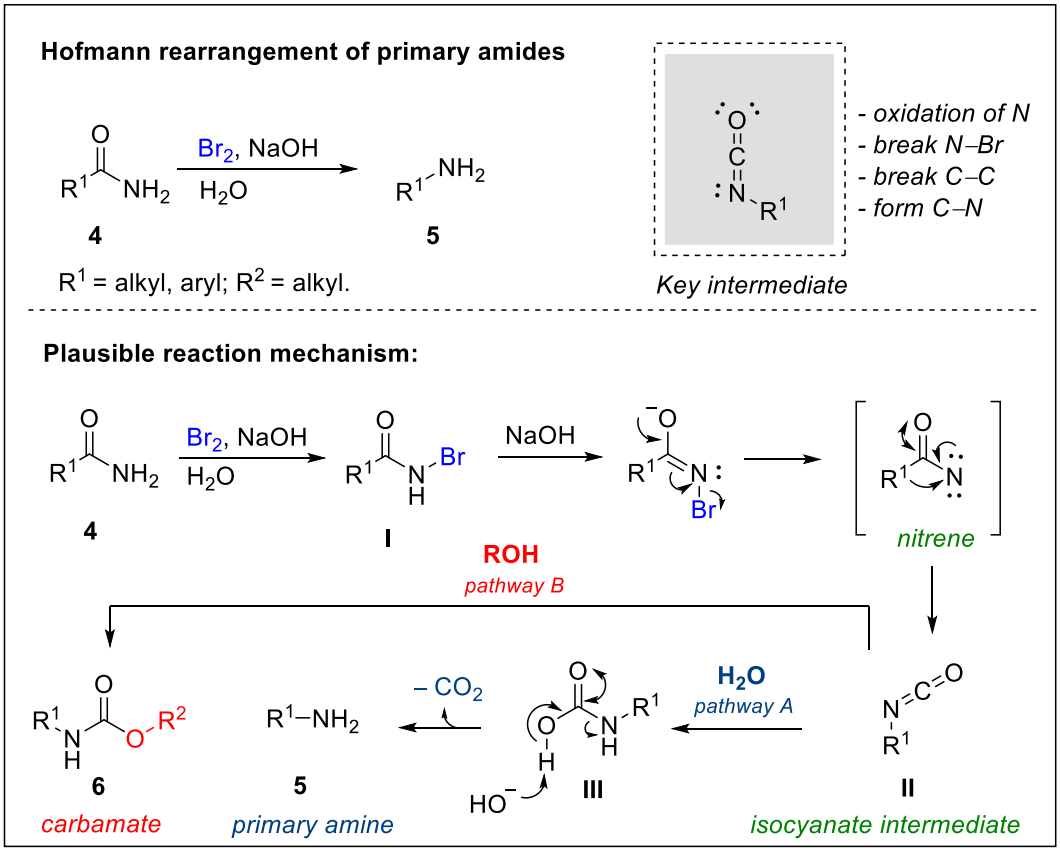

Scheme 2. Reaction mechanism of the Hofmann rearrangement of primary amides to amines (pathway A) and carbamates (pathway B) respectively.

The isocyanate intermediate **II** can also be trapped by other solvent molecules, such as alcohols, diverting the product formation to the corresponding carbamates **6** (pathway B, Scheme 2). Other reagents, such as *N*-bromosuccinimide,[55,56] hypohalites,[57] lead tetraacetate,[58,59] and hypervalent iodine species[50,60–65] can also induce the reaction, with bromine being the most common.

1.4 Challenges and motivation

The major challenges of bromination reactions are associated with the nature of bromination agents (Figure 9). The frequent bromination methods include using elemental bromine or hydrogen bromide, which is toxic, hazardous, and corrosive. Elemental bromine has a high density and volatility, which causes its handling and quantification challenging. Due to its poisonous nature, its large-scale transportation and storage also cause concerns.[66,67] Moreover, synthetic methodologies use super stoichiometric amount in the presence of chlorinated solvents creating hazardous reagents waste.

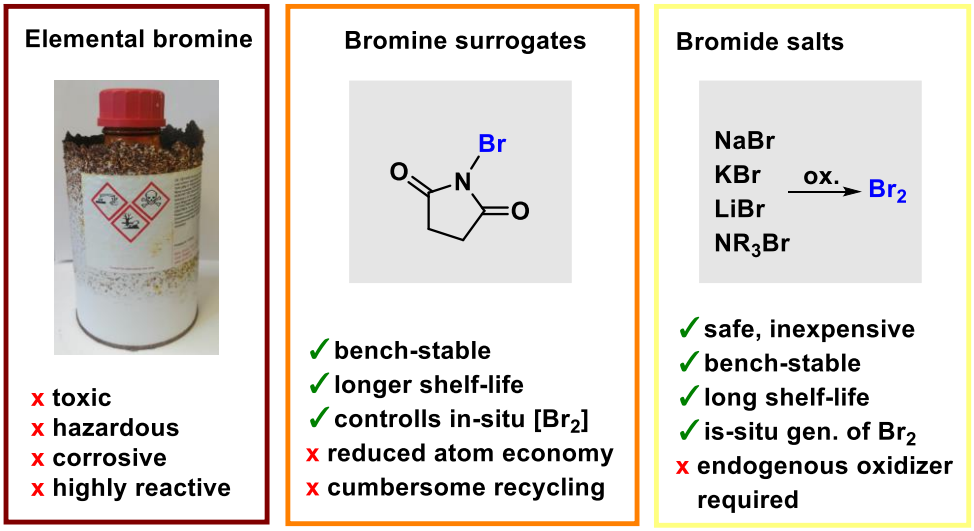

Figure 9. Advantages and disadvantages of different brominating agents.

Bench-stable bromine carriers overcome these disadvantages. These bromine surrogates liberate bromine in-situ, providing a safer alternative for synthetic bromination.[68] Their chemical stability allows them to keep the bromine concentration low in the solution upon liberation, which makes their handling less complicated. Moreover, due to their physical and chemical properties, they have a long shelf-life that overcomes the transportation issues associated with elemental bromine. Nevertheless, these reagents are hardly atom economic. Their production involves using elemental bromine under relatively harsh conditions, and after utilization are often discarded. The recycling of the carrier molecule and reformation of the bromine surrogate is tiresome and includes the discharge of elemental bromine again.[68]

In the presence of an external oxidizer, metal- and organic bromide salts are an attractive choice for substituting elemental bromine or low-atom efficiency bromine carriers.[69] Alkylammonium bromides are favored due to their better solubilities in a wide range of organic solvents and are frequently adopted as phase transfer catalysts.[70,71] Unfortunately, they are economically disfavored due to their high prices and strenuous recycling methods, accommodating metal bromides as the more sustainable choice.

In terms of endogenous oxidizers, oxygen or peroxide are preferred substances over harsh reagents such as Oxone® or hypervalent iodine. The generated by-products are H^+ and water, respectively, circumventing the implementation of surplus oxidizers and their corresponding toxic by-products.[69,72–74]

The scope of brominating agents and bromine surrogates is extensive; however, a green methodology is unavailable without compromising the reaction conditions or the success of the reaction outcome. Considering the current economic, environmental, and political pressure, the chemical industry is challenged to deliver a greener and more sustainable alternative to conventional methods.[75]

1.5 Synthetic electro-organic chemistry

The genesis of electrochemistry is set to 1800, and pioneering work for the foundation of synthetic electro-organic chemistry was laid decades later by M. Faraday and H. Kolbe (Figure 10).[76–78] The decarboxylative dimerization of carboxylic acids opened a new synthetic approach that catalyzed the growing interest in the field.[76,77] In the 1970s, the idea of indirect electrolysis provided the ground for electrochemical mediators such as *N*-oxyl radicals[79,80] and halogenide ions.[81–83] The anodic methoxylation of amides by Shono furnished a feasible C–C bond formation methodology involving an electrochemical step.[84,85] Yoshida introduced the electroauxiliary-concept[86,87] and the in-situ electrogenerated cationic reactive intermediates or "the pool method"[88,89] that significantly improved the selectivity of synthetic electrochemical reactions. These milestones served as the bedrock for today´s modern electrochemical developments.[90–95]

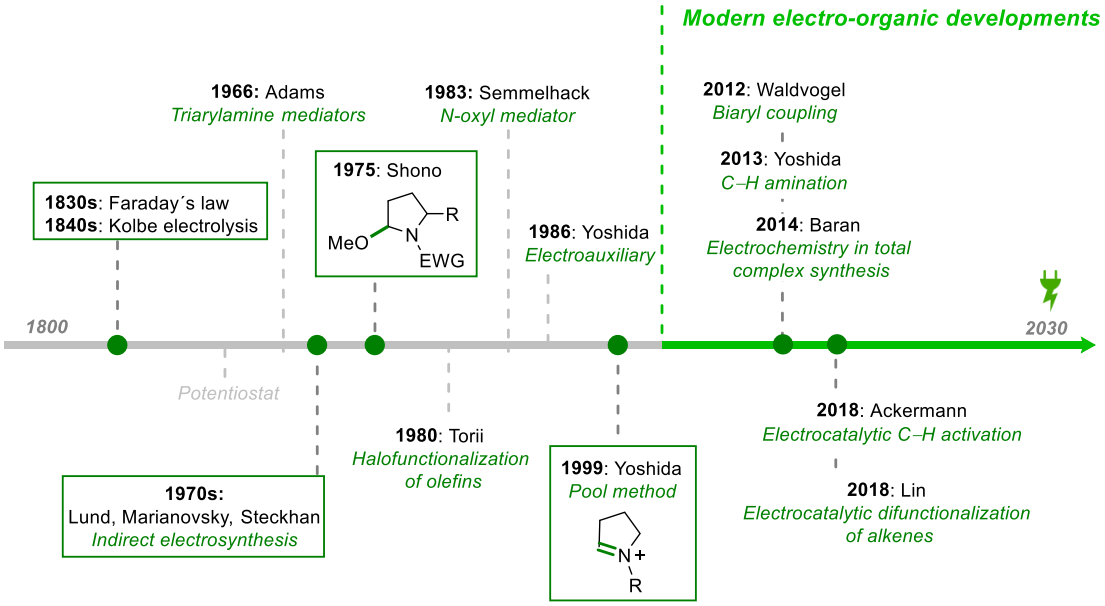

Figure 10. Selected representatives in the development of synthetic electro-organic chemistry.[96–98]

Electro-organic synthesis as an “electricity-driven” highly functional methodology is a leading research topic contributing to modern synthetic chemistry.[97,99–102] Using “traceless” electrons as sole redox reagents help to reduce the excessive use of harmful redox chemicals and reagent waste, contributing to higher atom efficiency.[103] Moreover, a simplified approach can be achieved by electro-generating highly reactive species and safe surrogates in situ, avoiding hazardous reagents.[88] Combining these green concepts with innovative methodologies contributes to the cleaner industrial productions and helps to raise awareness of the ecological footprint of today´s modern society.[72,104–108] These advantages, in combination with the valorization of renewable feedstock and “green electricity”, makes electrochemical functionalization particularly attractive (Figure 11).[108–112]

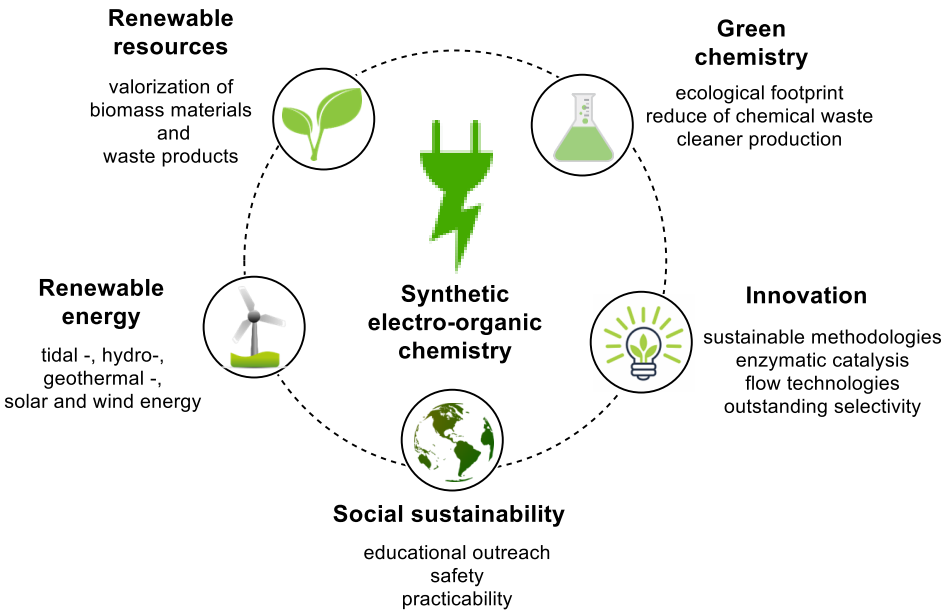

Figure 11. Sustainability aspects of modern synthetic electro-organic chemistry. License free icons can be found under https://pixabay.com/.

1.5.1. Basic parameters of electrochemical transformations

Synthetic electro-organic chemistry describes the chemical transformations of organic molecules forced by electricity. The amount of energy required to achieve the chemical transformation of interest is related to the cell potential and is described in the equations below. The free Gibbs energy (ΔG) is the maximum amount of work (w_{max}) that can be performed with the electrochemical cell (Equations 2, 3), and it is expressed as the result of the cell potential ($E°_{cell}$) and the total charge (nF) transferred

during the reaction in an ideal, reversible system (Equation 3). The *n* represents the total number of electrons transferred in the reaction, *F* is the Faraday constant (96,485 C/mol), and *K* represents the equilibrium constant. The standard cell potential ($E°_{cell}$) is the difference between the electrode potentials (Equation 4, Figure 12).

$$w_{max} = \Delta G \quad \textbf{(2)}$$

$$\Delta G = nFE_{cell} \quad \textbf{(3)}$$

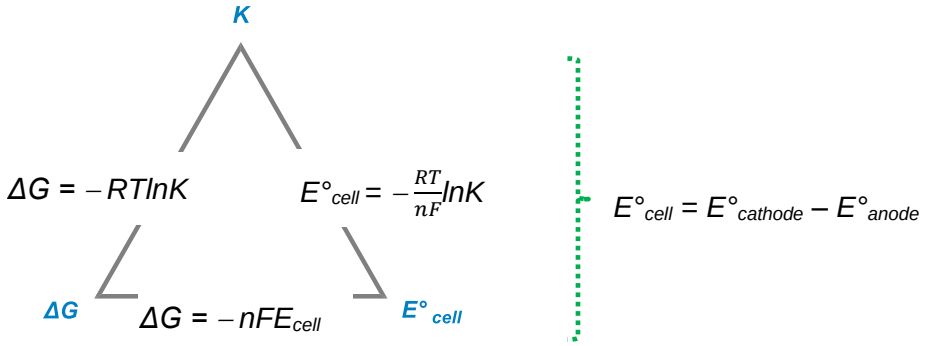

(4)

Figure 12. Relationship between activation energy, cell potential and kinetic equilibrium.[113] Adapted from reference [113], creative commons license: CC BY-NC-SA 4.0.

In a non-ideal system, electrode potential depends on the kinetics of the two electrode reactions, affected by many parameters and various overpotentials (η) that results in a voltage divergence.[114–117] This potential difference between the actual and the equilibrium cell potential when an external current is applied, is expressed as the anodic – and cathodic overpotential difference.

The cell potential is also associated with the ohmic resistance, calculated as the sum of conductivity loss correlated to the electrolyte, presence of membrane, and cell design under externally applied current (*I*, Equation 5).[109,118] Hence, the operating cell potential (U_{cell}) is the sum of the electrode potentials (E_{cell}), the electrode overpotentials (η_{cell}), and the cell resistance (R_{cell}) when the external current (*I*) applied and described as follows (Equation 5):

$$U_{cell} = E_{cathode} - E_{anode} + \eta_{cell} + IR_{cell} \quad \textbf{(5)}$$

Cell or half-reaction potential is measured against a reference electrode with a stable and known electrode potential. Standard hydrogen electrodes (SHE), calomel, or silver/silver chloride electrodes are frequently used reference electrodes.[119,120] The schematic representation of the overpotentials using a simplified redox reaction is described in Figure 13.

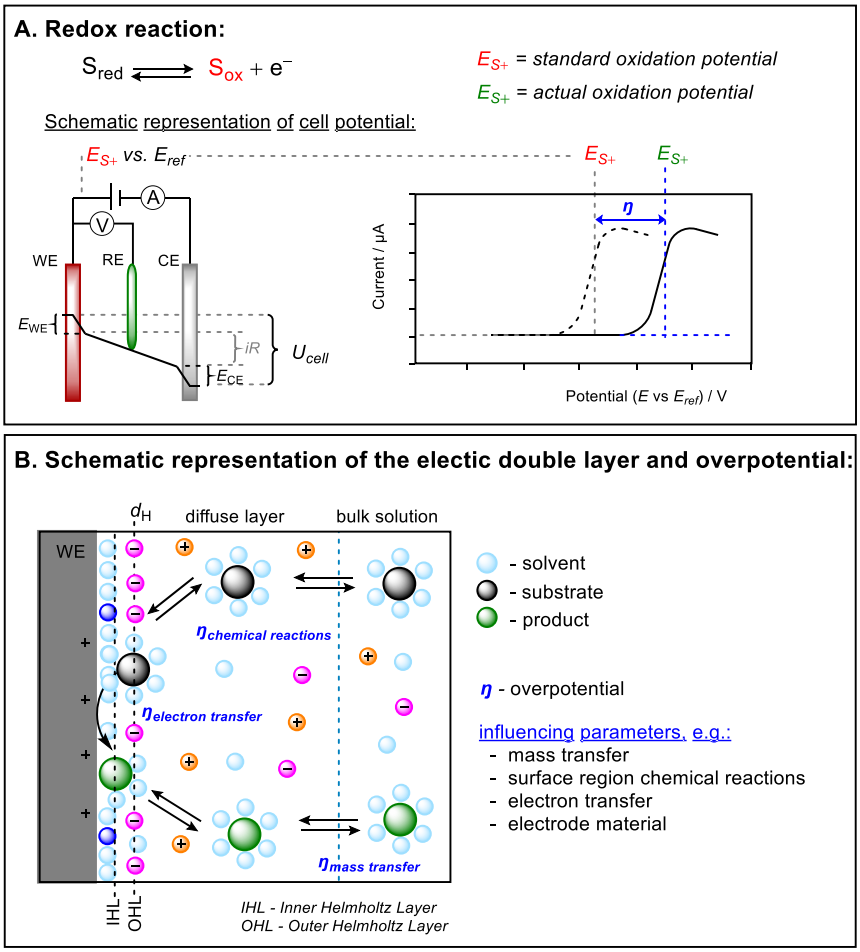

Figure 13. Schematic representation of understanding the overpotential of an electrochemical cell (A). The influencing parameters are summarized in part B.[78,121] S = substrate.

These single electron transformations (SET) occur at the electrode surface and are classified as anodic oxidative and cathodic reductive transformations. In terms of an electrochemical process, the kinetic barrier (η) must be overcome for an electron-transfer.

Applying positive or negative potential manipulates the energy of the Fermi level of the electrode, supplying enough activation energy to facilitate the charge transfer between the electrode and a substrate in the solvent (Figure 14). Therefore, the choice of electrode and electrolyte combination are determining factors in the success of the reaction.[100]

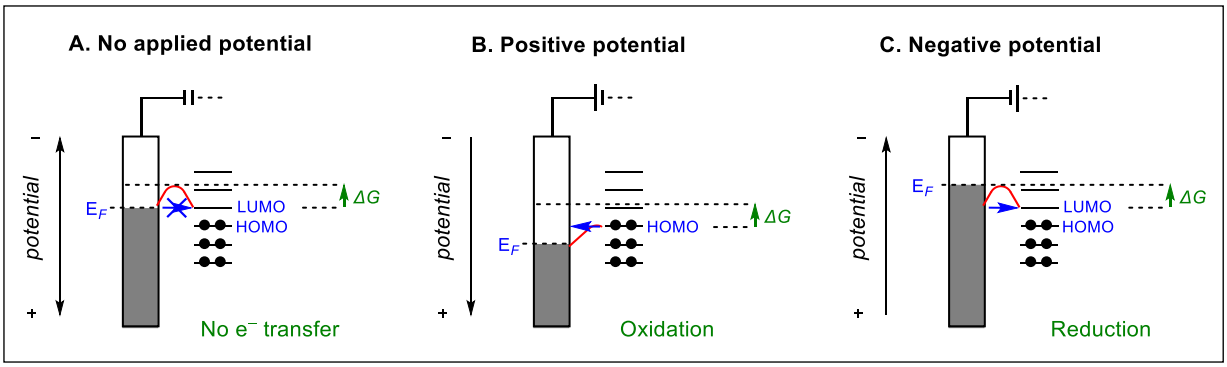

Figure 14. Possibilities of electron transfer in case of an applied potential. LUMO = lowest unoccupied molecular orbital. HOMO = highest occupied molecular orbital. Adapted from reference [78].

Regarding the nature of electrodes, inert, active, sacrificial, and high-surface electrodes are distinguished (Figure 15).[117] Inert electrodes serve only as a source or sink for electrons without chemically participating in the transformation. The common inert materials are noble metals (Pt), carbon-based electrodes (graphite, glassy carbon), or superior capacity electrodes (boron-doped diamond).[100] These electrodes are robust and electro-chemically stable, providing a convenient and economically advantageous operation.

Carbon-based electrodes are especially frequently employed due to their accessibility and low cost. The most common carbon-based electrodes are graphite, glassy carbon, and reticulated vitreous carbon (RVC) electrodes. Above their economic sustainability, they explicit versatile utilization and can be applied in exclusive transformations.[103,117] Graphite is considered a standard anode and cathode material, however, it has low mechanical stability.[122–124] Glassy carbon electrodes are prepared with thermosetting resins under controlled pyrolysis.[125] These types of carbon electrodes exhibit excellent conductivity, high temperature, and chemical stability, which is attributed to their tightly curled sp^2-carbon layers that are cross-linked via covalent C–C bonds resulting in fullerene-like microstructures.[125–127]

Active electrodes form an immobilized redox-active coating that expresses unique reactivity,[128,129] while sacrificial electrodes are consumed during electrolysis.[130] The ideal electrolyte minimizes the solution resistance and provides a steady flow of electrons across the bulk. Therefore, the solvent and the supporting electrolyte must be electro-chemically inert under the condition of interest (Figure 15).[100]

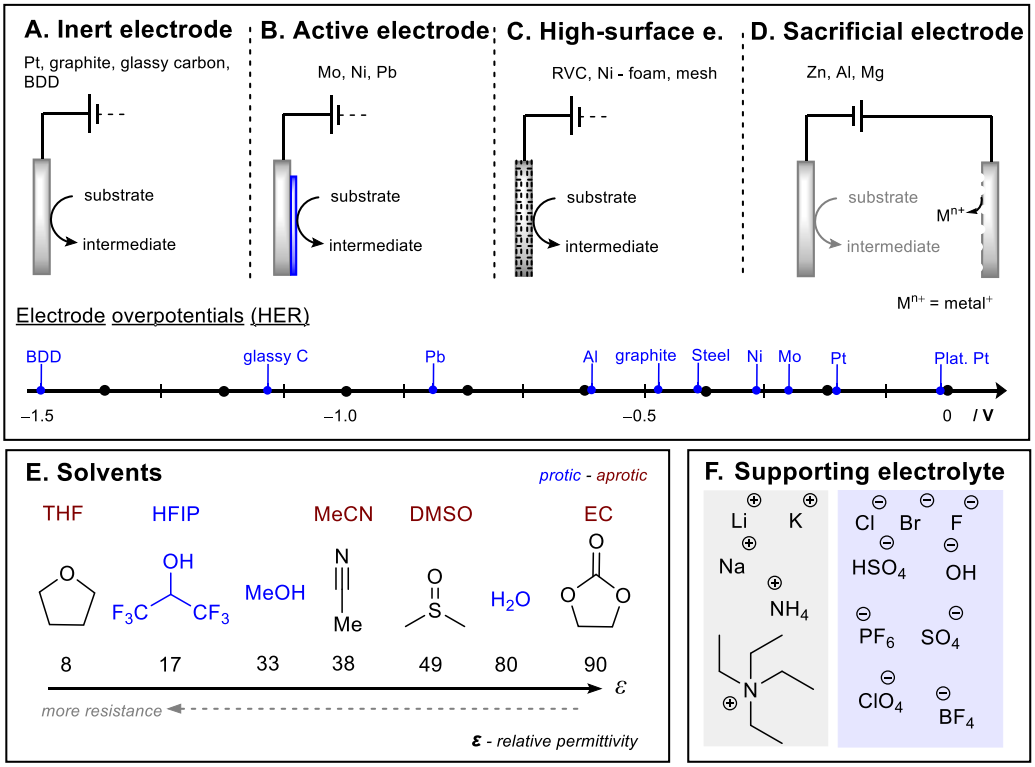

Figure 15. Schematic representation of electrode types, and their overpotentials to hydrogen evolution reaction (HER, j = 1 mA/cm^2, 25 °C, 1 M HCl (or H_2SO_4) in solvent specified in literature).[117] Solvents are listed according to their increasing permittivity (ε) value.[131,132] Protic solvents were indicated with blue colour. Supporting electrolytes were listed according to their charge.[78,131]

The electron transfer reactions can be described as direct electrolysis or indirect electrolysis (Figure 16). Direct electrolysis is a heterogenous action at the electrode surface that facilitates the conversion of a substrate into intermediate products. Direct electrolysis requires the transfer of the substrate of interest from the bulk solution to the interface region, its adsorption onto the electrode surface, upon which electrode transfer happens, and the desorption of intermediate product from the electrode and its migration back to the bulk solution where the subsequent reaction takes place (Figure 13). This implies that direct electrolysis in some cases can be associated with large overpotentials or is in danger of compromising the electrolysis via permanent adsorption on the electrode surface.[102] Regarding to indirect electrolysis, a redox mediator or an electrocatalyst with a lower redox potential as the substrate of interest undergoes electron transfer at the electrode forming a highly reactive species that provokes the reaction of interest.[99,133–135] The mediated approach is generally

favored, as the mediator can be regenerated as part of the electrochemical cycle, promoting selectivity and reducing the overall cell potential.

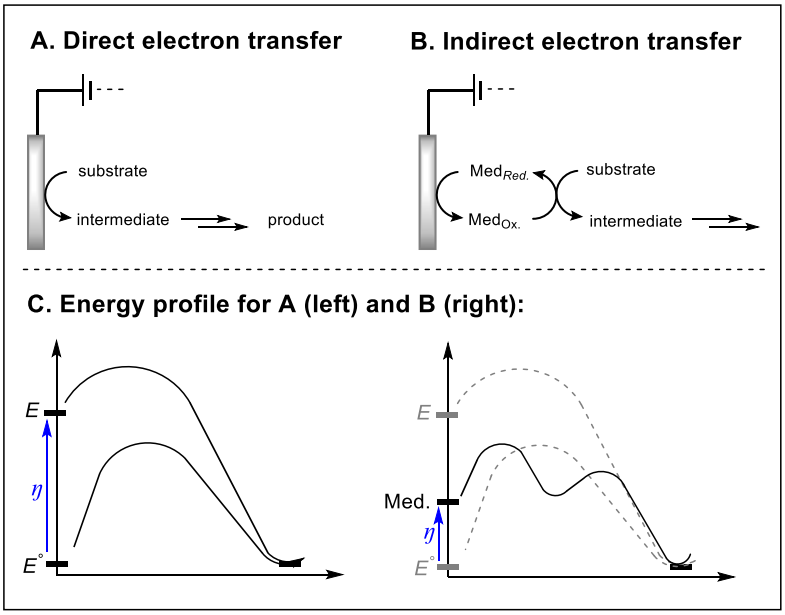

Figure 16. Schematic representations and simplified energy diagrams for direct (A) and indirect (B) electrontransfer. Adapted from reference [135].

Electro-organic transformations are carried out in a potentiostatic or galvanostatic operation (Figure 17). In a potentiostatic mode or a 3-electrode step-up, the working electrode's potential is steadily controlled against the reference electrode providing a stable and selective electrochemical window for synthetic transformations. In a galvanostatic, 2-electrode set-up, the current flow is maintained between the working and the auxiliary electrode facilitating a simple operation. The electrochemical reaction can be controlled by varying the current density (*j*) and the number of charges applied (*Q*). The current density (*j*) is derived as the applied current (*I*) per immersed electrode surface (*A*, Equation 6). The amount of applied charge required (*Q*) for the electrochemical process is determined by multiplying the number of electrons per substrate (*z*) with the number of moles (*N*) and the Faraday constant (*F*, 96485 C/mol) (Equation 7).

$$j = I / A \quad \textbf{(6)}$$

$$Q = z * N * F \quad \textbf{(7)}$$

Attributed to its simplicity, galvanostatic operations are more feasible for scale-up processes and preferred for industrial transfer.

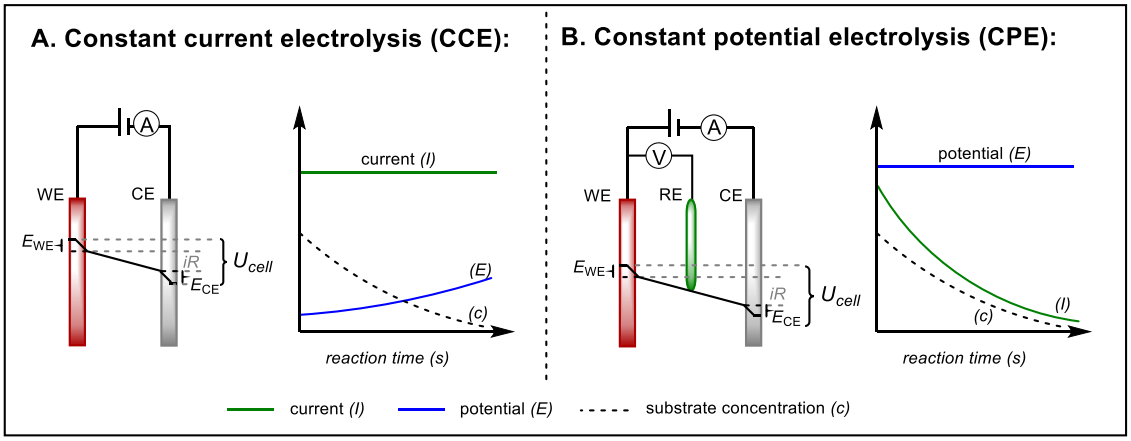

Figure 17. Schematic representation of constant current electrolysis (A) and constant potential electrolysis (B). The electrolysis time profiles represent the cell potential (*E*) – substrate concentration (*c*) relationship and current (*I*) – substrate concentration (*c*) relationship when constant current electrolysis (A) and constant potential electrolysis (B) are applied. WE: working electrode, CE: counter electrode, RE: reference electrode. Adapted from reference [78].

Depending on the nature of the chemical transformation, the reaction can be conducted in undivided, divided, or quasi-divided cells. Complete sets are commercially available as the IKA Screening System[136,137] or the ElectraSyn 2.0 Package[138] promoting harmonization of the reaction conditions.[139] The undivided cell provides a simple set-up and operation for an anodic or cathodic conversion, if the reaction remains intact from the counter-reaction, for example, hydrogen gas evolution at the cathode. In other cases, the counter-reaction is a complementary step in the reaction mechanism, conducted in a consecutive or convergent manner.[140–143] In a divided cell, the anodic and the cathodic compartment are separated via a membrane, protecting redox-vulnerable species from the complementary reaction. It is important to mention that the larger interelectrode distance and the presence of the cell membrane increase cell resistance.[102] A quasi-divided cell submerges the advantages of both undivided and divided electrochemical cells. The counter electrode (wire) usually has a minimal surface-to-current density ratio that hinders the mass transfer of the starting material or product and promotes the electrolysis of the solvent rather than the substrate of interest, creating a semi-divided environment.[102]

With careful consideration of the reaction parameters, a plausible synthetic route for a selective electrochemical process can be engineered. Regarding the oxidative

galvanostatic electrochemical processes, Figure 18 provides sufficient information about the basic reaction parameters for electro-organic transformations.

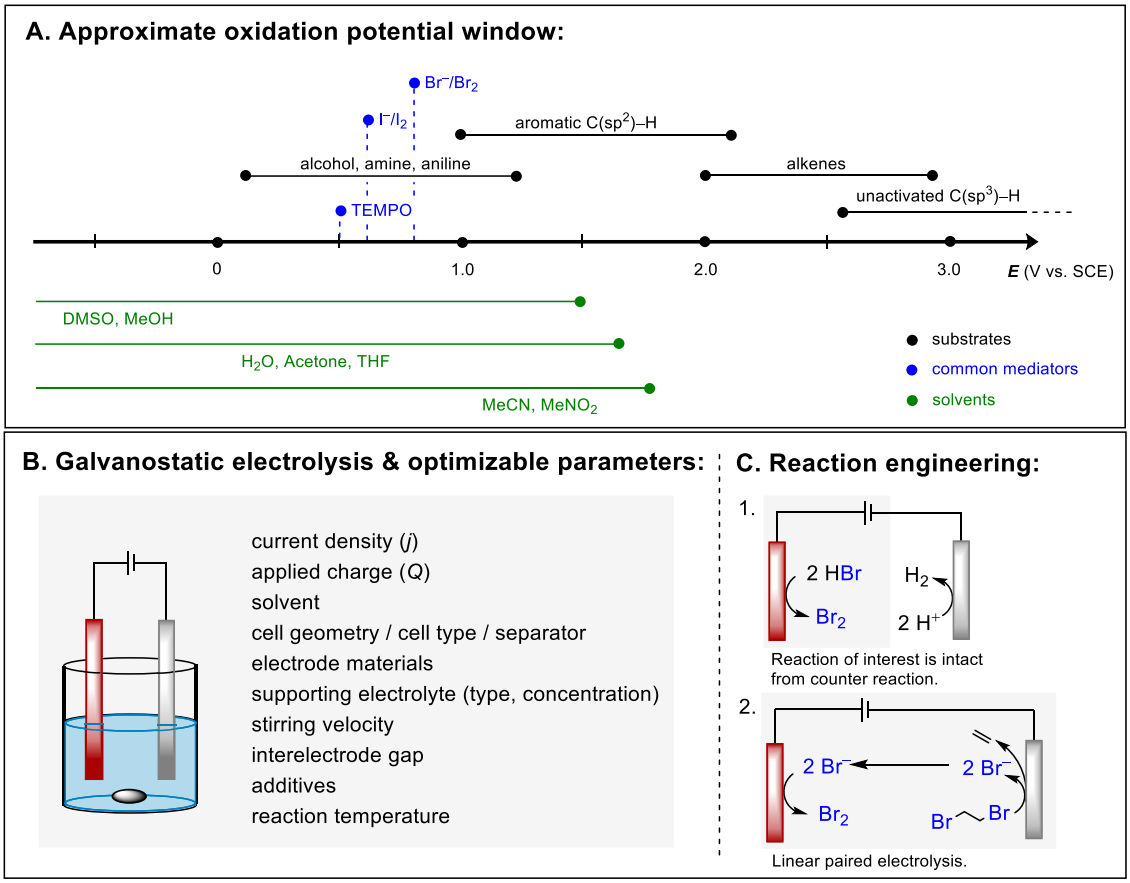

Figure 18. Schematic representation of approximate oxidation potential window for different substrates (black), common mediators (blue) and solvents (green, above). Schematic representation of a galvanostatic, two-electrode set-up with possible optimizable parameters listed on the right (below).[144–146]

In a nutshell, synthetic electro-organic chemistry demonstrates a highly sustainable approach that is readily established in research laboratories. The understanding of the principal reaction parameters and consideration of modern optimization strategies are crucial for transferring synthetic electro-organic chemistry into industrial processes.[103,147,148]

1.5.2. Organic electrochemistry in industry

Electrochemical processes demonstrate broad applicability and utilization in an interdisciplinary field. Therefore, their scalability in batch and transfer into flow reactors has been extensively researched.[149–151] As well as the new innovative technologies, the shifting of fossil-based resources to renewables and the already established industrial processes qualify electrochemical synthesis to be considered as a commonly accepted synthetic technique.[109–111]

Many electrochemical industrial processes are established on a commercial or pilot-plant scale. One of the most important ones is the chloralkali process generating chlorine gas and sodium hydroxide from sodium chloride brine.[152–154] The aluminium industry relies on the *Hall-Héroult* process or the electrochemical reduction of aluminium oxide in a molten cryolite bath using sacrificial carbon anodes.[155]

The most successful commercialized organic electrochemical process is *Baizer´s* adiponitrile synthesis, which started in the 1960s.[118,156] The electrohydrodimerization of acrylonitrile occurs at the cadmium cathode in the presence of quaternary ammonium salts, enhancing the reaction selectivity.[157] The product is mainly used to produce polyamides and polyurethanes.[118,156]

Another significant example was demonstrated by the company BASF, in a paired electrolysis fashion.[114,158] The simultaneous electrochemical generation of *t*-butylbenzaldehyde dimethyl acetate and phthalide takes place respectively in the unique capillary-gap cell. Methanol has a dual role as a reagent and a solvent, and the corresponding products are obtained in a combined 180% yield.[114,158,159]

Ontario Hydro and Hydro Quebec, Canada independently developed the cathodic hydrodimerization of formaldehyde on graphite electrodes.[156,160,161] The mechanism of action is comparable to the electrochemical adiponitrile formation.[157,160–162] Via this pilot plant process, ethylene glycol is produced in an aqueous solution at graphite electrodes with 98% current efficiency.[156,160] Table 1 shows a collection of industrial electrochemical processes on a commercial and pilot plant scale.[118,156]

Table 1. Selected examples of commercial and pilot plant scale industrial electrochemical processes.[118,156,158,163]

Starting material	Product	Scale [t/a]	Company
Acrylonitrile	Adiponitrile	300,000 t/a	Ascend Performance Materials, BASF, Asahi Chemical
Formaldehyde	Ethylene glycol	3,000,000 t/a	Ontairo Hydro, Hydro Quebec
L-Cystine	L-Cysteine	1500 t/a	Wacker Chemie AG
Dimethyl phthalate + *t*-Butyltoluene	Phthalide, *t*-Butylbenzaldehyde acetal	20,000 t/a	BASF

t/a: tonnes per annum.

The major disadvantage of industrial chemical and electrochemical processes is fossil-fuel dependence. Currently, the industrial sector contributes to 21% of the global greenhouse gas emissions.[164] In recent years, the development of renewable energy sources as feasible alternatives and the global action against climate change led to the desire to decarbonize the industry.[165] This ambition also encloses the shift towards non-fossil sources, such as carbon dioxide, nitrogen, and biomass sources, and their conversion into value-added chemicals. Respectively, the valorization of waste stream materials such as lignin, the electrochemical reduction of carbon dioxide, and nitrogen fixation are all considered emerging electrochemical processes.[165,166]

1.6 Electrochemical oxidation of bromide

The electrochemical generation of bromine has received increased attention since the second half of the 20th century, when polybrominated organic compounds were widely utilized as flame retardants, plastics, and coatings, and later were phased out due to their environmental damage[22,167,168] and toxic features.[168–170]

The electrochemical method joins the characteristic reactivities of elemental bromine and the advantages of bench-stable bromine carriers without the associated drawbacks.[99,100,103] Bromine can be easily electro-generated via anodic oxidation from its bromide salts.[152]

The electro-generation of bromine used in industrial flue gas desulfurization.[152,171] Bromine is generated at dimensionally stable ruthenium oxide-coated titanium anodes (DSA) and reacts with sulfur dioxide in an aqueous solution to form sulfuric acid and hydrobromic acid, respectively (Equation 8). HBr is oxidized back to bromine and supplied back to the cell (Equation 9).

$$Br_2 + SO_2 + 2\ H_2O \rightarrow 2\ HBr + H_2SO_4 \quad \textbf{(8)}$$

$$2\ HBr \rightarrow H_2 + Br_2 \quad \textbf{(9)}$$

The anodic oxidation of bromide to bromine has been extensively studied at various electrode materials and solvent systems. Vojinovic[172] and Halász[173] studied the rate-determining steps of bromide oxidation at single-crystal platinum and polycrystalline platinum electrodes in non-aqueous systems. Conway showed that the rate-determining step of the electro-generation of bromine depends on the recombination of bromine radicals to bromine.[174] These independent studies established that the oxidation of bromide is a two-step process in which bromide is oxidized to bromine and forms the stable tribromide salts in the presence of a sufficient bromide concentration. The second oxidation corresponds to the oxidation of tribromide salt to bromine.[172,173,175,176] Bromide can also be oxidized at various carbon-based electrodes. Graphite proved to be a versatile electrode material. However, under certain conditions, it is limited by the electrochemical intercalation of bromine into the graphite sheets causing corrosion.[122] Other carbon-based electrodes, such as glassy carbon and boron-doped diamond proven to be also suitable.[177,178]

M. Tariq showed the electro-generation of bromine at platinum and gold electrodes in aprotic, protic, and mixed media via cyclic voltammetry methods.[175] The study

showed that the ratio of the respectively generated “active bromine species” differ depending on the solvent system. Figure 19 shows the oxidation mechanism of bromide ions in different solvents with their respective voltammograms.

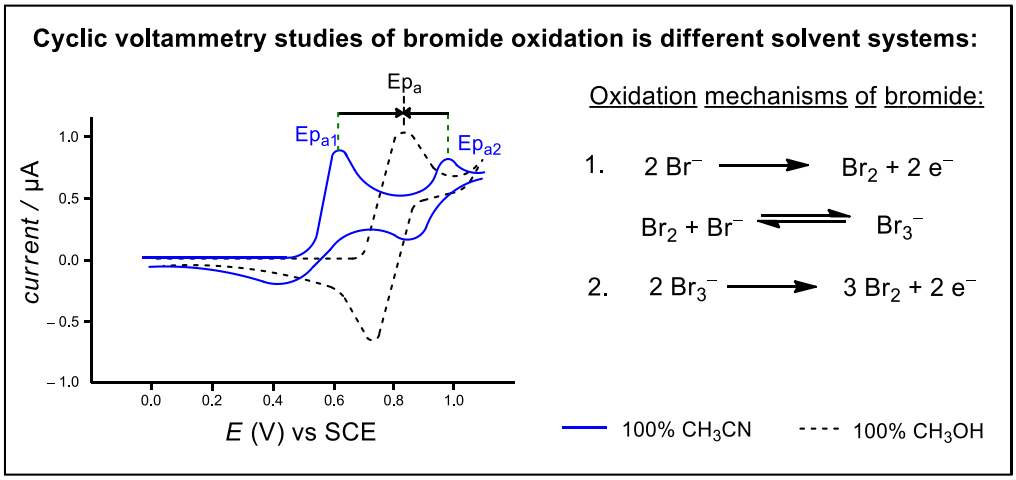

Figure 19. Schematic adaptation of cyclic voltammograms of bromide anion in different solvent systems. Conditions: NBu_4Br (5 mM), NBu_4ClO_4 (0.1 M), WE: platinum disk electrode (*d* = 1.6 mm), RE: saturated calomel electrode, CE: not indicated, scan rate: 50 mV/s, 25 °C.[175]

In situ generated bromine is in equilibrium with the corresponding Br_3^- when the bromide concentration is high. The second oxidation peak is governed by the oxidation of the stable salt to bromine. In acetonitrile, the stability of the tribromide salt is enhanced, driving the equilibrium towards Br_3^-. The voltammogram displays a quasi-reversible sweep which indicates the relatively low concentration of bromine in the solution. In contrast, the electro-oxidation of bromide in methanol displays different reactivity with a “one-step” oxidation process. Due to the higher dielectric constant of acetonitrile than methanol, the tribromide salt can be better stabilized in aprotic media.[179–181]

In terms of an aq. solution, unstable hypobromous acid can form, that easily dissociate to hypobromite and bromide according to the following equations.[182]

$$Br_2 + 2\ H_2O \rightleftharpoons HOBr + H_3O^+ + Br^- \quad \textbf{(10)}$$

$$HOBr + H_2O \rightleftharpoons BrO^- + H_3O^+ \quad \textbf{(11)}$$

In this case, the “active bromine agents” are a mixture of hypobromous acid, hypobromite, and bromine,[182] facilitating possible side reactions and reducing current efficiency.

Consequently, the majority of the electrochemically generated bromine is used for the oxidative electro-bromination of organic material, such as saturation of double bonds or the mediated synthesis of other synthetically highly relevant molecules.[112]

1.7. Electrochemical bromination and bromofunctionalization of alkenes

A manuscript was published on this chapter.

L. G. Gombos, S. R. Waldvogel, *The Electrochemical Bromofunctionalization of Alkenes and Alkynes – To Sustainability and Beyond*, *Sustain. Chem*. **2022**, *3*, 430–454.

DOI: 10.3390/suschem3040027

This manuscript was highlighted with a front cover picture.

Author contributions:

This manuscript was written and finalized by **me** under the supervision of S. R. Waldvogel.

The electrochemical bromination and bromofunctionalization of alkenes have been extensively researched due to the synthetic utility of the forming products. 1,2-dibromides, bromohydrins, and bromoesters are common structural motifs of fine chemicals and drug-candidate molecules.[1,183] Furthermore, these synthetically important intermediates can be easily further functionalized, contributing to a diverse platform of products. Figure 20 represents the comparison of conventional- and electrochemical bromination.

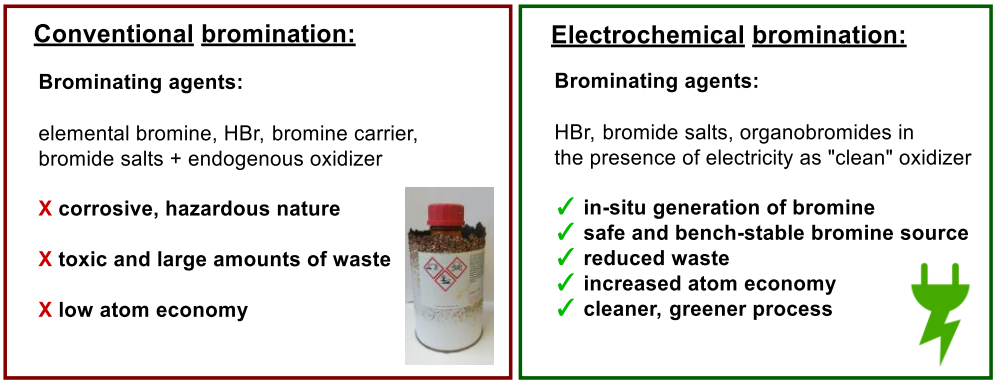

Figure 20. Comparison of conventional bromination and associated disadvantages with electrochemical bromination.[112]

Apart from generating bromine electrochemically in a highly sustainable manner, the product selectivity and outcome can be influenced depending on the complexity of the substrate, the presence of a co-nucleophile, or the employed solvent system. For instance, in the presence of protic solvents, the solvent acts as a co-nucleophile, affording the highly versatile bromohydrin or bromoester derivative.[184–187] Furthermore, certain structural features allow the bromine-mediated intramolecular cyclization, providing synthetically practical derivatives such as indanones,[188] isoxazolines, and lactones.[188–193]

In addition to the points listed in Figure 20, electrochemical bromination methods should be investigated on the following aspects: electrode materials, presence or absence of supporting electrolyte, the dual role of bromine salts, cathodic counter-reaction, and substrate source. Generally, carbon-based electrodes are favoured due to their sustainable nature. However, the electrode material and pairing depend on the nature of the reaction and the solvent.[103,194] Using the bromine source in a dual role as a supporting electrolyte increases the atom economy of the reaction and simplifies the system.[112] In terms of the cathodic counter-reaction, hydrogen evolution usually compliments the anodic generation of bromine.[143] Recently, many innovative methods aimed to incorporate the cathodic reaction as an inevitable part of the method to increase current efficiency and atom economy.[195–197]

Several electrochemical protocols touched the electrochemical dibromination of alkenes, including direct oxidative bromination,[198–200] electrocatalytic bromination,[201] and bromination of alkenes via linear paired electrolysis (Scheme 3).[195–197]

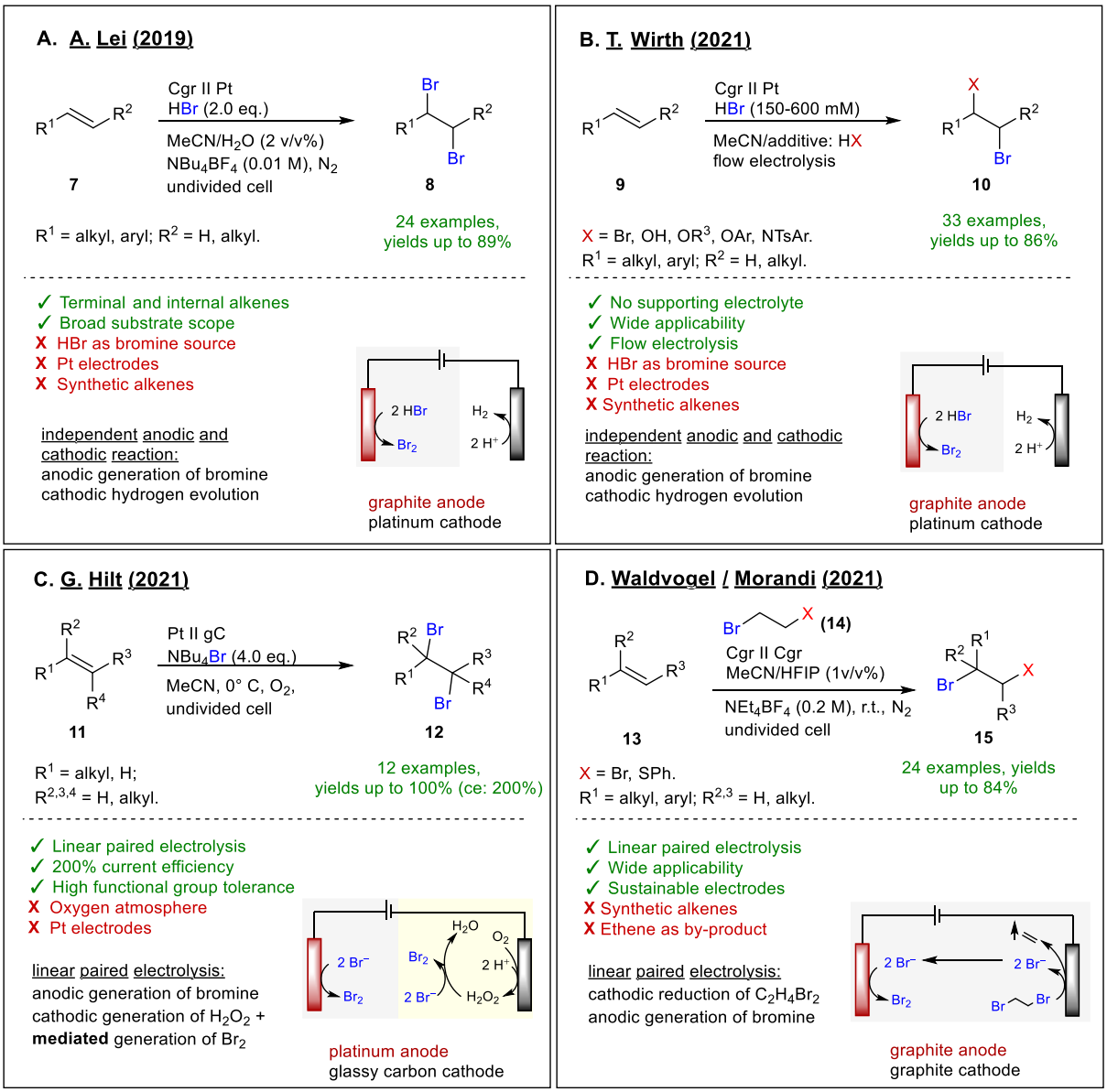

Scheme 3. State-of-art electrochemical bromination methods.[112,195,196,198,199] Cgr = graphite, gC = glassy carbon, Pt = platinum (anode II cathode).

In 2019, the Lei group published a widely applicable method for the electrochemical dibromination of terminal and internal alkenes **7** using HBr as a bromine source at graphite anode and platinum cathode. The method furnished a broad substrate scope of 24 examples with up to 89% yield.[199] Encouraged by these results, Wirth et al. reported the electrochemical dibromination and bromofunctionalization of activated and non-activated alkenes **9** in a flow reactor.[198] The small interelectrode distance featured a supporting electrolyte-free, single-pass method. Via switching the co-solvent, the procedure could also be extended to the formation of bromohydrins and bromoethers **10**.

Different electrochemical bromination methods have been developed within the concept of linear paired electrolysis.[195–197] Hilt and his group provided a convergent strategy for the electrochemical dibromination of alkenes **11** with the realization of 200% current efficiency for stoichiometric transformations in the presence of oxygen.[196] NBu_4Br is used in a dual role as a bromide source and supporting electrolyte. Bromine is generated at platinum anode and formed mediated via the cathodically generated hydrogen peroxide. This convergent system determines the theoretical applied charge of 1 *F* and current efficiency of 200%.

Recently, the merging e-shuttle method for the retro-dibromination of bromofunctionalization of alkenes was also reported.[195] This elegant shuttle reaction uses 1,2-dibromoethane (**14**) as a halogen promoter. The organohalide undergoes reductive dehalogenation at the cathode, and the forming bromide is anodically oxidized and transferred to the acceptor alkene. This innovative methodology was extended to the bromofunctionalization of alkenes as well.

While these methods are extensively applicable and provide exceptional selectivity and yields, they frequently employ dangerous or toxic bromine sources, such as HBr[198,199] and depleting metal electrodes.[196,198–200] Moreover, some require lower temperatures to ensure gas saturation[196] or the presence of fluorinated solvent additive to reduce side reactions.[195] In addition, almost all of them are based on fossil-based substrates.

1.8. Terpenes as potential substrates sources for electro-organic synthesis

With more than 50,000 different molecules identified, isolated, and characterized, terpenes represent one of the largest classes of natural compounds that is broadly utilized by the pharmaceutical, agricultural, and chemical industries.[202–204] The plant and fungi synthetized terpenes and terpenoids are considered readily available and inexpensive biomass from essential oils or as industrial by-products.[205,206] For example, the citrus juice by-product, limonene is produced on a 60,000 ton/year scale and used as a solvent.[207,208] Due to their biological activity[209] and unique structural features, they became a significant target of the polymer industry.[210] These diverse utilization methods promoted terpenes as one of the most significant valorization sources for preparing fine chemicals and valuable products.

The current functionalization methods are strenuous due to their delicate structures that result in undesired by-product formation and reduced chemoselectivity. Moreover, the traditional transformations rely on the use of several metal catalysts, such as Ru, Rh, Mn, or Ni, which makes the selective transformation of terpenes still challenging.[211–213]

While the electrochemical bromination of simple alkenes is extensively researched, the class of naturally derived olefins has been rather ignored. J. Malyszlo studied the kinetics of the electrochemical bromination of unsaturated fatty acids on a platinum rotating ring-disk electrode.[214] In 2005, the electrochemical dibromination of steroid-like structures **16** was reported (Scheme 4A).[215] In the presence of 2.5 eq. NEt_4Br in dichloromethane, the corresponding dibrominated products **17** could be obtained with up to 91% yield. In other solvents, the reaction had to be performed at elevated temperatures and casted only five examples.[215] Medeiros et al*.* reported the electro-epoxidation of natural and synthetic alkenes **18** in the presence of sodium bromide at platinum electrodes (Scheme 4B).[216] While this mediated approach proved promising in the case of stilbene and styrene, opposing to naturally derived olefins, it showed decreased yield and selectivity, forming the undesired brominated or oxidative by-products.

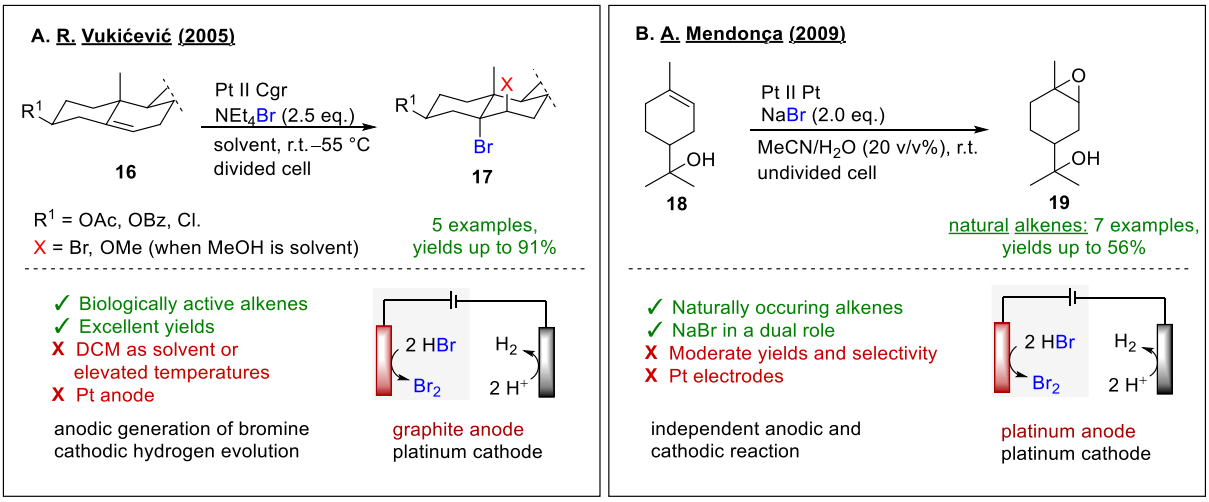

Scheme 4. State-of-art of electrochemical bromofunctionalization of natural alkenes.[215,216]

These examples demonstrate the few electrochemical bromination examples concerning naturally derived olefins shedding light on their challenging functionalization. In addition, the existing methods are associated with similar drawbacks emphasized earlier in the previous chapter. Accordingly, electrochemical dibromination methods are still lacking sufficient sustainability aspects.

1.9. Electrochemical formation of substituted hydrazines and derivatives

Hydrazine compounds are vital building blocks of synthetic organic chemistry and are readily used in their free or substituted forms in the pharmaceutical-, agrochemical-, dye- and energy sectors.[217–220]

Pioneering work in the establishment of hydrazine chemistry is connected to E. Fischer and T. Curtius.[219] The first industrial process was developed by O. Raschig, employing sodium hypochlorite and ammonia to form hydrazine as a 1:1 azeotrope mixture with water.[219,221] Today´s industrial hydrazine synthesis is still based on the *Raschig synthesis*, *ketazine process*, *peroxide process*, and their modifications (Scheme 5).[217,218]

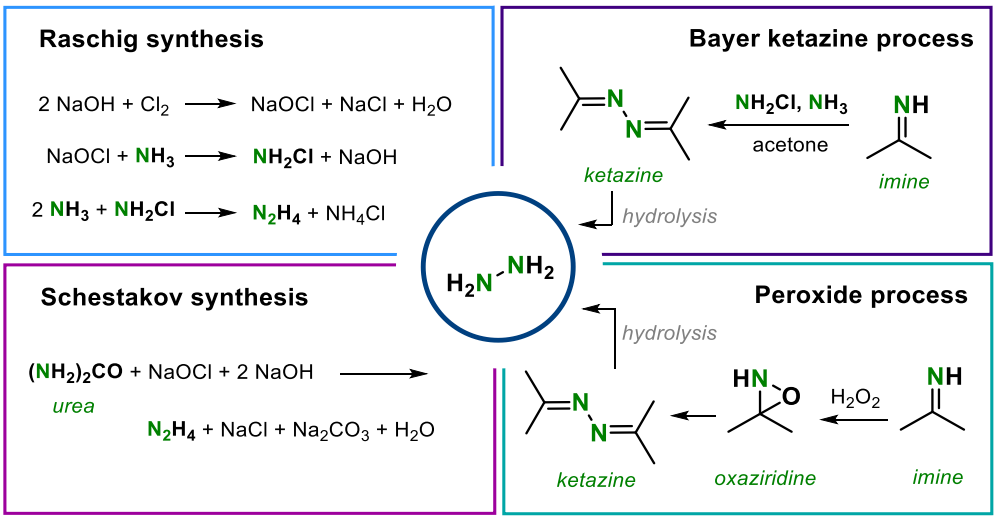

Scheme 5. Industrial hydrazine synthesis processes.[217–219,221]

The ketazine or *Bayer process* is based on the formation of chloramine from ammonia and chlorine or perchlorate in the presence of acetone, forming ketazine as an intermediate product.[217,218] Subsequent hydrolysis yields the hydrazine hydrate. The *Hayashi process* is based on the exact mechanism using cat. $ZnCl_2$ and CuCl, in the presence of molecular oxygen to form the azine intermediate.[217] The peroxide process is a modification of the *Bayer process* that relies on the formation of the corresponding imine that is oxidized to the oxaziridine intermediate. Subsequent condensations with ammonia and acetone yield the hydrazone, then the ketazine derivative.[217,218] This approach allows the exclusion of chlorine and sodium perchlorate as oxidizing agents, as a large amount of chlorinated by-products and NaCl salt reduces the atom efficiency of the reactions.[217] Moreover, free hydrazine and chloramine are unstable at higher temperatures and low pH.[217,219] Ureas are also employed as starting materials for commercial hydrazine synthesis.[217]

While commercial hydrazine synthesis is well-established, only a few electrochemical protocols are known. This can be reasoned due to the hydrazine species' electrochemical instability, resulting in the liberation of nitrogen.[222]

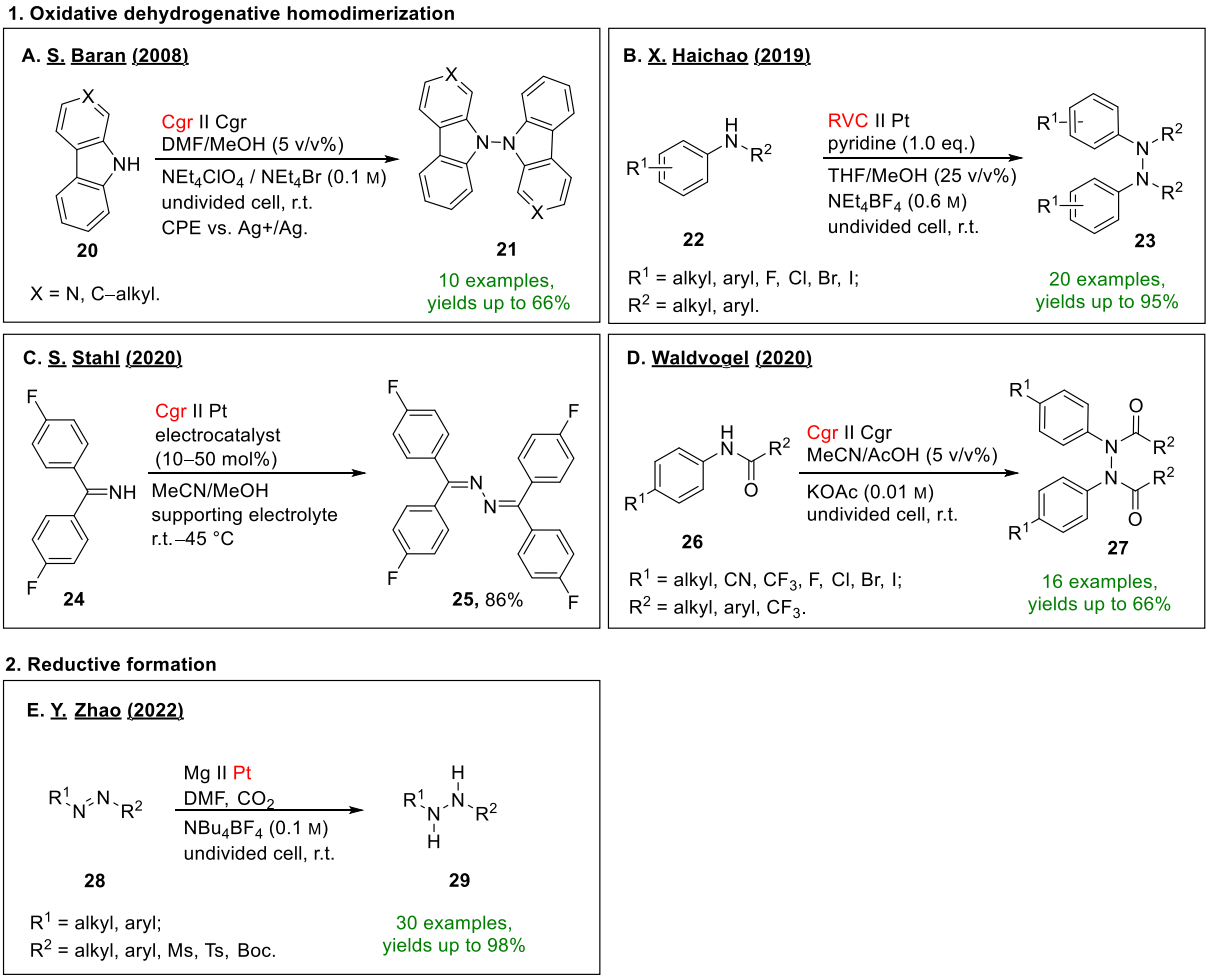

Scheme 6. State of art electrochemical hydrazine formation methods.[92,223–226] The reactions of interest take place at the electrodes emphasized in red. Cgr = graphite, gC = glassy carbon, Mg = magnesium, RVC = reticulated vitreous carbon, Pt = platinum (anode II cathode).

The electrochemical procedures can be classified into two approaches towards the formation of hydrazine derivatives (Scheme 6). One conveys the dehydrogenative homodimerization of diverse protected nitrogen compounds to the tetrasubstituted hydrazines (Scheme 6, 1.),[92,223–225] the other involves the reductive formation of mono- or disubstituted hydrazines (Scheme 6, 2.).[226,227]

P. Baran et al. reported the oxidative dehydrogenative homodimerization of carbazoles and carbolines **20** via direct oxidation at a carbon anode (Scheme 6A).[92] The reaction worked both using tetraethylammonium bromide or perchlorate as a supporting electrolyte, furnishing 10 examples with yields up to 66%. This method was used in the total synthesis of dixiamycin B with a yield of 28%. Similarly, the formation of tetrasubstituted hydrazines was reported.[223] The anodic oxidation of diphenylamine (**22**) followed by the pyridine-promoted formation of aminyl radicals

furnishes the desired homodimerized product **23**. The oxidative electrocatalytic imine coupling similar to the *Hayashi process* was described by Stahl et al.[224] The method yielded up to 86% of the desired product **25** with under constant potential electrolysis catalyzed by base, iodine, or copper (II/I) salt.[224] The electrochemical dehydrogenative intra- and intermolecular *N,N*-homocoupling via anodic N–N bond formation were reported in our group.[225,228,229] The electrochemical dehydrogenative coupling of anilides uses graphite electrodes to form 16 different *N,N*-diarylhydrazines **27** with up to 66% isolated yield.

Verma published a study of the electrochemical reduction of 1,3-diphenyl-3-hydroxytrianzene and showed the formation of phenyl hydrazine as a reductive by-product.[227] The electrochemical hydrogenation of azo compounds **28** was reported in the presence of CO_2.[226] Carbon dioxide serves as a critical reagent in the stabilization of highly reactive radical anions. The method features 30 disubstituted hydrazine **29** examples with up to 98% using a platinum cathode and a magnesium sacrificial anode.

As shown, the electrochemical formation of hydrazines has been investigated, with oxidative homodimerization (Scheme 6, 1.) being the preferred approach. However, the methods are somewhat limited to the formation of highly substituted hydrazine derivates, obligating a subsequent hydrolysis step. Moreover, the cathodic hydrogen evolution reaction usually requires the use of depleting metals.[223,224] Considering the structural dependence of hydrazines under electrochemical conditions and the limited methods available, the investigation of other electrochemical approaches in a more economical way is highly suggested.

2. Objectives

This thesis was inspired to provide a greener electrochemical bromination method for the bromination of olefines, electron-deficient enones, and for the bromocyclization of alkenoic acids compared to the already existing ones comprising multiple sustainability aspects (Figure 21):

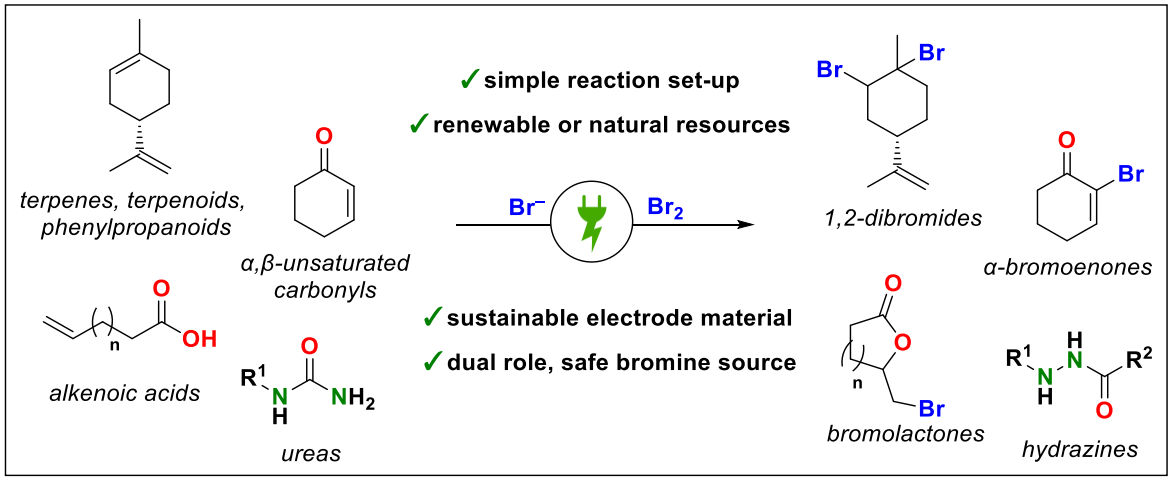

Figure 21. Objectives for the electrochemical bromination reactions.

As part of this methodology-based research, this work is focused on investigating the electrochemical dibromination of terpenes and naturally occurring olefins utilizing readily available and bench-stable bromide salt at carbon-based electrodes. The applicability of this highly sustainable method will be investigated in the frame of electrochemical bromolactonization of alkenoic acids and the selective α-bromination of deactivated alkenes. The initial investigation of the method and the optimization of the reaction parameters are highly desirable as the forming dibrominated products are of synthetic interest and can be subjected to further functionalization. This electrochemical methodology moves away from fossil-based dependence by exploiting terpenes as renewable resources.

Furthermore, the method will be extended to the study of the electrochemically generated bromine-mediated Hofmann rearrangement reactions involving ureas to the desired hydrazine compounds.

3. Results and discussion

3.1. Electrochemical dibromination of terpenes and naturally occurring olefins

A manuscript was published on this chapter:

L. G. Gombos, L. Werner, D. Schollmeyer; C. A. Martínez-Huitle, S. R. Waldvogel, *Selective Electrochemical Dibromination of Terpenes and Naturally Derived Olefins*, *Eur. J. Org. Chem*. **2022**, e202200857.

DOI: 10.1002/ejoc.202200857

The manuscript was appointed as a very important paper and was highlighted with a front cover picture. The cover picture was designed by M. Dörr and **me** and was created by M. Dörr.

Author contributions:

This manuscript was written and finalized by S. R. Waldvogel, C. A. Martínez-Huitle and **me**. The optimization reactions were carried out by C. A. Martínez-Huitle and **me**. Substrates were synthesized by L. Werner and **me**. D. Schollmeyer investigated the crystal structure of **30b.**

The naturally occurring (4*S*)-(–)-limonene (**30**) was chosen as a model substrate due to multiple functionalizable double bonds that offer regioselectivity issues. The initial reaction conditions were set to the ones shown in Scheme 7 and were optimized via the one-variable-at-time (OVAT) approach with respect to the following parameters: bromide source, cell geometry, solvent systems, electrode material, current density, applied charge, bromide concentration, and temperature.
Following the optimization process, the optimal reaction conditions were extended on different terpenes, terpenoids, and naturally derived olefins.

3.1.1. Optimization of the electrochemical reaction conditions

3.1.1.1. Optimization of bromide source

First, the bromide salts were screened under pre-set electrochemical conditions (Table 2). In this case, the bromide salt was designed to provide high performance in a dual role as a supporting electrolyte and as a bromine source.

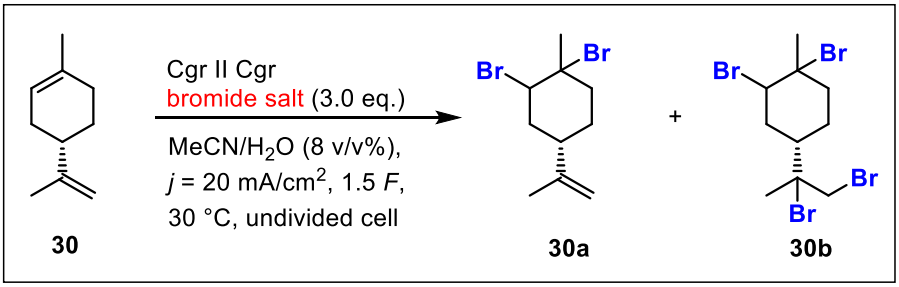

Scheme 7. Screening of bromide salts for the selective formation of **30a**. Cgr = graphite (anode II cathode).

Table 2. Screening of different type of bromide salts for the electrochemical bromination of (4*S*)-(–)-limonene (**30**).

Entry	Bromide salt	30a [%][a]	30b [%][a]	Conv. [%][b]
1*	NBu_4Br	0	0	n/a
2*	NMe_4Br	0	0	n/a
3*	NH_4Br	traces	0	n/a
4**	NBu_4Br	0	0	n/a
5	NaBr	30	4	57
6	LiBr	32	6	83
7	NBu_4Br	0	0	47
8	NEt_4Br	2	0	64

[a] Yields determined by ^{1}H NMR (internal standard: CH_2Br_2); [b] Conversion was determined via external GC calibration of **30**; [*] Conditions: **30** (0.7 mmol), bromide (1.5 mmol), acetonitrile (5 mL), j = 10 mA/cm^2, 4.4 *F* with resp. to **30**; [**] Acetone (5 mL) was used as solvent. n/a = not assessed.

After the initial screening experiments, the highest yields were obtained when metal bromide salts were employed. Sodium bromide and lithium bromide provided equally great results in obtaining the desired product **30a** with a yield of 30% and 32%, respectively (Table 2). However, heavy cathode corrosion was observed in the case of Entry 6 (Figure 22). This could be explained by the possible intercalation of lithium ions and the formation of lithium graphite intercalation compounds (Li-GIC) between the graphite layers.[230,231] Similar corrosion behavior was observed when using tetramethyl ammonium bromide (Entry 2). Interestingly, highly soluble tetraalkyl bromide salts inhibited the reaction, which could be attributed to the electrochemical double layer´s altered physical characteristics and the substrate´s solvation effect.[232]

The same results were observed in the presence of pure acetonitrile (Entry 1) and acetone (Entry 4) as well. As a result, further optimization reactions were concentrated on utilizing metal bromide salts that determined the solvent system´s composition and the need for the polar additive.

Figure 22. Heavy corrosion of graphite cathodes when LiBr was used.

3.1.1.2. Screening of cell geometry

To examine the effect of the cell geometry on the reaction outcome, the reaction with conditions from Entry 5 was carried out in a divided screening cell using a glass frit disk as a membrane (Scheme 8).

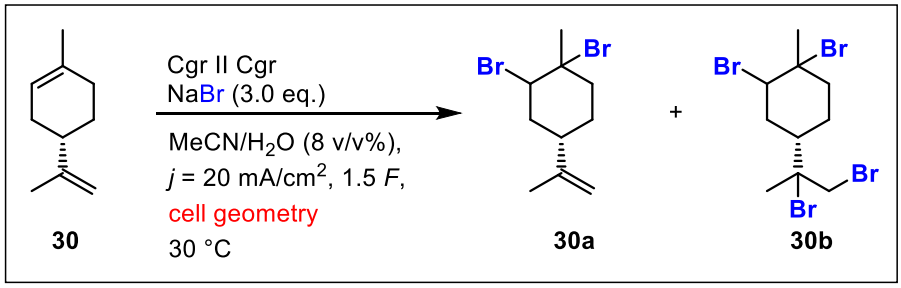

Scheme 8. Screening of cell geometry. Cgr = graphite (anode II cathode).

While a significant difference in the formation of **30a** was not observed, the formation of fully saturated product **30b** was increased to 8%, decreasing the selectivity of the reaction (Table 3).

Table 3. Screening of the cell geometry.

Entry	Cell geometry	30a [%][a]	30b [%][a]	Conv. [%][b]
9	undivided	30	4	57
10	divided	32	8	n/a

Conditions: **30** (0.7 mmol), NaBr (2.1 mmol), MeCN/H_2O (8 v/v%, 5 mL), graphite electrodes, j = 20 mA/cm^2, 1.5 F with resp. to **30**, 30 °C; [a] Yields determined by ^{1}H NMR (internal standard: CH_2Br_2); [b] Conversion was determined via external GC calibration of **30**. n/a = not assessed.

3.1.1.3. Optimization of the solvent system and the additive ratios

To determine the optimal solvent system of the electrochemical transformation, different sets of solvents and additives were tested (8 v/v%) first (Scheme 9). Protic solvents such as short-chained alcohols were avoided to reduce the competing reactions with the solvent.[184–187,198]

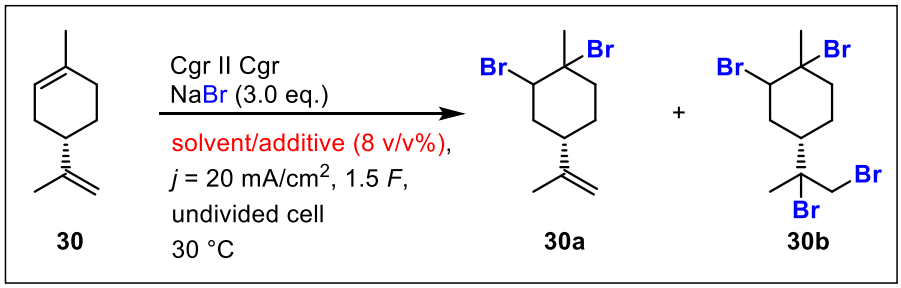

Scheme 9. Screening of solvent systems. Cgr = graphite (anode II cathode).

Table 4. Screening of different solvent systems in the presence of 8 v/v% additive.

Entry	Solvent/Additive (8 v/v%)	30a [%][a]	30b [%][a]	Conv. [%][b]
11	MeCN/H_2O	30	4	57
12	MeCN/AcOH	present	0	n/a
13	Acetone/H_2O	52	4	57
14	Acetone/AcOH	0	0	42
15	HFIP/acetone	0	0	42
16	Py/H_2O	12	6	43

Conditions: **30** (0.7 mmol), NaBr (2.1 mmol), solvent/additive (8 v/v%, 5 mL), graphite electrodes, j = 20 mA/cm^2, 1.5 F with resp. to **30**, 30 °C; [a] Yields determined by ^{1}H NMR

(internal standard: CH_2Br_2); [b] Conversion was determined via external GC calibration of **30**. HFIP = 1,1,1,3,3,3-hexafluoroisopropanol; Py = pyridine. n/a = not assessed.

The highest NMR yields were observed when acetone in the presence of 8 v/v% was employed, which can be attributed to the better solubility of the terpene in the solvent (Table 4, Entry 13). In the case of Entries 14 and 15, no desired products were formed, but conversion studies showed the consumption of the starting material to undetectable by-products. In the absence of water, no desired product was formed. Furthermore, less than 8 v/v% water did not promote the solution of NaBr in the reaction media, and electrolysis could not be carried out. To understand the role of water, different volume percentages were screened in acetonitrile, acetone, and pyridine solvents (Table 5).

Table 5. Screening of acetonitrile, acetone, and pyridine solvents with different water contents.

Entry	Solvent (20 v/v%)	30a [%][a]	30b [%][a]	Conv. [%][b]
17	MeCN/H_2O (20%)	9	0	63
18*	MeCN/H_2O (50%)	0	0	83
19	Acetone/H_2O (20%)	8	4	38
20	Py/H_2O (20%)	4	4	76

Conditions: **30** (0.7 mmol), NaBr (2.1 mmol), solvent/additive (5 mL), graphite electrodes, j = 20 mA/cm^2, 1.5 F with resp. to **30**, 30 °C; [a] Yields determined by ^{1}H NMR (internal standard: CH_2Br_2); [b] Conversion was determined via external GC calibration of **30**; [*] A current density (j) of 10 mA/cm^2 and 2.2 F with resp. to **30** was used. Py = pyridine.

With increased water content, the formation of desired compounds was reduced to 9% and 0%, respectively (Entries 17, 18). In the presence of 50 v/v% water, a complex mixture of products was detected. The nature of the by-products was not identified due to the complexity of the reaction mixture. The loss of selectivity could be explained by the decreased solubility of the lipophilic terpene with increasing water content. Moreover, the solvent can act as a co-nucleophile promoting the formation of different oxo-functionalized products. Furthermore, the type of “active brominating agents” are shifted toward the formation of HOBr and HBr. These aspects are all responsible for the different chemical reactivity observed and therefore, the diminished yields.
As acetone/water (8 v/v%) and acetonitrile/water (8 v/v%) proved the most promising, further optimization reactions were carried out parallel on both solvent systems.

3.1.1.4. Optimization of electrode materials

Both reaction conditions were tested at glassy carbon, boron-doped diamond (BDD), stainless steel, and platinum electrodes (Scheme 10, Table 6).

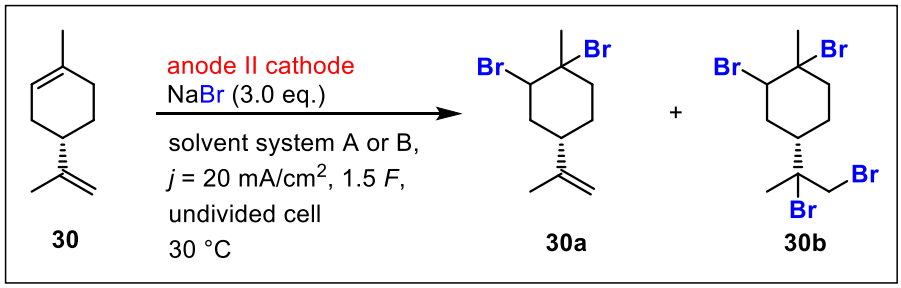

Scheme 10. Screening of different electrode materials. Solvent system A: MeCN/H_2O (8 v/v%, 5 mL), solvent system B: acetone/H_2O (8 v/v%, 5 mL).

Table 6. Screening of different electrode materials in both solvent systems. Solvent systems: MeCN/H_2O (8 v/v%, 5 mL) or acetone/H_2O (8 v/v%, 5 mL).

Entry	Solvent	Electrode	30a [%][a]	30b [%][a]	Conv. [%][b]
21	MeCN/H_2O	gC II gC	46	5	59
22*	MeCN/H_2O	gC II S.Steel	25	0	n/a
23	MeCN/H_2O	BDD II BDD	32	0	69
24	MeCN/H_2O	Pt II Pt	20	0	79
25	Acetone/H_2O	gC II gC	24	0	53
27	Acetone/H_2O	BDD II BDD	30	0	59
28	Acetone/H_2O	Pt II Pt	16	0	77

Conditions: **30** (0.7 mmol), NaBr (2.1 mmol), solvent/additive (8 v/v%, 5 mL), j = 20 mA/cm^2, 1.5 *F* with resp. to **30**, 30 °C; [a] Yields determined by ^{1}H NMR (internal standard: CH_2Br_2); [b] Conversion was determined via external GC calibration of **30**; [*] A current density (j) of 5 mA/cm^2 was used. gC = glassy carbon, S. Steel = stainless steel, BDD = boron-doped diamond, Pt = platinum. (anode II cathode). n/a = not assessed.

In the case of the acetonitrile/water solvent system, using glassy carbon electrodes resulted in an increased yield of 46% (Entry 21). For the acetone/water solvent system, graphite electrodes remained superior to other conditions (Table 4, Entry 13). However, graphite electrodes showed a tendency toward electrode amortization, affecting the reactions´ reproducibility. Similar tendencies were reported during the electrochemical oxidation of aq. KBr solution on graphite sheet by I. Izumi and

M. Inagaki.[122] Resistivity change was attributed to the intercalation of bromide in the graphite lattice layer. These findings urged the screening of more stable electrode materials. Inspired by the previous electrochemical approaches,[187,198,199,233] platinum electrodes and stainless steel as cathode material were also screened as possible alternatives (Entries 22, 24, and 28). Nevertheless, these electrode materials showed reduced product formation. To understand whether different carbon-based electrodes have a detrimental effect on the reaction, further optimization reactions were carried out on graphite, glassy carbon, and boron-doped diamond electrodes.

3.1.1.5. Screening of different current densities at carbon-based electrodes

Different current densities were tested in MeCN/H_2O (8 v/v%) and acetone/H_2O (8 v/v%) solvent systems in this optimization step (Scheme 11). In both cases, a range of current densities between 5 and 28 mA/cm^2 was applied on graphite, glassy carbon, and boron-doped diamond electrodes (Tables 7, 8).

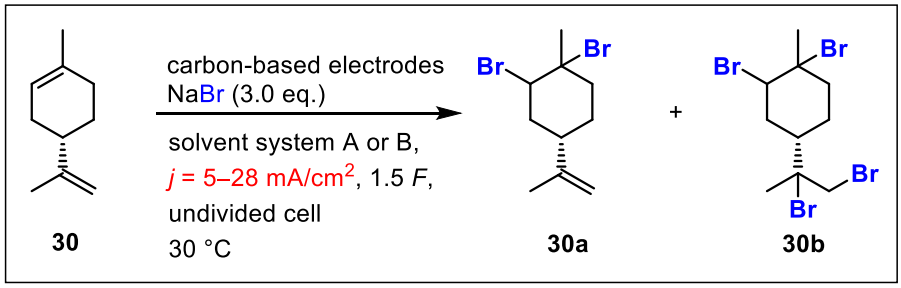

Scheme 11. Screening of different current densities in combination of different electrodes. Solvent system A: MeCN/H_2O (8 v/v%, 5 mL), solvent system B: acetone/H_2O (8 v/v%, 5 mL).

The best results were obtained when 5 mA/cm^2 was applied at glassy carbon and BDD electrodes (Entries 33, 37), obtaining **30a** with a 54% and 56% yield, respectively. At this point, the acetonitrile/water system proved superior to the acetone/water solvent system, and the latter was omitted from further optimization investigations.

Table 7. Screening of current density range on carbon-based electrode materials in MeCN/H_2O (8 v/v%, 5 mL).

Entry	Electrodes	*j* (mA/cm^2)	30a [%][a]	30b [%][a]	Conv. [%][b]
29	Cgr II Cgr	5	35	1	87
30	Cgr II Cgr	10	38	1	85
31	Cgr II Cgr	20	30	4	57
32	Cgr II Cgr	28	21	1	78
33	gC II gC	5	54	0	77
34	gC II gC	10	24	0	87
35	gC II gC	20	46	5	59
36	gC II gC	28	25	0	85
37	BDD II BDD	5	56	1	87
38	BDD II BDD	20	32	0	69

Conditions: **30** (0.7 mmol), NaBr (2.1 mmol), MeCN/H_2O (8 v/v%, 5 mL), 1.5 *F* with resp. to **30**, 30 °C; [a] Yields determined by ^{1}H NMR (internal standard: CH_2Br_2); [b] Conversion was determined via external GC calibration of **30**. Cgr = graphite, gC = glassy carbon, BDD = boron-doped diamond. (anode II cathode).

Table 8. Screening of current density range at carbon-based electrode materials in acetone/H_2O (8 v/v%, 5 mL).

Entry	Electrodes	*j* (mA/cm^2)	30a [%][a]	30b [%][a]	Conv. [%][b]
39	Cgr II Cgr	5	34	0	74
40	Cgr II Cgr	10	22	0	60
41	Cgr II Cgr	20	52	4	57
42	Cgr II Cgr	28	20	0	47
43	gC II gC	5	34	0	46
44	gC II gC	10	36	0	61
45	gC II gC	20	24	0	53
46	gC II gC	28	45	0	75
47	BDD II BDD	5	24	0	66
48	BDD II BDD	20	30	0	59

Conditions: **30** (0.7 mmol), NaBr (2.1 mmol), acetone/H_2O (8 v/v%, 5 mL), 1.5 *F* with resp. to **30**, 30 °C; [a] Yields determined by ^{1}H NMR (internal standard: CH_2Br_2); [b] Conversion was

determined via external GC calibration of **30**. Cgr = graphite, gC = glassy carbon, BDD = boron-doped diamond. (anode II cathode).

3.1.1.6. Optimization of the applied charge amount

The amount of applied charge with respect to the substrate was varied (Scheme 12). Due to the presence of starting material after electrolysis, higher charge quantities were applied up to 3.0 *F* at glassy carbon and BDD electrode materials (Table 9).

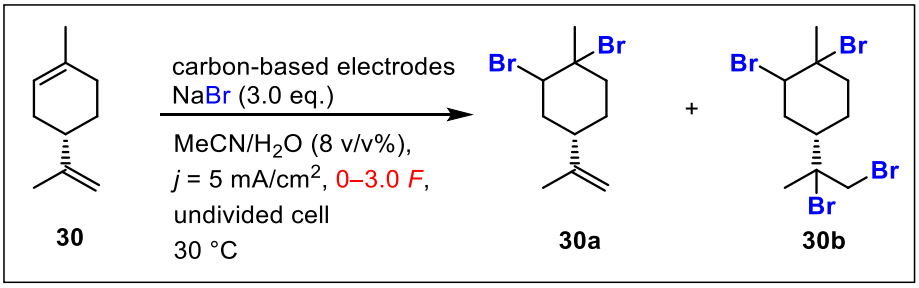

Scheme 12. Screening the applied charge amount (*Q*).

Table 9. Optimization of the applied charge amount (*Q*).

Entry	Electrodes	(Q)	30a [%][a]	30b [%][a]	Conv. [%][b]
49	gC II gC	1.5 *F*	54	0	77
50	gC II gC	2.2 *F*	36	4	83
51	gC II gC	3.0 *F*	49	1	98
52	gC II gC	0 *F*	0	0	2
53	BDD II BDD	1.5 *F*	56	1	87
54	BDD II BDD	3.0 *F*	44	1	88

Conditions: **30** (0.7 mmol), NaBr (2.1 mmol), acetonitrile/H_2O (8 v/v%, 5 mL), j = 5 mA/cm^2, 30 °C. [a] Yields determined by ^{1}H NMR (standard: CH_2Br_2); [b] Conversion was determined via external GC calibration of **30**. gC = glassy carbon, BDD = boron-doped diamond. (anode II cathode).

With increasing charge quantity, the formation of **30a** was decreased, while the starting material **30** diminished (Entry 51). According to previous studies, the theoretical charge for the formation of 1.0 eq. of bromine with respect to the substrate is 2.0 *F*.[173–175] Interestingly, the formation of **30a** was capped at 54% when 1.5 *F* was applied, indicating a possible side reaction that causes the consumption of starting material. The reaction mixture was analyzed qualitatively and quantitatively with GC,

GC-MS, and NMR spectroscopy. Apart from minor by-products, the reaction was highly selective, forming **30a** (Figure 23).

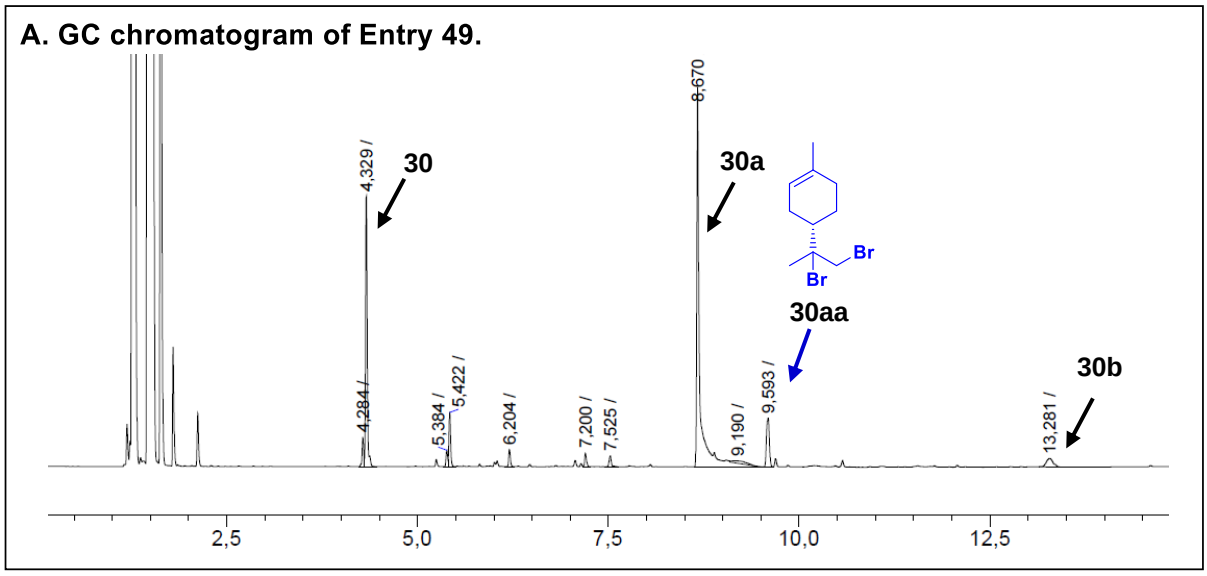

Figure 23. GC chromatogram of Entry 49 reaction mixture after electrolysis. Instrument: GC 2010 Shimadzu, method: HP5 hart.

Via GC and GC-MS chromatograms, it was revealed that a trace amount of brominated derivative was also present, where saturation was observed on the exo-bond (**30aa**, Figure 23, retention time: 9.593 min). After the work-up procedure, the yield and ratio of **30a** and **30b** could be quantified via NMR spectroscopy, and the obtained products were spectroscopically pure. However, in the case of Entry 49, 23% of diminished starting material still could not be reasoned, indicating the possible formation of highly volatile, short-chained hydrocarbon degradation products. The ideal electrode material was set to glassy carbon as a higher conversion of **30** was observed at BDD electrodes (Entries 53, 54). In the case of Entry 52, the reaction was left to stir overnight at the electrolysis temperature with no restriction on reducing heat transfer or disclosing air exchange. In the absence of electricity, no product was formed, and the starting material loss was insignificant.

3.1.1.7. Optimization of the bromide salt concentration

The reaction conditions were subjected to different amounts of bromide equivalents (Scheme 13). At this stage, 1, 2, and 4 equivalents (0.14 M, 0.28 M, and 0.56 M) of sodium bromide were tested (Table 10). As sodium bromide acts in a dual role as a

bromine source and supporting electrolyte, the concentration should be high enough that no detrimental effect is observed on the cell voltage when bromide is consumed.

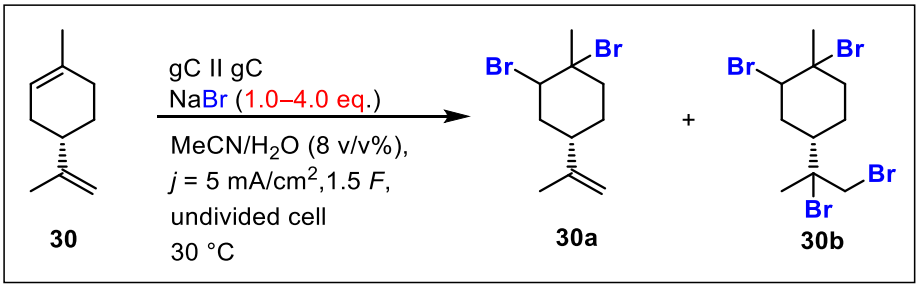

Scheme 13. Optimization of bromide salt concentration. gC = glassy carbon (anode II cathode).

Table 10. Optimization of bromide equivalents.

Entry	Equivalents / [M]	30a [%][a]	30b [%][a]	Conv. [%][b]
55	1.0 eq. / 0.14 M	21	0	57
56	2.0 eq. / 0.28 M	36	0	74
57	3.0 eq. / 0.42 M	54	0	77
58	4.0 eq. / 0.56 M	42	1	66

Conditions: **30** (0.7 mmol), acetonitrile/H_2O (8 v/v%, 5 mL), j = 5 mA/cm^2, 1.5 F with resp. to **30**, 30 °C. [a] Yields determined by ^{1}H NMR (internal standard: CH_2Br_2); [b] Conversion was determined via external GC calibration of **30**.

Both lower and higher quantities of NaBr than 3 eq. decreased the formation of the desired product **30a**. This can be attributed to NaBr being the limiting reagent in the reactions (Entries 55, 56). In the case of higher bromide content, the solvation of the salt was reduced, and efficient stirring of the solution was inhibited. This problem was tried to be solved via mechanical grinding of sodium bromide. However, higher yields were not obtained (Entry 58).

3.1.1.8. Screening of reaction temperature

To understand how temperature affects the reaction outcome, the now optimized conditions were carried out at different temperatures (Scheme 14). Interestingly, lower, and higher temperature ranges decreased the formation of **30a**. This could be reasoned by the volatile nature of **30** and the additional heat that is generated during the electrolysis (Table 11).

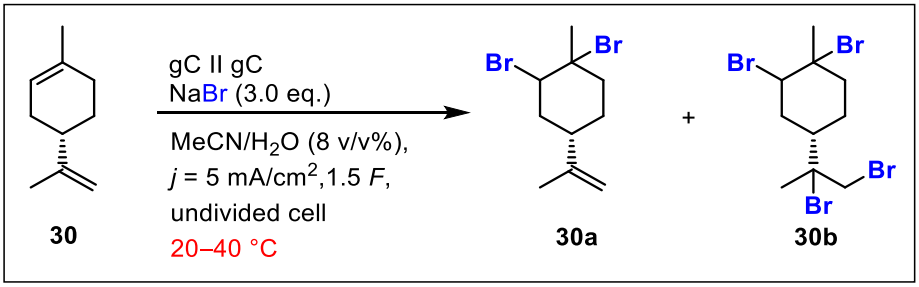

Scheme 14. Screening of optimal temperature range. gC = glassy carbon (anode II cathode).

Table 11. Variation of reaction temperatures.

Entry	Temperature (°C)	30a [%][a]	30b [%][a]	Conv. [%][b]
59	20	31	0	68
60	30	54	0	77
61	40	16	0	44

Conditions: **30** (0.7 mmol), NaBr (2.1 mmol), MeCN/H_2O (8 v/v%, 5 mL), j = 5 mA/cm^2, 1.5 F with resp. to **30**. [a] Yields determined by ^{1}H NMR (internal standard: CH_2Br_2); [b] Conversion was determined via external GC calibration of **30**.

As a result of the extensive screening reactions the following parameters were set as optimal (Scheme 15):

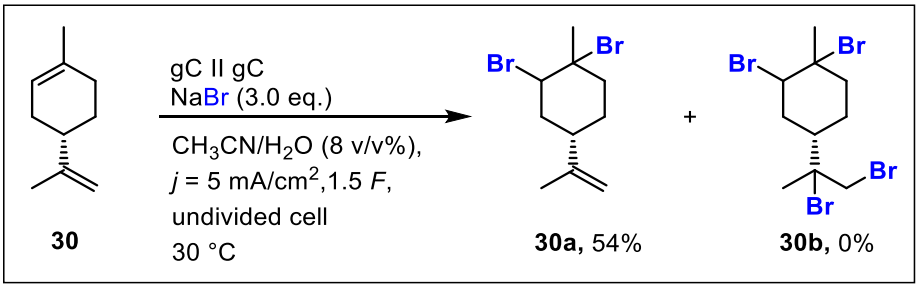

Scheme 15. Optimized reaction condition for the selective formation of **30a**.

The initial screening experiments revealed that limonene only tolerates NaBr as a bromine source, which determined the solvent composition and the necessity of H_2O as an additive. The best yields and selectivity were achieved when a charge of 1.5 F was applied in the presence of 3 eq. NaBr at glassy carbon electrodes (Entry 49). Even though the theoretical charge is 2.0 F for one equivalent of bromine formation with respect to the substrate, when more charge (Q) was applied (Entries 50, 51) or the bromide concentration was increased, the formation of **30a** was lowered (Entry 58).[234]

3.1.2. Extension of scope

Once the reaction conditions were optimized, the scope was extended with both structurally challenging mono- and polyunsaturated monoterpenes, terpenoids, and phenylpropanoids. The scope with respective yields, amount of applied charge, and diastereomeric ratio was included in the Scheme 16.

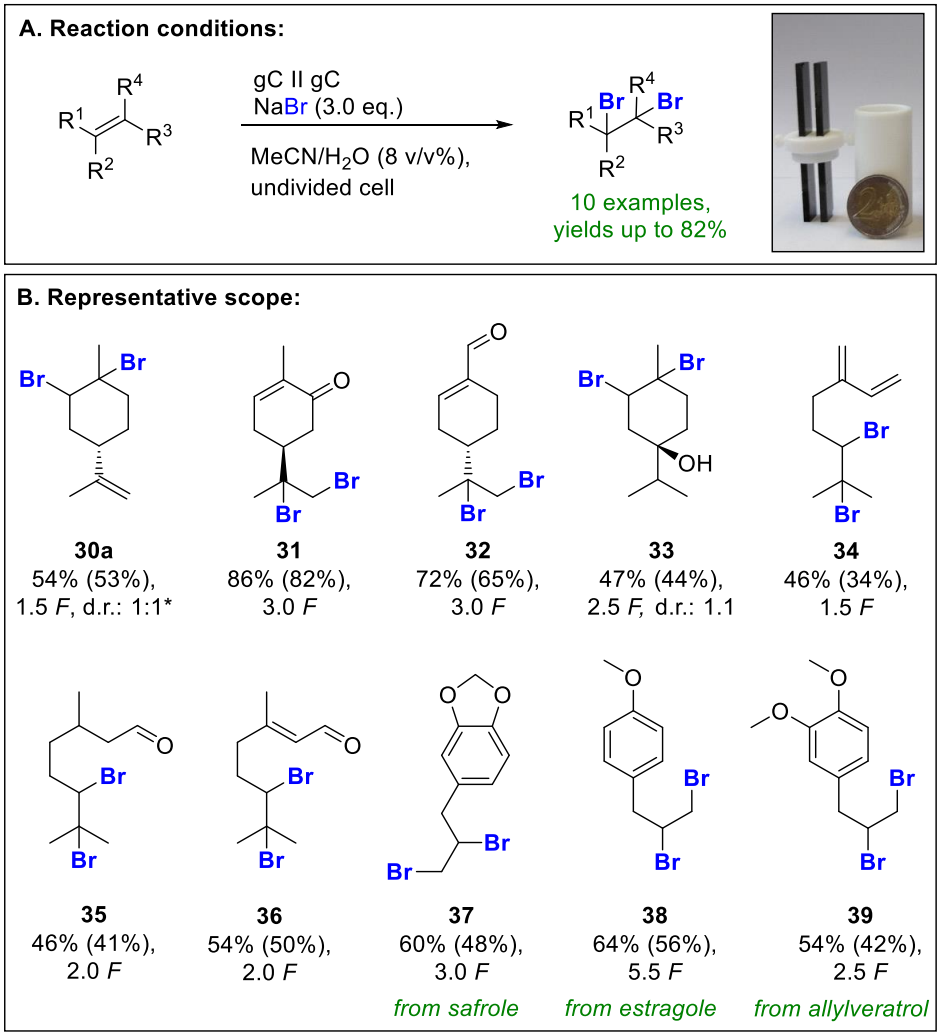

Scheme 16. Scope for the synthesis of dibrominated derivatives. Reaction conditions: substrate (0.7 mmol), NaBr (2.1 mmol), MeCN/H_2O (5 mL, 8 v/v%), glassy carbon electrodes, undivided cell, constant current, j = 5 mA/cm^2, 1.5–5.5 *F*, 30 °C. Yields were determined by ^{1}H NMR (standard: CH_2Br_2). Isolated yields are in brackets. gC = glassy carbon. [*] Diastereomeric ratio (d.r.) was postulated from the crystallographic data and d.r. of **30b**. Reproduced from reference [234], CC BY-NC-ND 4.0.

Among all the structures tested, **31** could be obtained with the highest isolated yield of 82%. Similarly, the electrochemical dibromination of perillaldehyde and 4-allylanisole formed **32** and **38** with an isolated yield of 65% and 56%, respectively.

The yields were higher in the presence of a deactivated olefin, and bromination was observed on the terminal alkenes. This can be attributed to the reduced nucleophilicity of the corresponding alkene, which enhanced the selectivity of our method as well. The method proved to be applicable to a wide range of natural alkenes, including various functional groups such as ketones, aldehydes, alcohol, and aromatic groups as well. In the case of α-pinene and 3-carene the method proved to be rather unsuccessful (Figure 24). While **40** could be obtained with an NMR yield of 20%, the product was subjected to degradation even when storing it under an inert atmosphere and low temperature. α-pinene yielded a complex mixture of unidentified products, and **41** could not be detected. This phenomenon was reasoned with the structural strain energy of the dimethylcyclobutyl moiety of α-pinene. Via an activation of the pinene olefin, the strained dimethylcyclobutyl ring can open, which leads to the unprofitable reaction outcome.[235] When pulegone was subjected to the optimized conditions, no conversion to **42** was observed (Figure 24).

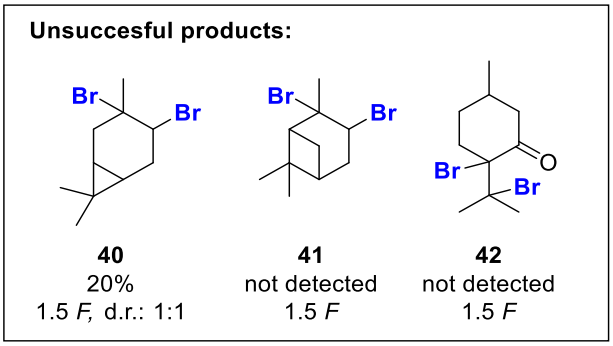

Figure 24. Unsuccessful products. Yields were determined by ^{1}H NMR (internal standard: CH_2Br_2). d.r. = diastereomic ratio.

The scalability of the reaction was tested on the formation of **31**. Carvone was scaled up from 0.7 mmol to 3.5 mmol in a 25 mL Telfon® cell to obtain the corresponding derivate in a yield of 72%. In the case of the 3.5 mmol scale, the reaction displayed a slightly decreased yield (Figure 25).

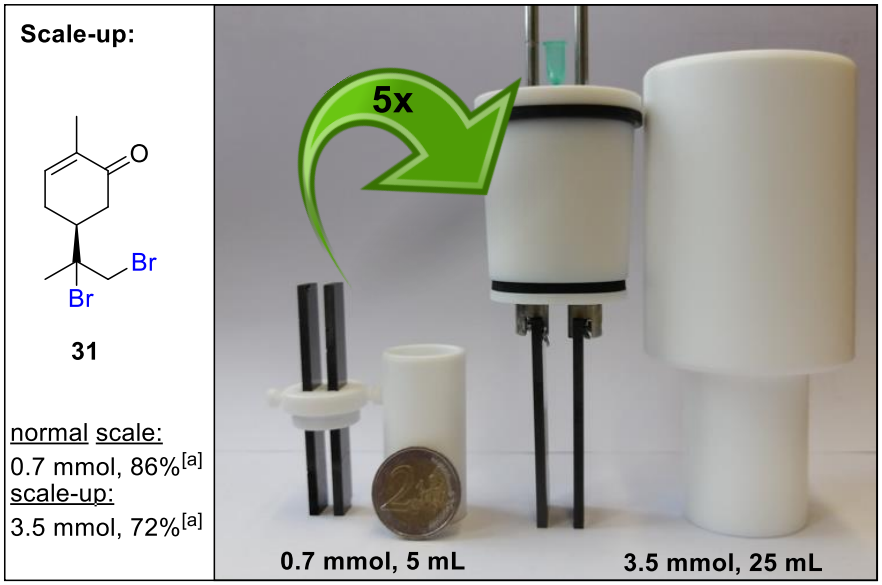

Figure 25. Transferring the synthesis of **31** from 0.7 mmol to 3.5 mmol scale. Reaction conditions: substrate (3.5 mmol), NaBr (10.5 mmol), MeCN/H_2O (25 mL, 8 v/v%), glassy carbon electrodes, undivided cell, constant current, j = 5 mA/cm^2, 3.0 *F*, stirring velocity: 400 rpm, 40 °C; [a] Yields determined by ^{1}H NMR (internal standard: CH_2Br_2). Reproduced from reference [234], CC BY-NC-ND 4.0.

When the reaction parameters and cell geometry were adjusted, the selectivity of the reaction was inversed to favour the formation of **30b** (Scheme 17). As carbon-halogen bond are cathodically labile,[236] a divided Teflon® cell with a ceramic glass frit was employed.[137] When 4.5 *F* was applied, 74% of **30b** was isolated. Only the (1*R*,2*R*,4*S*,8*S*)-diastereomer was obtained upon crystallization.

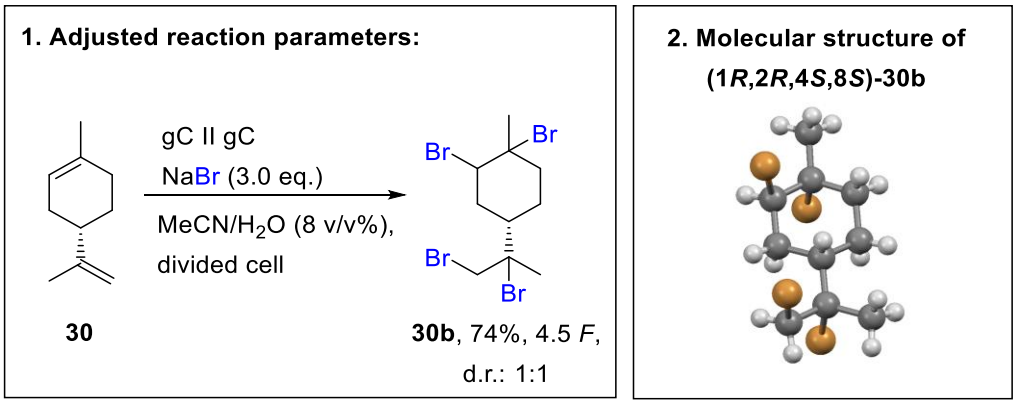

Scheme 17. Electrochemical tetrabromination of **30**. Reaction conditions: Anodic compartment: **30** (0.7 mmol), NaBr (2.1 mmol), MeCN/H_2O (5 mL, 8 v/v%). Cathodic compartment: NaBr (2.1 mmol), MeCN/H_2O (5 mL, 8 v/v%), glass frit membrane, glassy carbon electrodes, divided cell, constant current, j = 5 mA/cm^2, 4.5 *F*, 30 °C. Isolated yield.

The molecular structure of (1*R*,2*R*,4*S*,8*S*)-diastereomer of **30b** was obtained by crystallographic X-ray analysis (See experimental part for more information). Reproduced from reference [234], CC BY-NC-ND 4.0.

3.1.3. Mechanistic studies

For the elucidation of the electrochemical dibromination mechanism, cyclic voltammetry (CV) studies were carried out to understand the anodic counterpart. Three solutions were scanned subsequently, including **30** (black), sodium bromide (red), and **30** and sodium bromide (blue, Figure 26).

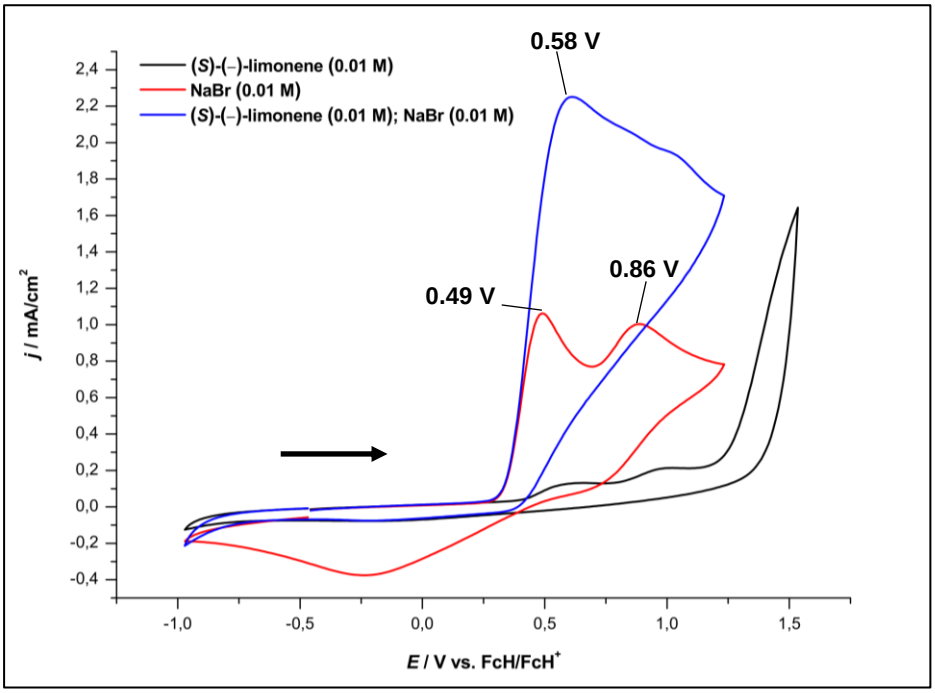

Figure 26. Cyclic voltammetry measurements of **30** (black), NaBr (red), and **30** and NaBr (blue) in MeCN/H_2O (8 v/v%) solution. Conditions: substrate (0.01 M), NBu_4BF_4 (0.10 M), WE: glassy carbon disk (*d* = 3.0 mm), RE: Ag/AgCl, CE: glassy carbon rod, scan rate: 100 mV/s. FcH = ferrocene. Instrument: Autolab PGSTAT101, Metrohm AG. Reproduced from reference [234], CC BY-NC-ND 4.0.

The red voltammogram postulates a quasi-reversible process with two distinctive oxidation potentials (red voltammogram, Figure 26). The first oxidation potential corresponds to the oxidation of bromide to bromine, according to Equation 12. In a polar aprotic media with excess bromide concentration, the electrochemically generated bromine is in equilibrium with the stable tribromide complexes (Equation

13). The second oxidation potential corresponds to the oxidation of these tribromide salts to bromine, which is in accordance with the literature (Equation 14).[172,173,175,176] In the presence of (4*S*)-(–)-limonene (**30**, blue voltammogram), the first oxidation potential was shifted from 0.49 V to 0.58 V, and the second oxidation potential was absent. This indicated the immediate saturation of the alkene by the generated bromine, shifting the equilibrium away from the formation of Br_3^-. The absence of the reduction potential in the blue voltammogram is also indicated that bromine is consumed by the alkene in the solution.

$$2\ Br^- \rightarrow Br_2 + 2\ e^- \qquad \textbf{(12)}$$

$$Br_2 + Br^- \rightleftharpoons Br_3^- \qquad \textbf{(13)}$$

$$2\ Br_3^- \rightarrow 3\ Br_2 + 2\ e^- \qquad \textbf{(14)}$$

Within the potential window, **30** displays no electrochemical reactivity (black). Therefore, NaBr should be anodically consumed before limonene (**30**) is affected.

The reaction was carried out in the presence of a radical scavenger, 2,2,6,6-tetramethylpiperidinyloxy (**43**, TEMPO) to support our findings. As a result, the formation of **30a** was suppressed entirely, resulting only in a trace amount of product, justifying the inhibition of active bromine agent formation (Figure 27).

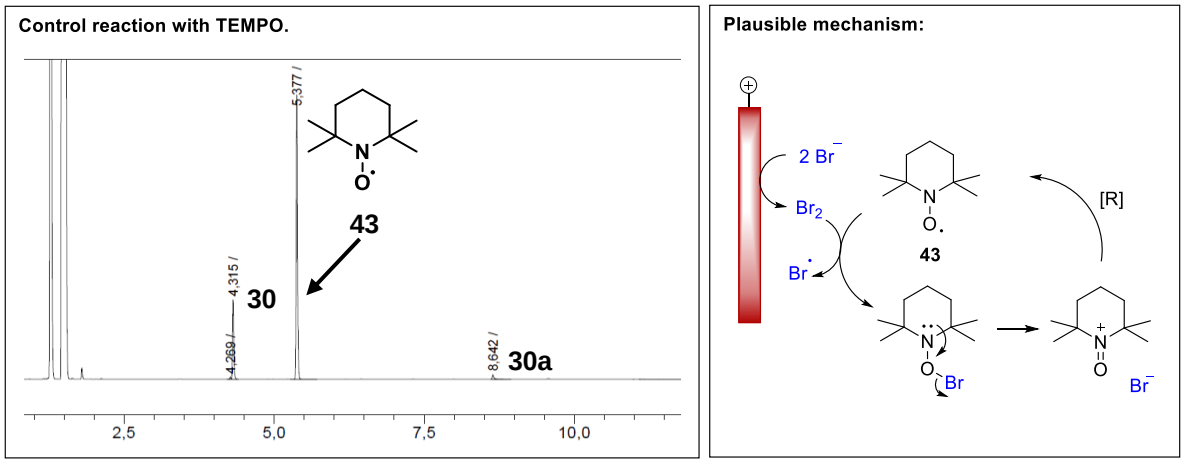

Figure 27. GC chromatogram of the reaction solution after electrolysis using TEMPO (5.377 min) as a radical scavenger. Instrument: GC 2010 Shimadzu, method: HP5 hart. Reaction conditions: **30** (0.7 mmol), NaBr (2.1 mmol), TEMPO (**43**, 2.1 mmol), MeCN/H_2O (5 mL, 8 v/v%), glassy carbon electrodes, j = 5 mA/cm^2, Q = 1.5 F. [R] = reduction.

As a cathodic reaction, hydrogen evolution is postulated, which is in accordance with previously recorded studies.[143] Moreover, in the case of the scale-up reaction, gas evolution was visually observed on the cathode. In case of divided cells, the pH value of the anodic and cathodic solutions was measured, indicating a strongly acidic and alkaline environment, respectively reinforcing our hypothesis (Scheme 18). In the case of an undivided cell, the pH value remained constant, suggesting the formation of hypobromite.[182]

As a result, the following reaction mechanism was postulated for the electrochemical dibromination of natural alkenes: bromide is oxidized via two-step at the anode to form bromine that immediately reacts with the respective olefin **30** to form the highly reactive halonium intermediate **IV**. Subsequently, the **IV** suffers nucleophilic ring opening by the free bromide in the solution forming the desired product. The reaction is complemented via cathodic hydrogen evolution. The formation of instable hypobromous acid cannot be disclosed (Scheme 18).

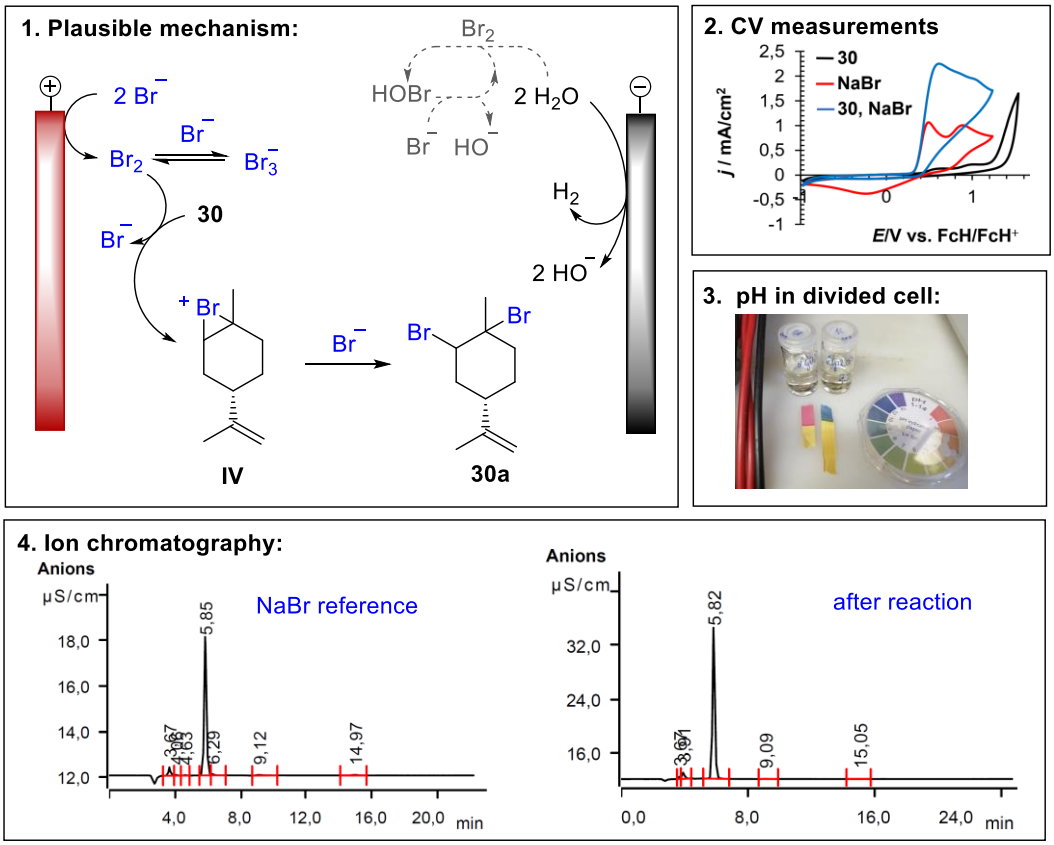

Scheme 18. Plausible reaction mechanism for the electrochemical dibromination of limonene (**30**). Cyclic voltammetry supports the anodic reaction. Visual observation of cathodic gas formation and pH measurements confirm the cathodic counter reaction. Ion chromatography shows Br^- as the sole anionic entity present after electrolysis. Bromate (BrO_3^-) was not

observed. Instruments: Autolab potentionstat PGSTAT101, Metrohm AG; 850 Professional IC, Metrohm AG.[234]

3.1.4. Control experiments

To demonstrate the superiority of the electrochemical method over the conventional bromination methods, the dibromination of (4*S*)-(–)-limonene (**30**) was conducted in the presence of elemental bromine and using DMSO/HBr (Table 12).[237,238]

Table 12. Control experiments for the dibromination of **30**.

Entry	Conditions	30a [%][a]	30b [%][a]
1	Br_2[237]	22	13
2	DMSO/HBr[238]	39	10
3	Electrochemical method	54	0

Control experiments. Reaction condition: 1) **30** (0.7 mmol), Br_2 (99.6 %,0.7 mmol), DCM (2.0 mL), 0 °C, 30 min. 2) **30** (0.7 mmol), DMSO (0.8 mmol), HBr (48 w/w% aq., 1.6 mmol), EtOAc (2.8 mL), 60 °C, 30 min. 3) **30** (0.7 mmol), NaBr (2.1 mmol), MeCN/H_2O (5 mL, 8 v/v%), glassy carbon electrodes, undivided cell, constant current, j = 5 mA/cm^2, 1.5 F, 30 °C. [a] Yield determined by ^{1}H NMR (internal standard: CH_2Br_2). [234]

In both cases, the desired product was obtained in lower yields with reduced selectivity. The reaction carried out in the presence of bromine proved unselective, accompanied by one main by-product and many unidentified by-products. According to GC-MS measurement, the signal was depicted as a monobrominated limonene derivative **30c**. Further characterization could not be carried out as the product decomposed upon isolation. The DMSO/HBr system reported by Jiao et al. showed higher selectivity providing **30a** in 39% and **30b** in 13% NMR yield (Table 12). The electrochemical method proved exceptional over the applied methodologies, which is credited to the slower and controlled in-situ generation of bromine during the electrolysis (Figure 28).[234]

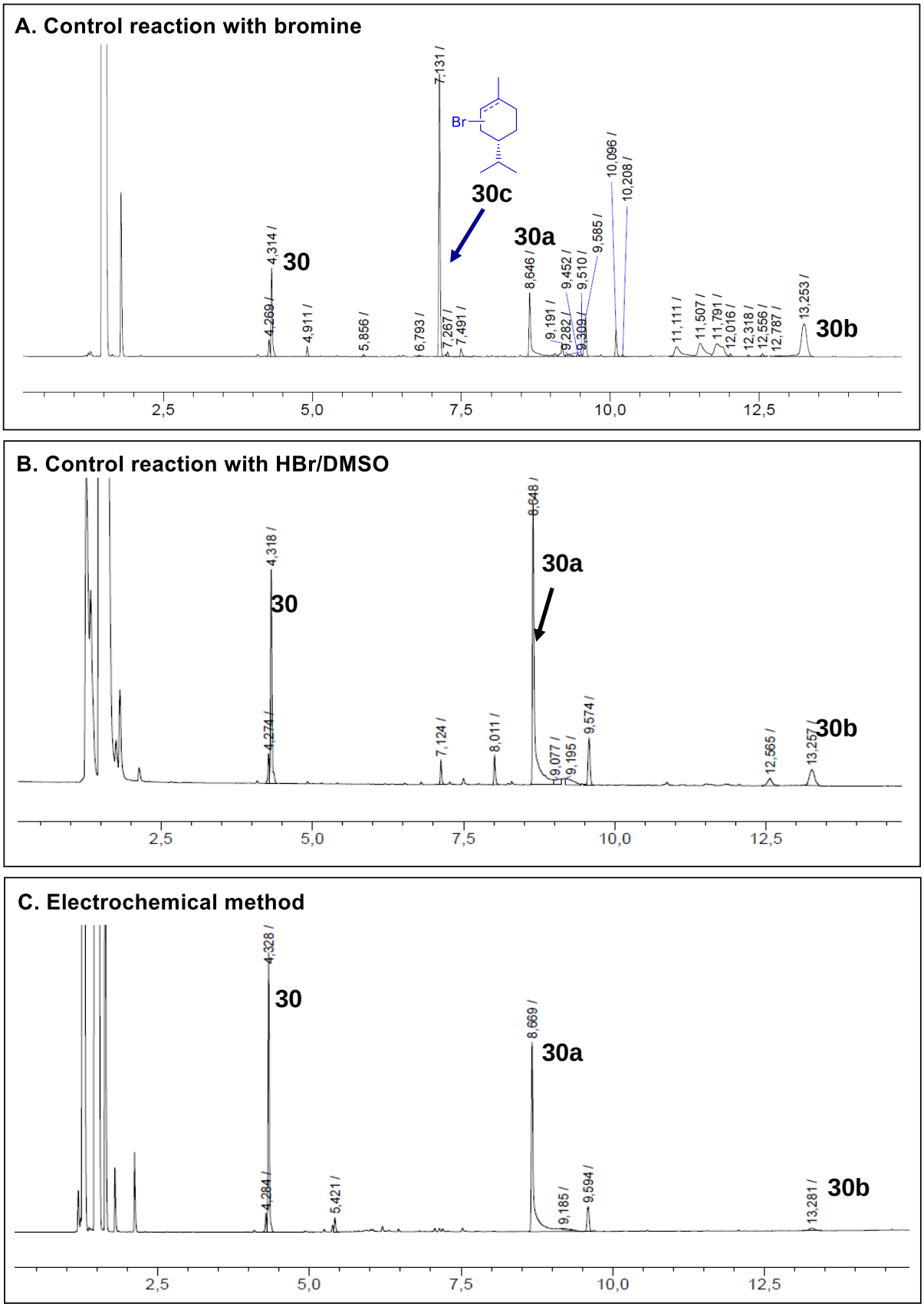

Figure 28. GC chromatograms of control reactions with bromine (A), DMSO/HBr (B), and electricity (C) for qualitative visualization of reaction selectivity. Signals of **30**, **30a**, **30b** and

30c were identified via GC, GC-MS and ^{1}H NMR measurements. Instrument: GC 2010 Shimadzu, method: HP5 hart. Reproduced from reference [234], CC BY-NC-ND 4.0.

3.1.5. Further functionalization of the electrochemically generated dibrominated products

To demonstrate the synthetic utility of the dibrominated derivatives, a series of further functionalization reactions were carried out according to Scheme 19.

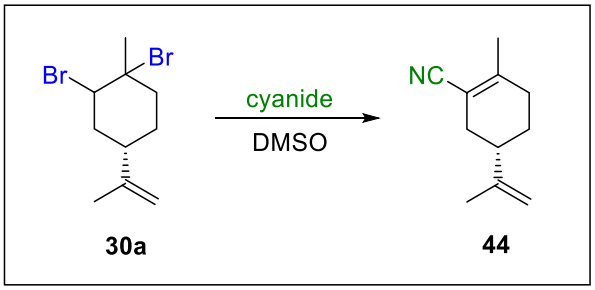

Scheme 19. Subsequent functionalization of **30a** to **44** via Kolbe-nitrile synthesis. Reproduced from reference [234], CC BY-NC-ND 4.0.

3.1.5.1. Kolbe-nitrile synthesis

Nitrile groups are indispensable functional groups in organic synthesis due to their ability to be converted into a plethora of significant products. The Kolbe-nitrile synthesis allows the formation of alkyl nitriles from alkyl halides via substitution with cyanide ion and shows excellent reactivity and selectivity in DMSO.[239]

30a was subjected to the well-known Kolbe-nitrile synthesis[240,241] and other alkyl nitrile forming methods[242,243] to form the corresponding α,β-unsaturated nitrile as a result of a one-pot substitution and subsequent elimination procedure. This approach was especially of interest as the forming α,β-unsaturated nitriles are excellent synthetic building blocks as polymer precursors from renewable resources.[244]

Moreover, the exact product under NaBr-mediated electrochemical conditions was not possible to achieve (Figure 29). The presence of NaCN inhibited the reaction by electrode passivation, forming white deposits on the immersed electrode surfaces. The reactions were monitored by TLC, GC, GC-MS, and ^{1}H NMR methods.

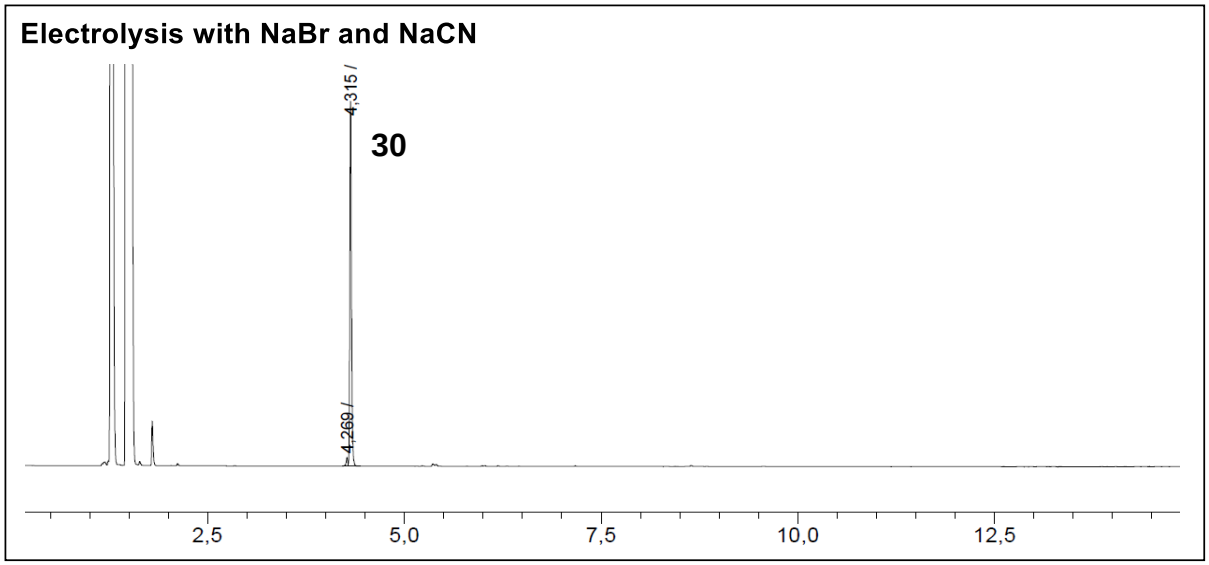

Figure 29. GC chromatogram of reaction solution after electrolysis in the presence of NaCN. Reaction conditions: **30** (0.7 mmol), NaBr (2.1 mmol), NaCN (1.4 mmol), MeCN/H_2O (8 v/v%, 5 mL), glassy carbon electrodes, j = 5 mA/cm^2, Q = 1.5 F, 30 °C. Instrument: GC 2010 Shimadzu, method: HP5 hart.

To promote the desired reaction, polar aprotic DMSO with surplus equivalents of cyanide salts was tested to facilitate the substitution. Subsequent to the S_N2 reaction, the inversion of stereochemistry at C2 allows the preferential antiperiplanar arrangement of C–H σ and C–Br σ* bonds to promote the β-elimination in a one-pot approach (Scheme 20). It is worth mentioning that trials in the reversed order to achieve **44** were unsuccessful, and no conversions were observed. This was justified by the ring distortion of **30a** due to the higher electron negativity of the bromine substituents that prevented the preferential arrangement for the β-elimination.

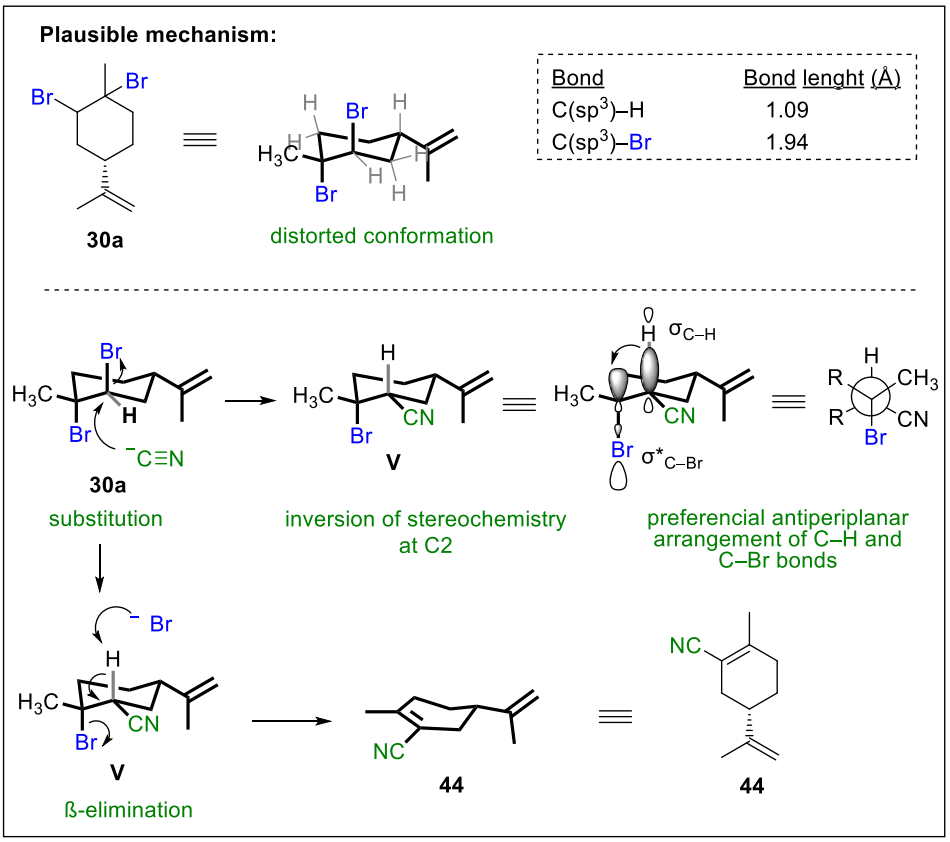

Scheme 20. Plausible mechanism for the formation of **44.**

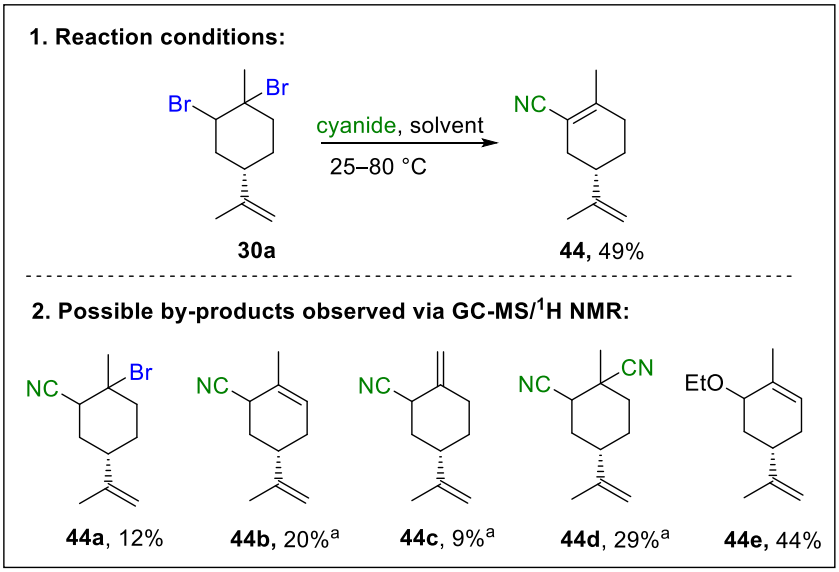

Scheme 21. Reaction conditions for **44** formation and possible by-products. [a] Yield was determined by ^{1}H NMR (internal standard: CH_2Br_2) or based on GC internal calibration (Table 14). Isolated yields.

The initial reactions showed that the conditions reported by U. Jahn et al. for the simple substitution of bromine functionality with cyanide could be applied to **30a** (Scheme

21). The proposed product was obtainable in a moderate yield and relative selectivity (Entry 1, Table 13).[240]

Table 13. Screening of Kolbe nitrile and other procedures for the formation of **44**.

Entry	Cyanide s.	Solvent	*T* (°C)	Yield [%][a,b]
1[240]	NaCN (2.2 eq.)	DMSO (2.0 mL, 0.25 M)	90 °C	**44** (49%)[b], **44a** (12%)[b]
2	KCN (2.0 eq.)	DMSO (2.0 mL 0.07 M)	25 °C	Complex mixture
3	KCN (2.0 eq.)	DMSO (1.0 mL, 0.14 M)	80 °C	Complex mixture
4	NaCN (4.0 eq.)	DMSO (10.0 mL, 0.10 M)	60 °C	**44,** 55%[a] (49%)[b]
5	NaCN (3.0 eq.)	DMSO 3.3 mL, 0.60 M)	40 °C	**44** (11%)[c], **44b** (20%)[b], **44c** (9%)[b]
6[242]	NaCN (2.2 eq.)	MeCN/H_2O (17 v/v%, 3.4 mL, 0.04 M)	25–50 °C, 12 h	No conversion
7[243]	KCN (4.5 eq.)	EtOH (5.0 mL, 0.12 M)	Reflux, 12 h	**44e** (44%)[b]
8	NBu_4CN (3.0 eq.)	MeCN (1.9 mL, 0.20 M)	50 °C	Complex mixture

[a] Yield determined by ^1H NMR (internal standard: CH_2Br_2); [b] Isolated yield; [c] Yield determined by GC internal calibration using octacosane ($C_{28}H_{58}$). Qualitative analysis was carried out with GC, GC-MS after 15 min, 30 min and 1 hour. Reaction conditions: substrate (0.135–0.610 mmol), cyanide (2.0–4.5 eq.), solvent (0.04–0.25 M refers to the solvated substrate as mM/mL), reactions were stopped after 1 hour, unless otherwise stated. DMSO = dimethyl sulfoxide.

Utilizing KCN under the same conditions reduced selectivity. In acetonitrile/water with NaCN no conversion was observed, while using tetrabutylammonium cyanide resulted in the mixture of the products (Entries 6, 8). Due to the complexity of the mixture, yields could not be provided (Figure 30). Characteristic shifts of **44a**, **44b** and **44c** were observed in ^1H NMR (Figure 31), however, their quantification was limited due to the overlapping signals.

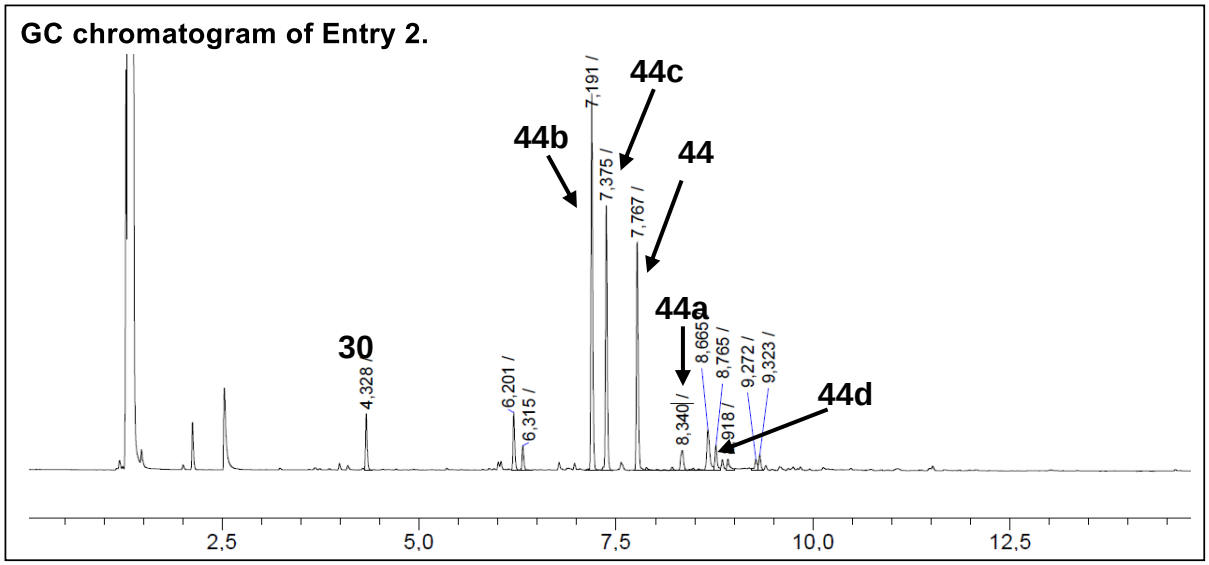

Figure 30. GC Chromatogram of Entry 2 (Table 13) after work-up procedure for the qualitative visualization of the product mixture. By-product **44a** was isolated and characterized via ^{1}H NMR. By-products **44b**, **44c** and **44d** were depicted via GC, GC-MS. Characteristic signals of **44b** and **44c** were observed in ^{1}H NMR (Figure 31). Instrument: GC 2010 Shimadzu, method: HP5 hart.

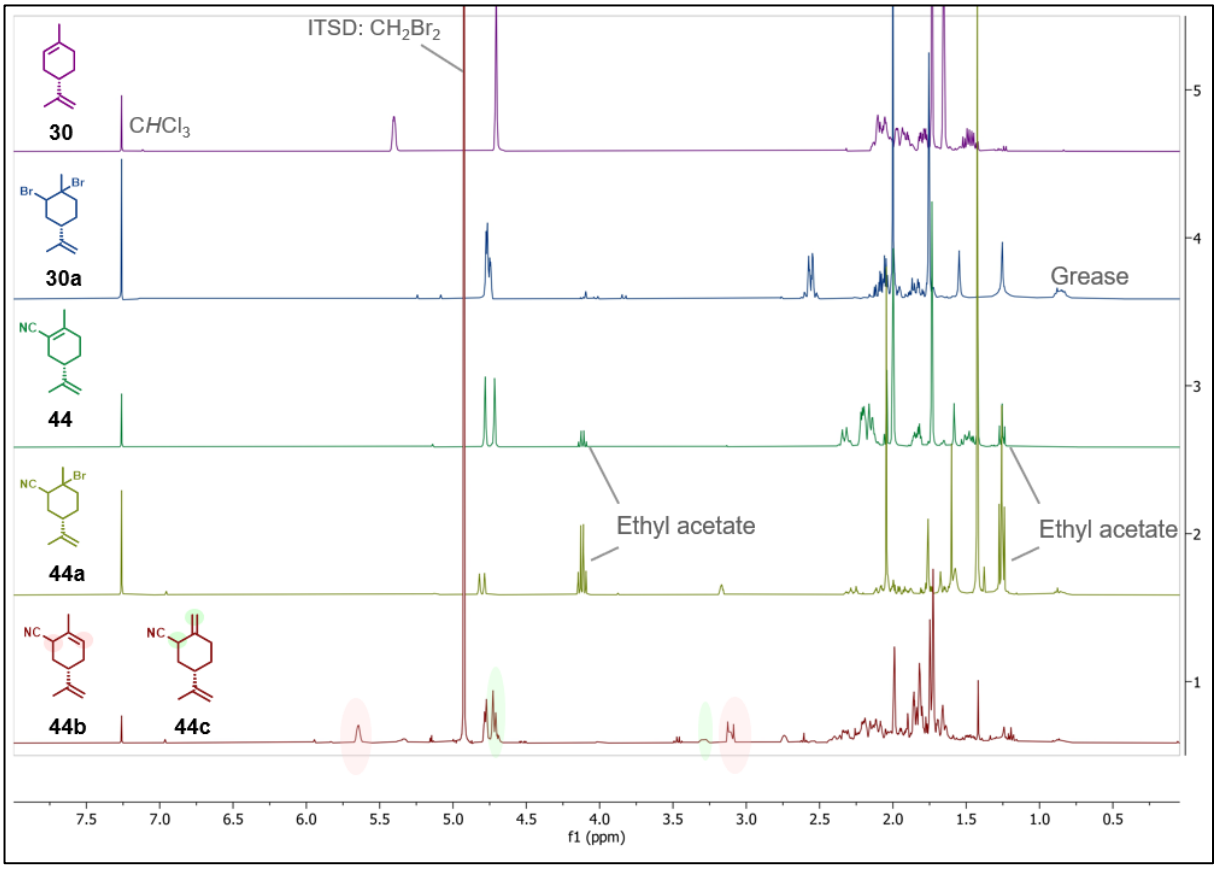

Figure 31. Stacked spectra of (4*S*)-(–)-limonene (**30**) and its functionalized derivatives. **30a**, **44** were isolated and fully characterized. Characteristic signals of the by-products **44a**, **44b**

and **44c** were observed via ^{1}H NMR (bordeaux spectrum, Entry 5, Table 13) and GC, GC-MS. Instrument: Bruker Avance III HD 400 (400 MHz, solvent: $CDCl_3$, internal standard: CH_2Br_2, 298 K).

Interestingly, when the protocol by Debarge et al. was applied, the unexpected allyl alkyl ether derivative **44e** was obtained with an isolated yield of 44% (Entry 7). Ethanol reduced the nucleophilicity of cyanide and acted as a co-nucleophile resulting in **44e**. The conditions in Entry 1 (Table 13) showed the highest affinity for the formation of **44**. However, all reactions carried out in DMSO at an elevated temperature resulted in the thermal degradation of **30a** to the limonene starting material **30**. Friedman and Shechter also described a similar finding that reason the phenomena with the coordination of the bromine functional group with the solvent in simple alkylbromides.[239] The reaction conditions were slightly modified to boost the selectivity of the reaction and reduce thermal degradation (Table 13, Entry 4). As a result, the by-product **44a** diminished entirely, and the desired product was obtained rapidly with a 55% ^{1}H NMR and 49% isolated yield. However, the thermal degradation of the substrate **30a** could not be completely declined.

To see if other solvents or the presence of an additive have a positive effect on the selectivity of the reaction, different solvent systems (Entries 9–11) and additives (Entries 12, 13) were employed (Table 14).

Table 14. Screening of different solvent systems and additives.

Entry	Deviation from reaction conditions[a]	Yield [%][b,c]
9	DMF/H_2O (2 v/v%)	**44** (22%)[b], **44d** (29%)[c]
10	NMP/H_2O (2 v/v%)	**44** (8%)[b], **44d** (14%)[c]
11	DMSO/H_2O (2 v/v%))	**44** (23%)[b], **44d** (16%)[c]
12	DMSO (100%), NaCN (2.0 eq.), KOtBu (1.2 eq.)	**44** (6%)[b]
13	DMSO (100%), NaCN (2.0 eq.), KOtBu (1.2 eq.), 25 °C	**44** (5%)[b]

[a] Reaction conditions: **30a** (0.24 mmol), NaCN (4.0 eq.), solvent/additive (2 v/v%, 2.42 mL), 80 °C; [b] Yield determined by GC internal calibration using octacosane ($C_{28}H_{58}$); [c] Yield estimated from GC integral ratios based on the yield of **44**. DMSO = dimethyl sulfoxide, DMF = dimethylformamide, NMP = *N*-methyl-2-pyrrolidon.

Even after screening the new conditions in Table 14, the DMSO system proved superior. The addition of water in DMF, NMP, or DMSO solvents increased the formation of double substituted product **44d**. In the case of Entries 9 and 10, water was obligatory to solvate NaCN in the solution mixture sufficiently. The increasing water content has a synergistic role of reducing the nucleophilicity of the cyanide anion and shielding the substituted bromide, reducing the elimination of the second bromine substituent, and promoting the side-reaction. The increased polarity of the solvent system has also a detrimental effect on E_2, explained by the Hughes and Ingold rules.[232] The competition between the β-elimination and substitution can be reasoned with the overall charge density of the transition states. In the case of the elimination, the charge is more widely dispersed compared to the transition state of the substitution reaction, resulting in a less compact solvation shell and therefore, decreased stabilization.[232] Therefore, with increasing solvent polarity, S_N2 will be favored. Adding a base causes the formation of limonene and other similar volatile products even at room temperature (Entries 12, 13).

The same reaction conditions were applied to the dibrominated myrcene derivative **34**. Surprisingly, instead of the desired nitrile derivate, **34a** was obtained with a yield of 74%, showing the structural dependence of the reaction. Utilizing CuCN in DMF, **34b** was obtained with a yield of 22% (Scheme 22).

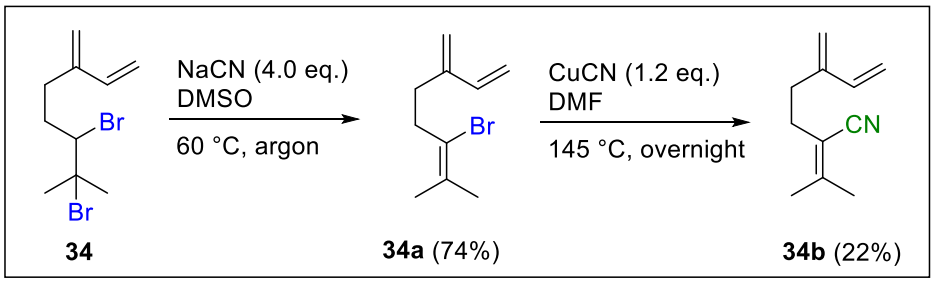

Scheme 22. Functionalization of **34** to **34b** via a 2-step synthesis. DMSO = dimethyl sulfide, DMF = dimethylformamide.

The exhibit the synthetic utility of the electrochemically dibrominated product **30a**, was subjected to the well-known Kolbe-nitrile synthesis.[239–241] After a series of optimization reactions, the desired α,β-unsaturated nitrile derivate **44** could be obtained in an isolated yield of 49% for the first time.[112,234] The reaction displays a rapid substitution and a subsequent functionalization in a one-pot approach with outstanding selectivity to the formation of **44**. However, the optimized conditions

proved to be structure-dependent (Scheme 22), shedding light on the overall structural delicacy of terpenes. The forming product is of high interest due to the multifunctional building nitrile functional group and its renewable resource.

3.2. Electrochemical bromination of enones

The electrochemical dibromination of natural alkenes showed that deactivated alkenes remained chemically intact. To tackle this challenge, the reaction conditions were slightly modified to enhance the electrophilicity of the bromine via a DMSO–Br complex.[245] To achieve the selective α-bromination of α,β-unsaturated carbonyls, 2-cyclohexene-1-one (**45**) was chosen as the model substrate, and initial optimization was carried out as follows (Scheme 23):

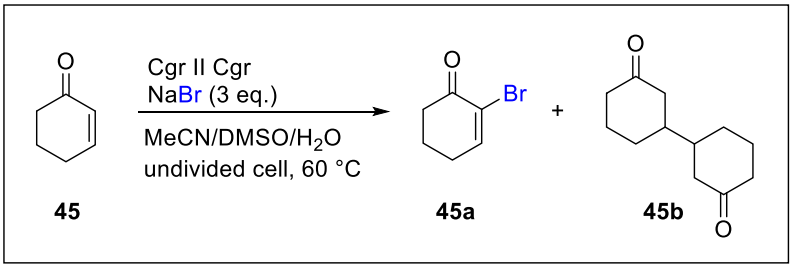

Scheme 23. Electrochemical α-bromination of **45**. DMSO = dimethyl sulfoxide. Cgr = graphite (anode II cathode).

Table15. Optimization of electrochemical α-bromoenone (**45a**) formation.

Entry	Deviation from standard conditions[a]	45a [%][b,c]	45b [%][b,c]
1	none	13%[b] (9%)[c]	0%
2	NaI	0%	0%
3	NBu_4Br	0%	0%
4	NaBr (5.0 eq.)	14%[b]	0%
5	25 °C	traces	traces
6	MeCN/H_2O (8 v/v%), no DMSO	0%	traces
7	MeCN/DMSO/H_2O (2.5 mL/2.5 mL/0.2 mL)	traces	19%[c]
8	MeCN/DMSO/H_2O (4.6 mL/0.5 mL/0.1 mL)	14%[b]	traces
9	MeCN/DMSO/H_2O (4.6 mL/0.1 mL/0.5 mL)	4%[b]	traces

[a] Standard conditions: **45** (0.5 mmol), NaBr (1.5 mmol), MeCN/DMSO/H_2O (4.6 mL/0.4 mL/0.2 mL), graphite electrodes, undivided cell, constant current, j = 10 mA/cm^2,

4.0 *F* (ref. substrate), 60 °C; [b] Yields determined by ^{1}H NMR (internal standard: CH_2Br_2); [c] Isolated yields. After electrolysis, the solution was left to stir overnight. DMSO = dimethyl sulfoxide.

The corresponding product was obtained using the initial conditions with an NMR yield of 13% (Entry 1, Table 15). When the halide source was changed to NaI or NBu_4Br, no product formation was observed, demanding the necessity of NaBr. Reducing the reaction temperature to 25 °C degrees or omitting DMSO from the solvent system diminished the formation of **45a,** and the hydrodimerized **45b** was obtained (Entries 5, 6). Interestingly, increasing the DMSO content to 2.5 mL displayed analogous behaviour furnishing **50b** with an isolated yield of 19%. The preliminary optimization conditions showed that both the presence of NaBr, and DMSO as well as the elevated temperature are influencing parameters in the formation of **45a,** and the following plausible mechanism is proposed (Scheme 24):

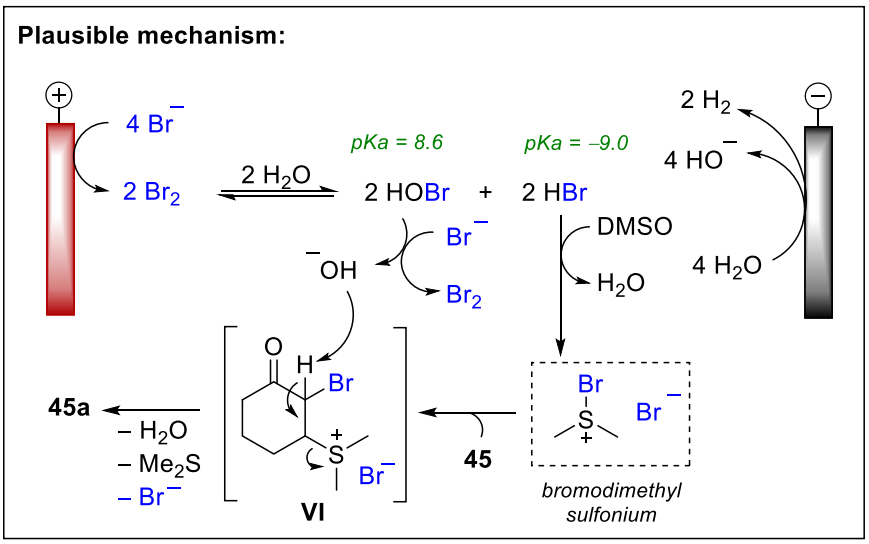

Scheme 24. Plausible reaction mechanism for the formation of **45a**.

According to the proposed mechanism, the electrochemically formed bromine reacts with water to form hypobromous and hydrobromic acid. The latter forms the highly efficient bromodimehtyl sulfonium bromide (BDMS)[245] agent that conveniently adds to the deactivated enone double bond **VI**. After subsequent deprotonation of the acidic α-proton and liberation of dimethyl sulfate in the β-position, **45a** is obtained. Heat is necessary for the liberation of volatile Me_2S, which drives the reaction forward. As Me_2S has a boiling point of 37 °C,[246] its liberation has a detrimental effect on the yield. Furthermore, its recycling was considered a priority to preserve the atom efficiency of

the reaction. The low yields of the desired **45a** could be justified by the HBr dependence of the reaction to form the "active brominating agent", BDMS. HBr has a pK_a of −9, which suggest that it is present mainly in its deprotonated form under the reaction conditions.[22] Moreover, the cathodic counter reaction consumes protons, shifting the reaction media into a rather alkaline environment. Both aspects limit the formation of BDMS.

To investigate if BDMS analogues can be directly generated by substituting DMSO, different sulfide sources were tested (Scheme 25).

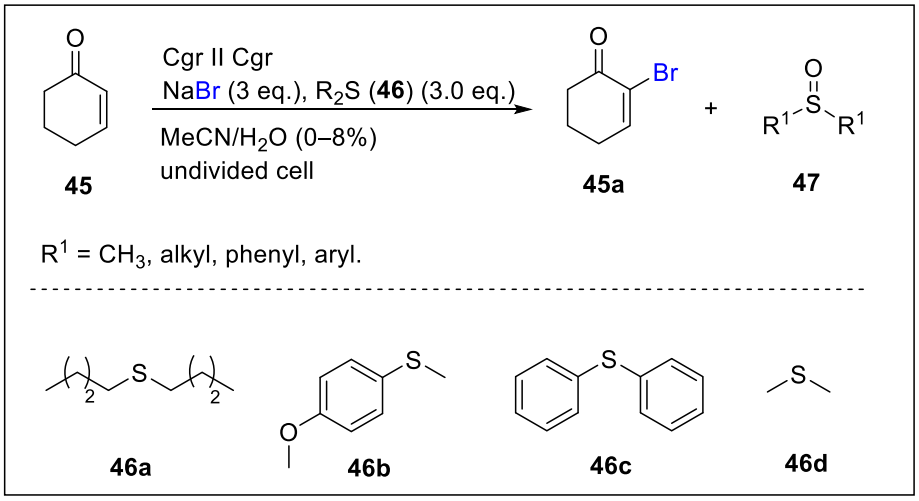

Scheme 25. NaBr mediated formation of bromodialkyl sulfonium [Br^+] from different sulfides. Cgr = graphite (anode II cathode).

In the case of the sulfides tested, no desired product was formed. Instead, the formation of sulfoxide derivates were observed (Table 16). When dibutyl sulfide was subjected to the standard conditions, dibutyl sulfoxide (**47a**) was obtained in 26% NMR yield. In the presence of other sulfide derivatives, oxidized derivates **47** were observed in trace amounts, or no formation of **47** was observed (Entries 16–19).

To see if different bromide sources facilitate the formation of the desired product, dibutyl sulfide (**46a**) was subjected to other reaction conditions (Table 16). Unfortunately, no formation of **45a** was observed. When ammonium bromide and tetramethylammonium bromide were used, 0.25 mL water was added to facilitate the solvation of the salt (Entries 20, 21). To avoid the use of water and possible oxidation of the sulfide derivate, tetrabutylammonium bromide was used (Entries 19, 22). However, even in the presence of pure HPLC-grade acetonitrile, **46a** is subjected to

oxidation with a trace amount of water in the system (Entry 22). Previous electrochemical protocols described similar findings.[247,248]

Table 16. Screening of other sulfide sources for the formation of [Br+].

Entry	Deviation from standard conditions[a]	45a [%][b]	47 [%][b]
15	**46a** (3.0 eq.)	0%	26%
16	**46b** (3.0 eq.)	0%	traces
17	**46c** (3.0 eq.)	0%	0%
18	**46d**, MeCN/H_2O (8 v/v%)	0%	0%
19	**46d**, NBu_4Br (3.0 eq.), MeCN (100 v/v%)	0%	0%
20*	**46a**, NH_4Br (3.0 eq.), MeCN /H_2O (5 v/v%)	0%	traces
21*	**46d**, NMe_4Br (3.0 eq.), MeCN /H_2O (5 v/v%)	0%	traces
22	**46a**, NBu_4Br (3.0 eq.), MeCN (100 v/v%), 60 °C	0%	traces

[a] Standard conditions: **45** (0.5 mmol), NaBr (1.5 mmol), **46** (3.0 eq.), MeCN/H_2O (4.6 mL/0.4 mL, 8 v/v%), graphite electrodes, undivided cell, constant current, j = 10 mA/cm^2, 2.0 F (ref. substrate) 25 °C; [b] Yields determined by ^{1}H NMR (internal standard: CH_2Br_2); [c] Isolated yields; [*] For sufficient solvation of the salt, 0.25 mL H_2O was added. After electrolysis was finished, the solution was left to stir overnight.

As the previous approaches did not promote the formation of the desired molecule, the standard conditions were carried out in the presence of different organic bases. The role of the base envisioned to have a catalytic effect via a Michael 1,4-addition forming intermediate **VII** (Scheme 26). **VII** reacts with the electrochemically generated bromine to form the α-brominated intermediate **VIII**. Upon deprotonation of the acidic hydrogen at α-position, **45a** is formed. The base is expected to reform as a part of the catalytic cycle. Pyridine (Py), imidazole, 1,1,3,3-tetramehtylguanadine, 2,6-lutidine and dimethylaminopyridine (DMAP) bulky bases were tested to see if the presence of a base has a positive effect on the reaction outcome (Table 17).

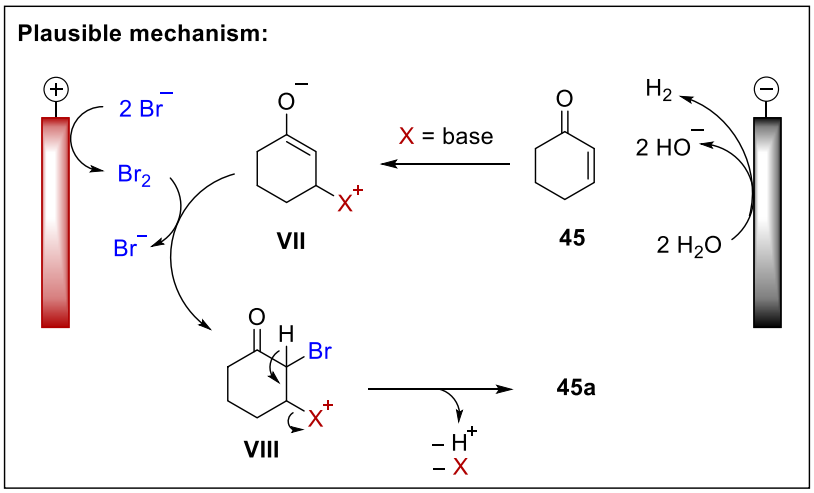

Scheme 26. Plausible reaction mechanism for the base catalyzed electrochemical generation of **45a**. X = base.

Table 17. Screening of different organic bases.

Entry	Deviations from standard conditions[a]	45a [%][b]	45b [%][b]
23*	**45** (0.5 mmol), NaBr (5 eq.), Py (1.0 mmol), 25 °C	0%	traces
24*,*	imidazole	0%	traces
25*	1,1,3,3-tetramehtylguanadine	0%	traces
26	2,6-lutidine	traces	0%
27**	DMAP	0%	0%
28	NBS/DBU (0.5 eq.), 2.0 *F*, 25 °C	traces	0%

[a] Standard conditions: **45** (0.7 mmol), NaBr (2.1 mmol), base (2.1 mmol), MeCN/H_2O (5.0 mL, 8 v/v%), graphite electrodes, undivided cell, constant current, j = 10 mA/cm^2, 4.0 *F* (ref. substrate), 60 °C; [b] Yields determined by ^{1}H NMR (internal standard: CH_2Br_2). [*] cathode passivation was observed. [**] Bromination of the base was depicted via GC, GC-MS. After electrolysis was finished, the solution was left to stir overnight. Py = pyridine, DMAP = 4-dimethylaminopyridine, NBS = *N*-bromosuccinimide, DBU = 1,8-diazabicyclo[5.4.0]undec-7-ene.

Out of the bases screened, only 2,6-lutidine featured the formation of the desired product in trace amounts (Entry 26). When pyridine, imidazole, or 1,1,3,3-tetramehtylguanadine was tested, heavy cathode passivation was observed, promoting the formation of by-product **45b**. In the presence of imidazole and DMAP, their brominated analogues were observed qualitatively (Entries 24, 27).

Next, the system was subjected to different aprotic polar solvents (Table 18).

Table 18. Screening of solvents.

Entry	Deviation from standard conditions[a]	45a [%]	45b [%]
29	THF (100 v/v%)	0%	0%
30	DMF (100 v/v%)	0%	traces

[a] Standard conditions: **45** (0.5 mmol), NBu_4Br (1.5 mmol), **46a** (1.0 eq.), graphite electrodes, undivided cell, constant current, j = 10 mA/cm^2, 2.0 F (ref. substrate), 60 °C; After electrolysis was finished, the solution was left to stir overnight. Reaction was monitored with GC and GC-MS methods. THF = tetrahydrofuran, DMF = dimethylformamide.

When utilizing other aprotic polar solvents, **45a** was not obtained. When THF was used, complete conversion of the starting material was observed (Entry 29). In the case of DMF, a trace amount of **45b** was obtained.

Parallel to the investigation of this project, the electrochemical chlorination and bromination of electron deficient C–H bonds in quinones, coumarins, quinoxalines and 1,3-diketones was published (Scheme 27).[249]

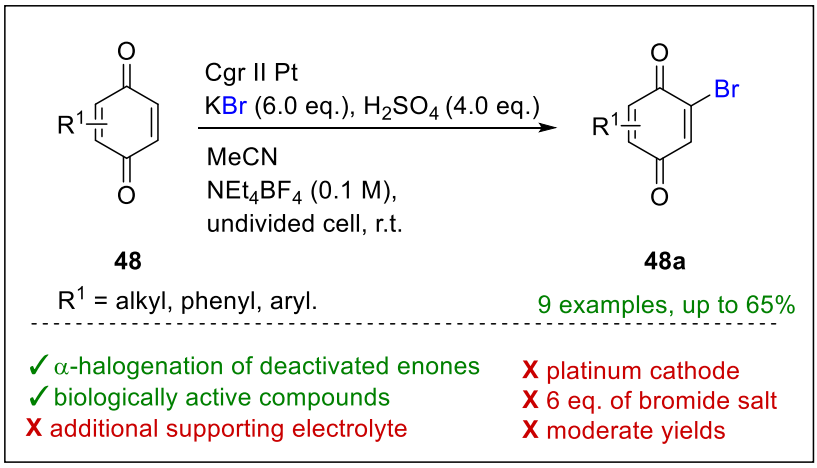

Scheme 27. Electrochemical activation of electron deficient C–H bonds. Cgr = graphite, Pt = platinum (anode II cathode).[249]

The electrochemical method presents 9 brominated derivates **48a** with moderate to good yields. KBr and H_2SO_4 serve as in-situ HBr source, which supports our HBr-dependence hypothesis of the reaction. Compared to our method, this procedure obligates the necessity of additional supporting electrolytes despite utilizing 6.0 eq. KBr salt. Moreover, it relies on a platinum metal cathode, which reduces the sustainability of this approach. In combination with our application of sustainable graphite electrodes, the dual role of NaBr both as a bromine source and supporting electrolyte, Scheme 27

sheds light on the possible drawbacks of Yu et al.´s approach and the necessity of further research on the efficient activation of electron-deficient C–H bonds.

3.3. Electrochemical bromolactonization of alkenoic acids

The successful dibromination protocol of terpenes was extended to the class of alkenoic acid to promote intramolecular bromocyclization to the corresponding bromolactone derivatives. 4-alkenoic acid (**49**) was chosen as a model substrate, and a short optimization was carried out according to Scheme 28. The reaction was monitored with GC, GC-MS, and ^{1}H NMR methods.

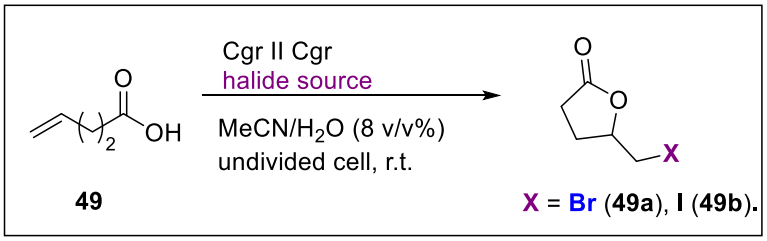

Scheme 28. Electrochemical halolactonization of **49**. Cgr = graphite (anode II cathode).

Table 19. Optimization of electrochemical halolactonization method.

Entry	Deviation from standard conditions[a]	Yield [%][b,c]	Conv. [%][b]
1	none	**49a**, 49%[b] (49%)[c]	100%[b]
2	NBu_4Br	**49a** (11%)[b]	62%[b]
3	NaOH (1.0 eq.)	**49a**, 15%[b] (14%)[c]	100%[b]
4	MeCN/MeOH/H_2O (4.2mL/0.4mL/0.4mL)	**49a** (42%)[b]	100%[b]
5	MeOH/H_2O (4.6mL/0.4mL)	**49a** (traces)	100%[b]
6	MeOH (5.0mL), NaI (3.0 eq.)	**49b** (traces)[b]	n/a
7	MeOH (5.0mL), NaI (3.0 eq.), $NaHCO_3$ (1.0 eq.)	**49b** (8%)[b]	70%[b]
8	MeOH (5.0mL), NaI (3.0 eq.), NaOH (1.0 eq.)	**49b** (10%)[b]	100%[b]
9	H_2O (5.0mL), NaI (3.0 eq.), $NaHCO_3$ (1.0 eq.), platinum electrodes	**49a** (0%)	n/a

[a] Standard conditions: **49** (0.7 mmol), NaBr (2.1 mmol), MeCN/H_2O (5.0 mL, 8 v/v%), graphite electrodes, undivided cell, constant current, j = 5 mA/cm^2, 2.0 F (ref. substrate),

25 °C; [b] Yields determined by ^{1}H NMR (internal standard: CH_2Br_2); [c] Isolated yields. Conversion was calculated using the ^{1}H NMR yield of **49a, b**. n/a = not assessed.

Upon applying the standard conditions on **49**, the corresponding bromolactone derivative **49a** was obtained with an NMR yield of 49% in a selective manner (Entry 1, Table 19). Upon a simple liquid-liquid extraction, the spectroscopically pure product was obtained with an isolated yield of 49%. The GC, GC-MS chromatogram, and crude NMR showed excellent selectivity; no trace of by-products was observed. Changing the bromide salt to NBu_4Br decreased the conversion of the starting material and the yield of **49a** to 11%. In the presence of one equivalent NaOH, the formation of the desired product was capped at 15% (Entry 3). The solvent system was complemented with MeOH to generate the base in situ. As a result, the desired product was formed with a yield of 42% (Entry 4). Using methanol as the major solvent or employing NaI as the halide source had a detrimental effect on the outcome of the reaction (Entries 5–9). When NaI in combination with a base was used, the iodolactone **49b** was obtained with reduced yields (Entries 8, 9). In water, no **49b** was formed, and the starting material was consumed completely.

As the initial conditions proved superior, further optimizations were performed on the original conditions. Next, the amount of applied charge was varied to study the relationship between the formation of product **49a** and the conversion of starting material **49** (Table 20).

Table 20. Varying the amount of applied charge (*Q*).

Entry	Deviation from standard conditions[a]	49a [%][b]	Conv. [%][b]
10	0.5 *F*	32%	80%
11	1.0 *F*	42%	84%
12	1.5 *F*	44%	92%
13	2.0 *F*	49%	100%

[a] Standard conditions: **49** (0.7 mmol), NaBr (2.1 mmol), MeCN/H_2O (5.0 mL, 8 v/v%), graphite electrodes, undivided cell, constant current, j = 5 mA/cm^2, 2.0 *F* (ref. substrate), 25 °C; [b] Yields determined by ^{1}H NMR (internal standard: CH_2Br_2); Conversion was calculated using the ^{1}H NMR yield of **49a**.

Via applying different amounts of charge (*Q*), it was revealed that with an increasing charge amount, the conversion of starting material increases. At 2.0 *F,* it reaches

100% conversion and limits the formation of the desired product **49a** (Entry 13). This finding explained the presence of HBr in the previous reports.[198] HBr acts as a bromine source and hinders the consumption of alkenoic acid by increasing its oxidation potential. Based on these findings, the following plausible mechanism was postulated (Scheme 29). Electrochemically generated bromine reacts with the alkenoic acid **49** to form the halonium intermediate **IX**. Spatial structural rearrangement and preferential overlap of the oxygen lone pair and the C–Br σ* bond at C5 allows the favoured 5-*exo*-*trig* cyclization of the molecule to **49a** following Baldwin´s rules.[250]

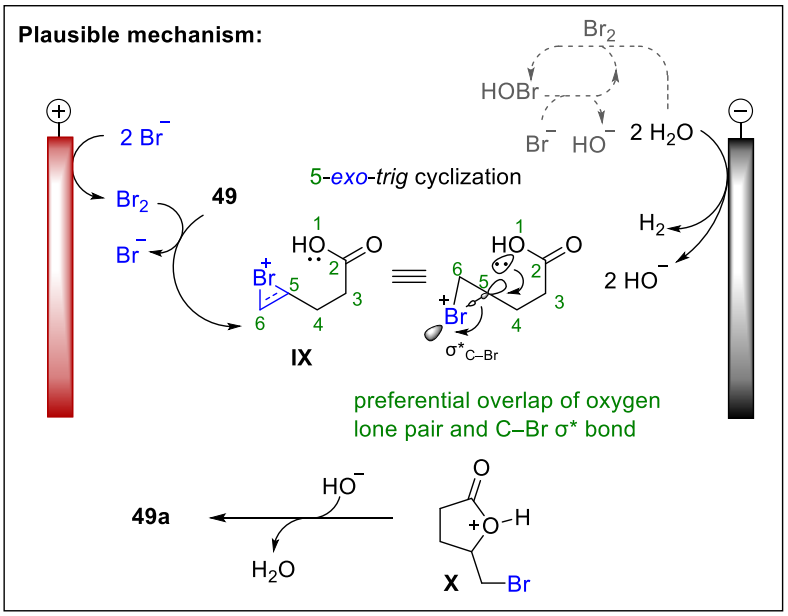

Scheme 29. Electrochemical bromocyclization of **49** to **49a**. Formation of HOBr cannot be closed out.

Parallel to the initial experiments conducted within the frame of this research project, the group of D. Y. Kim published an efficient electrochemical procedure for the bromocyclization of unsaturated carboxylic acids **50** using NaBr at graphite anode and nickel cathode electrodes (Scheme 30).[190] The procedure features 17 examples with up to 96% isolated yield.

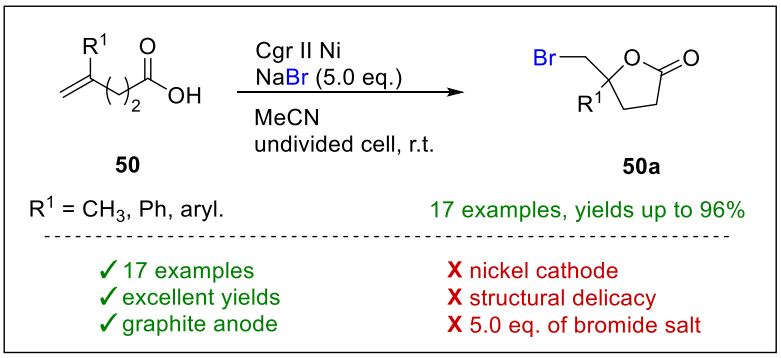

Scheme 30. Electrochemical bromolactonization of unsaturated carboxylic acid derivates reported by Kim et al.[190]

Excellent yields were obtained, especially when *R1* represented an aryl group suggesting the structural delicacy of the method. Nevertheless, the method showed the dependence on nickel metal cathode, which is a drawback due to the increasing economic demand and abundance of nickel metal.[251–253] Moreover, substrate **50** was utilized in 0.05 M concentration in the presence of 5.0 equivalent NaBr.

Utilizing cheap and sustainable graphite electrodes, higher substrate concentration, and using only 3 equivalents of NaBr qualifies our method still more advantageous. Moreover, the competing olefin saturation reaction, which is associated with conventional protocols, was not observed. Therefore, the initial experiments for the electrochemical bromolactonization published in this dissertation provide a solid base for potential further method development.

3.4. Hofmann rearrangement of urea derivatives

This project was inspired by the NaBr mediated Hofmann rearrangement of amides into bioactive carbamates (Scheme 31A).[254] We aimed to achieve an electrochemical protocol for the bromine-mediated transformation of urea derivatives to highly functional hydrazine derivates. Based on the mechanism postulated in the literature, the plausible rearrangement of urea **51** into its hydrazine derivatives proceeds via the following mechanism: the N–Br bond intermediate **XII** forms from the electrochemically generated bromine and **XI**. After a second deprotonation and rearrangement of amine functionality onto the bromine-activated nitrogen, the nitrene **XIV**, and subsequently, the amino isocyanate intermediate is formed **XV**. Following, **XV** is scavenged with methanol to form the desired protected hydrazine derivative **52**.

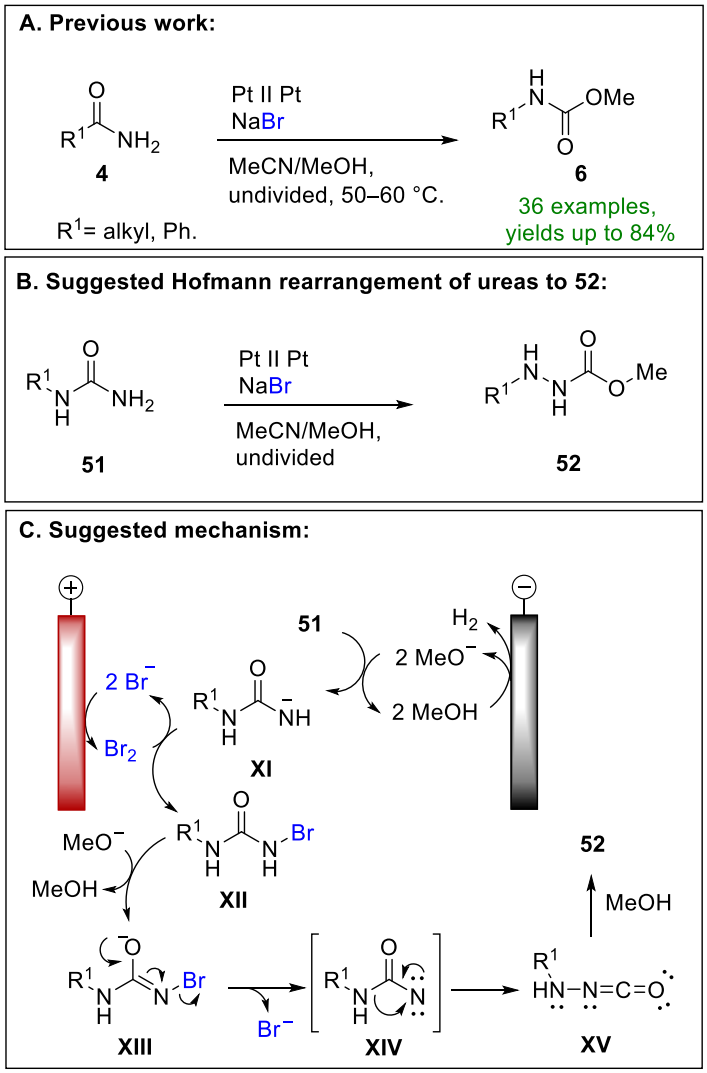

Scheme 31. Proposed electrochemical Hofmann rearrangement of urea derivatives **51** to hydrazines **52** based on previous literature. Pt = platinum (anode II cathode).[254–256]

3.4.1. Synthesis of urea derivates

First, the urea derivates were synthesized with slight modifications according to the literature.[257] Alkylamine and potassium isocyanate reacted in 1 M aq. HCl solution to furnish the following scope. The forming urea derivatives were recrystallized or subjected to column chromatography to yield the clean products **51** (Scheme 32).

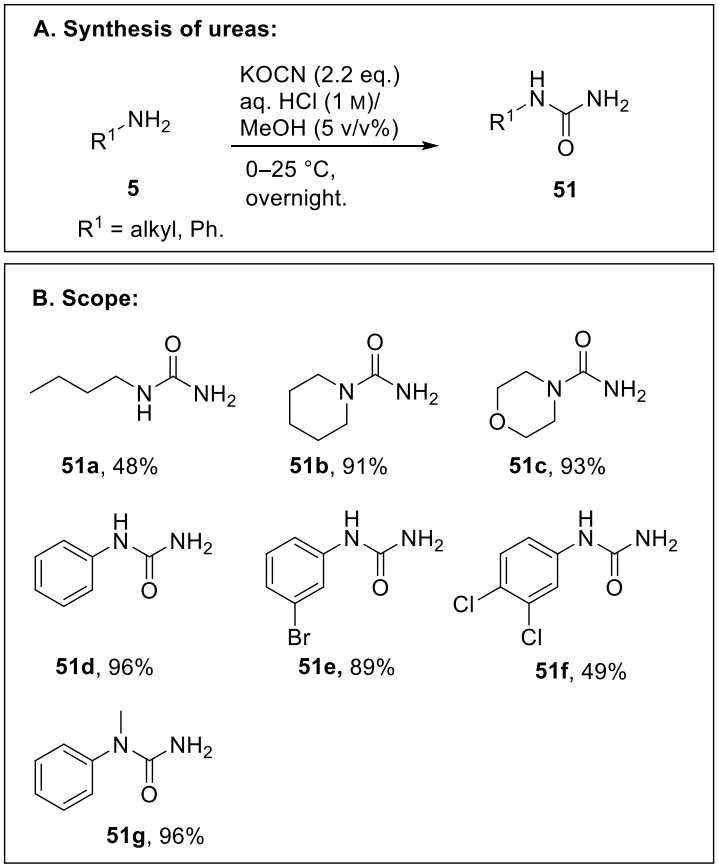

Scheme 32. Scope of urea derivatives. Isolated yields.

3.4.2. Preliminary optimization on urea derivatives

Opposed to the literature, *N*-butylurea (**51a**) was chosen as a model substrate over *N*-phenylurea (**51d**) to avoid bromination on the phenyl ring. **51a** was subjected to the electrochemical conditions taken over from the literature (Scheme 33).[254]

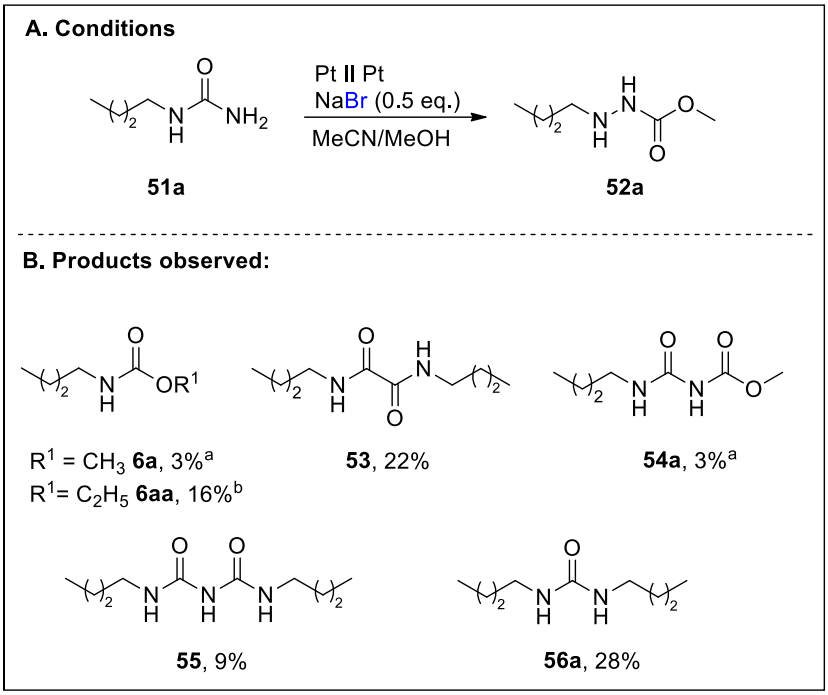

Scheme 33. Preliminary screening of **51a** for the formation of hydrazine derivate **52a**. [a] Yields determined by ^{1}H NMR (internal standard: CH_2Br_2). Isolated yields.

Under literature conditions, no presence of the desired urea was detected (Entry 1, Table 21). With a slight modification of the reaction conditions, the formation of carbamate **6a** and oxamide **53** was observed with 3% and 19% NMR yield, respectively (Entry 2). Using NEt_4Br as a bromine source or pure methanol diminished the conversion. Changing the electrode material to isostatic graphite decreased the conversion of starting material to 54%, but it did not affect the formation of oxalamide (Entry 5). When an increased amount of *F* was applied, the reaction selectivity decreased, yielding **6a**, **53**, **54a**, and **55** as a complex mixture (Entries 6, 9). Interestingly, the corresponding methylcarbamate derivative **6a** could be detected via GC and GC-MS methods when methanol was used as an additive. However, quantification via ^{1}H NMR failed, suggesting the compound´s instability.

When ethanol was utilized as an additive with NEt_4Br, **53** was obtained with an isolated yield of 22% (Entry 10). In the case of water as an additive, in combination with NaBr resulted in no conversion. When NaCl was used, the corresponding dialkyl urea **56a** was formed with a yield of 28% (Entry 8.)

Table 21. Initial screenings of electrochemical reactions conditions.

Entry	Deviations from conditions[a]	Yield [%][c,d,e]	Conv. [%][c,d,e]
1	literature conditions[b]	0%[e]	100%[e]
2*	none	**6a** (3%)[c], **53** (19%)[c]	66%[c]
3*	NEt_4Br	0%[e]	n/a
4	MeOH (100 v/v%), NEt_4Br	0%[e]	n/a
5*	Cgr II Cgr	**53** (20%)[c]	54%[c]
6*	Cgr II Cgr, 4.0 *F*	**53** (15%)[d], **54a** (3%)[d], **55** (9%)[d]	100%[e]
7	MeCN/H_2O (10 v/v%)	0%[e]	n/a
8	NaCl	**55** (8%)[c], **56a** (28%)[c]	40%[c]
9*	3.0 *F*	Complex mixture	n/a
10*	MeCN/EtOH (20 v/v%), NEt_4Br (1.0 eq.), NaOEt (1.0 eq.)	**53**, 24%[c] (22%)[d]	n/a
11*	MeCN/EtOH (10 v/v%), NEt_4Br (1.0 eq.), NaOEt (1.0 eq.), 3.0 *F*	**6aa** (16%)[c]	n/a
12	MeCN/EtOH (20 v/v%), NEt_4Cl (1.0 eq.), NaOEt (1.0 eq.)	**6aa** (2%)[c]	96%[c]

[a] Standard conditions: urea (0.5 mmol), NaBr (0.25 mmol), MeCN/MeOH (5.0 mL, 10 v/v%), platinum electrodes, undivided cell, constant current, j = 5 mA/cm^2, 2.0 *F* (ref. substrate), 30 °C; [b] Literature conditions: urea (0.5 mmol), NaBr (0.10 mmol), NBu_4BF_4 (1.0 mmol), MeCN/MeOH (5.0 mL, 10 v/v%), platinum electrodes, constant current, j = 6.7 mA/cm^2, 3.4 *F* (ref. substrate), 50 °C; [c] Yields determined by ^{1}H NMR (internal standard: CH_2Br_2); [d] Isolated yields; [e] Complete conversion of **51a** or absence of products were detected via GC, GC-MS; [*] Carbamate derivate was detected via GC, GC-MS. n/a = not assessed.

The initial reactions failed to provide the desired hydrazine compound, and the formed products suggested the decomposition of the urea. To understand whether the electrochemical instability relies on the structural features of **51a**, benzamide (**4**) and other urea derivatives were subjected to the literature and standard screening reaction conditions (Scheme 34, Tables 22, 23).

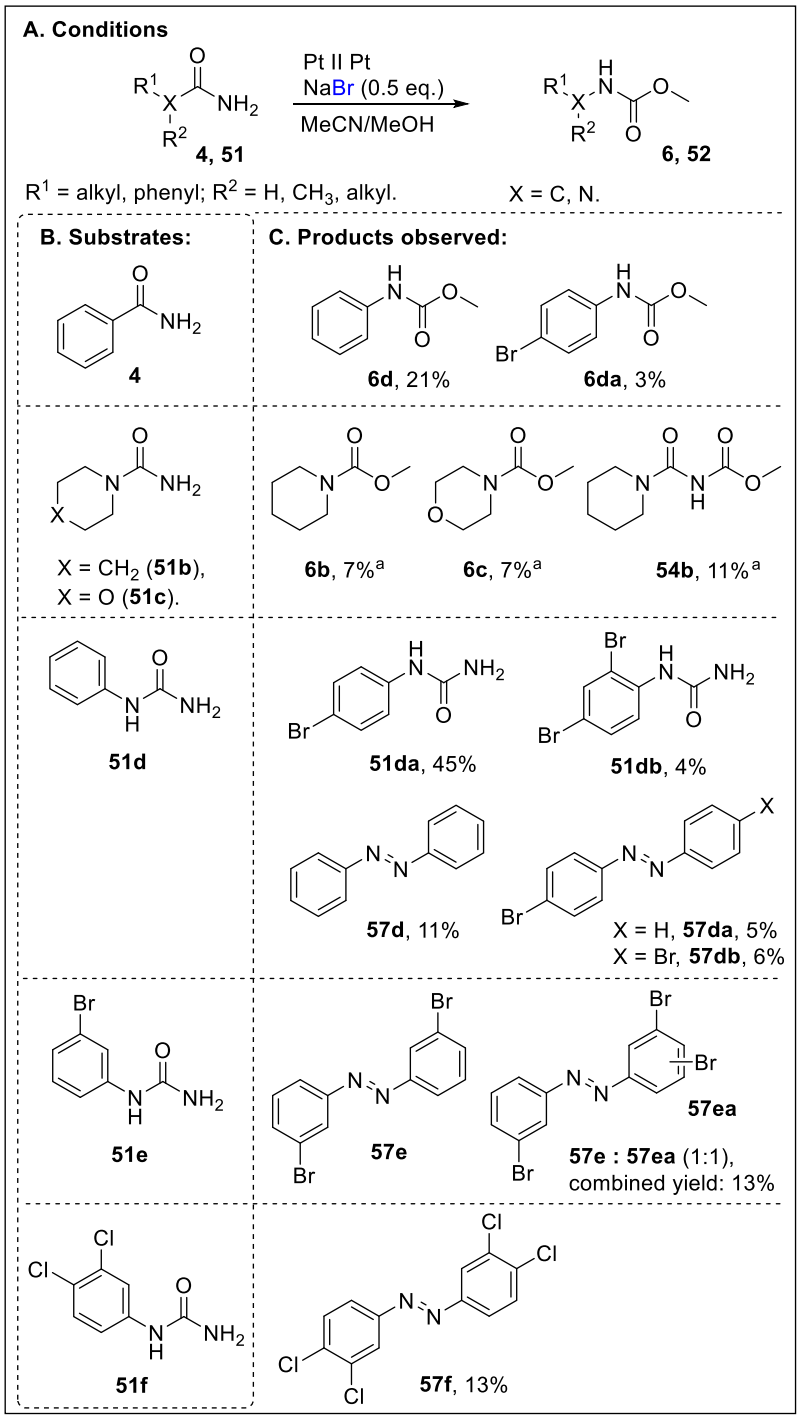

Scheme 34. Screening of **4** and other ureas **51** under literature and modified conditions.

[a] Characteristic signals were identified in ^{1}H and ^{13}C NMR.

Table 22. Screening of literature conditions on **4** and other urea derivatives.

Entry	Deviation from literature conditions[a]	Yield [%][b,c,d,]
13	none	**6d** (21%)[c], **6da** (3%)[c]
14	Cgr II Cgr	Decomposition of **4**[d]
15	**51d** (0.5 mmol)	Decomposition of **51d**[d]
16	**51d** (0.5 mmol), Cgr II Cgr	**57d** (7%)[b]
17	**51g** (0.5 mmol)	Decomposition of **51g**[d]

[a] Literature conditions: benzamide (**4**, 0.5 mmol), NaBr (0.1 mmol), NBu_4BF_4 (1.0 mmol), MeCN/MeOH (5.0 mL, 10 v/v%), constant current, j = 6.7 mA/cm^2, 3.4 F (ref. substrate), 50 °C; [b] Yields determined by ^{1}H NMR (internal standard: CH_2Br_2); [c] Isolated yields; [d] No conversion of the substrate was observed via GC, GC-MS and TLC. Cgr = graphite (anode II cathode).

Table 23. Screening of other conditions on other urea derivatives.

Entry	Deviation from standard conditions[a]	Yield [%][b,c,d,e]
18	none	**57da** (5%)[c], **57db** (6%)[c]
19	**51e** (0.5 mmol)	**57e**, **57ea** (1:1, 13%)[e]
20	**51f** (0.5 mmol)	**57f** (13%)[c]
21	**51d** (0.5 mmol), HBr (1.5 mmol)	**51da** (45%)[c], **51db** (4%)[c]
22	**51d** (0.5 mmol), Cgr II Cgr, MeOH/MTBE (10 v/v%), 60 °C	**57d** (11%)[c]
23	**51b** (0.5 mmol), Cgr II Cgr, MeOH/MTBE (10 v/v%), 60 °C	**6b** (7%)[b], **54b** (11%)[b]
24	**51c** (0.5 mmol), Cgr II Cgr, 50 °C	**6c** (7%)[b]

[a] Standard conditions: urea (0.5 mmol), NaBr (0.25 mmol), MeCN/MeOH (5.0 mL, 10 v/v%), platinum electrodes, undivided cell, constant current, j = 5 mA/cm^2, 2.0 F (ref. substrate), 30 °C; [b] Yields determined by ^{1}H NMR (internal standard: CH_2Br_2); [c] Isolated yields; [d] No conversion of the substrate was observed via GC, GC-MS and TLC; [e] Ratio was determined via GC-MS due to the overlapping signals in ^{1}H NMR. MTBE = methyl *tert*-butyl ether. Cgr = graphite (anode II cathode).

Reacting benzamide (**4**) under literature conditions, **6d** could be isolated with a 21% yield. As a by-product, a slight amount of brominated urethane **6da** was observed (Entry 13, Table 22).[254] Applying the same conditions to **51d** and **51g**, heavy electrode passivation occurred, and the reaction mixture was dark brown, indicating

urea decomposition. Changing the electrode material to graphite did not facilitate the reaction for benzamide (Entry 14). The slight modification of the reaction conditions facilitated the formation of the unexpected azobenzene derivatives **57** from the corresponding ureas (Table 23). Similar findings were reported independently through the oxidative coupling of anilines,[258–260] suggesting the electrochemical decomposition of urea to the corresponding anilines. The dark brown color of the reaction mixture after electrolysis and the poor yields of the corresponding azobenzenes indicate the same reaction mechanism and the overoxidation of the forming amine species.[261] When **51e** was used as a substrate, an isolated mixture of **57e** and **57ea** was obtained with a combined yield of 13%. The correct ratio could not be determined via NMR studies due to the overlapping signals of the two products. The electrode material had a detrimental effect on the outcome of the reaction, with platinum promoting the decomposition of urea derivatives (Entries 14, 16). The Yang group reported the oxidation of urea on different anode electrodes under physiological conditions.[262] Platinum electrodes promote efficient C–N bond breakage resulting in the liberation of ammonia, carbon monoxide, or carbon dioxide.[262] When piperidine urea (**51b**) and morpholine urea (**51c**) was subjected to the reaction conditions, the corresponding carbamates **6b**, **6c** were detected with a 7% NMR yield, respectively (Table 23).

3.4.3. Investigation of the formation of symmetric dialkyl urea derivatives

To investigate the formation of **56**, the role of water as an additive and different supporting electrolyte salts were investigated (Scheme 35).

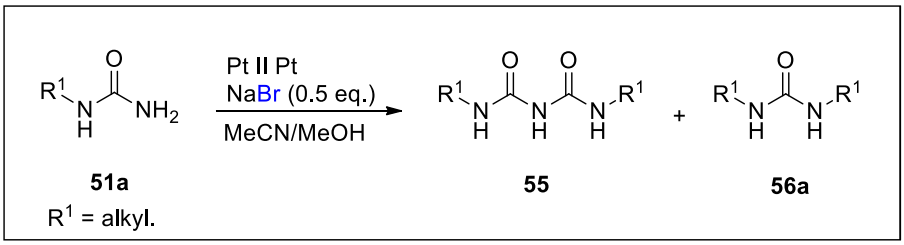

Scheme 35. Investigation of the formation of **56a**. Pt = platinum (anode II cathode).

Table 24. Screening of different conditions for the formation of symmetric dialkyl urea derivatives.

Entry	Deviation from conditions[a]	Yield [%][b,c]	Conv. [%][b,c]
25	none	0%[b]	n/a
26	NaI, Cgr II Cgr	0%[b]	75%[b]
27	NaCl, Cgr II Cgr	**55** (8%)[c], **56a** (28%)[c]	40%[c]
28	NaCl, NaOH (0.5 eq.), Cgr II Cgr	**55** (23%)[c]	83%[c]
29	KCl, Cgr II Cgr	**55** (5%)[b], **56a** (24%)[b]	79%[b]
30	LiCl, Cgr II Cgr	**55** (3%)[b], **56a** (8%)[b]	69%[b]
31	NEt_4Cl, MeCN/MeOH (10 v/v%), Cgr II Cgr	**56a** (24%)[b]	78%[b]
32	$LiClO_4$, Cgr II Cgr	**55** (4%)[b], **56a** (16%)[b]	73%[b]
33	NBu_4BF_4, Cgr II Cgr	**56a** (26%)[b]	72%[b]

[a] Standard conditions: urea (0.5 mmol), NaBr (0.25 mmol), MeCN/H_2O (5.0 mL, 10 v/v%), platinum electrodes, undivided cell, constant current, j = 5 mA/cm^2, 2.0 F (ref. substrate), 30 °C; [b] Yields determined by ^{1}H NMR (internal standard: CH_2Br_2); [c] Isolated yields. Conversion is calculated from ^{1}H NMR yield or isolated yield of starting material. Cgr = graphite electrode (anode II cathode).

The formation of **56a** was only observed when water was used as an additive in combination with chloride or other electrochemically stable supporting electrolytes (Table 24). In the presence of sodium bromide or iodide, no product was formed. In the presence of NaCl, the corresponding dialkyl urea **56a** was formed with an isolated yield of 28% (Entry 27). As a by-product, **55** was detected. The isolated 60% starting material showed good selectivity and mass balance of the reactions, suggesting a different reaction mechanism than those involving bromide salts (Entry 27). When NaOH was added as an additive, the yield of **56a** was reduced (Entry 28). Interestingly, $LiClO_4$ and NBu_4BF_4 afforded the same product closing out the role of chlorine, or possible hydrochloric acid or hypochlorous acid in the reaction mechanism.

Extending the initial conditions to ureas **51b** and **51c** gave similar results, and **56b** and **56c** could be obtained with an isolated yield of 10% and 20%, respectively (Scheme 36). Moreover, no formation of the corresponding biuret was observed, suggesting these derivatives´ robustness. No diphenylurea was formed, when phenylurea (**51d**) was used as a substrate (Table 25).

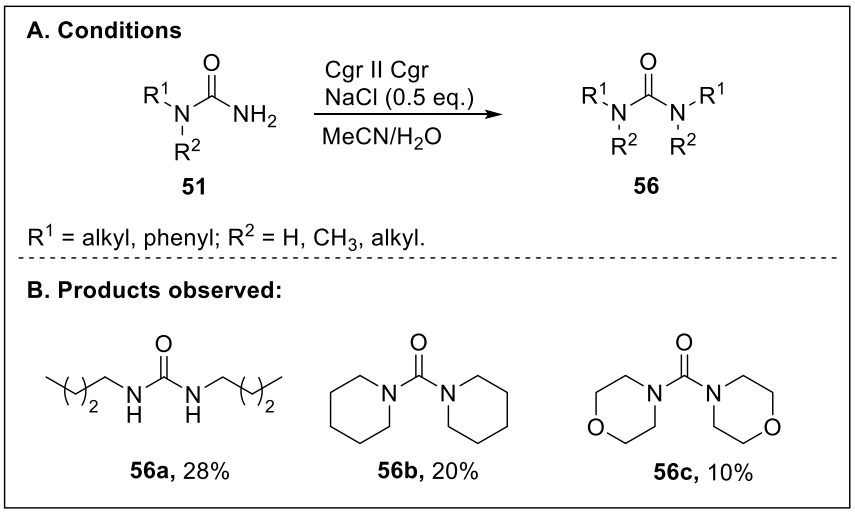

Scheme 36. Scope of symmetric dialkyl urea derivatives. Cgr = graphite (anode II cathode).

Table 25. Screening conditions for the formation of dialkylureas.

Entry	Deviation from conditions[a]	Yield [%][b,c]	Conv. [%][b,c]
34	**51b** (0.5 mmol)	**56b** (20%)[c]	50%[c]
35	**51c** (0.5 mmol)	**56c** (10%)[c]	n/a
36	**51d** (0.5 mmol)	Decomposition of **51d**	53%[b]

[a] Standard conditions: urea (0.5 mmol), NaCl (0.25 mmol), MeCN/H_2O (5.0 mL, 10 v/v%), graphite electrodes, undivided cell, constant current, j = 5 mA/cm^2, 2.0 F (ref. substrate), 30 °C; [b] Yields determined by ^{1}H NMR (internal standard: CH_2Br_2); [c] Isolated yields. Conversion is calculated from ^{1}H NMR yield or isolated yield of starting material. Cgr = graphite electrode (anode II cathode). n/a = not assessed.

3.4.4. CV studies und mechanism proposal for observed products

The observed products suggest the formation of the isocyanate intermediate, confirming the ureas' decomposition and/or hydrolysis under the electrochemical conditions. Cyclic voltammetry measurements were carried out to verify whether the proposed redox-mediated steps take place. Three solutions were scanned subsequently, including the solvent (green), **51a** (black), sodium bromide (blue), and **51a** and sodium bromide (red, Figure 32).

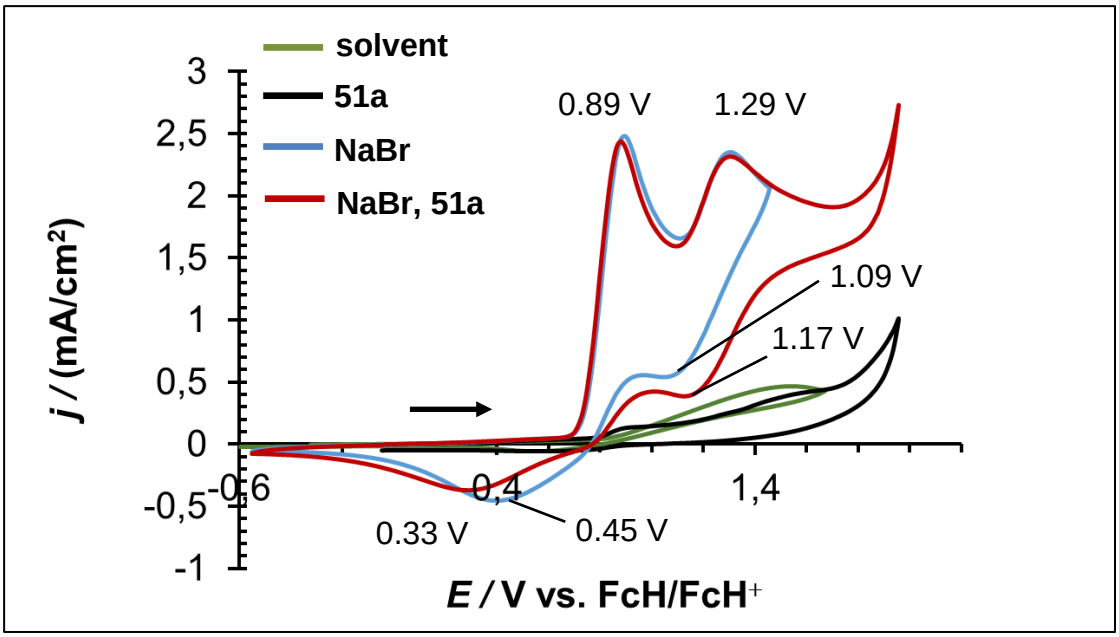

Figure 32. Cyclic voltammetry measurements of the solvent (green), **51a** (black), sodium bromide (blue) and **51a** and sodium bromide (red) in MeCN/MeOH (10 v/v%) solution. Conditions: substrate (0.01 M), NBu_4BF_4 (0.10 M), WE: glassy carbon disk (*d* = 3.0 mm), RE: Ag/AgCl, CE: glassy carbon rod, scan rate: 100 mV/s. FcH = ferrocene. Instrument: Autolab PGSTAT101, Metrohm AG.

The blue voltammogram (NaBr) postulates a quasi-reversible process with two distinctive oxidations (0.89 V, 1.29 V) and reduction peak potentials (1.09 V, 0.45 V). As previously mentioned, the first oxidation peak potential corresponds to the oxidation of bromide to bromine, which forms the stable tribromide complex. The second oxidation potential corresponds to the oxidation of this tribromide salt to bromine, which is in accordance with the literature (Section 1.6.).[172,173,175,176,234] Respectively, the two reduction peak potentials correspond to the reverse reactions, with the reduction of bromine at 0.45 V. Interestingly, the presence of the substrate does not have a significant effect on the oxidation of the bromide (red voltammogram). However, the reduction potentials are slightly shifted to 1.17 V from 1.09 V and to 0.33 V from 0.45 V, respectively. This could be due to a coordinative interaction between the bromine and the urea nitrogens, which donates electron density to the bromine molecule, making it less susceptible to reduction. Overall, the two voltammograms display similar activity, which might indicate that the forming bromine has little role in forming the observed products. In the investigated electrochemical window, the solvent system (green) and **51a** (black) display little to no reactivity.

In addition to the redox activity of NaBr, NaI, and NaCl salts were also tested. Sodium iodide displays a two-electron oxidation similar to bromide, suggesting the formation of relatively stable I_3^- (purple graph, Figure 33). While the oxidation of iodide takes place at lower potentials compared to bromide (0.53 V, 0.84 V), no electrochemical activity in the presence of NaI was observed (Section 3.4.2., Table 24). NaCl displays an inefficient one-electron oxidation at 1.34 V. This proposes the idea of a possible direct oxidation of urea under electrochemical conditions involving chloride salts.

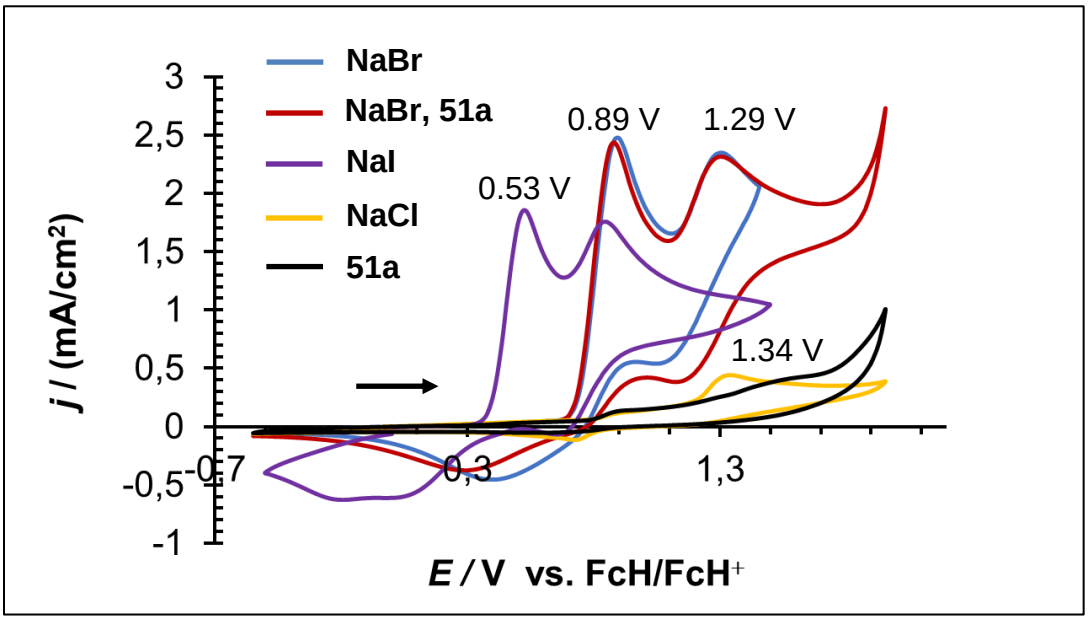

Figure 33. Cyclic voltammetry measurements of sodium bromide (blue), NaBr and **51a** (red), sodium iodide (purple), sodium chloride (yellow) and **51a** (black) in MeCN/MeOH (10 v/v%) solution. Conditions: substrate (0.01 M), NBu_4BF_4 (0.10 M), WE: glassy carbon disk (*d* = 3.0 mm), reference electrode: Ag/AgCl, CE: glassy carbon rod, scan rate: 100 mV/s. FcH = ferrocene. Instrument: Autolab PGSTAT101, Metrohm AG.

The following plausible mechanisms were proposed explaining the formation of the observed by-products (Scheme 37).

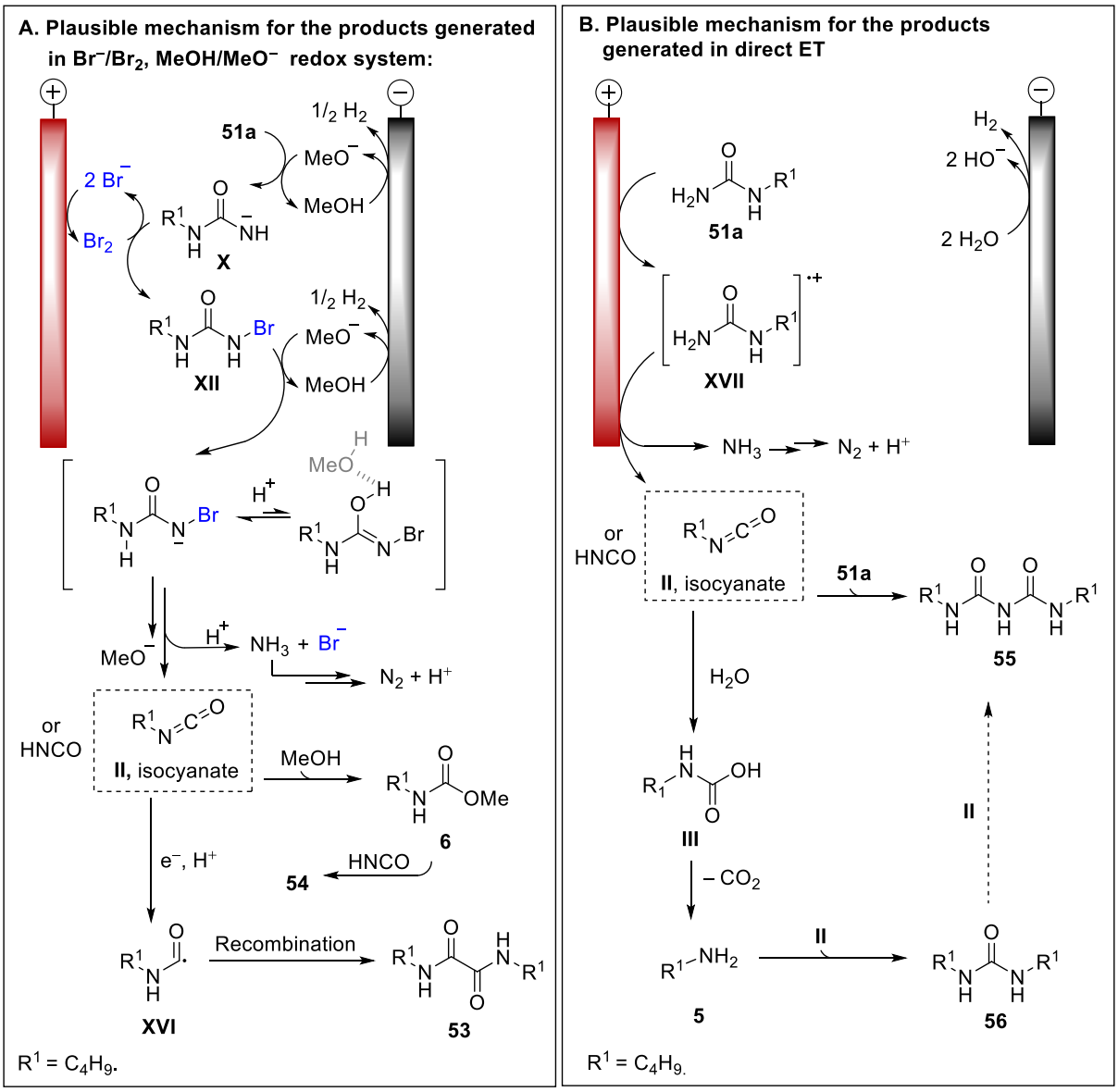

Scheme 37. Plausible mechanism for the electrochemical carbamate **6**, oxalamide **53**, biuret **55** and dialkyl urea **56** formation. ET = electron transfer.

In the mediated system, the cathodically generated base reacts with **51a** to form intermediate **X**, which reacts with the anodically generated bromine to form bromourea **XII**. Here, it decomposes to the isocyanate intermediate liberating ammonia and bromide as a possible by-product through a further deprotonation and an internal proton transfer, or via tautomerization and a proton transfer.[263] Similar findings were reported upon the decomposition of urea in the presence of active chlorine species, with NH_2Cl and $NHCl_2$, as leaving groups.[264,265] However, analogous leaving groups with bromine are thought to be unstable and were not described.[263] Possible hydrogen-bond interactions with methanol could stabilize the tautomer.[179,232] The forming alkyl isocyanate is scavenged by the solvent forming **6** or can be reduced to

its radical form **XV**. Following radical recombination, the formation of **53** could be explained. Formation of **54** was postulated via the reaction of electrochemically generated isocyanate, and **6**.[266] In terms of direct oxidation, **51a** suffers two-electron oxidation, liberating isocyanate, and amine as feasible by-products. The forming isocyanate can be scavenged by urea forming **55** or by the water to form carbamic acid **III**. Upon simultaneous decarboxylation, the corresponding amine **5** forms. Reaction with isocyanate, the formation of **56** is proposed. Formation of **55** can also be postulated from the reaction of **II** with **56**.[267] The products **6b**, **6c,** and **54** were also observed when morpholine- and piperidine urea were subjected to electrochemical conditions supporting the plausible mechanism (Table 20, Entry 22, 23).[266,267] Interestingly, other urea decomposition products,[266] such as cyanuric acid was not observed.

The reaction displayed a slightly different behavior when aromatic ureas were tested (Scheme 38). The presence of an electron-rich aromatic group promotes the liberation of aniline instead of the proposed amine or bromoamine product. The radical cation **XVII** forms via direct oxidation, which is trapped by **5** to form intermediate **XVIII**. Via subsequent oxidation and deprotonation, azobeneze (**57**) is formed in low amounts. The product was confirmed via GC, GC-MS comparing to the reference compound and NMR spectroscopic studies. The relatively low yield can be explained by the overoxidation of aniline, which was also indicated by the dark brown color of the reaction solution after electrolysis and the low counting of the qualitative measurements.[261] The role of electrochemically generated bromine was not investigated.

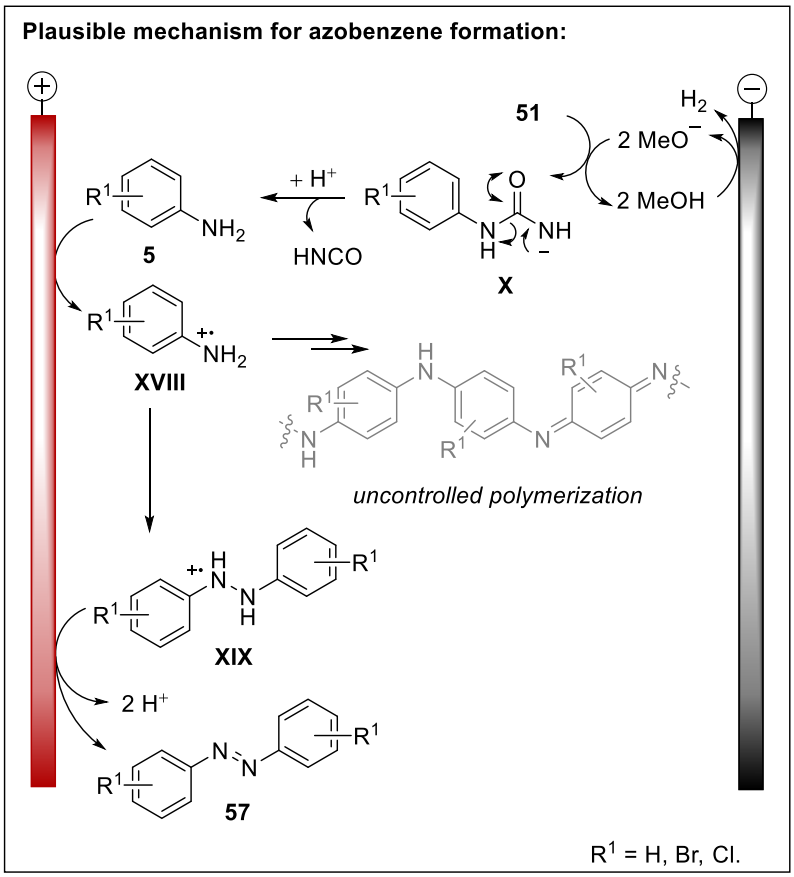

Scheme 38. Plausible mechanism for the formation of azobenzenes.[261,268]

Under the tested reaction conditions, the formation of **52** was not observed. The identified products can be explained via the electrochemical decomposition of ureas into their isocyanate or amine derivatives furnishing the unexpected molecules. The electrochemical lability can be reasoned with the electron-rich nature of the urea. The electrode material seemed to have a detrimental effect on the reactivity, promoting the decomposition of the ureas.

3.4.5. Further electrochemical and synthetic approaches for hydrazine formation

Eventually, different control reactions were carried out to understand the feasibility of the desired rearrangement. As the reaction proceeds via a simultaneous multistep process including first a deprotonation, N–Br bond formation, second deprotonation, isocyanate formation, and nucleophilic attack of the solvent, the separation of the N–Br bond formation and the rearrangement part was aimed (Scheme 39). Based on the

commercial hydrazine production,[217,218,220,221,269] we intended that electrochemically generated hypobromous acid would facilitate the reaction (Table 26).

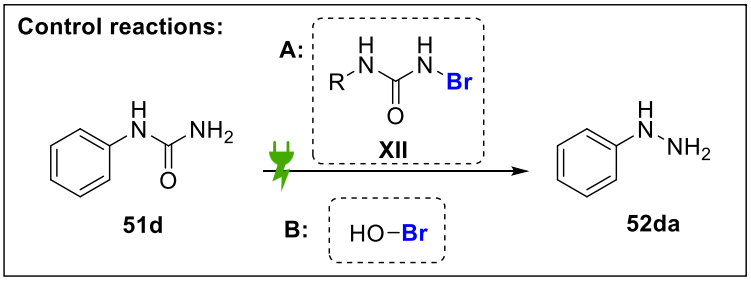

Scheme 39. Control reactions aiming the formation of **XII** (Pathway A) and hypobromous acid (B) in an ex-cell approach.

Table 26. Electrochemical control reactions via a subsequent addition (A) and ex-cell (B) approach.

Entry	Conditions	Results
1	A: Subsequent addition via **XII** intermediate[a]	**57d** (traces)
2	B: Ex-cell approach via in situ generated HOBr[b]	**52da** not observed

Reaction conditions: [a] 1. **51d** (0.5 mmol), NBu_4Br (1.0 mmol), acetonitrile (5 mL), graphite electrodes, 2.0 *F*, *j* = 5 mA/cm^2, 300 rpm, 25 °C, 2. NaOH (0.5 mmol), H_2O (1 mL), 50 °C, 1 h; [b] 1. NBu_4Br (1.0 mmol), NaOH (0.5 mmol), acetonitrile (5 mL), graphite electrodes, 2.0 *F*, *j* = 5 mA/cm^2, 300 rpm, 25 °C, 2. **51d** (0.5 mmol), H_2O (1 mL), 50 °C, 1 h. Reactions were monitored via TLC, GC and LC.

First, the electrochemical reaction was carried out in a subsequent addition and an ex-cell approach. The electrolysis of the urea with NBu_4Br was carried out at room temperature, following the addition of aq. NaOH and heating the reaction mixture to 50 °C to facilitate the rearrangement (Entry 1). In reaction B, tetrabutylammonium bromide and NaOH were electrolyzed, and an aq. solution of the urea was subsequently followed (Entry 2). In both cases, no rearrangement was observed to either the hydrazine **52da** or the carbamate **6d**. In the case of Entry 1, a trace amount of azobenzene **57d** was detected.

Next, electrolysis was carried out orientating on the industrially known chlor-alkali method. In the chlor-alkali electrolysis, aqueous sodium chloride solution is electrolyzed at relatively high current densities, in which chlorine gas is generated on the DSA anode and hydroxide on the nickel cathode.[153] In an undivided cell, chlorine and NaOH react to form sodium chloride, hypochlorite, and water (Section 1.9).

Industrially, hypochlorite is used for the Hofmann rearrangement of ureas to hydrazines.[217,218,220,221,269]

Ureas were subjected to the following conditions to form the corresponding hydrazines (Scheme 40).

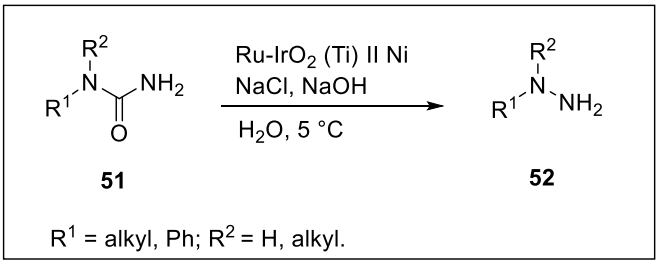

Scheme 40. Screening for the formation of **52** under chlor-alkali conditions. Ru-IrO_2 (Ti) = Ru/TiO_2 supported on titanium net.

Table 27. Screening of reaction conditions for the formation of **52**.

Entry	Deviation from standard conditions[a,b]	52 [%][c]
3	**51d** (0.25 mmol)[a]	0%
4	**51a**, *j* = (100 mA/cm^2)[a]	0%
5	**51c**, NaBr (5.0 M)[b]	**52c** (traces)
6	Ex-cell: **51c**[b]	**52c** (present)
7	Ex cell: **51c**, NaBr (5.0 M)[b]	0%

[a] Standard conditions: urea (0.50 mmol), NaCl (5.0 M), NaOH (1.0 M), H_2O (5 mL), Ru-IrO_2 (Ti) II Ni, *j* = 200 mA/cm^2, 4.0 *F* (with resp. formation of 1 mmol NaOCl), undivided Telfon® cell, 5–35 °C, 350 rpm, [b] Modified conditions: urea (0.5 mmol), NaCl (5.0 M), NaOH (1.0 M), H_2O (10 mL), Ru-IrO_2 (Ti) II Ni, *j* = 200 mA/cm^2, 8.0 *F* (with resp. formation of 1 mmol NaOCl), undivided beaker-type glass cell with cooling jacket, 0–60 °C, 400 rpm; [c] Qualitative measurements were carried out with GC, GC-MS, TLC, TLC-MS.

The initial reactions in a 5 mL PTFE cell using **51a** and **51d** did not facilitate the formation of the desired product (Table 27). When **51d** was used, the dialkyl derivative (**56d**) was detected with TLC-MS (Entry 3). As temperature control is crucial for forming the N–Cl bond and liberating CO_2, the cell was exchanged for a 25 mL beaker-type cell with a cooling jacket (Entries 5, 6, 7).[220] The new cell type allowed the cooling of the reaction solution to 0 °C. Using **51c** and NaBr as the halide source, the electrolysis was carried out by applying 8.0 *F* (Entry 3). After the electrolysis, the solution was heated to 60 °C to facilitate the rearrangement. Qualitative TLC showed

no presence of the starting material urea. The solution was acidified to pH 5, then extracted with acetonitrile forcing the hydrazine to the organic layer and minimizing the solvation of the urea starting material. TLC-MS showed poor formation of the corresponding hydrazine (**52c**) product (Entry 5). To see if the formation of hydrazine can be promoted, electrolysis was carried out via an ex-cell approach. During the NaCl, NaOH mixture electrolysis, the solution turned cloudy. After the electrolysis, urea in 1 mL water was added at 0 °C, then heated to 60 °C. The reaction solution became transparent, and the heating was accompanied by gentle bubbling. After one hour, the reaction was left to cool to room temperature and was neutralized. Upon analysis with GC, GC-MS, and TLC-MS, the corresponding **52ca** was detected (Entry 6, Figure 34).

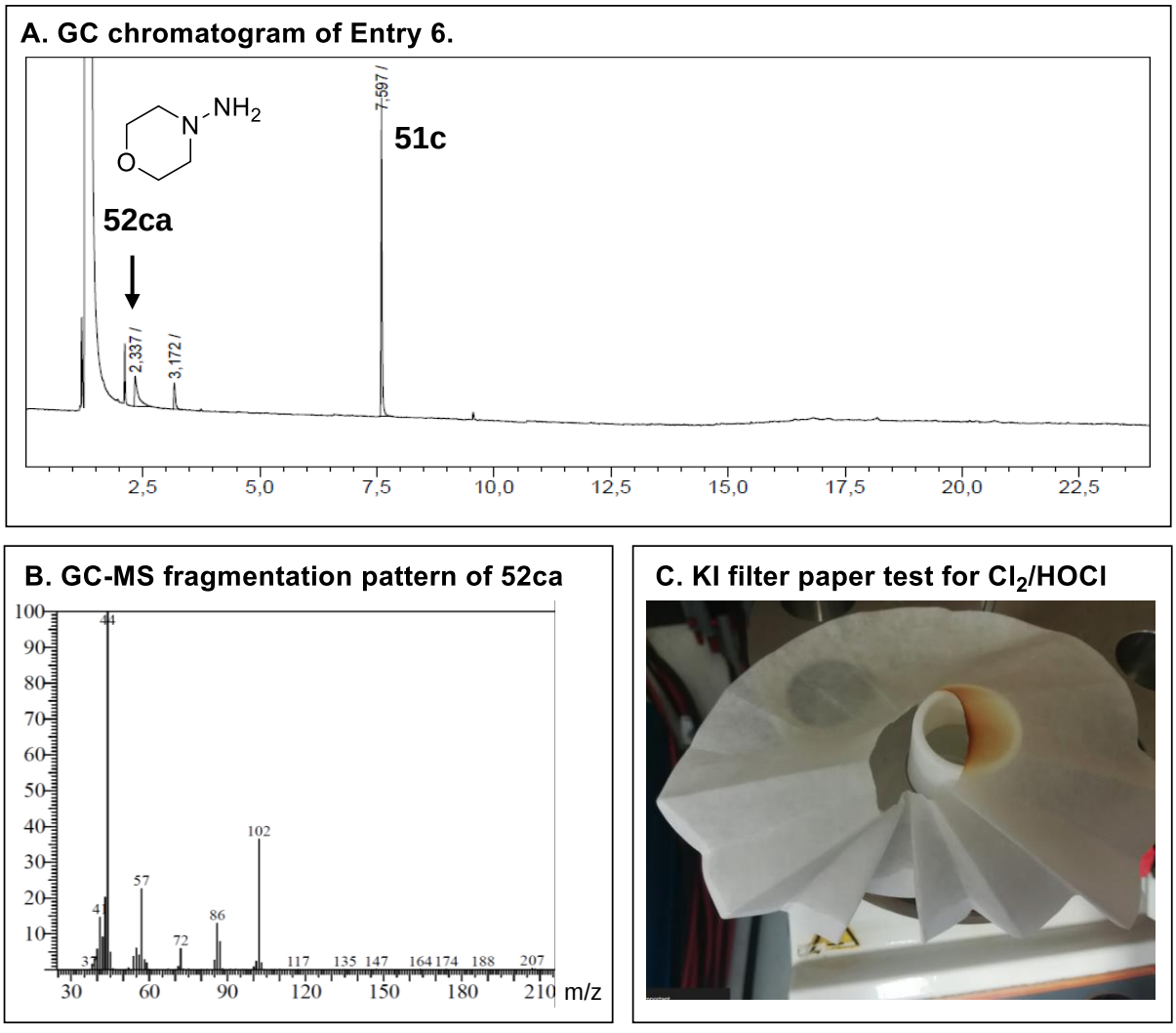

Figure 34. GC Chromatogram of Entry 4 showing the trace amounts of hydrazine **52ac** product. The signals were depicted via GC, GC-MS methods. Instruments: GC 2010 Shimadzu, method: HP5 hart; Shimadzu GC-2025 coupled with HI-5MS column, Avantor

VWR. KI test: KI (0.1 M) in 1 M HCl (5 mL). Filter paper was wettened with the acidic KI solution and placed above the reaction mixture after electrolysis.

Repeating the reaction conditions using NaBr as the halide source did not afford **52ca,** showing that temperature and the halide source are detrimental for the formation of the desired product.

Eventually, possible synthetic methodologies were tested that proved to be excellent for the formation of carbamates **6** from benzamides **4** (Scheme 41). First, the approaches reported by Moriarty[270] and Kalesse[271] were employed and tested parallel on both benzamide (**4**) and *N*-phenylurea (**51d**). Using this method, **4d** could be isolated with a moderate yield of 40% (Entry 8, Table 28). When the same conditions were applied to **51d**, the reaction was kept stirring at 0 °C for 2 hours. Surprisingly, the protected hydrazine derivative **52d** was formed in traces (Entry 9). The product was elucidated with GC and GC-MS methods (Figure 35).

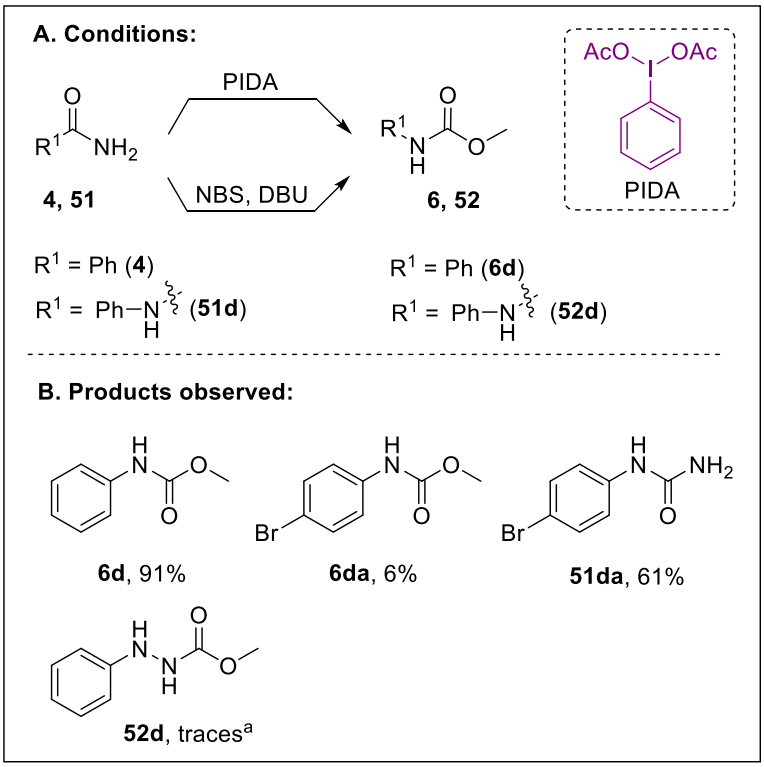

Scheme 41. Control reactions with PIDA and NBS/DBU conducted on **4** and **51d**.[270,271] [a] Qualitative measurements via GC, GC-MS. Isolated yields. PIDA = phenyliodine(III) diacetate, DBU = 1,8-diazabicyclo[5.4.0]undec-7-ene, NBS = *N*-bromosuccinimide.

Table 28. PIDA and NBS assisted Hofmann rearrangement of **4** and **50d**.[55,270]

Entry	Deviation from standard conditions[a,b]	[%][c,d]
8	none[a]	**6d** (40%)[c]
9	**51d** (0.5 mmol), 0 °C for 2 hours[a]	**52d** (traces)[d]
10	none[b]	**6d** (91%)[c]
11	**51d** (0.5 mmol)[b]	**6da** (6%)[c], **51da** (61%)[c]

[a] Standard condition A: benzamide (**4**, 0.50 mmol), KOH (1.25 mmol), PIDA (0.65 mmol), MeOH (5 mL), 0–25 °C, 12 h; [b] Standard conditions B: benzamide (**4**, 0.50 mmol), DBU (1.00 mmol), NBS (2.00 mmol), reflux, 45 mins; [c] Isolated yields; [d] Identified with GC, GC-MS methods. PIDA = phenyliodine(III) diacetate, DBU = 1,8-diazabicyclo[5.4.0]undec-7-ene, NBS = *N*-bromosuccinimide.

Second, the NBS-promoted Hofmann rearrangement was conducted on both substrates.[55] Applying conditions to benzamide (**4**), the corresponding carbamate **6d** was afforded an excellent yield of 91%. Using the same approach on **51d**, the desired product was not formed. Instead, the conditions promoted the bromination of urea **51d** in the para position and its rearrangement to the carbamate derivative **6da**. The brominated urea **51da** was obtained with a yield of 61%. The obtained products were similar to the ones observed during electrolysis using HBr as a bromine source (Table 23, Entry 21).

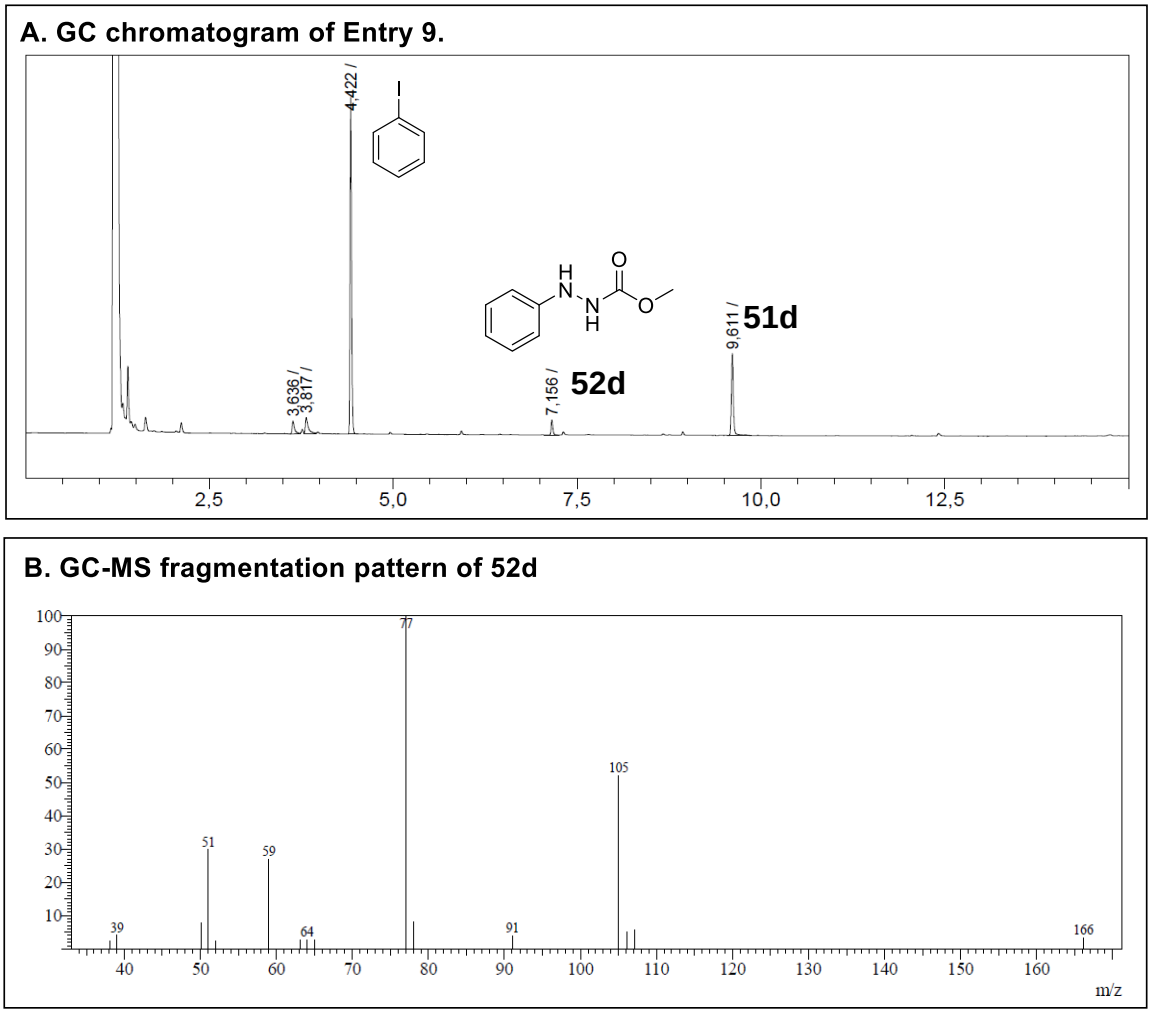

Figure 35. GC chromatogram of reaction solution of Entry 9 after 12 hours. **52d** was identified via GC-MS. Instruments: GC 2010 Shimadzu, method: HP5 hart; Shimadzu GC-2025 coupled with HI-5MS column, Avantor VWR.

Investigating different approaches, the desired hydrazine was observed. The chlor-alkali electrolysis inspired conditions afforded **52ca** in trace amount. Similarly, when applying the conventional approach from Landsberg and Kalessee on **51d**,[271] the corresponding protected hydrazine **52d** could be observed.

4. Conclusion

4.1. Electrochemical dibromination of terpenes and naturally derived olefins

The safe, selective, and sustainable electrochemical bromination protocol of terpenes, terpenoids, and naturally derived olefins was established. The highlights of this approach are the utilization of NaBr, which serves both as a reagent and supporting electrolyte, the application of sustainable carbon electrodes as well as the use of renewable molecules as substrates. This method facilitates the selective functionalization of mono- and polyunsaturated terpenes, demonstrated in 11 examples with yields up to 82 % (Scheme 42). The electrochemical bromination of structurally delicate compounds has been proven superior to the already existing methods using elemental bromine or hydrogenbromide. Scalability, as well as further functionalization, has been demonstrated.[112,234]

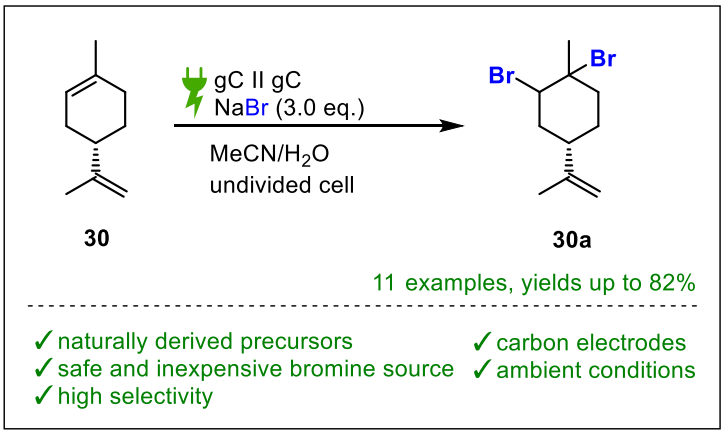

Scheme 42. Summary of electrochemical dibromination of naturally derived olefins.

4.2. Electrochemical bromination of electron-deficient enones

With a slight modification of the reaction conditions in Section 3.1, preliminary research of the selective electrochemical bromination of electron-deficient enone **45** was achieved. The method relies on the formation of bromodimethylsulfonium bromide (BDMS) in the presence of DMSO at sustainable graphite electrodes at elevated temperatures. Screening of other sulfide sources suggests the possible reformation of DMSO under the electrochemical conditions, contributing to this approach´s sustainability aspect. The method selectively provides the desired product **45a** in poor

yields, which is inferior so far to other electrochemical procedures known (Scheme 43).[249]

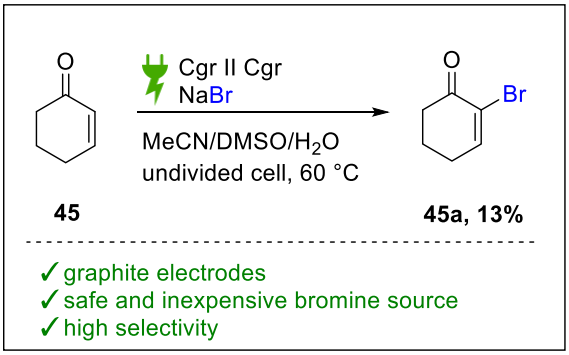

Scheme 43. Summary of electrochemical α-bromoenone formation.

4.3. Electrochemical bromolactonization of alkenoic acids

The successful bromocyclization of alkenoic acid (**49**) to γ-lactones (**49a**) was established (Scheme 44). The collective advantages of this approach are the dual role of NaBr as a bench-stable and safe bromide source, the use of graphite electrodes, and the exclusion of additional supporting electrolytes. The desired product was obtained in a selective manner and with moderate yields without optimization. Furthermore, it excludes the use of hazardous hydrogen bromide as bromine source associated with existing procedures.[190,198]

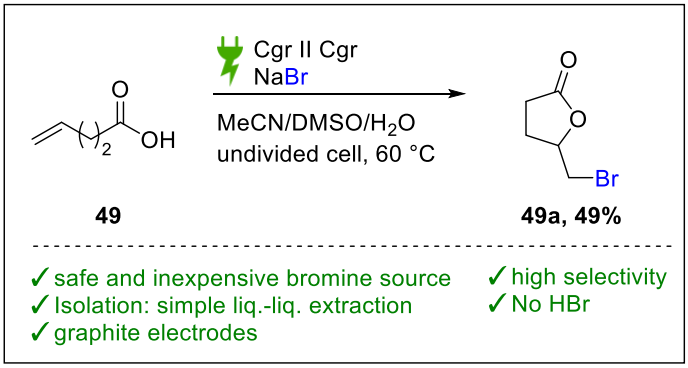

Scheme 44. Summary of electrochemical bromolactonization of **49**.

4.4. Electrochemical Hofmann rearrangement of urea derivatives

The tested electrochemical approaches did not facilitate the formation of the desired hydrazine derivatives (**52**) but afforded the in-situ formation of isocyanate (**II**) that

served as an intermediate for the products identified in the reaction. The reactions were also proved structural dependent. While mono- and dialkylated ureas afforded the formation of different decomposition derivatives, phenylurea derivatives facilitated the formation of unexpected azobenzene **57** products (Scheme 45). Control reactions based on the chlor-alkali electrolysis method could facilitate to formation of desired hydrazine **52ca** in traces. Applying the conventional literature using PIDA,[271] **52d** was detected in trace amount using GC, GC-MS methods.

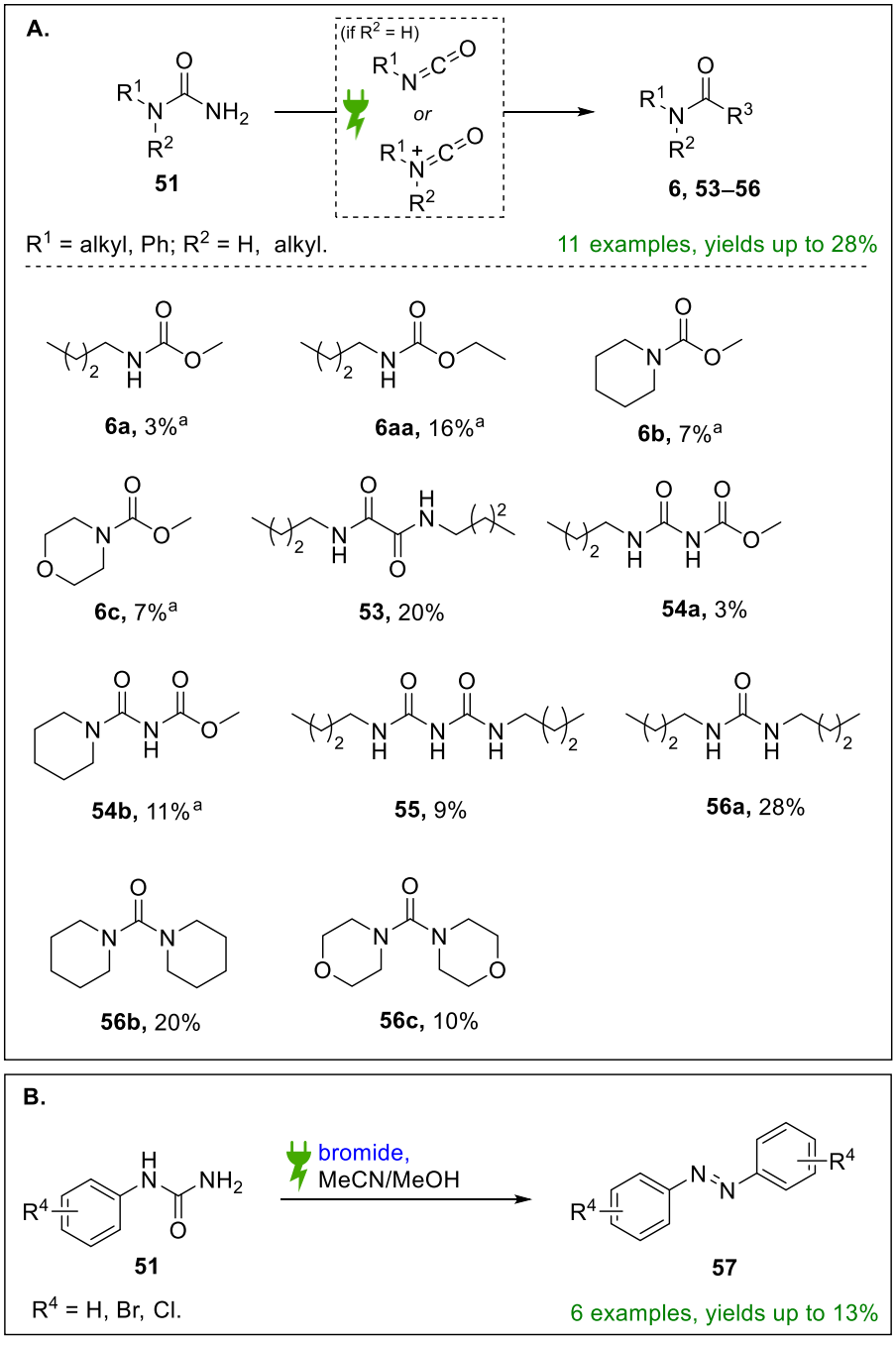

Scheme 45. Summary of the electrochemical Hofmann rearrangement of **51**. [a] Yield determined via ^{1}H NMR (internal standard: CH_2Br_2). Isolated yields.

5. Outlook

5.1. Electrochemical bromofunctionalization of terpenes

The electrochemical bromofunctionalization methodologies and bromine-mediated synthetic approaches gained significant attention in recent years. Based on the successful electrochemical bromination of terpenes and naturally occurring alkenes, the investigation of a possible one-pot bromofunctionalization in an electrochemical flow approach is envisioned.

Utilizing NaBr in a mediated approach in the presence of a nucleophilic additive can result in terpene-based bromohydrins, bromoethers (**30aa**). Especially sulfur- and nitrogen-containing nucleophiles are of interest as the resulting products can give rise to highly functional biobased monomer derivatives (Scheme 46).[210,272]

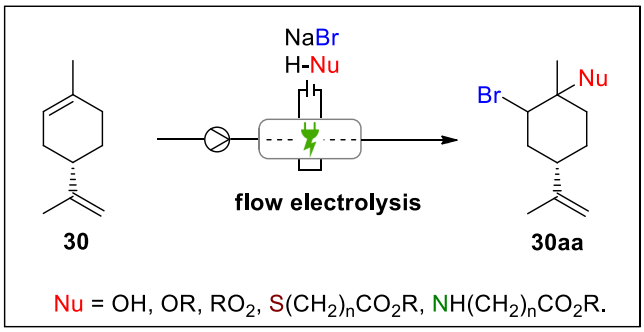

Scheme 46. Possible electrochemical bromine mediated functionalization of terpenes in flow electrolysis.

5.2. Electrochemical halogen-mediated hydrazine formation

The initial research carried out in the scope of this dissertation revealed the electrochemical instability of certain urea derivatives suggesting the structural modification of the substrate. A possible alternative is a protected *N*-alkyl urea with an electron-withdrawing moiety (**51**) that could direct the selectivity of the Hofmann rearrangement and enhance the *N*-migration during the rearrangement.

Moreover, the in-situ electro-generated HOBr, HOCl[273,274] could be tested, as these agents proved successful in promoting the formation of the corresponding hydrazine derivates.[217,219–221]

Furthermore, based on the control reaction carried out with phenyliodine(III) diacetate (PIDA), electrochemically generated hypervalent iodine species[275] could promote the desired rearrangement (Scheme 47).

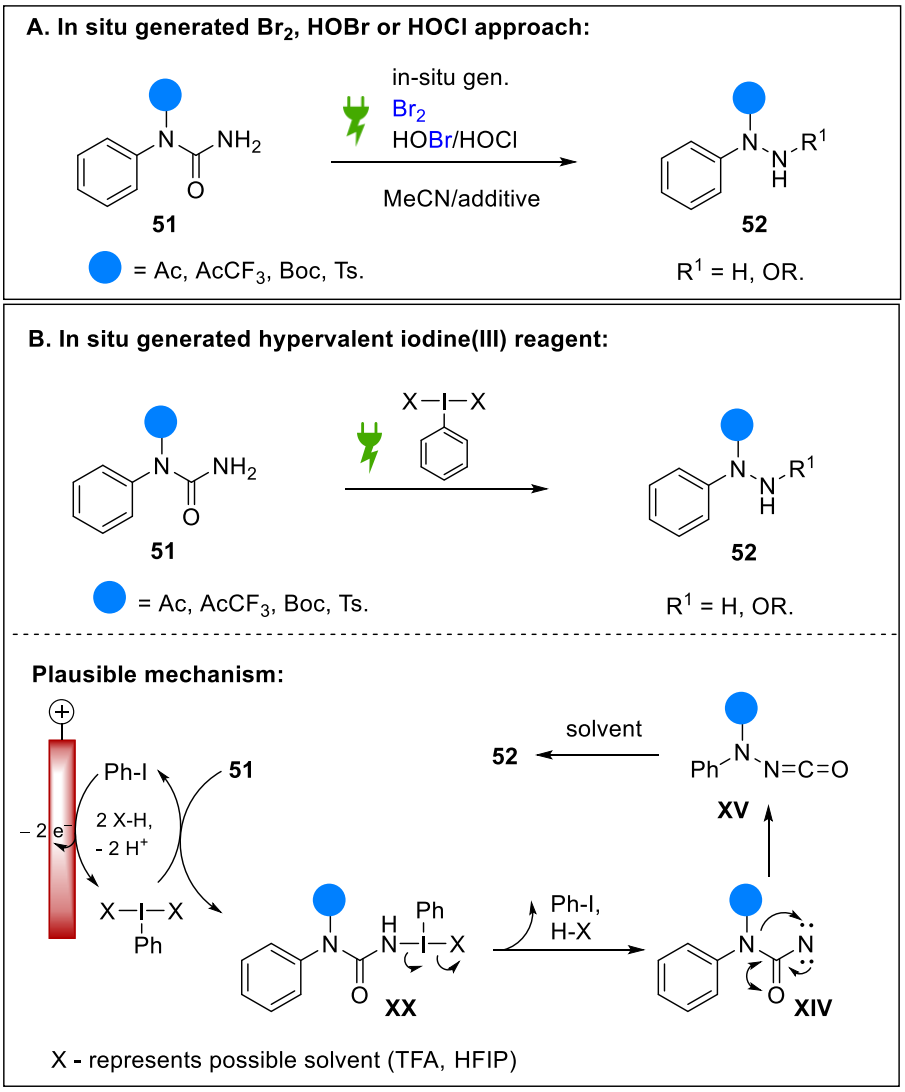

Scheme 47. Possible electrochemical methodologies for the formation of hydrazine derivates (**52**). The blue functionality represents the electron-withdrawing protecting group.[273–275]

Alternatively, protected hydrazine derivatives could be achieved via an electrophilic amination of oxaziridines (**58**, Scheme 47).[269] The formation of *N*-protected oxaziridine is envisioned using a redox bromine/peroxide system,[276,277] or employing electrochemically generated peroxodicarbonate[278] or periodide species[279,280] (Scheme 48). The forming oxaziridine is subsequently reacted with an amine (**5**) to form the desired hydrazine derivatives (**52**).[219,281]

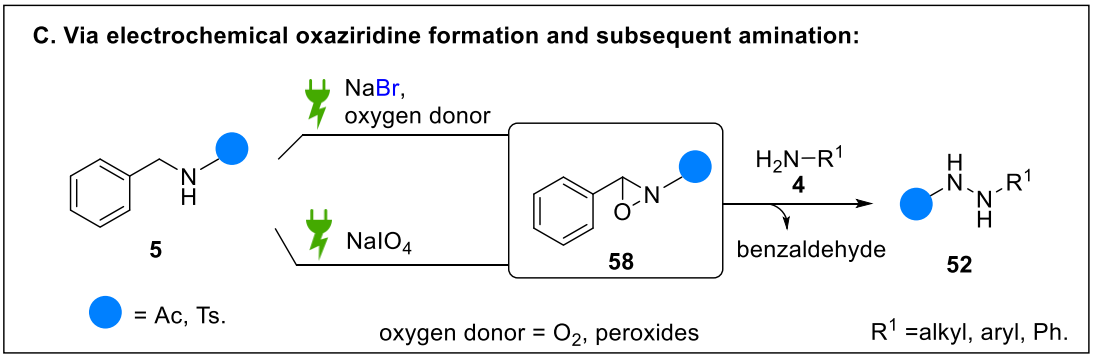

Scheme 48. Possible hydrazine formation via electrochemically generated oxaziridines (**58**) based on previous conventional and electrochemical methodologies.[276–281]

6. Experimental section

6.1. General information

All reagents were obtained from commercial suppliers and used in analytical grades unless stated otherwise. Cyclohexane and ethyl acetate were redistilled under reduced pressure before use. All other solvents were purified by standard methods.[282]

NMR spectroscopy: All ^{1}H, ^{13}C and 2D NMR spectra were recorded at 25 °C, using a *Bruker* Avance III HD 400 (400 MHz, Analytische Messtechnik, Karlsruhe, Germany). Chemical shifts (δ) are reported in parts per million (ppm) relative to traces of non-deuterated solvent in the corresponding deuterated solvent. Dibromomethane served as internal standard for ^{1}H NMR (in $CDCl_3$ δ = 4.947 ppm).[283]

Gas chromatography: Quantitative and qualitative analysis of reactions mixtures and purified products were conducted via gas chromatography on a Shimadzu GC-2025 (*Shimadzu*, Kyoto, Japan) device. HP-5MS column (*Agilent Technologies*, Santa Clara, California; length: 30 m, inner diameter: 0.25 mm, film: 0.25 µm, carrier gas: hydrogen).

Gas chromatography coupled mass spectrometry (GC-MS) measurements were carried out on a Shimadzu GC-2025 (*Shimadzu*, Kyoto, Japan) equipped with a flame ionization detector using a HI-5MS column (*Avantor VWR*, Radnor, USA, length: 30 m, inner diameter: 0.25 mm, ((5%-phenyl)-dimethylsiloxane) film: 0.25 µm, carrier gas: helium). The chromatograph was coupled to a mass spectrometer Shimadzu GC-MS-QP2025 (*Shimadzu*, Kyoto, Japan) with an injection temperature of 250 °C and detection inlet temperature of 250 °C.

High Resolution Mass Spectrometry: High-resolution mass spectra were obtained by using an Aligent 6545 QTOF-MS (*Aligent*, Santa Clara (SC), USA) apparatus employing electronspray chemical ionization (ESI±) and atmospheric pressure chemical ionization (APCI±). In some cases, $AgNO_3$ was added to the analyte solution for better ionization of the compounds.

Thin Layer Chromatography Mass Spectrometry was performed on an Advion Expresslon CMS with Plate Express Interface (Advion, Ithaca, NY, USA) apparatus employing electronspray chemical ionization (ESI±). For the measurements Silica gel

60 sheets deposited on aluminium (F254, *Merck KGaA*, Darmstadt, Germany) were used.

IR spectroscopy: For IR measurements, a “Bruker Alpha II FTIR” spectrometer (*Bruker Corporation*, Massachusetts, USA) with a Platinum-ATR unit was used.

Melting points: The melting ranges were measured with “Melting Point Apparatus M-565” (*Büchi*, Essen, Germany). Heating rate of 1 °C min^{-1} was used.

X-ray crystallography: X-ray analysis data were collected on a STOE IPDS-2T diffractometer (*STOE & Cie GmbH*, Darmstadt, Germany) using graphite monochromated Mo-Kα radiation (λ= 0.71073 Å). Intensities were measured using fine-slicing ω and corrected for background, polarization and Lorentz effects. The structures were solved by direct methods and refined anisotropically by the least-squares procedure implemented in the SHELX program system. The supplementary crystallographic can be obtained free of charge from the Cambridge Crystallographic Data Center via www.ccdc.cam.ac.uk/data_request/cif. Deposition numbers and further details are given with the individual characterization data.

Preparative chromatography: Column chromatography was performed on silica gel 60 M (0.040–0.063 mm, *MachereyNagel GmbH & Co*, Düren, Germany) using a mixture of cyclohexane/ethyl acetate, cyclohexane/dichloromethane or dichloromethane/methanol as eluent. Automated column chromatography was performed on a preparative chromatography system (*Büchi*, Flawil, Switzerland) with a Büchi Conrol Unit C-620, an UV detector Büchi UV photometer C-635, a Büchi fraction collector C-660 and two Pump Modules C-605 for adjusting the solvent mixtures. Thin layer chromatography was conducted on Silica gel 60 sheets deposited on aluminium (F254, *Merck KGaA*, Darmstadt, Germany). For visualization of the components, a potassium permanganate stain (3 g $KMnO_4$, 20 g K_2CO_3, 5 mL NaOH (5%), 300 mL water) and a *p*-anisaldehyde stain (135 mL EtOH, 5 mL conc. H_2SO_4, 1.5 mL of AcOH (100%), 3.7 mL *p*-anisaldehyde) were used.

High Performance Liquid Chromatography: High performance liquid chromatography was performed on a Shimadzu HPLC-MS system using an autosampler SIL-20AHT, a column oven CTO-20AC, two pump modules LC-20AD for adjusting the solvent mixtures, a LCMS-2020 mass spectrometer, a diode array detector SPD-M20A, a communication BUS module CBM-20A, and an Eurospher II

100-5 C18 column 150 x 4 mm (*Knauer*, Berlin, Germany). As eluting system, a solvent mixture of acetonitrile/water with 1 vol.% formic acid was used.

Ion chromatography was performed on an 850 Professional IC (Metrohm AG, Herisau, Switzerland) equipped with a Metrosep A Supp 4 anion exchange column (Metrohn AG, Herisau, Switzerland). Eluent system: Na_2CO_3 (0.9 mmol/L) and $NaHCO_3$ (0.85 mmol/L) in H_2O with 5 vol.% acetone.

Cyclic voltammetry: Cyclic voltammetry measurements were conducted in a 10 mL snap-cap vial equipped with an Autolab PGSTAT101 potentiostat (*Metrohm AG*, Herisau, Switzerland). Working electrode; a glassy carbon electrode tip (3 mm diameter); counter electrode: glassy carbon rod; reference electrode: Ag/AgCl in saturated LiCl/EtOH. All measurements were referenced against FcH/FcH^+.[284,285] A solvent mixture of acetonitrile/water or acetonitrile/methanol were used employing Bu_4NBF_4 (0.10 M) as supporting electrolyte. The substrate concentration was 0.01 M, and the scan rate was 100 mV/s. The solution of interest was purged with argon for 5 minutes before collection of data.

6.2. General protocol for quantification via GC calibration

6.2.1. External standard calibration of (4*S*)-(–)-limonene (**30**)

5.0 mL solutions of (4*S*)-(–)-limonene (**30**) in acetonitrile/deionized water (8 v/v%) with known concentrations (5.2 mmol/cm^3; 8.7 mmol/cm^3; 19.2 mmol/cm^3; 50.6 mmol/cm^3, 68.1 mmol/cm^3) were prepared in 25.0 mL round-bottom flasks. Three 1.5 mL GC-vial-samples were prepared via taking an aliquant of 50 µL from the round-bottom flasks and filtered via approx. 245 mg silica gel 60M, using ethyl acetate as eluent. The resulting 15 samples were analyzed via GC and the response was plotted in the diagram giving the straight-line equation (Equation 15) below:

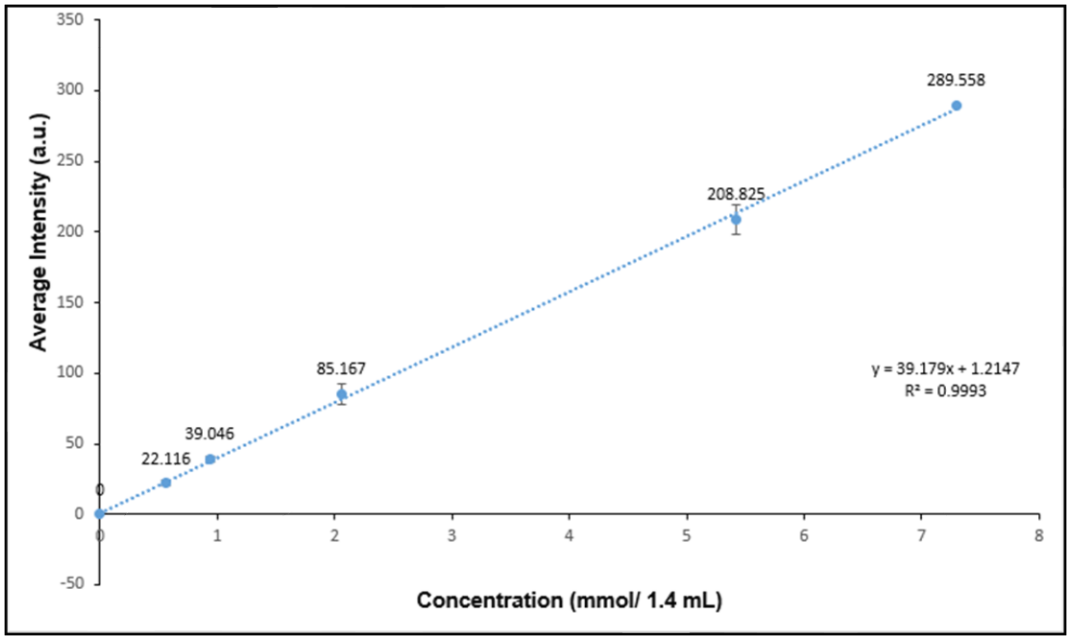

Figure 36. External standard calibration of the starting material **30**. Adapted from reference [234], CC BY-NC-ND 4.0.

$$y = b_0 + b_1 c \qquad \textbf{(15)}$$

The straight-line equation (Equation 15) was used to calculate the analysis function (Equation 16) to determine the concentration of an unknown sample. Hence, conversion of **30** was determined.

$$c = \frac{y - b_0}{b_1} \qquad \textbf{(16)}$$

6.2.2. Internal standard calibration of (4*S*)-*p*-mentha-1,8-diene-2-carbonitrile (**44**)

5.0 mL solutions of **44** in acetonitrile/dichloromethane (50 v/v%) with known concentrations (0.0132 mmol/cm^3; 0.0158 mmol/cm^3; 0.0572 mmol/cm^3; 0.0690 mmol/cm^3) with a known concentration of 0.0069 mmol/cm^3 octacosane ($C_{28}H_{58}$) as internal standard were prepared in 25.0 mL round-bottom flasks. Three 1.5 mL GC-vial-samples were prepared via taking an aliquant of 50 µL from the round-bottom flasks and filtered via approx. 245 mg silica gel 60M, using ethyl acetate as eluent. The resulting 12 samples were analyzed via GC and the ratio of **44**/ITSD response (*x*–axis) was plotted against molar ratio of **44**/ITSD (*y*–axis), giving the straight-line equation (Equation 17) below:

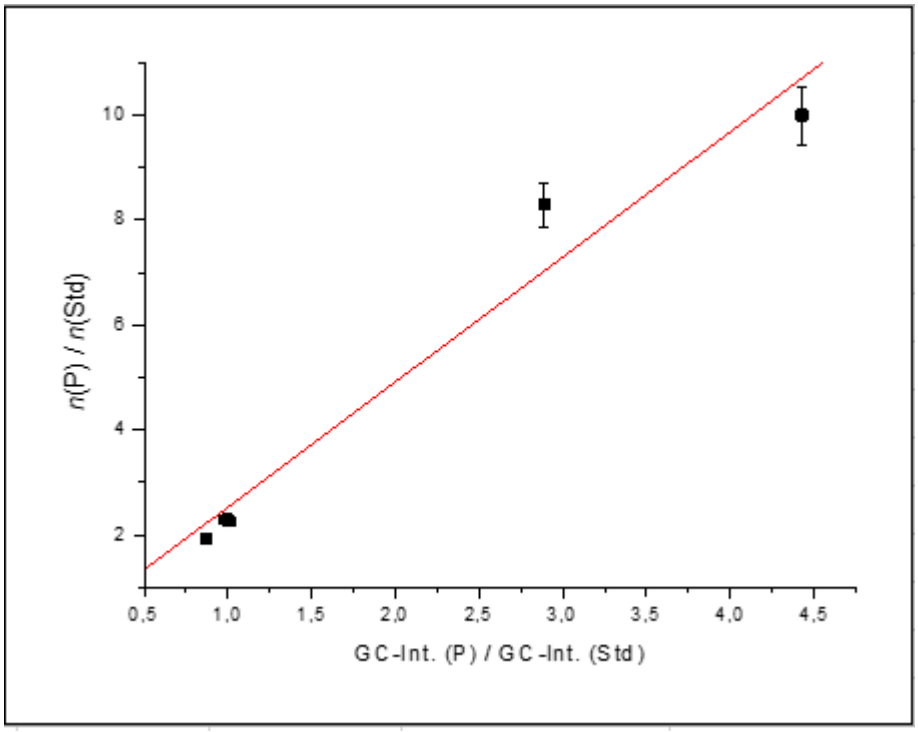

Figure 37. GC internal standard calibration of **44** with octacosane ($C_{28}H_{58}$).

$$y = a + bx \qquad \textbf{(17)}$$

a = 0.14383

b = 2.38534.

6.3. Electrochemical set-up and synthesis protocols

Electrochemical reactions were carried out with a two-electrode set-up under galvanostatic conditions.

6.3.1. Electrode information

Dimensions of electrodes:

5 mL PTFE screening cell: 0.7 x 1.0 x 0.3 cm

25 mL PTFE beaker-type cell: 0.6 x 6.0 x 2.0 cm

Isostatic graphite

SIGRAFINE® V2100, *SGL Carbon*, Bonn, Germany

Glassy carbon

SIGRADUR® G, *HTW GmbH*, Thierhaupten, Germany

Boron-doped diamond (BDD)

DIACHEM®, 15 µm boron-doped diamond layer on 3 mm silicon support, *CONDIAS GmbH*, Itzehoe, Germany

Platinum

Platinum sheet, 99.9% Pt, *ÖGUSSA Ges.m.b.H.,* Wien, Austria

Dimensionally stable anode (DSA®)

De Nora, Ru/TiO_2 (5 g Ru/m^2) supported on Titanium net, Milan, Italy

Nickel

IKA Werke GmbH & Co. KG, Staufen, Germany

Stainless steel (VA 1.4571)

6.3.2. Experimental set-up for electrochemical synthesis in screening cells

The electrochemical reactions were conducted in 5 mL undivided or divided Teflon™ screening cells that are homemade by the university´s mechanical workshop or commercially available as IKA screening system.[136,137,286]

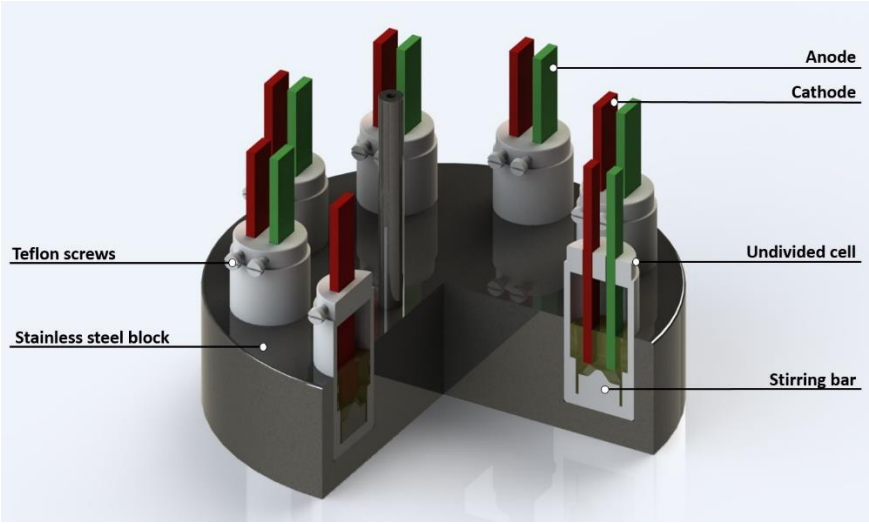

Figure 38. Schematic visualization of 5 ml undivided screening system allowing the simultaneous running of 8 reactions with an interelectrode distance of 5.0 mm.

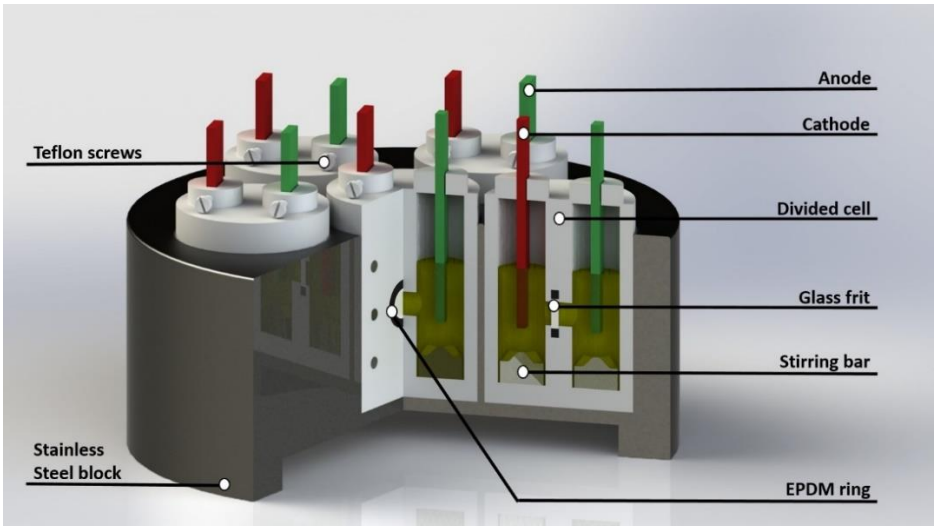

Figure 39. Schematic visualization of divided screening system allowing the simultaneous running of 6 reactions divided by a porous glass frit membrane with an interelectrode distance of 10.0 mm.

6.3.3. Experimental set-up for the electrochemical synthesis in 25 mL cells

5-fold scale-up reactions and control reactions were conducted in an undivided beaker-type Teflon™ cell or undivided beaker-type glass cell with a cooling jacket. The Teflon™ cell consists of a 25 ml beaker and a Teflon™ plug with an interelectrode distance of 10.0 mm. The glass beaker-type cell consists of a 25 mL glass beaker with

a cooling jacket and a Teflon™ plug with an interelectrode distance of 10.0 mm. Electrochemcial synthesis was carried out at glassy carbon, DSA (Ru-IO_2 (Ti net)) and nickel electrodes.

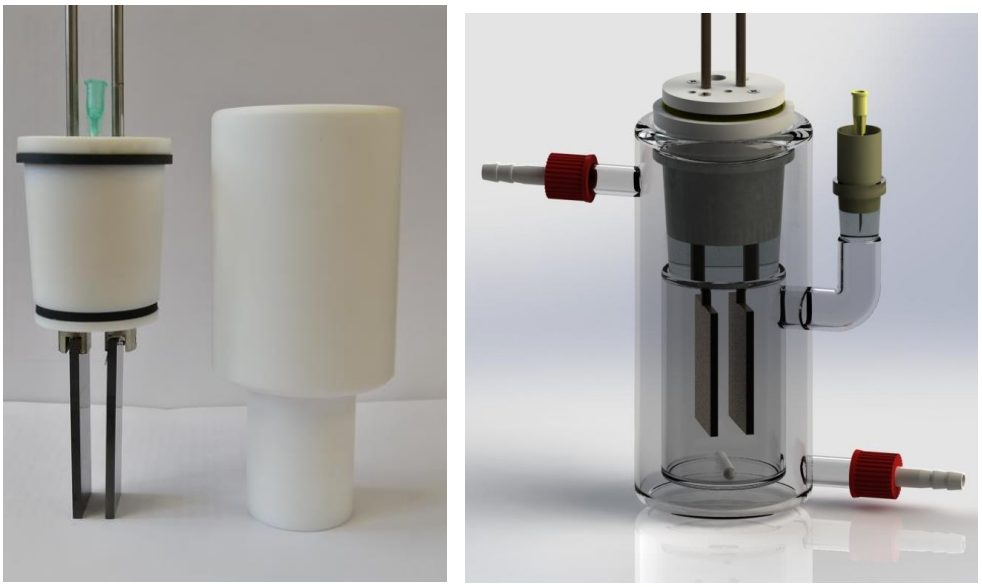

Figure 40. 25 mL Teflon™ beaker-type cell (left) and the schematic representation of beaker-type glass cell (right) with an interelectrode distance of 10.0 mm.

6.3.4. Electrochemical bromination of terpenes

The solvation of metal bromide salt in the solvent system is crucial to the success of the reaction. After reaching reaction temperature, a waiting time of 30 minutes is highly recommended before the addition of terpene to the solution.

6.3.4.1. General protocol for the optimization reactions in undivided screening cells (GP1)

Electrochemical bromination of terpenes was carried out according to literature.[234]

A 5.0 mL solution of sodium bromide (2.1 mmol) in acetonitrile/deionized water (8v/v%) was transferred into an undivided 5 mL screening cell and warmed to 30 °C. After electrolysis temperature was reached, terpene (0.7 mmol) was added via a 100 µL Hamilton™ syringe and electrolyzed at isostatic graphite, glassy carbon, BDD, platinum or stainless-steel electrodes. The immersed part of the electrodes had dimensions of 0.3 x 1.0 x 1.8 cm. A constant current electrolysis with current densities of 5–28 mA/cm^2 was performed at 30 °C. After applying 1.5–5.5 *F*, an aliquant of

approx. 50 µL was taken from the reaction solution and filtered via approx. 245 mg silica gel 60M, whereby 1.5 mL ethyl acetate was used as eluent. The filtrate was examined via GC and GC-MS analysis. The reaction solution was then transferred into a 100 mL separatory funnel followed by the addition of 15.0 mL ethyl acetate and 15.0 mL deionized water. After phase separation, the organic layer was further washed two times with deionized water (15.0 mL). The organic layer was washed with brine, dried over magnesium sulfate, and concentrated under *vacuo*. The product was quantified *via* ^{1}H NMR using CH_2Br_2 as internal standard. In most cases, the crude product was spectroscopically pure.

6.3.4.2. General protocol for the optimization reactions in divided screening cells (GP2)

A solution of sodium bromide (2.1 mmol) in 5 mL of solvent mixture constructed of acetonitrile (4.6 mL) and deionized water (0.4 mL, 8 v/v%) was transferred into the anodic compartment of PTFE cell. The same step was repeated for the cathodic compartment. The cell is warmed to 30 °C. Once the electrolysis temperature was reached, terpene (0.7 mmol) was added to the anodic compartment via a 100 µL Hamilton™ syringe and electrolyzed at glassy carbon electrodes. A constant current electrolysis with a current density of 5 mA/cm^2 was performed at 30 °C. After applying 4.5 *F*, an aliquant of approx. 50 µL was taken from the reaction solution and filtered via approx. 245 mg silica gel 60 M, whereby 1.5 mL ethyl acetate was used as eluent. The filtrate was examined via GC and GC-MS analysis. The reaction solution was then transferred into a 100 mL separatory funnel followed by the addition of 15 mL ethyl acetate and 15 mL deionized water. After phase separation, the organic layer was further washed two times with deionized water (15.0 mL). The organic layer was washed with brine, dried over magnesium sulfate and concentrated under *vacuo*.

6.3.4.3. General protocol for the electrochemical synthesis in 25 mL PTFE cell (GP3)

A solution of sodium bromide (10.5 mmol) in 25.0 mL solvent mixture constructed of acetonitrile (23.0 mL) and deionized water (2.0 mL, 8 v/v%) was transferred into an undivided 25.0 mL PTFE cell warmed to 30 °C. Once the electrolysis temperature was reached, terpene (3.5 mmol) was added via a 500 µL Hamilton™ syringe and

electrolyzed at glassy carbon electrodes. A constant current electrolysis with a current density of 5 mA/cm^2 was performed at 30 °C. After applying 3.0 *F*, an aliquant of approx. 50 µL was taken from the reaction solution and filtered via approx. 245 mg silica gel 60M, whereby 1.5 mL ethyl acetate was used as eluent. The filtrate was examined via GC and GC-MS analysis. The reaction solution was then transferred into a 250.0 mL separatory funnel followed by the addition of 80 mL ethyl acetate and 80 mL deionized water. After phase separation, the organic layer was washed two times with deionized water (80 mL). The organic layer was washed with brine, dried over magnesium sulfate and concentrated under *vacuo*. The product was quantified by ^{1}H NMR using CH_2Br_2 as internal standard.

6.3.5. Electrochemical control reactions

6.3.5.1. Control reaction with TEMPO (**43**)

Reaction was carried out according to GP1, where (4*S*)-(–)-limonene (**30**) was used as terpene. A solution of **30** (0.7 mmol), NaBr (2.1 mmol), TEMPO (**43**, 2.1 mmol) in MeCN/H_2O (5 mL, 8 v/v%) was electrolyzed at glassy carbon electrodes with a current density of j = 5 mA/cm^2 (9 mA/1.8cm^2) at 30 °C. After applying 1.5 *F*, the reaction mixture was analyzed qualitatively via GC method.

6.3.5.2. Control reaction with NaCN

Reaction was carried out according to GP1, where (4*S*)-(–)-limonene (**30**) was used as terpene. A solution of **30** (0.7 mmol), NaBr (2.1 mmol), NaCN (1.4 mmol) in MeCN/H_2O (5 mL, 8 v/v%) was electrolyzed at glassy carbon electrodes with a current density of j = 5 mA/cm^2 (9 mA/1.8cm^2) at 30 °C. After applying 1.5 *F*, the reaction mixture was analyzed qualitatively via GC method.

6.3.6. Electrochemical α-haloenone formation (GP4)

Sodium halide (1.5 mmol), water (11.1 mmol., 0.2 mL) was added to a 5.0 mL solvent mixture of acetonitrile/dimethyl sulfoxide (8 v/v%) and transferred into an undivided 5 mL screening cell and warmed to 60 °C. Once the electrolysis temperature was reached, cyclohex-1-one (**45**, 0.5 mmol) was added to the reaction solution via a

100 µL Hamilton™ syringe and electrolyzed at graphite electrodes. A constant current electrolysis was performed with a current density of 10 mA/cm^2 (18 mA/1.8cm^2). After applying 4.0 *F*, an aliquant of approx. 50 µL was taken from the reaction solution and filtered via approx. 245 mg silica gel 60M, whereby 1.5 mL ethyl acetate was used as eluent. The filtrate was examined via GC and GC-MS analysis. The reaction solution was then transferred into a 100 mL separatory funnel followed by the addition of 15.0 mL ethyl acetate and 15.0 mL deionized water. After phase separation, the organic layer was washed two times with deionized water (15 mL). The organic layer was washed with brine, dried over magnesium sulfate and concentrated under *vacuo* to give the spectroscopically pure compound. The product was quantified by ^{1}H NMR using CH_2Br_2 as internal standard.

6.3.7. Electrochemical halolactonization of alkenoic acids (GP5)

A 5.0 mL solution of sodium halide (2.1 mmol) in a solvent mixture of acetonitrile/deionized water (8 v/v%) was transferred into an undivided 5 mL screening cell. Alkenoic acid (**49**, 0.7 mmol) was added to the solution and electrolyzed at graphite electrodes. A constant current electrolysis with a current density of 5 mA/cm^2 (9 mA/1.8cm^2) was performed at room temperature (25 °C). After applying 2.0 *F*, an aliquant of approx. 50 µL was taken from the reaction solution and filtered via approx. 245 mg silica gel 60M, whereby 1.5 mL ethyl acetate was used as eluent. The filtrate was examined via GC and GC-MS analysis. The reaction solution was then transferred into a 100 mL separatory funnel followed by the addition of 15.0 mL ethyl acetate and 15.0 mL deionized water. After phase separation, the organic layer was further washed two times with deionized water (15.0 mL). The organic layer was washed with brine, dried over magnesium sulfate, and concentrated under *vacuo* to give the spectroscopically pure compound. The product was quantified by ^{1}H NMR using CH_2Br_2 as internal standard.

6.3.8. Electrochemical Hofmann rearrangement of urea derivatives

6.3.8.1. General electrochemical conditions (GP6)

The synthesis of precursors was carried out according to literature (Section 6.5).[257]

The reaction conditions for the electrochemical Hofmann rearrangement of urea derivatives were adapted from S. Zhang et al.[254]

A solution of urea (0.5 mmol), sodium halide (0.25–1.50 mmol) in 5.0 mL solvent mixture of acetonitrile/methanol, acetonitrile/water, acetonitrile or alcohol was transferred to a 5.0 mL screening cell and warmed to 30–60 °C. A constant current electrolysis was performed with a current density of 5.0–6.7 mA/cm^2. The reaction was monitored via TLC, GC and GC-MS methods. After electrolysis, the reaction solution was reduced under reduced pressure and subjected to column chromatography (cyclohexane/ethyl acetate, cyclohexane/dichloromethane or dichloromethane/methanol) to yield the corresponding azobenzene, carbamate or urea derivatives.

6.3.8.2. General electrochemical conditions using electrochemically generated HOCl in PTFE cell (GP7)

The reaction conditions for the electrochemical Hofmann rearrangement of urea derivatives were adapted from the chlor-alkali electrolysis.[153]

A solution of urea (0.5 mmol), sodium halide (25 mmol), sodium hydroxide (5 mmol) in 5 mL deionized water was transferred to a 5.0 mL screening cell and cooled to 5 °C. A constant current electrolysis was performed with a current density of 100–200 mA/cm2. The reaction was monitored via TLC, TLC-MS, GC and GC-MS methods. After electrolysis, the reaction solution was heated to 35 °C and kept on this temperature whilst continuously stirring. Following that, it was acidified with 1 M aq. HCl to pH 1, where upon vigorous gas evolution was observed. The reaction solution was stirred for 15 mins, basified with 1 M aq. NaOH to pH 9. Eventually, the reaction solution was extracted with dichloromethane (3x25 mL). The organic phase was dried with $MgSO_4$ and concentrated under vacuo.

6.3.8.3. General electrochemical conditions using electrochemically generated HOCl in beaker-type cell with a cooling jacket (GP8)

The reaction conditions for the electrochemical Hofmann rearrangement of urea derivatives were adapted from the chlor-alkali electrolysis.[153]

A solution of urea (0.5 mmol), sodium halide (50 mmol), sodium hydroxide (10 mmol) in 10 mL deionized water was transferred to a 25 mL beaker-type glass cell with a

cooling jacket and cooled to 0 °C. A constant current electrolysis was performed with a current density of 200 mA/cm^2 using a stirring rate of 400 rpm. The reaction was monitored via TLC, TLC-MS, GC and GC-MS methods. After electrolysis, the reaction solution was heated to 60 °C and kept at this temperature whilst continuously stirring. Followed, it was acidified with 1 M aq. HCl to pH 5 or pH 7 and let to cool to room temperature. Eventually, the reaction solution was extracted with MeCN using the salting out method. The organic phase was dried with $MgSO_4$ and concentrated under vacuo.

6.4. General protocol for the conventional bromination of **30**

6.4.1. Protocol for the conventional bromination using Br_2

(4*S*)-(–)-limonene (**30**) was subjected to dibromination method using elemental bromine.[237]

Bromine (99.6%, 0.7 mmol) was added dropwise to the continuously stirring solution of **30** (0.7 mmol) and dichloromethane (2.0 mL) at 0 °C. The solution remained transparent. After 30 minutes, the solution was left to warm to room temperature and it was quenched with 2 mM aq. metabisulfite solution. The organic layer was washed with brine, dried over $MgSO_4$, and concentrated under *vacuo*. The product was quantified by ^{1}H NMR using CH_2Br_2 as internal standard.

6.4.2. Protocol for the conventional bromination using DMSO/HBr system

(4*S*)-(–)-limonene (**30**) was subjected to dibromination method published by Jiao et al.[238]

HBr (aq. 48 w/w%, 1.6 mmol) was added to a continuously stirring solution of **30** (0.7 mmol), DMSO (0.8 mmol) and ethyl acetate at 60 °C. The solution turned from transparent to bright orange. After 30 minutes, the solution was left to cool down to room temperature and it was concentrated under vacuo. The product was quantified by ^{1}H NMR using CH_2Br_2 as internal standard.

6.5. General protocol for the synthesis of urea precursors

The urea precursors were synthesized according to the adjusted protocol adopted from D. Mahajan et al.[257]

KOCN (2.2 eq.) was added in two portions to a stirring solution of amine **5** (5.0–20.0 mmol) dissolved in 7.5–30.0 mL solution mixture consisting of aq. HCl (1 M) and methanol (5 v/v%) at 0 °C. The mixture was left to stir at 0 °C for 10 minutes, followed by stirring overnight at room temperature. After reaction completion, the solvent was distilled off under reduced pressure and the crude mixture was subjected to column chromatography (DCM/MeOH 5%) or recrystallization to yield the desired urea derivative.

6.6. General protocol for the Hofmann rearrangement using PIDA

The general procedure was carried out according to literature.[270]

Phenyliodine(III) diacetate (0.65 mmol) was added to the solution of the substrate (0.5 mmol), KOH (1.25 mmol) in 5 mL MeOH at 0 °C and let to stir for 15 minutes. The reaction mixture was warmed to room temperature and stirred overnight. The rection was monitored via TLC and GC and GC-MS. After reaction completion, the mixture was extracted with EtOAc/H_2O and concentrated under *vacuo*. The crude product was isolated via column chromatography.

6.7. General protocol for the Hofmann rearrangement using NBS/DBU

The general procedure was carried out according to literature.[55]

DBU (1.15 mmol) was added to a stirring solution of the substrate (0.50 mmol) and NBS (1.00 mmol) at room temperature. The reaction mixture was refluxed for 15 mins, where NBS (1.00 mmol) was added again, and refluxed for an additional 30 mins. The rection was monitored via TLC and GC and GC-MS. After reaction completion, the mixture was concentrated under reduced pressure and extracted with EtOAc/H_2O. The crude product was isolated via column chromatography.

6.8. Characterization

6.8.1. Methyl *N*-phenylcarbamate (**6d**)

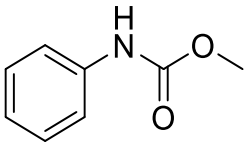

6d was prepared according to protocol adopted from J. Lichtenecker et al.[55]

According to section 6.7, 1,8-diazabicyclo(5.4.0)undec-7-ene (171 µL, 1.15 mmol, 2.3 eq.) was added to a continuously stirring solution of benzamide (**4**, 61 mg, 0.50 mmol, 1.0 eq.), *N*-bromosuccinimide (90 mg, 1.00 mmol, 2.0 eq.) in 11.3 mL methanol at room temperature. The resulting solution was refluxed for 15 minutes, followed by the further addition of NBS (90 mg, 1.00 mmol, 2.0 eq.) and refluxed for an additional 30 minutes.

After reaction completion, the solvent was evaporated under reduced pressure. The crude product was subjected to manual column chromatography (CH/EA 50%) to yield **6d** (69 mg, 0.46 mmol, 91%) as a yellow oil.

^{1}H NMR (400 MHz, $CDCl_3$): δ [ppm] = 7.39–7.37 (m, 2H), 7.33–7.28 (m, 2H), 7.09–7.04 (m, 1H), 6.70 (bs, 1H), 3.78 (s, 3H).

^{13}C NMR (101 MHz, $CDCl_3$): δ [ppm] = 154.2, 138.0, 129.2, 123.6, 118.9, 52.5.

HRMS for $C_8H_{10}NO^+$ (ESI+) $[M+H]^+$: calc.:152.0706, found: 152.0700.

R*f* = 0.73 (CH/EA 50%).

GC: t_R 7.315 min.

The spectroscopic data are in accordance with literature.[55,287]

6.8.2. Methyl *N*-(4-bromophenyl)carbamate (**6da**)

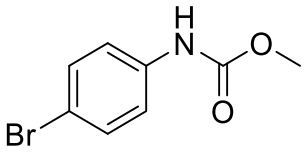

6da was prepared according to protocol adopted from J. Lichtenecker et al.[55]

According to section 6.7, 1,8-diazabicyclo(5.4.0)undec-7-ene (171 µL, 1.15 mmol, 2.3 eq.) was added to a continuously stirring solution of *N*-phenylurea (68 mg, 0.50 mmol, 1.0 eq.), *N*-bromosuccinimide (90 mg, 1.00 mmol,

2.0 eq.) in 11.3 mL methanol at room temperature. The resulting solution was refluxed for 15 minutes, followed by the further addition of NBS (90 mg, 1.00 mmol, 2.0 eq.) and refluxed for an additional 30 minutes.

After reaction completion, the solvent was evaporated under reduced pressure. The crude product was subjected to manual column chromatography (CH/EA 50%) to yield **6da** (7 mg, 0.03 mmol, 6%) as a highly viscous yellow oil.

^{1}H NMR (400 MHz, $CDCl_3$): δ [ppm] = 7.43–7.39 (m, 2H), 7.31–7.26 (m, 2H), 6.64 (bs, 1H), 3.77 (s, 3H).

^{13}C NMR (101 MHz, $CDCl_3$): δ [ppm] = 154.0, 137.1, 129.2, 120.4, 116.1, 52.7.

R*f* = 0.70 (CH/EA 50%).

GC: t_R 12.165 min.

GC-MS: t_R 11.893 min, *m/z* 231.

The spectroscopic data are in accordance with literature.[55,287]

6.8.3. (4*S*)-1,2-Dibromo-*p*-menth-8-ene (**30a**)

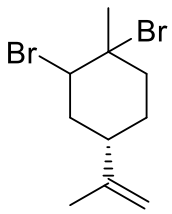

According to the general protocol (GP1), **30** (95 mg, 0.70 mmol, 1.00 eq.) was electrolyzed until 1.5 *F* (101 C) were applied at 5 mA/cm^2 (9 mA/1.8 cm^2). After the extraction procedure, 116 mg of crude product were obtained. NMR quantification with internal standard gave a yield of 54% **30a**. Minor impurities were removed under vacuo to yield **30a** (110 mg, 0.37 mmol, 53%) as a yellow oil.

Diastereomeric ratio 1:1*

The crude product was used for the formation of **44** without further purification.

^{1}H NMR (400 MHz, $CDCl_3$): δ [ppm] = 4.78–4.74 (m, 3H), 2.60–2.51 (m, 2H), 2.13–2.03 (m, 2H), 2.01–1.94 (m, 1H), 2.00 (s, 3H), 1.88–1.72 (m, 2H), 1.74 (s, 3H).

^{13}C NMR (101 MHz, $CDCl_3$): δ [ppm] = 148.5, 109.8, 70.7, 61.4, 38.1, 36.9, 36.5, 35.5, 28.0, 21.1.

The spectroscopic data are in accordance with literature.[234,288]

[*] Diastereomeric ratio was postulated as 1:1 from the crystallographic data and d.r. of **30b**.

6.5.2. (4*S*)-1,2,8,9-Tetrabromo-*p*-menthane (**30b**)

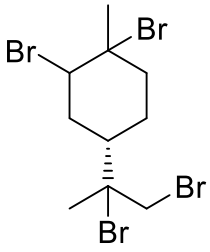

According to the general protocol (GP2), **30** (95 mg, 0.70 mmol, 1.00 eq.) was electrolyzed until 4.5 *F* (304 C) were applied at 5 mA/cm^2 (9 mA/1.8 cm2). After the extraction procedure, minor impurities were removed under vacuo to yield **30b** (236 mg, 0.52 mmol, 74%) as highly viscous oil.

Diastereomeric ratio 1:1 (NMR data refer to both diastereomers).

^{1}H NMR (400 MHz, $CDCl_3$): δ [ppm] = 4.77–4.73 (m, 2H), 4.02 (d, *J* = 10.1 Hz, 1H), 3.95 (d, *J* = 10.1 Hz, 1H), 3.84 (d, *J* = 10.1 Hz, 1H), 3.83 (d, *J* = 10.1 Hz, 1H), 2.76 (ddd, *J* = 14.5 Hz, 11.5 Hz, 3.1 Hz, 1H), 2.65 (ddd, *J* = 14.5 Hz, 11.5 Hz, 3.1 Hz, 1H), 2.30–2.22 (m, 2H), 2.21–2.11 (m, 4H), 2.04–1.98 (m, 3H), 2.00 (s, 3H), 2.00 (s, 3H), 1.91 (s, 3H), 1.87 (s, 3H), 1.87–1.83 (m, 3H).

^{13}C NMR (101 MHz, $CDCl_3$): δ [ppm] = 71.6, 71.6, 69.5, 69.4, 60.7, 60.3, 41.7, 41.4, 38.8, 38.6, 35.9, 35.7, 35.2, 35.2, 34.9, 34.1, 29.4, 29.3, 25.1, 24.8.

The spectroscopic data are in accordance with literature.[10, 232]

Crystallization was performed by dissolving **30b** (50 mg) in dichloromethane (1 mL) and cyclohexane (2 mL) at room temperature, whereby crystals of one diastereomer were obtained. Crystal structure determination of (1*R*,2*R*,4*S*,8*S*)-1,2,8,9-tetrabromo-*p*-menthane (also see Scheme 17): $C_{10}H_{16}Br_4$, M = 455.87 g/mol; colorless plate (0.050 x 0.300 x 0.420 mm^3), T = 120 K, λ(Mo-Kα) = 0.71073 Å, space group $P2_12_12_1$, a = 7.9502(2) Å, b = 18.5812(6) Å, c = 18.7339(4) Å, α = 90(2)°, ß = 90(6)°, γ = 90(4)°, V = 2767.45(13) Å^3 , z = 8, ρ_{xray} = 2.188 mg/m^3 , $2\theta_{max}$ = 56,9°, μ = 11.599 mm^{-1}, F(000) = 1728, 27602 reflections, 6601 unique reflections (R_{int} = 0.0293), final R-values [I > 2σ(I)]: R_1 = 0.0339, *w*R_2 = 0.0728, R-values (all data): R_1 = 0.0406, *w*R_2 = 0.0767, CCDC-2123110.

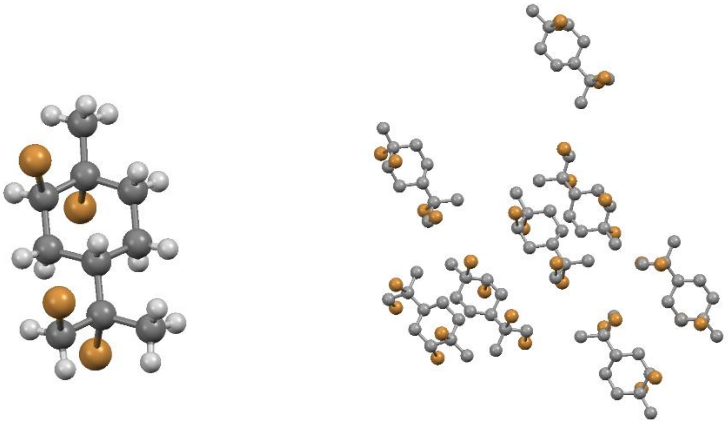

Figure 41. Molecular structure of (1*R*,2*R*,4*S*,8*S*)-1,2,8,9-tetrabromo-*p*-menthane (**30b**) of the unit cell (left) and in packing (right) determined by X-ray analysis. Hydrogen atoms are omitted for better visualization (right).[234]

6.8.4. (4*S*)-8,9-Dibromo-*p*-menth-6-en-2-one (**31**)

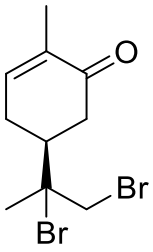

According to general protocol (GP1), (4*S*)-(+)-carvone (105 mg, 0.70 mmol, 1.00 eq.) was electrolyzed until 3.0 *F* (202 C) were applied at 5 mA/cm^2 (9 mA/1.8 cm^2). After the extraction procedure, 178 mg of crude product were obtained. NMR quantification with internal standard gave a yield of 86% **31.** Minor impurities were removed under *vacuo* to yield **31** (178 mg, 0.57 mmol, 82%) as a yellow oil.

Diastereomeric ratio 1:1 (NMR data refer to both diastereomers).

^{1}H NMR (400 MHz, $CDCl_3$): δ [ppm] = 6.78–6.73 (m, 2H), 3.96 (d, *J* = 10.6 Hz, 1H), 3.94 (d, *J* = 10.6 Hz, 1H), 3.86 (d, *J* = 10.6 Hz, 1H), 3.82 (d, *J* = 10.6 Hz, 1H), 2.68–2.35 (m, 10H), 1.89 (s, 3H), 1.88 (s, 3H), 1.80 (s, 6H).

^{13}C NMR (101 MHz, $CDCl_3$): δ [ppm] = 198.7, 198.2, 143.8, 143.6, 135.5, 135.5, 71.2, 71.1, 42.4, 42.1, 40.8, 40.7, 40.7, 40.1, 28.9, 28.5, 28.0, 15.8, 15.7.

The spectroscopic data are in accordance with literature.[234,289]

6.8.5. (4*S*)-8,9-Dibromo-*p*-menth-1-en-7-al (**32**)

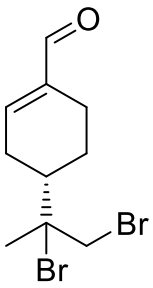

According to general protocol (GP1), (4*S*)-(–)-perillaldehyde (105 mg, 0.7 mmol, 1.00 eq.) was electrolyzed until 3.0 *F* (202 C) were applied at 5 mA/cm^2. (9 mA/1.8 cm^2). After the extraction procedure, 175 mg of crude product were obtained. NMR quantification with internal standard gave a yield of 72% **32**. Minor impurities were removed under *vacuo* to yield **32** (140 mg, 0.45 mmol, 65%) as a yellow oil.

Diastereomeric ratio 1:1 (NMR data refer to both diastereomers).

^{1}H NMR (400 MHz, $CDCl_3$): δ [ppm] = 9.46 (s, 2H), 6.82–6.80 (m, 2H), 4.13 (d, *J* = 10.3 Hz, 1H), 3.97 (d, *J* = 10.3 Hz, 1H), 3.87 (d, *J* = 10.3 Hz, 1H), 3.85 (d, *J* = 10.3 Hz, 1H), 2.61–2.46 (m, 5H), 2.41–2.32 (m, 1H), 2.14–1.93 (m, 6H), 1.95 (s, 3H), 1.89 (s, 3H), 1.88–1.82 (m, 1H), 1.52–1.31 (m, 2H).

^{13}C NMR (101 MHz, $CDCl_3$): δ [ppm] = 193.6, 193.5, 149.3, 149.1, 141.3, 72.0, 71.8, 41.6, 41.5, 41.3, 41.1, 29.3, 29.3, 29.2, 28.7, 24.3, 23.7, 21.7, 21.5.

The spectroscopic data are in accordance with literature.[234]

6.8.6. (4*R*)-1,2-Dibromo-*p*-menthan-4-ol (**33**)

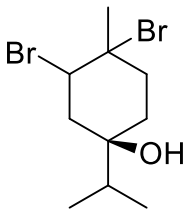

According to general protocol (GP1), (4*R*)-(–)-terpinen-4-ol (108 mg, 0.70 mmol, 1.00 eq.) was electrolyzed until 2.5 *F* (169 C) were applied at 5 mA/cm^2 (9 mA/1.8 cm^2). After the extraction procedure, 112 mg of crude product were obtained. NMR quantification with internal standard gave a yield of 46% **33**. Minor impurities were removed under *vacuo* to yield **33** (96 mg, 0.31 mmol, 44%) as a yellow oil.

Diastereomeric ratio 1:1 (NMR data refer to both diastereomers).

^{1}H NMR (400 MHz, $CDCl_3$): δ [ppm] = 4.87 (dd, *J* = 12.5, 4.6 Hz, 1H), 4.73–4.70 (m, 1H), 2.76 (ddd, *J* = 13.5, 13.5, 4.6 Hz, 1H), 2.72 (dd, *J* = 16.0, 4.4 Hz, 1H), 2.38 (ddd, *J* = 13.6, 4.1, 3.0 Hz, 1H), 2.38–2.37 (m, 1H), 2.24–2.14 (m, 3H), 2.04 (s, 3H),

2.00–1.87 (m, 3H), 1.86 (s, 3H), 1.78–1.72 (m, 1H), 1.66–1.53 (m, 5H), 1.52–1.44 (m, 1H), 0.96 (s, 3H), 0.94 (s, 3H), 0.92 (s, 3H), 0.90 (s, 3H).

^{13}C NMR (101 MHz, $CDCl_3$): δ [ppm] = 75.3, 72.4, 70.8, 68.0, 61.7, 58.4, 43.6, 39.7, 38.9, 38.4, 38.3, 35.0, 33.0, 32.4, 31.7, 24.8, 16.8, 16.8, 16.7, 16.6.

The spectroscopic data are in accordance with literature.[234]

6.8.7. 6,7-Dibromo-7-methyl-3-methyleneoct-1-ene (**34**)

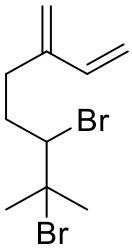

According to general protocol (GP1), myrcene (95 mg, 0.70 mmol, 1.00 eq.) was electrolyzed until 1.5 *F* (101 C) were applied at 5 mA/cm^2 (9 mA/1.8 cm^2). After the extraction procedure, 131 mg of crude product were obtained. NMR quantification with internal standard gave a yield of 46% **34**. The crude residue was subjected to flash column chromatography (cyclohexane, 100%) to yield **34** (70 mg, 0.24 mmol, 34%) as a colorless oil.

Caution is to be taken due to the volatile nature of this product.

^{1}H NMR (400 MHz, $CDCl_3$): δ [ppm] = 6.38 (dd, *J* = 17.5, 11.1 Hz, 1H), 5.30 (d, *J* = 17.5 Hz, 1H), 5.12–5.08 (m, 3H), 4.20 (dd, *J* = 10.7, 1.5 Hz, 1H), 2.71–2.57 (m, 3H), 2.38–2.31 (m, 1H), 1.98 (s, 3H), 1.81 (s, 3H).

^{13}C NMR (101 MHz, $CDCl_3$): δ [ppm] = 144.8, 138.5, 117.1, 114.0, 68.6, 66.5, 35.4, 34.7, 3.2, 28.4.

The spectroscopic data are in accordance with literature.[234,289,290]

6.8.8. 6-Bromo-7-methyl-3-methyleneoct-1,6-diene (**34a**)

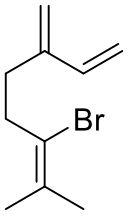

34a was prepared according to literature.[240]

34 (295 mg, 1.00 mmol) in 2 mL DMSO was added via a syringe pump (0.2 mL/min) to a continuously stirring solution of NaCN (196 mg, 4.00 mmol) in 8 mL DMSO at 60 °C under argon atmosphere. After addition, the reaction was left to stir for 30 mins at 60 °C. The reaction was monitored via TLC, GC. Once the reaction was complete, the mixture was left to cool to room

temperature. It was partitioned with 50 mL Et_2O and 50 mL water. The organic phase was washed with water (4 x 50 mL). The organic layer was washed with brine (50 mL), dried over $MgSO_4$ and concentrated under *vacuo*. The residue was subjected to flash column chromatography (cyclohexane/ethyl acetate, 10:0 → 9:1) to yield **34a** (159 mg, 0.74 mmol, 74%) as a transparent oil.

^{1}H NMR (400 MHz, $CDCl_3$): δ [ppm] = 6.36 (dd, 1H, *J* = 17.6, 10.8 Hz), 5.31 (dd, 1H, *J* = 17.6, 1.0 Hz), 5.09 (dd, 1H, *J* = 10.8, 1.0 Hz), 5.03–5.01 (m, 2H), 2.68–2.64 (m, 2H), 2.47–2.43 (m, 2H), 1.87 (s, 3H), 1.74 (s, 3H).

^{13}C NMR (101 MHz, $CDCl_3$): δ [ppm] = 145.3, 138.7, 130.9, 121.4, 116.7, 113.6, 37.0, 30.0, 25.5, 20.5.

GC-MS: t_R 7.762 min, *m/z* 160.

R*f* = 0.9 (Cyclohexane/EtOAc 10%).

6.8.9.5-Methylene-2-(propan-2-ylidene)hept-6-enenitrile (**34b**)

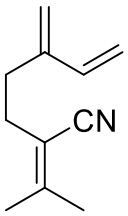

A mixture of **34a** (159 mg, 0.74 mmol) and CuCN (79 mg, 0.88 mmol, 1.2 eq.) in 5 mL DMF was refluxed for 12 h. The reaction was monitored via TLC and GC. After reaction completion, the crude mixture was filtered and washed with 50 mL hexane. The organic layer was washed with water (2 x 50 mL) and brine. The first aq. phase was extracted with hexane (50 mL). The organic layers were combined, washed with brine, dried over $MgSO_4$ concentrated under *vacuo* to give the spectroscopically clean product (**34b**, 26 mg, 0.16 mmol, 22%) as a yellow oil.

^{1}H NMR (400 MHz, $CDCl_3$): δ [ppm] = 6.36 (dd, 1H, *J* = 17.6, 10.8 Hz), 5.26 (dd, 1H, *J* = 17.6, 1.0 Hz), 5.09 (dd, 1H, *J* = 10.8, 1.0 Hz), 5.05 (d, 1H, *J* = 1.0 Hz), 5.03 (d, 1H, *J* = 1.0 Hz), 2.42–2.39 (m, 4H), 3.17 (s, 3H), 1.81 (s, 3H).

^{13}C NMR (101 MHz, $CDCl_3$): δ [ppm] = 152.5, 144.6, 138.4, 119.4, 117.0, 113.7, 109.1, 30.1, 28.9, 24.8, 20.3.

HRMS for $C_{11}H_{15}N^+$ (ESI+) $[M+H]^+$: calc.: 162.1277, found: 162.1274.

R*f* = 0.42 (Cyclohexane/EtOAc 10%).

6.8.10. 6,7-Dibromo-3,7-dimethyloctan-1-al (**35**)

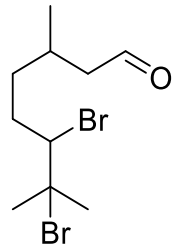

According to general protocol (GP1), citronellal (105 mg, 0.70 mmol, 1.00 eq.) was electrolyzed until 2.0 *F* (135 C) were applied at 5 mA/cm^2 (9 mA/1.8 cm^2). After the extraction procedure, 116 mg of crude product were obtained. NMR quantification with internal standard gave a yield of 46% **35**. Minor impurities were removed under *vacuo* to yield **35** (90 mg, 0.29 mmol, 41%) as a colorless oil.

Diastereomeric ratio 1:1 (NMR data refer to both diastereomers).

^{1}H NMR (400 MHz, $CDCl_3$): δ [ppm] = 9.77 (dd, *J* = 1.7, 1.7 Hz, 2H), 4.16 (dd, *J* = 9.4, 1.7 Hz, 1H), 4.14 (dd, *J* = 9.4, 1.7 Hz, 1H), 2.50–2.40 (m, 4H), 2.43–2.32 (m, 2H), 2.16–2.08 (m, 2H), 1.97 (s, 3H), 1.97 (s, 3H), 1.80 (s, 3H), 1.79 (s, 3H), 1.64–1.57 (m, 2H), 1.53–1.47 (m, 2H), 1,39–1.31 (m, 2H), 1.01 (d, *J* = 7.0 Hz, 3H), 1.00 (d, *J* = 7.0 Hz, 3H).

^{13}C NMR (101 MHz, $CDCl_3$): δ [ppm] = 202.6, 202.5, 69.0, 68.9, 66.8, 66.5, 51.4, 50.6, 35.7, 35.6, 35.5, 33.7, 33.4, 28.1, 28.1, 27.8, 27.3, 20.4, 19.6.

The spectroscopic data are in accordance with literature.[234]

6.8.11. 6,7-Dibromo-3,7-dimethyloct-2-en-1-al (**36**)

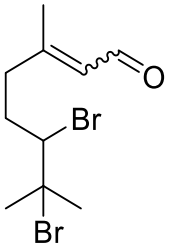

According to general protocol (GP1), citral (E/Z: 2:3) (107 mg, 0.70 mmol, 1.00 eq.) was electrolyzed until 2.0 *F* (135 C) were applied at 5 mA/cm^2 (9 mA/1.8 cm^2). After the extraction procedure, 141 mg of crude product were obtained. NMR quantification with internal standard gave a yield of 54% **36**. Minor impurities were removed under vacuo to yield **36** (110 mg, 0.35 mmol, 50%) as a colorless oil.

Diastereomeric ratio (E/Z) 2:3 (NMR data refer to both diastereomers).

^{1}H NMR (400 MHz, $CDCl_3$): δ [ppm] = 10.05 (d, *J* = 8.0 Hz, 1H), 10.01 (d, *J* = 8.0 Hz, 1H), 5.97–5.95 (m, 2H), 4.11 (dd, *J* = 11.3, 1.4 Hz, 1H), 4.10 (dd, *J* = 11.3, 1.4 Hz, 1H), 3.02–2.92 (m, 1H), 2.80–2.57 (m, 5H), 2.44–2.35 (m, 1H), 2.21 (s, 3H), 2.03 (s, 3H), 2.02 (s, 6H), 1.98 (s, 3H), 1.81 (s, 3H), 1.80 (s, 3H).

^{13}C NMR (101 MHz, $CDCl_3$): δ [ppm] = 191.3, 190.9, 161.6, 161.5, 130.2, 128.3, 68.4, 68.2, 65.0, 64.8, 40.0, 35.6, 34.4, 33.3, 31.0, 28.0, 27.9, 24.8, 17.7.

The spectroscopic data are in accordance with literature.[234]

6.8.12. 5-(2,3-Dibromopropyl)-1,3-benzodioxole (**37**)

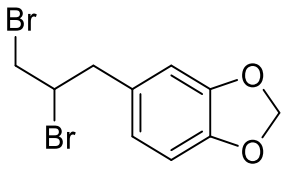

According to general protocol (GP1), 5-allyl-1,3-benzodioxole (113 mg, 0.70 mmol, 1.00 eq.) was electrolyzed until 3.0 *F* (203 C) were applied at 5 mA/cm^2 (9 mA/1.8 cm^2). After the extraction procedure, 187 mg of the crude product were obtained. NMR quantification with internal standard gave a yield of 60% **37**. The crude product was subjected to high performance liquid chromatography (acetonitrile/H_2O 1:1 → 4:1) to yield **37** as a pale, yellow oil (109 mg, 0.34 mmol, 48%).

^{1}H NMR (400 MHz, $CDCl_3$): δ [ppm] = 6.79–6.73 (m, 3H), 5.96 (s, 2H), 4.30 (dddd, *J* = 8.9, 7.6, 4.9, 4.2 Hz, 1H), 3.82 (dd, *J* = 10.5, 4.2 Hz, 1H), 3.62 (dd, *J* = 10.5, 9.0 Hz, 1H), 3.40 (dd, *J* = 14.7, 4.9 Hz, 1H), 3.06 (dd, *J* = 14.7, 7.6 Hz, 1H).

^{13}C NMR (101 MHz, $CDCl_3$): δ [ppm] = 147.8, 146.9, 130.6, 122.9, 110.0, 108.4, 101.2, 52.8, 41.8, 36.0.

The spectroscopic data are in accordance with literature.[234]

6.8.13. 4-(2,3-Dibromopropyl)anisole (**38**)

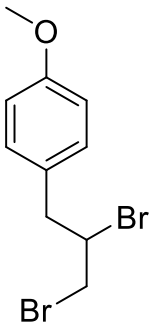

According to general protocol (GP1), 4-allylanisole (104 mg, 0.70 mmol, 1.00 eq.) was electrolyzed until 5.5 *F* (371 C) were applied at 5 mA/cm^2 (9 mA/1.8 cm^2). After the extraction procedure, 165 mg of crude product were obtained. NMR quantification with internal standard gave a yield of 64% **38**. The crude product was subjected to high performance liquid chromatography (acetonitrile/H_2O 1:1 → 4:1) to yield **38** as a colorless oil (119 mg, 0.34 mmol, 56%).

^{1}H NMR (400 MHz, $CDCl_3$): δ [ppm] = 7.26–7.20 (m, 2H), 6.89–6.86 (m, 2H), 4.33 (dddd, *J* = 8.9, 7.6, 4.9, 4.2 Hz, 1H), 3.81 (dd, *J* = 10.5, 4.2 Hz, 1H), 3.81 (s, 3H),

3.62 (dd, *J* = 10.5, 8.9 Hz, 1H), 3.42 (dd, *J* = 14.7, 4.9 Hz, 1H), 3.11 (dd, *J* = 14.7, 7.6 Hz, 1H).

^{13}C NMR (101 MHz, $CDCl_3$): δ [ppm] =158.9, 130.7, 128.9, 114.0, 55.4, 53.0, 41.4, 36.1.

The spectroscopic data are in accordance with literature.[234,291,292]

6.8.14. 4-(2,3-Dibromopropyl)-1,2-dimethoxybenzene (**39**)

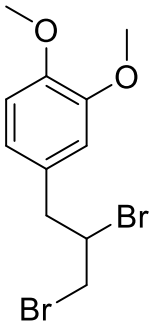

According to general protocol (GP1), 4-allyl-1,2-dimethoxybenzene (125 mg, 0.07 mmol, 1.00 eq.) was electrolyzed until 4.0 *F* (270 C) were applied at 5 mA/cm^2 (9 mA/1.8 cm^2). After the extraction procedure, 204 mg of the crude product were obtained. NMR quantification with internal standard gave a yield of 57% **39**. The crude product was subjected to high performance liquid chromatography (acetonitrile/H_2O 1:1 → 4:1) to yield **39** as a pale, yellow oil (99 mg, 0.29 mmol, 42%).

^{1}H NMR (400 MHz, $CDCl_3$): δ [ppm] = 6.84–6.82 (m, 3H), 4.35 (dddd, *J* = 8.9, 7.6, 5.0, 4.2 Hz, 1H), 3.89 (s, 3H), 3.88 (s, 3H), 3.81 (dd, *J* = 10.5, 4.2 Hz, 1H), 3.61 (dd, *J* = 10.5, 8.9 Hz, 1H) 3.41 (dd, *J* = 14.7, 4.9 Hz, 1H), 3.12 (dd, *J* = 14.7, 7.6 Hz, 1H).

^{13}C NMR (101 MHz, $CDCl_3$): δ [ppm] = 149.0, 148.3, 129.3, 121.9, 112.9, 111.2, 56.1, 52.8, 41.6, 36.2.

The spectroscopic data are in accordance with literature.[234]

6.8.15. 3,4-Dibromocarane (**40**)

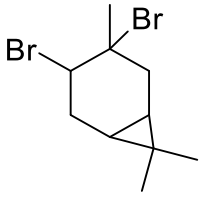

According to general protocol (GP1), 3-carene (95 mg, 0.70 mmol, 1.00 eq.) was electrolyzed until 1.5 *F* (101 C) were applied at 5 mA/cm^2 (9 mA/1.8 cm^2). After the extraction procedure, 73 mg of crude product were obtained. NMR quantification with internal standard gave a yield of 20% **40**.

^{1}H NMR (400 MHz, $CDCl_3$): δ [ppm] = 4.25 (dd, *J* = 10.8, 7.3 Hz, 1H), 2.77 (dd, *J* = 15.0, 10.3 Hz, 1H), 2.54–2.38 (m, 3H), 2.15–2.11 (dd, *J* = 15.0, 4.9 Hz, 1H), 1.91 (s, 3H), 1.03 (s, 3H), 0.97 (s, 3H), 0.83 (ddd, *J* = 9.7, 9.7, 4.9 Hz, 1H), 0.75–0.70 (m, 1H).

^{13}C NMR (101 MHz, $CDCl_3$): δ [ppm] = 68.6, 62.7, 39.2, 31.7, 28.3, 25.6, 21.5, 20.4, 18.2, 15.7.

6.8.16. (4S)-*p*-Mentha-1,8-diene-2-carbonitrile (**44**)

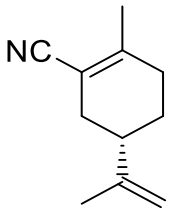

44 was prepared according to a literature.[240]

30a (295 mg, 1.00 mmol) in 2 mL DMSO was added via a syringe pump (0.2 mL/min) to a continuously stirring solution of NaCN (196 mg, 4.00 mmol) in 8 mL DMSO at 60 °C under argon atmosphere. After addition, the reaction was left to stir for 30 mins at 60 °C. The reaction was monitored via TLC, GC. Once the reaction was complete, the mixture was left to cool to room temperature. It was partitioned with 50 mL Et_2O and 50 mL water. The organic phase was washed with water (4 x 50 mL). The organic layer was washed with brine (50 mL), dried over $MgSO_4$ and concentrated under *vacuo*. The residue was subjected to flash column chromatography (cyclohexane/ethyl acetate, 10:0 → 9:1) to yield **44** (79 mg, 0.49 mmol, 49%) as a transparent oil.

^{1}H NMR (400 MHz, $CDCl_3$): δ [ppm] = 4.78–4.78 (m, 1H), 4.72–4.71 (m, 1H), 2.38–2.28 (m, 1H), 2.23–2.11 (m, 4H), 2.00 (s, 3H), 1.87–1.81 (m, 1H), 1.73 (s, 3H), 1.53–1.43 (m, 1H).

^{13}C NMR (101 MHz, $CDCl_3$): δ [ppm] = 153.3, 147.7, 119.2, 110.0, 106.0, 40.0, 32.2, 32.0, 26.7, 22.7, 20.9.

The spectroscopic data are in accordance with literature.[234]

6.8.17. (4S)-*p*-Mentha-1,8-diene-6-ethylether (**44e**)

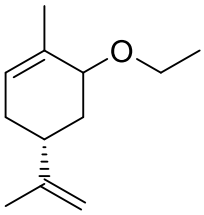

44e was prepared according to literature.[243]

A continuously stirring solution of **30a** (100 mg, 0.33 mmol) and KCN (65 mg, 1.00 mmol) in 2 mL EtOH was refluxed overnight. The reaction was monitored via TLC, GC and GC-MS. Once the reaction was complete, the mixture was concentrated under reduced pressure. The crude product was partitioned with 50 mL Et_2O and 50 mL water. The organic phase was washed with water (2 x 50 mL), then with brine (50 mL), dried over $MgSO_4$ and concentrated under *vacuo*. The residue was subjected to flash column chromatography (cyclohexane/ethyl acetate, 10:0 → 9:1) to yield **44e** (26 mg, 0.14 mmol, 44%) as a yellow oil.

^{1}H NMR (400 MHz, $CDCl_3$): δ [ppm] = 5.60–5.58 (m, 1H), 4.74–4.70 (m, 2H), 3.71-3.64 (m, 1H), 3.61-3.59 (m, 1H), 3.46-3.39 (m, 1H), 2.39–2.32 (m, 1H), 2.17–2.10 (m, 1H), 2.07–2.02 (m, 1H), 1.77 (bs, 3H), 1.74 (bs, 3H), 1.72–1.70 (m, 1H), 1.40 (td, 1H, *J* = 13.30, 3.8 Hz.), 1.22 (t, 3H, *J* = 7.0 Hz).

^{13}C NMR (101 MHz, $CDCl_3$): δ [ppm] = 150.0, 133.29, 125.6, 108.7, 76.1, 65.0, 35.6, 32.2, 31.3, 21.1, 21.1, 16.0.

The spectroscopic data are in accordance with literature.[293]

6.8.18. 2-Bromo-2-cyclohexen-1-one (**45a**)

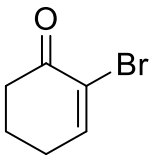

According to GP4, 2-cyclohexene-1-one (**45**, 48 mg, 0.5 mmol, 1.00 eq.) was electrolyzed until 2.0 *F* (97 C) were applied at 10 mA/cm^2 (18 mA/1.8 cm^2). After the extraction procedure, minor impurities were removed under *vacuo* to yield **45a** (8 mg, 0.05 mmol, 9%) as a transparent oil.

^{1}H NMR (400 MHz, $CDCl_3$): δ [ppm] = 7.42 (t, *J* = 7.4 Hz, 1H), 2.65–2.61 (m, 2H), 2.47–2.43 (m, 2H), 2.11–2.04 (m, 2H).

^{13}C NMR (101 MHz, $CDCl_3$): δ [ppm] = 191.4, 151.3, 124.0, 38.5, 28.5, 22.8.

HRMS for $C_6H_7BrONa^+$ (ESI+) $[M+Na]^+$: calc.: 196.9572, found: 196.9563.

The spectroscopic data are in accordance with literature.[37,294]

6.8.19. [1,1´-Bicyclohexyl]-3,3´-dione (**45b**)

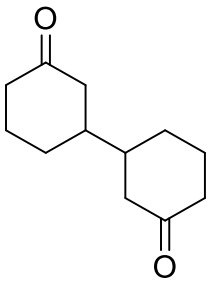

According to GP4, 2-cyclohexene-1-one (**45**, 48 mg, 0.5 mmol, 1.00 eq.) was used as substrate in a 5 mL solvent mixture of acetonitrile/dimethyl sulfoxide (50 v/v%). The reaction solution was electrolyzed until 2.0 *F* (97 C) were applied at 10 mA/cm^2 (18 mA/1.8 cm^2). After the extraction procedure, minor impurities were removed under *vacuo* to yield **45b** (9 mg, 0.046 mmol, 19%) as a transparent oil.

Diastereomeric ratio 1:1. NMR data refers to both diastereomers.

^{1}H NMR (400 MHz, $CDCl_3$): δ [ppm] = 2.47–2.35 (m, 4H), 2.30–2.21 (m, 2H), 2.14–2.04 (m, 4H), 1.94–1.87 (m, 2H), 1.78–1.55 (m, 4H), 1.45–1.33 (m, 2H).

^{13}C NMR (101 MHz, $CDCl_3$): δ [ppm] = 211.4, 211.4, 45.5, 45.0, 43.9, 43.9, 41.5, 28.6, 28.4, 25.4, 25.3.

HRMS for $C_{12}H_{18}O_2K^+$ (ESI+) $[M+K]^+$: calc.: 233.0939, found: 233.0934.

The spectroscopic data are in accordance with literature.[295]

6.8.20. 5-(Bromomethyl)dihydrofuran-2-one (**49a**)

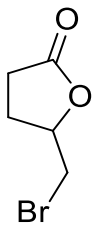

According to GP5, 4-pentenoic acid (**49**, 70 mg, 0.7 mmol, 1.00 eq.) was electrolyzed until 2.0 *F* (135 C) were applied at 5 mA/cm^2 (9 mA/1.8 cm^2). After the extraction procedure, minor impurities were removed under *vacuo* to yield **49a** (61 mg, 0.34 mmol, 49%) as a transparent oil.

^{1}H NMR (400 MHz, $CDCl_3$): δ [ppm] = 4.65 (tt, *J* = 7.1, 4.9 Hz, 1H), 3.51–3.43 (m, 2H), 2.57–2.41 (m, 2H), 2.35–2.28 (m, 1H), 2.02–1.94 (m, 1H).

^{13}C NMR (101 MHz, $CDCl_3$): δ [ppm] = 176.1, 77.7, 34.3, 28.1, 25.8.

GC-MS: t_R 8.097 min, *m/z* 179.

The spectroscopic data are in accordance with literature.[198]

6.8.21. *N*-Butylurea (**51a**)

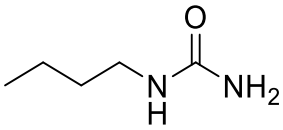

According to section 6.5, 1-butylamine (1.46 g, 0.02 mol, 1.0 eq.) was used as substrate. After reaction completion, the solvent was reduced approximately to half and placed into the fridge overnight. The forming crystals were filtered off, washed with ice cold water and recrystallized from boiling water according to literature to form the desired product **51a** as a white flaky solid (1.11 g, 9.54 mmol, 48%).[282]

^{1}H NMR (400 MHz, DMSO–d_6): δ [ppm] = 5.89 (s, 1H), 5.34 (s, 2H), 2.95–2.91 (m, 2H), 1.34–1.22 (m, 4H), 0.86 (t, *J* = 7.2 Hz, 3H).

^{13}C NMR (101 MHz, DMSO–d_6): δ [ppm] = 158.7, 39.5*, 32.2, 19.6, 13.8.

HRMS for $C_5H_{13}N_2O^+$ (ESI+) $[M+H]^+$: calc.: 117.1023, found: 117.1024.

R*f* = 0.16 (DCM/MeOH 5%).

Mp: 94–96 °C.

* Due to the overlapping signals with the solvent, signal was depicted via HSQC NMR.

The spectroscopic data are in accordance with literature.[257]

6.8.22. 1-Piperidinecarboxamide (**51b**)

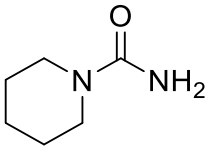

According to section 6.5, piperidine (428 mg, 5.00 mol, 1.0 eq.) was used as substrate. After reaction completion, the solvent was reduced under *vacuo*. The crude product was subjected to manual column chromatography (DCM/MeOH 5%) to yield **51b** (581 mg, 4.53 mmol, 91%) as a white solid.

^{1}H NMR (400 MHz, DMSO–d_6): δ [ppm] = 5.82 (s, 2H), 3.24–3.21 (m, 4H), 1.53–1.48 (m, 2H), 1.42–1.36 (m, 4H).

^{13}C NMR (101 MHz, DMSO–d_6): δ [ppm] = 158.0, 44.3, 25.4, 24.1.

HRMS for $C_6H_{12}N_2ONa^+$ (ESI+) $[M+Na]^+$: calc.: 151.0842, found: 151.0847.

R*f* = 0.32 (DCM/MeOH 5%).

Mp: 104–105 °C.

The spectroscopic data are in accordance with literature.[257,296]

6.8.23. 4-Morpholinecarboxamide (**51c**)

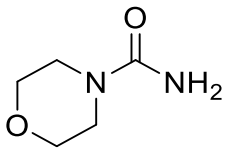

According to section 6.5, morpholine (431 mg, 5.00 mol, 1.0 eq.) was used as substrate. After reaction completion, the solvent was reduced under *vacuo*. The crude product was subjected to manual column chromatography (DCM/MeOH 5%) to yield **51c** (604 mg, 4.64 mmol, 93%) as a white solid.

^{1}H NMR (400 MHz, DMSO–d_6): δ [ppm] = 6.02 (s, 2H), 3.52–3.50 (m, 4H), 3.24–3.22 (m, 4H).

^{13}C NMR (101 MHz, DMSO–d_6): δ [ppm] = 158.3, 66.0, 43.8.

HRMS for $C_5H_{11}N_2O_2^+$ (ESI+) $[M+H]^+$: calc.: 131.0815, found: 131.0821.

R*f* = 0.30 (DCM/MeOH 5%).

Mp: Decomposes over 195 °C.

The spectroscopic data are in accordance with literature.[257,297]

6.8.24. *N*-Phenylurea (**51d**)

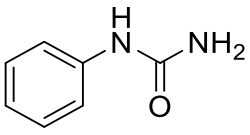

According to section 6.5, aniline (456 mg, 5.00 mol, 1.0 eq.) was used as substrate. After reaction completion, the solvent was reduced under *vacuo*. The crude product was subjected to manual column chromatography (DCM/MeOH 5%) to yield **51d** (651 mg, 4.79 mmol, 96%) as a white solid.

^{1}H NMR (400 MHz, DMSO–d_6): δ [ppm] = 8.55 (s, 1H), 7.40–7.34 (m, 2H), 7.22–7.18 (m, 2H), 6.90–6.89 (m, 1H), 5.85 (s, 2H).

^{13}C NMR (101 MHz, DMSO–d_6): δ [ppm] = 156.0, 140.6, 128.6, 121.0, 117.8.

HRMS for $C_7H_9N_2O^+$ (ESI+) $[M+H]^+$: calc.: 137.0709, found: 137.0712.

R*f* = 0.32 (DCM/MeOH 5%).

Mp: 104–105 °C.

The spectroscopic data are in accordance with literature.[257,298]

6.8.25. *N*-(4-Bromophenyl)urea (**51da**)

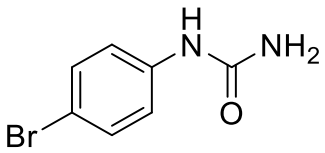

According to GP6, a solution of *N*-phenylurea (**51d**, 68 mg, 0.50 mmol, 1 eq.), hydrobromic acid (303 mg, 1.5 mmol, 3 eq.) in 5.0 mL solvent mixture of acetonitrile/H_2O (10 v/v%) was transferred to a 5.0 mL screening cell and warmed to 30 °C. After reaction temperature was reached, the solution was electrolyzed at platinum electrodes until 2.0 *F* (97 C) were applied at 5 mA/cm^2 (9 mA/1.8cm^2). After electrolysis, the reaction was reduced under vacuo and subjected to column chromatography (CH/EA 50→100%) to yield **51da** (48 mg, 0.22 mmol, 45%) as a white solid.

^{1}H NMR (400 MHz, DMSO–d_6): δ [ppm] = 8.66 (s, 1H), 7.37 (s, 4H), 5.90 (s, 2H).

^{13}C NMR (101 MHz, DMSO–d_6): δ [ppm] = 155.8, 140.0, 131.3, 119.6, 112.3.

HRMS for $C_7H_8{}^{79}BrN_2O^+$ (ESI+) $[M+H]^+$: calc.:214.9815, found: 214.9809.

GC: t_R 12.155 min.

R*f* = 0.33 (EA 100%).

Mp: Decomposes over 205 °C.

The spectroscopic data are in accordance with literature.[296]

6.8.26. *N*-(2,4-Dibromophenyl)urea (**51db**)

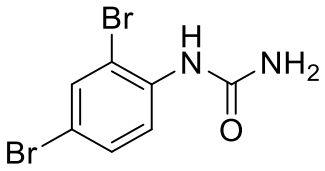

According to GP6, a solution of *N*-phenylurea (**51d**, 68 mg, 0.50 mmol, 1 eq.), hydrobromic acid (303 mg, 1.5 mmol, 3 eq.) in 5.0 mL solvent mixture of acetonitrile/H_2O (10 v/v%) was transferred to a 5.0 mL screening cell and warmed to 30 °C. After reaction temperature was reached, the solution was electrolyzed at platinum electrodes until 2.0 *F* (97 C) were applied at 5 mA/cm^2 (9 mA/1.8cm^2). After electrolysis, the reaction was reduced under vacuo and subjected to column chromatography (CH/EA 50→100%) to yield **51db** (6 mg, 0.02 mmol, 4%) as a white solid.

^{1}H NMR (400 MHz, DMSO–d_6): δ [ppm] = 8.04 (d, *J* = 9.0 Hz, 1H), 7.94 (s, 1H), 7.77 (d, *J* = 2.3 Hz, 1H), 7.46 (dd, *J* = 9.0, 2.3 Hz, 1H), 6.48 (s, 2H).

^{13}C NMR (101 MHz, DMSO–d_6): δ [ppm] = 155.4, 137.5, 134.0, 130.7, 122.9, 113.4, 112.9.

GC: t_R 12.902 min.

R*f* = 0.37 (CH/EA 50%).

6.8.27. *N*-(3-Bromophenyl)urea (**51e**)

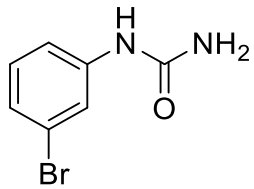

According to section 6.5, 3-bromoaniline (860 mg, 5.00 mol, 1.0 eq.) was used as substrate. After reaction completion, the forming precipitate was filtered off, washed with ice cold water (10 mL) to form **51e** (959 mg, 4.46 mmol, 89%) as an off-white solid.

^{1}H NMR (400 MHz, DMSO–d_6): δ [ppm] = 8.75 (s, 1H), 7.84–7.83 (m, 1H), 7.21 (ddd, *J* = 8.0, 2.0, 1.3 Hz, 1H), 7.16 (dd, *J* = 8.0, 8.0 Hz, 1H), 7.05 (ddd, *J* = 8.0, 2.0, 1.2 Hz, 1H), 5.90 (bs, 2H).

^{13}C NMR (101 MHz, DMSO–d_6): δ [ppm] = 155.8, 142.3, 130.5, 123.5, 121.7, 119.9, 116.5.

HRMS for $C_7H_8{}^{79}BrN_2O^+$ (ESI+) $[M+H]^+$: calc.: 214.9815, found: 214.9813.

R*f* = 0.37 (DCM/MeOH 5%).

Mp: Decomposes over 150 °C.

The spectroscopic data are in accordance with literature.[257,299]

6.8.28. *N*-(3,4-Dichlorophenyl)urea (**51f**)

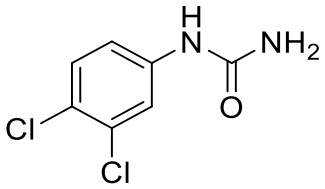

According to section 6.5, 3,4-dichloroaniline (810 mg, 5.00 mol, 1.0 eq.) was used as substrate. After reaction completion, the solvent was reduced under *vacuo*. The crude product was subjected to manual column chromatography (DCM/MeOH 5%) to yield **51f** (501 mg, 2.44 mmol, 49%) as an off-white solid.

^{1}H NMR (400 MHz, DMSO–d_6): δ [ppm] = 8.85 (s, 1H), 7.85 (d, *J* = 2.4 Hz, 1H), 7.43 (d, *J* = 8.8 Hz, 1H), 7.24 (dd, *J* = 8.8, 2.4 Hz, 1H), 6.03 (s, 2H).

^{13}C NMR (101 MHz, DMSO–d_6): δ [ppm] = 155.7, 140.8, 130.9, 130.4, 122.2, 118.7, 117.8.

HRMS for $C_7H_7{}^{35}Cl_2N_2O^+$ (ESI+) $[M+H]^+$: calc.: 204.9930, found: 204.9929.

R*f* = 0.37 (DCM/MeOH 5%).

Mp: 153–155 °C.

The spectroscopic data are in accordance with literature.[257,300]

6.8.29. *N*-Methyl-*N*-phenylurea (**51g**)

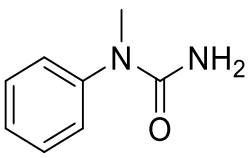

According to section 6.5, *N*-methylaniline (536 mg, 5.00 mol, 1.0 eq.) was used as substrate. After reaction completion, the solvent was reduced under *vacuo*. The crude product was subjected to manual column chromatography (DCM/MeOH 5%) to yield **51g** (747 mg, 4.97 mmol, 99%) as a white solid.

^{1}H NMR (400 MHz, DMSO–d_6): δ [ppm] = 7.38–7.32 (m, 2H), 7.28–7.25 (m, 2H), 7.21–7.17 (m, 1H), 5.78 (s, 2H), 3.12 (s, 3H).

^{13}C NMR (101 MHz, DMSO–d_6): δ [ppm] = 157.4, 144.5, 129.0, 126.1, 125.4, 37.0.

HRMS for $C_8H_{11}N_2O^+$ (ESI+) $[M+H]^+$: calc.: 151.0868, found: 151.0866.

R*f* = 0.44 (DCM/MeOH 5%).

Mp: 73–75 °C.

The spectroscopic data are in accordance with literature.[257,301]

6.8.30. *N,N´*-Dibutyloxalamide (**53**) and methyl *N*-(Butylcarbamoyl)carbamate (**54a**)

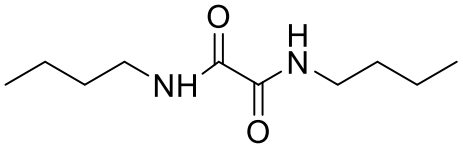

53

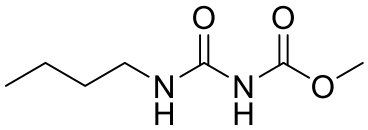

54a

According to GP6, a solution of 1-butylurea (**51a**, 58 mg, 0.50 mmol, 1 eq.), sodium bromide (15 mg, 0.25 mmol, 0.5 eq.) in 5.0 mL solvent mixture of acetonitrile/MeOH (10 v/v%) was transferred to a 5.0 mL screening cell and warmed to 30 °C. After reaction temperature was reached, the solution was electrolyzed at graphite electrodes until 4.0 *F* (194 C) were applied at 5 mA/cm^2 (9 mA/1.8cm^2). After electrolysis, the reaction was reduced under vacuo and subjected to column chromatography (DCM/MeOH 5%) to yield a mixture of **53** (8 mg, 0.04 mmol, 15%) and **54a** (2 mg, 0.01 mmol, 3%) as an orange solid.

Product ratio **53**:**54a** = 1:2.9 was determined via NMR studies.

53:[302]

^{1}H NMR (400 MHz, DMSO–d_6): δ [ppm] = 8.83 (t, *J* = 5.8 Hz, 2H),.3.22 (td, *J* = 7.0, 5.7 Hz, 4H), 1.53–1.45 (m, 4H), 1.36–1.28 (m, 4H), 0.89 (t, *J* = 7.3 Hz, 6H).

^{13}C NMR (101 MHz, DMSO–d_6): δ [ppm] = 161.7, 39.7, 30.9, 19.4, 13.6.

R*f* = 0.55 (DCM/MeOH 5%).

The spectroscopic data are in accordance with literature.[302]

54a:

^{1}H NMR (400 MHz, DMSO–d_6): δ [ppm] = 9.98 (s,1H), 7.74 (t, *J* = 5.5 Hz, 1H), 3.64 (s, 3H), 3.14 (td, *J* = 7.0, 5.7 Hz, 2H), 1.39–1.37 (m, 2H), 1.28–1.26 (m, 2H), 0.87 (t, *J* = 7.3 Hz, 3H).

^{13}C NMR (101 MHz, DMSO–d_6): δ [ppm] = 155.1, 152.7, 52.3, 38.7, 31.3, 19.5, 13.6.

HRMS for $C_7H_{14}N_2O_3Na^+$ (ESI+) $[M+Na]^+$: calc.: 197.0896, found: 197.0877.

GC-MS: t_R 8.948 min, *m/z* 174.

R*f* = 0.55 (DCM/MeOH 5%).

6.8.31. *N,N'*-Dibutylimidodicarbonic diamide (**55**)

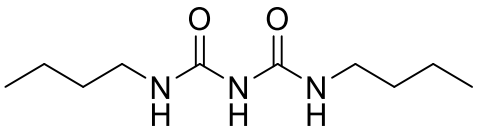

According to GP6, a solution of 1-butylurea (**51a**, 58 mg, 0.50 mmol, 1 eq.), sodium bromide (15 mg, 0.25 mmol, 0.5 eq.) in 5.0 mL solvent mixture of acetonitrile/MeOH (10 v/v%) was transferred to a 5.0 mL screening cell and warmed to 30 °C. After reaction temperature was reached, the solution was electrolyzed at graphite electrodes until 4.0 *F* (194 C) were applied at 5 mA/cm^2 (9 mA/1.8cm^2). After electrolysis, the reaction was reduced under vacuo and subjected to column chromatography (DCM/MeOH 5%) to yield **55** (5 mg, 0.02 mmol, 9%) as an orange solid.

^{1}H NMR (400 MHz, DMSO–d_6): δ [ppm] = 8.50 (s,1H), 7.33 (bs, 2H), 3.07 (td, *J* = 7.0, 5.7 Hz, 4H), 1.42–1.35 (m, 4H), 1.31–1.24 (m, 4H), 0.87 (t, *J* = 7.3 Hz, 6H).

^{13}C NMR (101 MHz, DMSO–d_6): δ [ppm] = 154.50, 38.4, 31.5, 19.5, 13.6.

HRMS for $C_{10}H_{21}N_3O_2Na^+$ (ESI+) $[M+Na]^+$: calc.: 238.1526, found: 238.1521.

R*f* = 0.37 (DCM/MeOH 5%).

6.8.32. *N,N´*-Dibutylurea (**56a**)

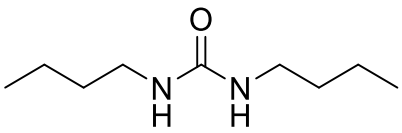

According to GP6, a solution of 1-butylurea (**51a**, 58 mg, 0.50 mmol, 1 eq.), sodium chloride (15 mg, 0.25 mmol, 0.5 eq.) in 5.0 mL solvent mixture of acetonitrile/water (10 v/v%) was transferred to a 5.0 mL screening cell and warmed to 30 °C. After reaction temperature was reached, the solution was electrolyzed at graphite electrodes until 2.0 *F* (97 C) were applied at 5 mA/cm^2 (9 mA/1.8cm^2). After electrolysis, the reaction was reduced under vacuo and subjected to column chromatography (DCM/MeOH 5%) to yield **56a** (12 mg, 0.07 mmol, 28%) as a white solid.

^{1}H NMR (400 MHz, DMSO–d_6): δ [ppm] = 5.72 (t, *J* = 5.5 Hz, 2H), 2.97–2.93 (m, 4H), 1.34–1.22 (m, 8H), 0.86 (t, *J* = 7.2 Hz, 2H).

^{13}C NMR (101 MHz, DMSO–d_6): δ [ppm] = 158.1, 38.9, 32.2, 19.6, 13.8.

GC-MS: t_R 7.936 min, *m/z* 172.

R*f* = 0.31 (DCM/MeOH 5%).

The spectroscopic data are in accordance with literature.[303]

6.8.33. 1,1´-Carbonyldipiperidine (**56b**)

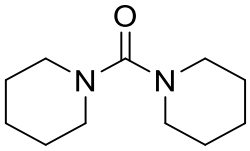

According to GP6, a solution of piperidine-1-carboxamide (**51b**, 64 mg, 0.50 mmol, 1 eq.), sodium chloride (15 mg, 0.25 mmol, 0.5 eq.) in 5.0 mL solvent mixture of acetonitrile/water (10 v/v%) was transferred to a 5.0 mL screening cell and warmed to 30 °C. After reaction temperature was reached, the solution was electrolyzed at graphite electrodes until 2.0 *F* (97 C) were applied at 5 mA/cm^2 (9 mA/1.8cm^2). After electrolysis, the reaction was reduced under vacuo and subjected to column chromatography (DCM/MeOH 5%) to yield **56b** (10 mg, 0.05 mmol, 20%) as a highly viscous oil.

^{1}H NMR (400 MHz, MeOH–d_4): δ [ppm] = 3.21–3.18 (m, 8H), 1.64–1.53 (m, 12H).

^{13}C NMR (101 MHz, MeOH–d_4): δ [ppm] = 164.7*, 49.1, 26.9, 25.7.

*Due to low substance amount, the assigned signal was depicted via HMBC NMR ($^3J_{C–H}$). See figure 56 in section 10.

R*f* = 0.50 (DCM/MeOH 5%).

GC-MS: t_R 11.259 min, *m/z* 196.

The spectroscopic data are in accordance with literature.[304]

6.8.34. 4,4´-Carbonyldimorpholine (**56c**)

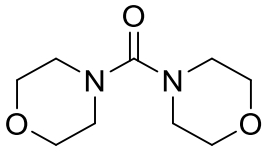

According to GP6, a solution of morpholine-4-carboxamide (**51c**, 65 mg, 0.50 mmol, 1 eq.), sodium chloride (15 mg, 0.25 mmol, 0.5 eq.) in 5.0 mL solvent mixture of acetonitrile/water (10 v/v%) was transferred to a 5.0 mL screening cell and warmed to 30 °C. After reaction temperature was reached, the solution was electrolyzed at graphite electrodes until 2.0 *F* (97 C) were applied at 5 mA/cm^2 (9 mA/1.8cm^2). After electrolysis, the reaction was reduced under vacuo and subjected to column chromatography (DCM/MeOH 5%) to yield **56c** (5 mg, 0.02 mmol, 10%) as a highly viscous oil.

^{1}H NMR (400 MHz, MeOH–d_4): δ [ppm] = 3.67–3.64 (m, 8H), 3.28–3.26 (m, 8H).

^{13}C NMR (101 MHz, MeOH–d_4): δ [ppm] = 164.6*, 67.6, 48.4.

*Due to low substance amount, the assigned signal was depicted via HMBC NMR ($^3J_{C–H}$). See figure 59 in section 10.

R*f* = 0.37 (DCM/MeOH 5%).

GC: t_R 10.018 min.

The spectroscopic data are in accordance with literature.[304,305]

6.8.35. Diphenyldiazene (**57d**)

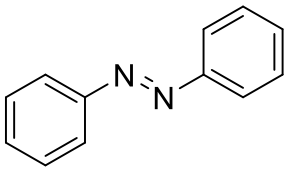

According to GP6, a solution of *N*-phenylurea (**51d** ,68 mg, 0.50 mmol, 1 eq.), sodium bromide (155 mg, 1.50 mmol, 1.5 eq.) and sodium hydroxide (20 mg, 0.50 mmol, 1 eq.) in 5.0 mL solvent mixture of methanol/MTBE (10 v/v%) was transferred to a 5.0 mL screening cell and warmed to 60 °C. After reaction temperature was reached, the solution was electrolyzed at graphite electrodes until 2.0 *F* (97 C) were applied at 5 mA/cm^2 (9 mA/1.8cm^2). After electrolysis, the reaction was reduced under vacuo and subjected to column chromatography (CH/DCM 10%) to yield **57d** (5 mg, 0.03 mmol, 11%) as a yellow solid.

^{1}H NMR (400 MHz, $CDCl_3$): δ [ppm] = 7.94–7.91 (m, 4H), 7.55–7.48 (m, 6H).

^{13}C NMR (101 MHz, $CDCl_3$): δ [ppm] = 152.8, 131.1, 129.2, 123.0.

HRMS for $C_{12}H_{11}N_2^+$ (ESI+) $[M+H]^+$: calc.: 183.0917, found: 183.0908.

R*f* = 0.43 (CH/DCM 10%).

GC: t_R 9.774 min.

GC-MS: t_R 11.042 min, *m/z* 182.

The spectroscopic data are in accordance with literature.[306]

6.8.36. 1-(4-Bromophenyl)-2-phenyldiazene (**57da**)

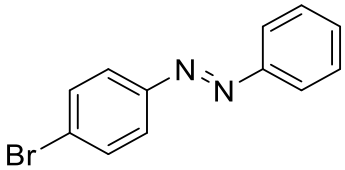

According to GP6, a solution of *N*-phenylurea (**51d**, 68 mg, 0.50 mmol, 1 eq.), sodium bromide (26 mg, 0.25 mmol, 0.5 eq.) in 5.0 mL solvent mixture of acetonitrile/MeOH (10 v/v%) was transferred to a 5.0 mL screening cell and warmed to 30 °C. After reaction temperature was reached, the solution was electrolyzed at graphite electrodes until 2.0 *F* (97 C) were applied at 5 mA/cm^2 (9 mA/1.8cm^2). After electrolysis, the reaction was reduced under vacuo and subjected to column chromatography (CH/DCM 50%) to yield **57da** (3 mg, 0.01 mmol, 5%) as an orange solid.

^{1}H NMR (400 MHz, $CDCl_3$): δ [ppm] = 7.93–7.90 (m, 2H), 7.82–7.78 (m, 2H), 7.67–7.64 (m, 2H), 7.53–7.49 (m, 3H).

^{13}C NMR (101 MHz, $CDCl_3$): δ [ppm] = 152.7, 151.5, 132.5, 131.5, 129.3, 125.5, 124.5, 123.1.

HRMS for $C_{12}H_{10}{}^{79}BrN_2^+$ (ESI+) $[M+H]^+$: calc.:261.0022, found: 261.0014.

R*f* = 0.68 (CH/DCM 10%).

GC: t_R 11.945 min.

GC-MS: t_R 13.269 min, *m/z* 260.

The spectroscopic data are in accordance with literature.[306,307]

6.8.37. 1,2-Bis(4-bromophenyl)diazene (**57db**)

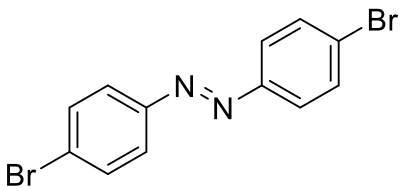

According to GP6, a solution of *N*-phenylurea (**51d**, 68 mg, 0.50 mmol, 1 eq.), sodium bromide (26 mg, 0.25 mmol, 0.5 eq.) in 5.0 mL solvent mixture of acetonitrile/MeOH (10 v/v%) was transferred to a 5.0 mL screening cell and warmed to 30 °C. After reaction temperature was reached, the solution was electrolyzed at graphite electrodes until 2.0 *F* (97 C) were applied at 5 mA/cm^2 (9 mA/1.8cm^2). After electrolysis, the reaction was reduced under vacuo and subjected to column chromatography (CH/DCM 50%) to yield **57db** (5 mg, 0.02 mmol, 6%) as an orange solid.

^{1}H NMR (400 MHz, $CDCl_3$): δ [ppm] = 7.81–7.78 (m, 4H), 7.67–7.64 (m, 4H).

^{13}C NMR (101 MHz, $CDCl_3$): δ [ppm] = 151.3, 132.6, 125.9, 124.6.

R*f* = 0.72 (CH/DCM 10%).

GC: t_R 13.984 min.

GC-MS: t_R 16.139 min, *m/z* 340.

The spectroscopic data are in accordance with literature.[306,307]

6.8.38. 1,2-Bis(3,4-dichlorophenyl)diazene (**57f**)

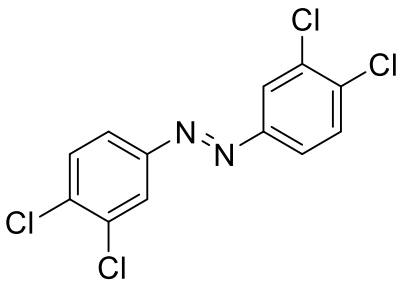

According to GP6, a solution of 1-(3,4-dichlorophenyl)urea (**51d**, 103 mg, 0.50 mmol, 1 eq.), sodium bromide (26 mg, 0.25 mmol, 0.5 eq.) in 5.0 mL solvent mixture of acetonitrile/MeOH (10 v/v%) was transferred to a 5.0 mL screening cell and warmed to 30 °C. After reaction temperature was reached, the solution was electrolyzed at platinum electrodes until 2.0 *F* (97 C) were applied at 5 mA/cm^2 (9 mA/1.8cm^2). After electrolysis, the reaction was reduced under vacuo and subjected to column chromatography (CH/DCM 10%) to yield **57f** (10 mg, 0.03 mmol, 13%) as a pale-yellow solid.

^{1}H NMR (400 MHz, $CDCl_3$): δ [ppm] = 8.01 (d, *J* = 2.2 Hz, 2H), 7.80 (dd, *J* = 8.5, 2.2 Hz, 2H), 7.62 (d, *J* = 8.5 Hz, 2H).

^{13}C NMR (101 MHz, $CDCl_3$): δ [ppm] = 151.2, 135.9, 133.8, 131.2, 124.2, 123.2.

HRMS for $C_{12}H_7{}^{35}Cl_4N_2^+$ (ESI+) $[M+H]^+$: calc.:318.9358, found: 381.9364.

R*f* = 0.70 (CH/DCM 10%).

GC: t_R 15.054 min.

GC-MS: t_R 17.167 min, *m/z* 320.

The spectroscopic data are in accordance with literature.[306,307]

7. List of Abbreviations

ΔE	Energy difference	E_{pa}	Anodic peak potential
ΔG	Gibbs free energy	E_{pc}	Cathodic peak potential
°C	Degree Celsius	eq.	Equivalent
A	Ampere	ET	Electron transfer
Å	Ångström	Et	Ethyl
Ac	Acetyl	*F*	Faraday´s constant, 96,485 C/mol
AcOH	Acetic acid	FcH	Ferrocene
API	Active pharmaceutical ingredient	g/L	Grams per litre
aq.	Aqueous	gC	Glassy carbon
Ar	Aryl	GC	Gas chromatography
atm	Standard atmosphere	GM-MS	Gas chromatography - mass spectrometry
BDD	Boron-doped diamond	h	Hour
BDE	Bond dissociation energy	HER	Hydrogen evolution reaction
BDMS	Bromodimehtyl sulfonium bromide	HFIP	1,1,1,3,3,3-Hexafluoroisopropanol
Boc	*tert*-Butoxycarbonyl	HOMO	Highest occupied molecular orbital
Bu	Butyl	*i*	*Ipso*
CE	Counter electrode	*I*	Current (A)
CV	Cyclic voltammerty	*IHL*	Inner Helmholtz Layer
d.r.	Diastereomeric ratio	*j*	Current density (A/m^2)
D°	Bond dissociation energy	*K*	Equilibrium constant
DSA	Dimensionally stable anode	kJ/mol	Kilojoule per mol
d	Diameter	LUMO	Lowest unoccupied moleculer orbital
DMAP	4-Dimethylaminopyridine	*m*	*Meta*
DMF	Dimethylformamide	M	Molar
DMSO	Dimethyl sulfoxide	Me	Methyl
E°cell	Cell potential	MeCN	Acetonitrile
E_F	Fermi level energy	min	Minutes

mmHg	Milimetre of mercury	*t*	*Tert*
MTBE	Methyl *tert*-butyl ether	*T (K)*	Temperature (Kelvin)
n	Number of moles	t/a	Tonnes per annum
NBS	*N*-bromosuccinimide	TFA	Trifluoroacetic acid
NMP	*N*-methyl-2-pyrrolidone	THF	Tetrahydrofuran
NMR	Nuclear magnetic resonance	TLC	Thin layer chromatography
ŋ	Overpotential	TLC-MS	Thin layer chromatography - mass spectrometry
OHL	Outer Helmholtz Layer	Ts	Tosyl, *p*-toluenesulfonyl group
o	*Ortho*	U_{cell}	Operating cell potential
p	*Para*	V	Volt
pH	Potential of hydrogen	v/v%	Concentration, volume per volume
Ph	Phenyl	WE	Working electrode
PIDA	Phenyliodine(III) diacetate	w_{max}	Maximum amount of work
PTFE	Polytetrafluoroethylene	*z*	Charge number
Py	Pyridine	*ε*	Permittivity
Q	Applied charge (C/mol)	σ	Sigma bond
R	Ideal gas constant, 8.314 J/mol	σ*	Sigma star bond
R_{cell}	Cell resistance		
RE	Reference electrode		
RVC	Reticulated vitreous carbon		
s	Lat. secundum		
S	Substrate		
SCE	Saturated calomel electrode		
SET	Single electron transfer		
SHE	Standard hydrogen electrode		

8. Literature

[1] M. M. Häggblom, I. D. Bossert, in *Dehalogenation*, Kluwer Academic Publishers, Boston, **2005**, pp. 3–29.

[2] T. Kosjek, E. Heath, *Halogenated heterocycles as pharmaceuticals* in *Halogenated Heterocycles*, (Ed.: J. Iskra), Springer Berlin, Heidelberg, **2011**, *27*, pp. 219–246.

[3] C. J. Löwig, *Das Brom Und Seine Chemischen Verhältnisse*, C. F. Winter, Heidelberg, **1829**.

[4] C. J. Löwig, *Liebigs Ann. Chem.* **1828**, *90*, 485–499.

[5] A. J. Balard, *Rev. Hist. Pharm.* **2007**, *356*, 495–504.

[6] E. Salameh, A. Tarawneh, M. Al-Raggad, *Arab. J. Geosci.* **2016**, *9*, 414.

[7] L. Fernandez, "Market volume of bromine wordwide from 2015 to 2021, with a forecast for 2022 to 2029," can be found under https://www.statista.com/statistics/1245240/bromine-market-volume-worldwide/, accessed: 13.08.2023.

[8] M. Kesner, *Bromine and Bromine Compounds from the Dead Sea, Israel*, The Department Of Science Teaching, The Weizmann Institute Of Science, Rehovot, Israel, **1999**.

[9] F. Ge, Y. Li, X. Ye, H. Liu, *Progress on the Extraction Techniques of Bromine in Proceedings of the 2015 International Symposium on Energy Science and Chemical Engineering* (Ed.: Y. He), Atlantis Press, Springer Nature, Berlin, Germany, **2015**, pp. 23–27.

[10] L. C. Stewart, *Ind. Eng. Chem.***1934**, *26*, 361–369.

[11] "Bromine recovery plants," can be found under https://www.ablazeexport.com/bromine-recovery-plants/, accessed: 13.08.2023.

[12] M. Soyluoglu, M. S. Ersan, M. Ateia, T. Karanfil, *Chemosphere* **2020**, *238*, 124583.

[13] Y. Liu, Y. Qin, Q. Li, Y. Wang, Y. Zhang, L. Zhang, L. Liu, *J. Memb. Sci.* **2017**, *543*, 222–232.

[14] H. Wang, C. Y. Xiao, B. Zhao, *Lect. Not. El. Engr.* **2012**, 81–87.

[15] X.-L. Zhou, Z.-J. Ji, J. Wang, X. Zhang, X.-F. Gou, J. Liu, P.-P. Zhang, J.-T. Bi, Y.-Y. Zhao, J.-S. Yuan, *J. Environ. Chem. Eng.* **2022**, *10*, 107946.

[16] M. B. Heeb, J. Criquet, S. G. Zimmermann-Steffens, U. von Gunten, *Water Res.* **2014**, *48*, 15–42.

[17] J. J. Rook, A. A. Gras, B. G. V. der Heijden, J. de Wee, *J. Environ. Sci. Health* **1978**, *13*, 91–116.

[18] W. Jiao, S. Luo, Z. He, Y. Liu, *Chem. Eng. J.* **2017**, *313*, 912–927.

[19] A. R. Horrocks, D. Price, *Fire Retardant Materials*, Woodhead Publishing Limited, Cambridge, UK, **2001**.

[20] D. Yoffe, A. Kampf, in *Kirk-Othmer Encyclopedia of Chemical Technology*, John Wiley & Sons Inc., Hoboken, NJ, USA, **2002**.

[21] H. A. U. Monro, *Anz. Schädlingskd. Pfl.* 1971, *52*, 44–47.

[22] D. Yoffe, R. Frim, S. D. Ukeles, M. J. Dagan, H. J. Barda, T. J. Benya, David. C. Sanders, *Ullmann´s Encyclopedia of Industrial Chemistry*, Wiley-VCH, Weinheim, Germany, **2013**.

[23] "Bromine - The Essential Chemical Industry," can be found under https://www.essentialchemicalindustry.org/chemicals/bromine.html, accessed: 13.08.2023.

[24] Y. R. Luo, *Comprehensive Handbook of Chemical Bond Energies*, CRC Press, Boca Raton, FL, US, **2007**.

[25] A. D. White, F. Gallou, *Iron(III)Chloride* in *Encyclopedia of Reagents for Organic Synthesis*, John Wiley & Sons, Hoboken, NJ, USA, **2006**.

[26] Y. Xiao, P. Liu, *Angew. Chem. Int. Ed.* **2008**, *47*, 9722–9725; *Angew. Chem.* **2008**, *120*, 9868–9871.

[27] E. Puchl'ová, M. Dendys, I. Špánik, P. Szolcsányi, *Molecules* **2019**, *24*, 4497.

[28] R. Jana, T. P. Pathak, M. S. Sigman, *Chem. Rev.* **2011**, *111*, 1417–1492.

[29] I. Roberts, G. E. Kimball, *J. Am. Chem. Soc.* **1937**, *59*, 947–948.

[30] J. Clayden, N. Greeves, S. Warren, *Organic Chemistry*, Oxford University Press, Oxford, UK, **2001**.

[31] William Reusch, "Addition reactions of alkenes," can be found under https://www2.chemistry.msu.edu/faculty/reusch/virttxtjml/addene1.htm, **2013**, accessed: 13.08.2023.

[32] A. U. Ubaidullaev, V. I. Vinogradova, Sh. N. Zhurakulov, N. I. Mukarramov, Kh. M. Bobakulov, K. A. Turgunov, B. Tashkhodzhaev, *Chem. Nat. Compd.* **2022**, *58*, 1101–1107.

[33] M. D. Dowle, D. I. Davies, *Chem. Soc. Rev.* **1979**, *8*, 171.

[34] R. S. Brown, *Acc. Chem. Res.* **1997**, *30*, 131–137.

[35] A. B. Smith, T. A. Rano, N. Chida, G. A. Sulikowski, J. L. Wood, *J. Am. Chem. Soc.* **1992**, *114*, 8008–8022.

[36] S. H. Lone, K. A. Bhat, M. A. Khuroo, *Chem. Biol. Interact.* **2015**, *240*, 180–198.

[37] C. Ye, J. M. Shreeve, *J. Org. Chem.* **2004**, *69*, 8561–8563.

[38] K.-M. Kim, I.-H. Park, *Synthesis* **2004**, 2641–2644.

[39] L. Engman, K. W. Törnroos, *J. Organomet. Chem.* **1990**, *391*, 165–178.

[40] S. V. Ley, A. J. Whittle, *Tetrahedron Lett.* **1981**, *22*, 3301–3304.

[41] K. C. Nicolaou, H. Ding, J.-A. Richard, D. Y.-K. Chen, *J. Am. Chem. Soc.* **2010**, *132*, 3815–3818.

[42] N. Holub, J. Neidhöfer, S. Blechert, *Synfacts* **2005**, 0098–0098.

[43] L. K. G. Ackerman, M. M. Lovell, D. J. Weix, *Nature* **2015**, *524*, 454–457.

[44] M. G. Banwell, B. D. Kelly, O. J. Kokas, D. W. Lupton, *Org. Lett.* **2003**, *5*, 2497–2500.

[45] "Drugbank Online," can be found under https://go.drugbank.com/drugs/DB07757, accessed: 13.08.2023.

[46] R. W. Hoffmann, *Chem. Soc. Rev.* **2016**, *45*, 577–583.

[47] W. Markownikoff, *Liebigs Ann. Chem.* **1870**, *153*, 137–264.

[48] A. W. Hofmann, *Ber. Dtsch. Chem. Ges.* **1881**, *14*, 2725–2736.

[49] A. W. Hofmann, *Ber. Dtsch. Chem. Ges.* **1882**, *15*, 762–775.

[50] A. Kimishima, H. Umihara, A. Mizoguchi, S. Yokoshima, T. Fukuyama, *Org. Lett.* **2014**, *16*, 6244–6247.

[51] T. Hakogi, M. Taichi, S. Katsumura, *Org. Lett.* **2003**, *5*, 2801–2804.

[52] K. G. Poullennec, D. Romo, *J. Am. Chem. Soc.* **2003**, *125*, 6344–6345.

[53] T. Hakogi, Y. Monden, S. Iwama, S. Katsumura, *Org. Lett.* **2000**, *2*, 2627–2629.

[54] A. G. Schultz, A. Wang, *J. Am. Chem. Soc.* **1998**, *120*, 8259–8260.

[55] J. Schörghuber, T. Sára, M. Bisaccia, W. Schmid, R. Konrat, R. J. Lichtenecker, *ChemBioChem* **2015**, *16*, 746–751.

[56] X. Huang, M. Seid, J. W. Keillor, *J. Org. Chem.* **1997**, *62*, 7495–7496.

[57] K. A. Monk, R. S. Mohan, *J. Chem. Educ.* **1999**, *76*, 1717.

[58] D. A. Evans, K. A. Scheidt, C. W. Downey, *Org. Lett.* **2001**, *3*, 3009–3012.

[59] T. Katagiri, M. Irie, K. Uneyama, *Org. Lett.* **2000**, *2*, 2423–2425.

[60] A. Vasudevan, G. F. Koser, *J. Org. Chem.* **1988**, *53*, 5158–5160.

[61] V. V. Zhdankin, P. J. Stang, *Chem. Rev.* **2002**, *102*, cr010003+.

[62] D. E. DeMong, R. M. Williams, *J. Am. Chem. Soc.* **2003**, *125*, 8561–8565.

[63] E. Hernández, J. M. Vélez, C. P. Vlaar, *Tetrahedron Lett.* **2007**, *48*, 8972–8975.

[64] A. A. Zagulyaeva, C. T. Banek, M. S. Yusubov, V. V. Zhdankin, *Org. Lett.* **2010**, *12*, 4644–4647.

[65] A. Yoshimura, K. R. Middleton, M. W. Luedtke, C. Zhu, V. V. Zhdankin, *J. Org. Chem.* **2012**, *77*, 11399–11404.

[66] D. R. Addis, A. Molyvdas, N. Ambalavanan, S. Matalon, T. Jilling, *Ann. NY. Acad. Sci.* **2020**, *1480*, 30–43.

[67] D. R. Addis, S. Aggarwal, A. Lazrak, T. Jilling, S. Matalon, *Physiology* **2021**, *36*, 272–291.

[68] M. Eissen, D. Lenoir, *Chem. Eur. J.* **2008**, *14*, 9830–9841.

[69] R. Van Kerrebroeck, T. Horsten, C. V. Stevens, *Eur. J. Org. Chem.* **2022**, e202200310.

[70] Y. Marcus, *J. Solution Chem.* **2008**, *37*, 1071–1098.

[71] A. W. Herriott, D. Picker, *J. Am. Chem. Soc.* **1975**, *97*, 2345–2349.

[72] P. Anastas, N. Eghbali, *Chem. Soc. Rev.* **2010**, *39*, 301–312.

[73] V. Patil, G. Shankarling, *J. Org. Chem.* **2015**, *80*, 7876–7883.

[74] A. Podgoršek, M. Zupan, J. Iskra, *Angew. Chem. Int. Ed.* **2009**, *48*, 8424–8450.

[75] O. Hoegh-Guldberg, "Global Warming of 1.5° C," can be found under https://www.ipcc.ch/sr15/, accessed: 13.08.2023.

[76] H. Kolbe, *Liebigs Ann. Chem.* **1849**, *69*, 257–294.

[77] H. Kolbe, *Liebigs Ann. Chem.* **1848**, *64*, 339–341.

[78] T. Fuchigami, S. Inagi, M. Atobe, *Fundamentals and Applications of Organic Electrochemistry: Synthesis, Materials, Devices*, John Wiley & Sons, Chichester, West Sussex, UK, **2014**.

[79] J. E. Nutting, M. Rafiee, S. S. Stahl, *Chem. Rev.* **2018**, *118*, 4834–4885.

[80] M. F. Semmelhack, C. R. Schmid, *J. Am. Chem. Soc.* **1983**, *105*, 6732–6734.

[81] S. Torii, K. Uneyama, K. Ueda, *J. Org. Chem.* **1984**, *49*, 1830–1832.

[82] K. Uneyama, Y. Masatsugu, S. Torii, *Bull. Chem. Soc. Jpn.* **1985**, *58*, 2361–2365.

[83] T. Inokuchi, S. Matsumoto, M. Tsuji, S. Torii, *J. Org. Chem.* **1992**, *57*, 5023–5027.

[84] T. Shono, *Electroorganic Chemistry in Organic Synthesis*, Pergamon Press Ltd., Kyoto, Japan, **1984**.

[85] T. Shono, Y. Matsumura, K. Tsubata, *J. Am. Chem. Soc.* **1981**, *103*, 1172–1176.

[86] J. I. Yoshida, M. Watanabe, H. Toshioka, M. Imagawa, S. Suga, *J. Electroanal. Chem.* **2001**, *507*, 55–65.

[87] J. I. Yoshida, S. Isoe, *Tetrahedron Lett.* **1987**, *28*, 6621–6624.

[88] J. Yoshida, A. Shimizu, R. Hayashi, *Chem. Rev.* **2018**, *118*, 4702–4730.

[89] J. I. Yoshida, S. Suga, S. Suzuki, N. Kinomura, A. Yamamoto, K. Fujiwara, *J. Am. Chem. Soc.* **1999**, *121*, 9546–9549.

[90] G. S. Sauer, S. Lin, *ACS Catal.* **2018**, *8*, 5175–5187.

[91] N. Sauermann, T. H. Meyer, Y. Qiu, L. Ackermann, *ACS Catal.* **2018**, *8*, 7086–7103.

[92] B. R. Rosen, E. W. Werner, A. G. O'Brien, P. S. Baran, *J. Am. Chem. Soc.* **2014**, *136*, 5571–5574.

[93] T. Morofuji, A. Shimizu, J. Yoshida, *J. Am. Chem. Soc.* **2013**, *135*, 5000–5003.

[94] J. L. Röckl, D. Pollok, R. Franke, S. R. Waldvogel, *Acc. Chem. Res.* **2020**, *53*, 45–61.

[95] A. Kirste, B. Elsler, G. Schnakenburg, S. R. Waldvogel, *J. Am. Chem. Soc.* **2012**, *134*, 3571–3576.

[96] C. Zhu, N. W. J. Ang, T. H. Meyer, Y. Qiu, L. Ackermann, *ACS Cent. Sci.* **2021**, *7*, 415–431.

[97] M. Yan, Y. Kawamata, P. S. Baran, *Chem. Rev.* **2017**, *117*, 13230–13319.

[98] M. D. Kärkäs, *Chem. Soc. Rev.* **2018**, *47*, 5786–5865.

[99] L. F. T. Novaes, J. Liu, Y. Shen, L. Lu, J. M. Meinhardt, S. Lin, *Chem. Soc. Rev.* **2021**, *50*, 7941–8002.

[100] D. Pollok, S. R. Waldvogel, *Chem. Sci.* **2020**, *11*, 12386–12400.

[101] A. Shatskiy, H. Lundberg, M. D. Kärkäs, *ChemElectroChem* **2019**, *6*, 4067–4092.

[102] G. Hilt, *ChemElectroChem* **2020**, *7*, 395–405.

[103] S. B. Beil, D. Pollok, S. R. Waldvogel, *Angew. Chem. Int. Ed.* **2021**, *60*, 14750–14759; *Angew. Chem.* **2021**, *133*, 14874–14883.

[104] C. J. Clarke, W.-C. Tu, O. Levers, A. Bröhl, J. P. Hallett, *Chem. Rev.* **2018**, *118*, 747–800.

[105] C. Roth, A. N. Simonov, *Curr. Opin. Electrochem.* **2022**, *36*, 101158.

[106] H. Chen, E. Kätelhön, R. G. Compton, *Curr. Opin. Electrochem.* **2023**, *38*, 101214.

[107] T. Wiedmann, J. Barrett, *Sustainability* **2010**, *2*, 1645–1693.

[108] R. A. Sheldon, D. Brady, *ChemSusChem* **2022**, *15*, e202102628.

[109] J. Seidler, J. Strugatchi, T. Gärtner, S. R. Waldvogel, *MRS Energy & Sustainability* **2020**, *7*, 42.

[110] M. Breiner, M. Zirbes, S. R. Waldvogel, *Green Chem.* **2021**, *23*, 6449–6455.

[111] A. L. Rauen, F. Weinelt, S. R. Waldvogel, *Green Chem.* **2020**, *22*, 5956–5960.

[112] L. G. Gombos, S. R. Waldvogel, *Sustain. Chem.* **2022**, *3*, 430–454.

[113] D. S. Gho, S. Singh, “Connection between Cell Potential, ΔG, and K ,” can be found under https://chem.libretexts.org/Bookshelves/Analytical_Chemistry/Supplemental_Modules_(Analytical_Chemistry)/Electrochemistry/Electrochemistry_and_Thermodynamics, accessed: 13.08.2023.

[114] O. Hammerich, B. Speiser, *Organic Electrochemistry, Fifth Edition: Revised and Expanded*, CRC Press, Boca Raton, FL, USA, **2015**.

[115] J. E. Nutting, J. B. Gerken, A. G. Stamoulis, D. L. Bruns, S. S. Stahl, *J. Org. Chem.* **2021**, *86*, 15875–15885.

[116] K. D. Moeller, *Chem. Rev.* **2018**, *118*, 4817–4833.

[117] D. M. Heard, A. J. J. Lennox, *Angew. Chem. Int. Ed.* **2020**, *59*, 18866–18884.

[118] G. G. Botte, *Electrochem. Soc. Interface* **2014**, *23*, 49–55.

[119] A. J. Bard, L. R. Faulkner, *Electrochemical Methods: Fundamentals and Applications, 2nd Edition*, John Wiley & Sons, New York, NY, USA, **2001**.

[120] G. Jerkiewicz, *ACS Catal.* **2020**, *10*, 8409–8417.

[121] M. Dunwell, Y. Yan, B. Xu, *Curr. Opin. Chem. Eng.* **2018**, *20*, 151–158.

[122] I. Izumi, J. Sato, N. Iwashita, M. Inagaki, *Synth. Met.* **1995**, *75*, 75–77.

[123] B. Juettner, *J. Am. Chem. Soc.* **1937**, *59*, 208–213.

[124] A.-L. Cui, G.-X. Feng, Y.-F. Zhao, H.-Z. Kou, H. Li, G.-H. Zhu, H.-S. Hwang, H.-C. Oh, Y.-J. Kwon, D.-C. Lee, *Electrochem. Commun.* **2009**, *11*, 409–412.

[125] S. Sharma, C. N. Shyam Kumar, J. G. Korvink, C. Kübel, *Sci. Rep.* **2018**, *8*, 16282.

[126] P. J. F. Harris, *Philos. Mag.***2004**, *84*, 3159–3167.

[127] G. M. Jenkins, K. Kawamura, *Nature* **1971**, *231*, 175–176.

[128] S. Möhle, M. Zirbes, E. Rodrigo, T. Gieshoff, A. Wiebe, S. R. Waldvogel, *Angew. Chem. Int. Ed.* **2018**, *57*, 6018–6041; *Angew. Chem.* **2018**, *130*, 6124–6149.

[129] S. B. Beil, T. Müller, S. B. Sillart, P. Franzmann, A. Bomm, M. Holtkamp, U. Karst, W. Schade, S. R. Waldvogel, *Angew. Chem. Int. Ed.* **2018**, *57*, 2450–2454; *Angew. Chem.* **2018**, *130*, 2475–2479.

[130] G. Silvestri, S. Gambino, G. Filardo, *Acta. Chem. Scand.* **1991**, *45*, 987–992.

[131] C. Kingston, M. D. Palkowitz, Y. Takahira, J. C. Vantourout, B. K. Peters, Y. Kawamata, P. S. Baran, *Acc. Chem. Res.* **2020**, *53*, 72–83.

[132] C. Wohlfarth, *Handbook of Chemistry and Physics*, (Eds.: W.M. Haynes, D.R. Lide, T.J. Bruno), CRC Press, Boca Raton, FL, USA, **2016**, pp. 199–220.

[133] C. A. Malapit, M. B. Prater, J. R. Cabrera-Pardo, M. Li, T. D. Pham, T. P. McFadden, S. Blank, S. D. Minteer, *Chem. Rev.* **2022**, *122*, 3180–3218.

[134] A. R. Akbashev, *ACS Catal.* **2022**, *12*, 4296–4301.

[135] F. Wang, S. S. Stahl, *Acc. Chem. Res.* **2020**, *53*, 561–574.

[136] "IKA Screening System Package (8 cells)," can be found under https://www.ika.com/en/Products-Lab-Eq/Screening-System-csp-913/Screening-System-Package-(8-Cells)-cpdt-40003642/, accessed: 12.08.2023.

[137] "IKA Screening System Package (6 cells)," can be found under https://www.ika.com/en/Products-LabEq/Screening-System-pg913/Screening-System-Package-(6-cells)-40003631/, accessed: 12.08.2023.

[138] “IKA ElectraSyn 2.0 Package,” can be found under: https://www.ika.com/en/Products-LabEq/Electrochemistry-Kit-pg516/ElectraSyn-20-pro-Package-40003261/, accessed: 12.08.2023.

[139] M. Yan, Y. Kawamata, P. S. Baran, *Angew. Chem. Int. Ed.* **2018**, *57*, 4149–4155; *Angew. Chem.* **2018**, *130*, 4219–4225.

[140] T. Wu, K. D. Moeller, *Angew. Chem. Int. Ed.* **2021**, *60*, 12883–12890; *Angew. Chem.* **2021**, *133*, 12993–13000.

[141] T. Wu, B. H. Nguyen, M. C. Daugherty, K. D. Moeller, *Angew. Chem. Int. Ed.* **2019**, *58*, 3562–3565; *Angew. Chem.* **2019**, *131*, 3600–3603.

[142] F. Marken, A. J. Cresswell, S. D. Bull, *Chem. Rec.* **2021**, *21*, 2585–2600.

[143] M. Klein, S. R. Waldvogel, *Angew. Chem. Int. Ed.* **2022**, *61*, e202204140; *Angew. Chem.* **2022**, *134*, e202204140.

[144] C. Schotten, T. P. Nicholls, R. A. Bourne, N. Kapur, B. N. Nguyen, C. E. Willans, *Green Chem.* **2020**, *22*, 3358–3375.

[145] L. M. Reid, T. Li, Y. Cao, C. P. Berlinguette, *Sustainable Energy Fuels* **2018**, *2*, 1905–1927.

[146] Y. Kawamata, M. Yan, Z. Liu, D.-H. Bao, J. Chen, J. T. Starr, P. S. Baran, *J. Am. Chem. Soc.* **2017**, *139*, 7448–7451.

[147] M. Dörr, M. M. Hielscher, J. Proppe, S. R. Waldvogel, *ChemElectroChem* **2021**, *8*, 2621–2629.

[148] N. Tanbouza, T. Ollevier, K. Lam, *iScience* **2020**, *23*, 101720.

[149] M. Selt, R. Franke, S. R. Waldvogel, *Org. Process. Res. Dev.* **2020**, *24*, 2347–2355.

[150] M. Selt, B. Gleede, R. Franke, A. Stenglein, S. R. Waldvogel, *J. Flow. Chem.* **2021**, *11*, 143–162.

[151] D. Pollok, B. Gleede, A. Stenglein, S. R. Waldvogel, *Aldrichimita ACTA* **2021**, *54*, 3–15.

[152] F. Marken, *The Electrochemistry of Halogens* in *Encyclopedia of Electrochemistry*, (Eds.: A. J. Bard, M. Stratmann, Wiley-VCH, Weinheim, Germany, **2006**.

[153] T. F. O’Brien, T. V. Bommaraju, F. Hine, *Handbook of Chlor-Alkali Technology*, Springer, New York, NY, USA, **2005**.

[154] S. Trasatti, *Electrochim. Acta.* **2000**, *45*, 2377–2385.

[155] E. Balomenos, D. Panias, I. Paspaliaris, *Min. Proc. Ext. Met. Rev.* **2011**, *32*, 69–89.

[156] C. A. C. Sequeira, D. M. F. Santos, *J. Braz. Chem. Soc.* **2009**, *20*, 387–406.

[157] D. E. Blanco, R. Atwi, S. Sethuraman, A. Lasri, J. Morales, N. N. Rajput, M. A. Modestino, *J. Electrochem. Soc.* **2020**, *167*, 155526.

[158] K. Jüttner, *Technical Scale of Electrochemistry* in *Encyclopedia of Electrochemistry*, (Eds.: A. J. Bard, M. Stratmann, Wiley-VCH, Weinheim, Germany, **2007**.

[159] H. Hannebaum, H. Pütter, *Chem. Unserer Zeit* **1999**, *33*, 373–374.

[160] N. L. Weinberg, D. J. Mazur, *J. Appl. Electrochem.* **1991**, *21*, 895–901.

[161] A. P. Doherty, P. A. Christensen, A. Hamnett, K. Scott, *J. Electroanal. Chem.* **1995**, *386*, 39–44.

[162] M. I. Montenegro, D. Pletcher, E. A. Liolios, D. J. Mazur, C. Zawodzinski, *J. Appl. Electrochem.* **1990**, *20*, 54–59.

[163] M. J. Orella, Y. Román-Leshkov, F. R. Brushett, *Curr. Opin. Chem. Eng.* **2018**, *20*, 159–167.

[164] AR5 Climate Change 2014: Mitigation of Climate Change," **2014**, can be found under: https://www.ipcc.ch/report/ar5/wg3/, accessed: 13.08.2023.

[165] R. Xia, S. Overa, F. Jiao, *JACS Au* **2022**, *2*, 1054–1070.

[166] M. Zirbes, T. Graßl, R. Neuber, S. R. Waldvogel, *Angew. Chem. Int. Ed.* **2023**, *62*, e202219217; *Angew. Chem.* **2023**, *135*, e202219217.

[167] C. Lassen, S. Løkke, L. I. Andersern, *Brominated Flame Retardants*, Environmental Project Nr. 494, Miljøprojekt, Danish Institute of Fire Technology, Hvidovre, Denmark, **1999**.

[168] K. L. Kirk, *Biochemistry of the Elemental Halogens and Inorganic Halides*, Plenum Press, New York, NY, US, **1991**.

[169] D. Schrenk, M. Bignami, L. Bodin, J. K. Chipman, J. del Mazo, B. Grasl-Kraupp, C. Hogstrand, L. Hoogenboom, J. C. Leblanc, C. S. Nebbia, E. Nielsen, E. Ntzani, A. Petersen, S. Sand, T. Schwerdtle, H. Wallace, D. Benford, P. Fürst, M. Rose, S. Ioannidou, M. Nikolič, L. R. Bordajandi, C. Vleminckx, *EFSA Journal* **2021**, *18,* e05991.

[170] D. Klinčić, M. Dvoršćak, K. Jagić, G. Mendaš, S. Herceg Romanić, *Environ. Sci. Pol. Res.* **2020**, *27*, 5744–5758.

[171] D. Pletcher, F. C. Walsh, *Industrial Electrochemistry*, Springer, London, UK, **1993**, pp. 331–384.

[172] V. Vojinovic, S. Mentus, V. Komnenic, *J. Electroanal. Chem.* **2003**, *547*, 109–113.

[173] D. Halász, C. Visy, A. Szucs, M. Novák, *React. Kinet. Catal. L.* **1992**, *48*, 177–188.

[174] B. E. Conway, Y. Phillips, S. Y. Qian, *J. Chem. Soc., Faraday Trans.* **1995**, *91*, 283.

[175] M. Tariq, *Z. Phys. Chem.* **2020**, *234*, 295–312.

[176] J. G. Bell, J. Wang, *J. Electroanal. Chem.* **2015**, *754*, 133–137.

[177] W. K. Behl, *J. Electrochem. Soc.* **1989**, *136*, 2305–2310.

[178] N. Vinokur, B. Miller, Y. Avyigal, R. Kalish, *J. Electrochem. Soc.* **1996**, *143*, L238–L240.

[179] R. Giernoth, *Angew. Chem. Int. Ed.* **2011**, *50,* 11289–11289; *Angew. Chem.* **2011**, *123,* 11485–11485.

[180] H. Tanida, H. Sakane, I. Watanabe, *J. Chem. Soc., Dalton Trans.* **1994**, 2321.

[181] R. Ayala, J. M. Martínez, R. R. Pappalardo, E. Sánchez Marcos, *J. Phys. Chem. A* **2000**, *104*, 2799–2807.

[182] B. N. Grgur, *J. Electrochem. Soc.* **2019**, *166*, E50–E61.

[183] X. Salom-Roig, C. Bauder, *Synthesis* **2020**, *52*, 964–978.

[184] O. V. Bityukov, V. A. Vil', G. I. Nikishin, A. O. Terent'ev, *Adv. Synth. Catal.* **2021**, *363*, 3070–3078.

[185] A. Shimizu, R. Hayashi, Y. Ashikari, T. Nokami, J. Yoshida, *Beilstein J. Org. Chem.* **2015**, *11*, 242–248.

[186] Y. Ashikari, A. Shimizu, T. Nokami, J. Yoshida, *J. Am. Chem. Soc.* **2013**, *135*, 16070–16073.

[187] X. Sun, H.-X. Ma, T.-S. Mei, P. Fang, Y. Hu, *Org. Lett.* **2019**, *21*, 3167–3171.

[188] T.-S. Zhang, W.-J. Hao, R. Wang, S.-C. Wang, S.-J. Tu, B. Jiang, *Green Chem.* **2020**, *22*, 4259–4269.

[189] J. Zhang, S.-Q. Shi, W.-J. Hao, G.-Y. Dong, S.-J. Tu, B. Jiang, *J. Org. Chem.* **2021**, *86*, 15886–15896.

[190] R. Kim, J. Ha, J. Woo, D. Y. Kim, *Tetrahedron Lett.* **2022**, *88*, 153567.

[191] Y. He, X. Qin, X. He, X. Wu, Z. Yin, *Eur. J. Org. Chem.* **2021**, 5831–5834.

[192] A. Prabhakar Kale, P. Nikolaienko, K. Smirnova, M. Rueping, *Eur. J. Org. Chem.* **2021**, 3496–3500.

[193] J. Wu, H. Abou-Hamdan, R. Guillot, C. Kouklovsky, G. Vincent, *Chem. Commun.* **2020**, *56*, 1713–1716.

[194] L. Schulz, S. Waldvogel, *Synlett* **2019**, *30*, 275–286.

[195] X. Dong, J. L. Roeckl, S. R. Waldvogel, B. Morandi, *Science* **2021**, *371*, 507–514.

[196] J. Strehl, M. L. Abraham, G. Hilt, *Angew. Chem. Int. Ed.* **2021**, *60*, 9996–10000; *Angew. Chem.* **2021**, *133*, 10084–10088.

[197] X. Shang, X. Liu, Y. Sun, *Green Chem.* **2021**, *23*, 2037–2043.

[198] J. Seitz, T. Wirth, *Org. Biomol. Chem.* **2021**, *19*, 6892–6896.

[199] Y. Yuan, A. Yao, Y. Zheng, M. Gao, Z. Zhou, J. Qiao, J. Hu, B. Ye, J. Zhao, H. Wen, A. Lei, *iScience* **2019**, *12*, 293–303.

[200] K. Kulangiappar, M. Ramaprakash, D. Vasudevan, T. Raju, *Synth. Commun.* **2016**, *46*, 145–153.

[201] J. C. Siu, N. Fu, S. Lin, *Acc. Chem. Res.* **2020**, *53*, 547–560.

[202] S. Zwenger, C. Basu, *Biotechnol. Mol. Biol. Rev.* **2008**, *3,* 1–7.

[203] E. J. N. Helfrich, G.-M. Lin, C. A. Voigt, J. Clardy, *Beilstein J. Org. Chem.* **2019**, *15*, 2889–2906.

[204] Y. Yamada, T. Kuzuyama, M. Komatsu, K. Shin-ya, S. Omura, D. E. Cane, H. Ikeda, *PNAS,* **2015**, *112*, 857–862.

[205] F. R. Marín, C. Soler-Rivas, O. Benavente-García, J. Castillo, J. A. Pérez-Alvarez, *Food Chem.* **2007**, *100*, 736–741.

[206] A. Corma, S. Iborra, A. Velty, *Chem. Rev.* **2007**, *107*, 2411–2502.

[207] E. Jongedijk, K. Cankar, M. Buchhaupt, J. Schrader, H. Bouwmeester, J. Beekwilder, *Appl. Microbiol. Biotechnol.* **2016**, *100*, 2927–2938.

[208] B. M. Lange, *Biosynthesis and Biotechnology of High-Value p-Menthane Monoterpenes, Including Menthol, Carvone, and Limonene* in *Biotechnology of Isoprenoids*, (Eds.: J. Schrader, J. Bohlmann), Springer International, Basel, Switzerland, **2015**, pp. 319–353.

[209] A. Masyita, R. Mustika Sari, A. Dwi Astuti, B. Yasir, N. Rahma Rumata, T. Bin Emran, F. Nainu, J. Simal-Gandara, *Food Chem. X* **2022**, *13*, 100217.

[210] F. Della Monica, A. W. Kleij, *Polym. Chem.* **2020**, *11*, 5109–5127.

[211] L. A. Parreira, L. Menini, E. V. Gusevskaya, *Catal. Sci. Technol.* **2014**, *4*, 2016–2022.

[212] W. Schwab, C. Fuchs, F. Huang, *Eur. J. Lipid Sci. Tec.* **2013**, *115*, 3–8.

[213] M. E. G. Mosquera, G. Jiménez, V. Tabernero, J. Vinueza-Vaca, C. García-Estrada, K. Kosalková, A. Sola-Landa, B. Monje, C. Acosta, R. Alonso, M. Á. Valera, *Sustain. Chem.* **2021**, *2*, 467–492.

[214] J. Malyszko, E. Malyszko, E. Rutkowska-Ferchichi, M. Kaczor, *Anal. Chim. Acta* **1998**, *376*, 357–364.

[215] S. Milisavljevic, K. Wurst, G. Laus, M. Vukicevic, R. Vukicevic, *Steroids* **2005**, *70*, 867–872.

[216] M. Inês, A. J. Mendonça, A. P. Esteves, D. I. Mendonça, M. J. Medeiros, *C. R. Chim.* **2009**, *12*, 841–849.

[217] H. Hayashi, *Res. Chem. Intermediat.* **1998**, *24*, 183–196.

[218] J.-P. Schirmann, P. Bourdauducq, in *Ullmann's Encyclopedia of Industrial Chemistry*, Wiley-VCH, Weinheim, Germany, **2001**.

[219] U. Ragnarsson, *Chem. Soc. Rev.* **2001**, *30*, 205–213.

[220] P. Rademacher, in *Category 5, Compounds with One Saturated Carbon Heteroatom Bond* (Eds.: Enders, Schaumann), Georg Thieme, Stuttgart, **2009**.

[221] J. W. Cahn, R. E. Powell, *J Am Chem Soc* **1954**, *76*, 2565–2567.

[222] S. W. Tatarchuk, J. J. Medvedev, F. Li, Y. Tobolovskaya, A. Klinkova, *Angew. Chem. Int. Ed.* **2022**, *61*, e202209839.

[223] E. Feng, Z. Hou, H. Xu, *Chinese J. Org. Chem.* **2019**, *39*, 1424.

[224] F. Wang, J. B. Gerken, D. M. Bates, Y. J. Kim, S. S. Stahl, *J. Am. Chem. Soc.* **2020**, *142*, 12349–12356.

[225] V. M. Breising, J. M. Kayser, A. Kehl, D. Schollmeyer, J. C. Liermann, S. R. Waldvogel, *Chem. Commun.* **2020**, *56*, 4348–4351.

[226] Y. Zhao, X. Guo, S. Li, Y. Fan, G. Ji, M. Jiang, Y. Yang, Y. Jiang, *Angew. Chem. Int. Ed.* **2022**, *61*, e202213636.

[227] M. Gupta, B. S. Bairwa, R. Karnawat, I. K. Sharma, P. S. Verma, *Indian J. Chem.* **2008**, *47*, 383–386.

[228] A. Kehl, T. Gieshoff, D. Schollmeyer, S. R. Waldvogel, *Chemistry - A European Journal* **2018**, *24*, 590–593.

[229] T. Gieshoff, D. Schollmeyer, S. R. Waldvogel, *Angewandte Chemie International Edition* **2016**, *55*, 9437–9440; *Angew. Chem.* **2016**, *128*, 9587 – 9590.

[230] S. S. Popova, L. N. Ol'shanskaya, T. V. Pominova, *Russ. J. Electrochem.* **2002**, *38*, 362–368.

[231] Z. X. Shu, R. S. McMillan, J. J. Murray, *J. Electrochem. Soc.* **1993**, *140*, 922–927.

[232] C. Reichardt, T. Welton, in *Solvents and Solvent Effects in Organic Chemistry*, Wiley-VCH, Weinheim, Germany, **2010**.

[233] C. Wan, R.-J. Song, J.-H. Li, *Org. Lett.* **2019**, *21*, 2800–2803.

[234] L. G. Gombos, L. Werner, D. Schollmeyer, C. A. Martínez-Huitle, S. R. Waldvogel, *Eur. J. Org. Chem.* **2022**, e202200857.

[235] P. R. Khoury, J. D. Goddard, W. Tam, *Tetrahedron* **2004**, *60*, 8103–8112.

[236] C. Gütz, M. Selt, M. Bänziger, C. Bucher, C. Römelt, N. Hecken, F. Gallou, T. R. Galvão, S. R. Waldvogel, *Chem. Eur. J.* **2015**, *21*, 13878–13882.

[237] G. S. Buchanan, K. P. Cole, G. Li, Y. Tang, L.-F. You, R. P. Hsung, *Tetrahedron* **2011**, *67*, 10105–10118.

[238] S. Song, X. Li, X. Sun, Y. Yuan, N. Jiao, *Green Chem.* **2015**, *17*, 3285–3289.

[239] L. Friedman, H. Shechter, *J. Org. Chem.* **1960**, *25*, 877–879.

[240] E. Dinca, P. Hartmann, J. Smrček, I. Dix, P. G. Jones, U. Jahn, *Eur. J. Org. Chem.* **2012**, 4461–4482.

[241] G. E. Ham, J. Stevens, *J. Org. Chem.* **1962**, *27*, 4638–4639.

[242] H.-S. Chong, X. Sun, Y. Chen, M. Wang, *Tetrahedron Lett.* **2015**, *56*, 946–948.

[243] S. Debarge, P. McDaid, P. O'Neill, J. Frahill, J. W. Wong, D. Carr, A. Burrell, S. Davies, M. Karmilowicz, J. Steflik, *Org. Process. Res. Dev.* **2014**, *18*, 109–121.

[244] O. Hauenstein, S. Agarwal, A. Greiner, *Nat. Commun.* **2016**, *7*, 11862.

[245] L. H. Choudhury, T. Parvin, A. T. Khan, *Tetrahedron* **2009**, *65*, 9513–9526.

[246] Sigma Aldrich Merck, “Dimethylsulfid SDS,” can be found under https://www.sigmaaldrich.com/DE/en/sds/sial/471577, accessed: 13.08.2023.

[247] M. Klein, S. R. Waldvogel, *Angew. Chem. Int. Ed.* **2021**, *60*, 23197–23201; *Angew. Chem.* **2021**, *133*, 23382–23387.

[248] M. Klein, D. L. Troglauer, S. R. Waldvogel, *JACS Au* **2023**, *3*, 575–583.

[249] D. Yu, R. Ji, Z. Sun, W. Li, Z.-Q. Liu, *Tetrahedron Lett.* **2021**, *86*, 153514.

[250] I. V. Alabugin, K. Gilmore, *Chem. Commun.* **2013**, *49*, 11246.

[251] X. Zhou, S. Zheng, H. Zhang, Q. Liu, W. Xing, X. Li, Y. Han, P. Zhao, *Entropy* **2022**, *24*, 1221.

[252] G. M. Mudd, *Ore. Geol. Rev.* **2010**, *38*, 9–26.

[253] H. U. Sverdrup, K. V. Ragnarsdottir, *Resour. Conserv. Recycl.* **2016**, *114*, 130–152.

[254] L. Li, M. Xue, X. Yan, W. Liu, K. Xu, S. Zhang, *Org. Biomol. Chem.* **2018**, *16*, 4615–4618.

[255] T. Cantin, A. B. Charette, T. Poisson, P. Jubault, *Synthesis* **2023**, 55, A–H.

[256] Y. Matsumura, T. Maki, Y. Satoh, *Tetrahedron Lett* **1997**, *38*, 8879–8882.

[257] L. Tiwari, V. Kumar, B. Kumar, D. Mahajan, *RSC Adv.* **2018**, *8*, 21585–21595.

[258] S. Wawzonek, T. W. McIntyre, *J. Electrochem. Soc.* **1972**, *119*, 1350.

[259] G. Liu, S. Liu, Z. Li, H. Chen, J. Li, Y. Zhang, G. Shen, B. Yang, X. Hu, X. Huang, *RSC Adv.* **2022**, *12*, 118–122.

[260] A. M. Sheta, A. Alkayal, M. A. Mashaly, S. B. Said, S. S. Elmorsy, A. V. Malkov, B. R. Buckley, *Angew. Chem. Int. Ed.* **2021**, *60*, 21832–21837; *Angew. Chem.* **2021**, *133*, 22003–22008.

[261] D. M. Mohilner, R. N. Adams, W. J. Argersinger, *J. Am. Chem. Soc.* **1962**, *84*, 3618–3622.

[262] X. Wang, J. Li, Y. Duan, J. Li, H. Wang, X. Yang, M. Gong, *ChemCatChem* **2022**, *14*, e202101906.

[263] J. I. de Jong, J. de Jonge, *Recl. Trav. Chim. Pays-Ba.* **1953**, *72*, 169–172.

[264] Ernest R. Blatchley, M. Cheng, *Environ. Sci. Technol.* **2010**, *44*, 8529–8534.

[265] F. D. Chattaway, *Proceedings of the Royal Society of London* in *Series A, Containing Papers of a Mathematical and Physical Character* **1908**, *81*, 381–388.

[266] E. Delebecq, J.-P. Pascault, B. Boutevin, F. Ganachaud, *Chem. Rev.* **2013**, *113*, 80–118.

[267] A. Lapprand, F. Boisson, F. Delolme, F. Méchin, J.-P. Pascault, *Polym. Degrad. Stab*. **2005**, *90*, 363–373.

[268] A. K. V. Mruthunjaya, A. A. J. Torriero, *Molecules* **2023**, *28*, 471.

[269] U. Ragnarsson, *Chem. Soc. Rev.* **2001**, *30*, 205–213.

[270] R. M. Moriarty, C. J. Chany, R. K. Vaid, O. Prakash, S. M. Tuladhar, *J. Org. Chem.* **1993**, *58*, 2478–2482.

[271] D. Landsberg, M. Kalesse, *Synlett* **2010**, 1104–1106.

[272] M. Firdaus, L. Montero de Espinosa, M. A. R. Meier, *Macromolecules* **2011**, *44*, 7253–7262.

[273] D. Wang, Z. Wan, H. Zhang, A. Lei, *Adv. Synth. Catal.* **2021**, *363*, 1022–1027.

[274] Z. Li, Q. Sun, P. Qian, K. Hu, Z. Zha, Z. Wang, *Chinese Chem. Let.* **2020**, *31*, 1855–1858.

[275] R. Francke, *Curr. Opin. Electrochem.* **2021**, *28*, 100719.

[276] P. Becker, T. Duhamel, C. Martínez, K. Muñiz, *Angew. Chem. Int. Ed.* **2018**, *57*, 5166–5170; *Angew. Chem.* **2018**, *130*, 5262–5266.

[277] Q. Yao, X. Huang, J. Pu, X. Xi, X. Fang, L. Zhao, Y. Mai, C. He, *Chinese J. Org. Chem.* **2017**, *37*, 116.

[278] A. Seitz, P. J. Kohlpaintner, T. van Lingen, M. Dyga, F. Sprang, M. Zirbes, S. R. Waldvogel, L. J. Gooßen, *Angew. Chem. Int. Ed.* **2022**, *61*, e202117563; *Angew. Chem.* **2022**, *134*, e202117563.

[279] S. Arndt, D. Weis, K. Donsbach, S. R. Waldvogel, *Angew. Chem. Int. Ed.* **2020**, *59*, 8036–8041; *Angew. Chem.* **2020**, *132*, 8112–8118.

[280] S. Arndt, P. J. Kohlpaintner, K. Donsbach, S. R. Waldvogel, *Org. Process. Res. Dev.* **2022**, *26*, 2564–2613.

[281] J. Vidal, J.-C. Hannachi, G. Hourdin, J.-C. Mulatier, A. Collet, *Tetrahedron Lett.* **1998**, *39*, 8845–8848.

[282] W. L. F. Armarego, C. L. L. Chai, *Purification of Laboratory Chemicals*, Butterworth-Heinemann, Elsevier, Oxford, UK, **2013**.

[283] R. K. Harris, E. D. Becker, S. M. C. de Menezes, R. Goodfellow, P. Granger, *Solid State Nucl. Magn. Reason.* **2002**, *22*, 458–483.

[284] R. R. Gagne, C. A. Koval, G. C. Lisensky, *Inorg. Chem.* **1980**, *19*, 2854–2855.

[285] S. Trasa'tti, *Pure Appl. Chem.* **1986**, *58*, 955–966.

[286] C. Gütz, B. Klöckner, S. R. Waldvogel, *Org. Process. Res. Dev.* **2016**, *20*, 26–32.

[287] Z. H. Guan, H. Lei, M. Chen, Z. H. Ren, Y. Bai, Y. Y. Wang, *Adv Synth Catal* **2012**, *354*, 489–496.

[288] U. Husstedt, H. J. Schäfer, *Synthesis* **1979**, *12*, 966–998.

[289] Y. Kitahara, T. Kato, I. Ichinose, *Chem. Lett.* **1976**, *5*, 1051–1056.

[290] L. Peilleron, T. D. Grayfer, J. Dubois, R. H. Dodd, K. Cariou, *Beilstein J. Org. Chem.* **2018**, *14*, 1103–1111.

[291] D. G. Vassão, D. R. Gang, T. Koeduka, B. Jackson, E. Pichersky, L. B. Davin, N. G. Lewis, *Org. Biomol. Chem.* **2006**, *4*, 2733–2744.

[292] T. Ying, W. Bao, Y. Zhang, *J. Chem. Res.* **2004**, 806–807.

[293] J. A. Gonçalves, A. C. Bueno, E. V. Gusevskaya, *J Mol. Catal. A* **2006**, *252*, 5–11.

[294] Y. Sun, H. Wang, R. Prins, *Tetrahedron Lett.* **2008**, *49*, 2063–2065.

[295] A. Jones, H. Kronenwetter, R. Manchanayakage, *Electrochem. Commun.* **2012**, *25*, 8–10.

[296] N. Saraiva Rosa, T. Glachet, Q. Ibert, J. F. Lohier, X. Franck, V. Reboul, *Synthesis* **2020**, *52*, 2099–2105.

[297] B. N. Atkinson, A. R. Chhatwal, H. v. Lomax, J. W. Walton, J. M. J. Williams, *Chem. Commun.* **2012**, *48*, 11626–11628.

[298] I. Jain, P. Malik, *Synlett* **2022**, *33*, 93–97.

[299] D. Habibi, S. Heydari, A. Faraji, H. Keypour, M. Mahmoudabadi, *Polyhedron* **2018**, *151*, 520–529.

[300] J. Li, X. Wang, Z. Wang, Y. Shi, *Org. Lett.* **2021**, *23*, 8958–8962.

[301] I. D. Inaloo, S. Majnooni, M. Esmaeilpour, *Eur. J. Org. Chem.* **2018**, 3481–3488.

[302] T. Meyer, J. Rabeah, A. Brückner, X. F. Wu, *Chem. Eur. J.* **2021**, *27*, 5642–5647.

[303] R. Hauptmann, A. Petrosyan, F. Fennel, M. A. Argüello Cordero, A. E. Surkus, J. Pospech, *Chem. Eur. J.* **2019**, *25*, 4325–4329.

[304] T. Mizuno, T. Nakai, M. Mihara, *Synthesis* **2010**, 4251–4255.

[305] Y. Cao, J. G. Yang, Y. Deng, S. Wang, Q. Liu, C. Shen, W. Lu, C. M. Che, Y. Chen, L. He, *Angew. Chem. Int. Ed.* **2020**, *59*, 2080–2084.

[306] J. Qin, Y. Long, F. Sun, P. P. Zhou, W. D. Wang, N. Luo, J. Ma, *Angew. Chem. Int. Ed.* **2022**, *61*, e202112907.

[307] Y. Su, X. Liu, J. Yu, G. Cao, R. Zhang, Y. Zhao, D. Huang, K. H. Wang, C. Huo, Y. Hu, *Synthesis* **2020**, *52*, 1103–1112.

9. Publications and student mentoring

Publications

- L. G. Gombos, S. R. Waldvogel, *Electrochemical Bromofunctionalization of Alkenes and Alkynes – To Sustainability and Beyond*, *Sustain. Chem*. **2022**, *3*, 430–454.

  DOI: 10.3390/suschem3040027

- L. G. Gombos, L. Werner, D. Schollmeyer; C. A. Martínez-Huitle, S. R. Waldvogel, *Selective Electrochemical Dibromination of Terpenes and Naturally Derived Olefins*, *Eur. J. Org. Chem*. **2022**, e202200857.

  DOI: 10.1002/ejoc.202200857

Student mentoring

- 2022, personal data, Undergraduate research assistant.

  Studies of the electrochemical Hofmann rearrangement of ureas to hydrazine derivatives.

- 2021, personal data, Bachelor thesis.

  Title: *Electrochemical bromination of naturally derived compounds.*

10. Spectra of unreported compounds

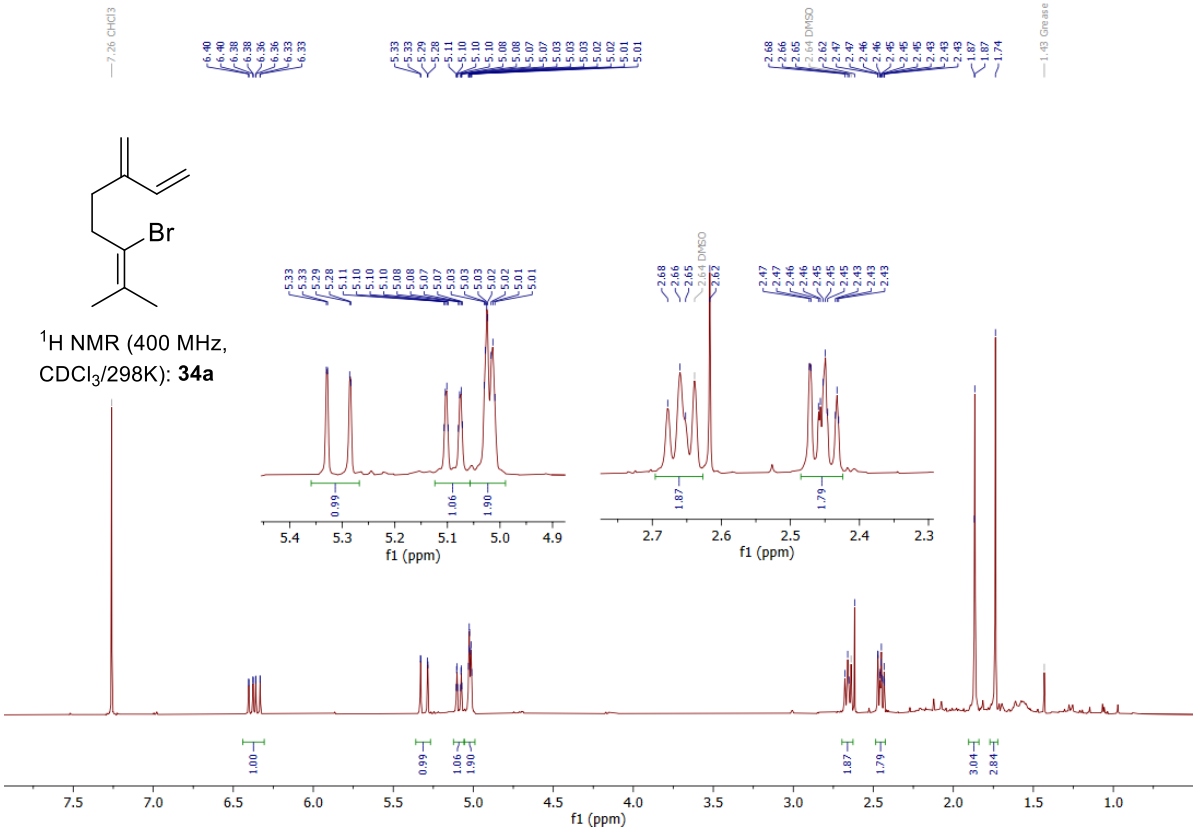

Figure 42. 400 MHz ^{1}H NMR spectrum of 6-bromo-7-methyl-3-methyleneoct-1,6-diene (**34a**).

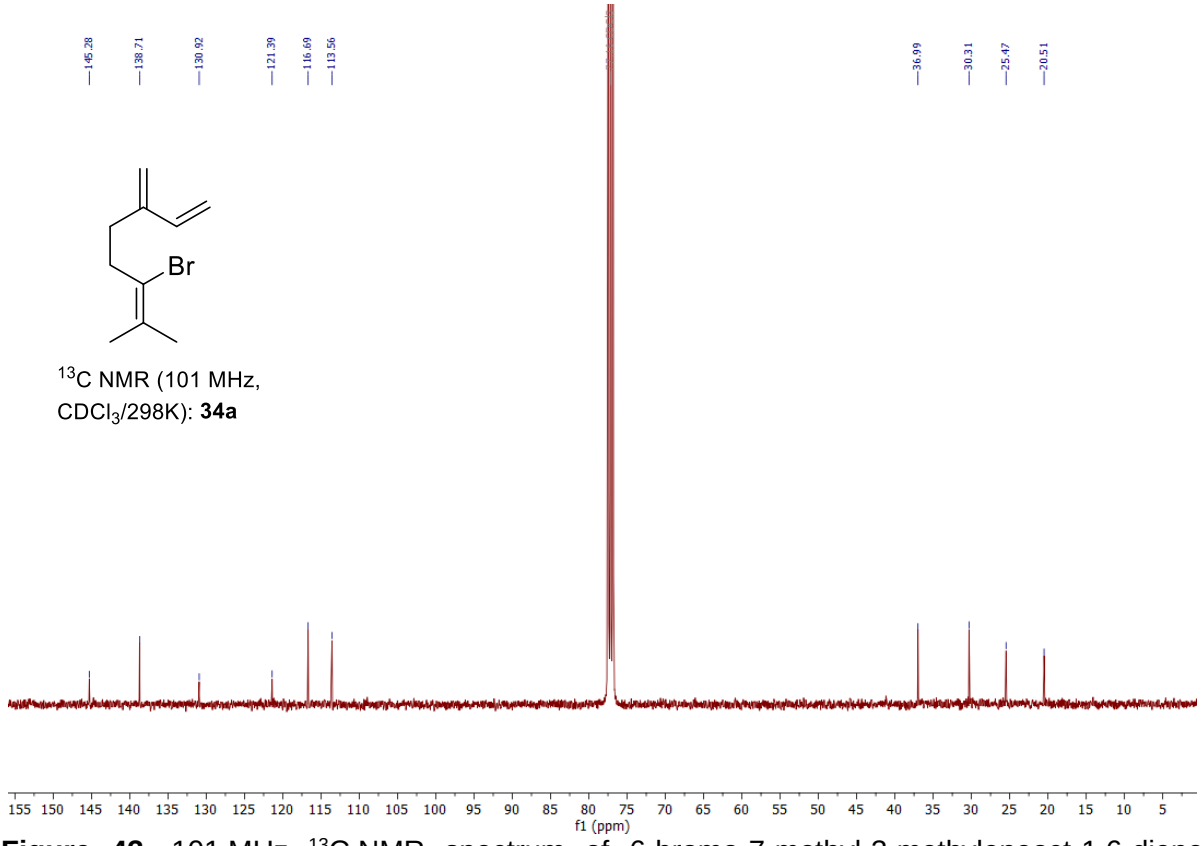

Figure 43. 101 MHz ^{13}C NMR spectrum of 6-bromo-7-methyl-3-methyleneoct-1,6-diene (**34a**).

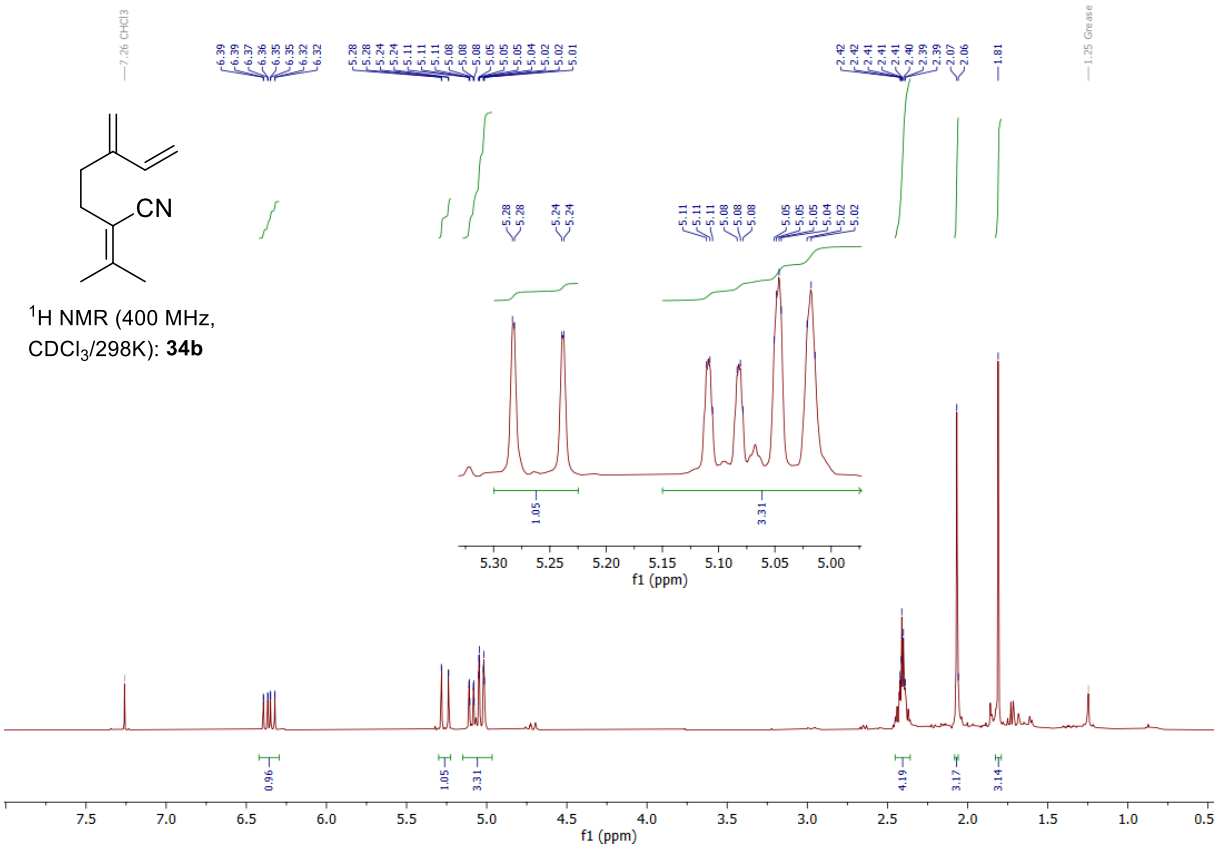

Figure 44. 400 MHz ^{1}H NMR spectrum of 5-methylene-2-(propan-2-ylidene)hept-6-enenitrile (**34b**).

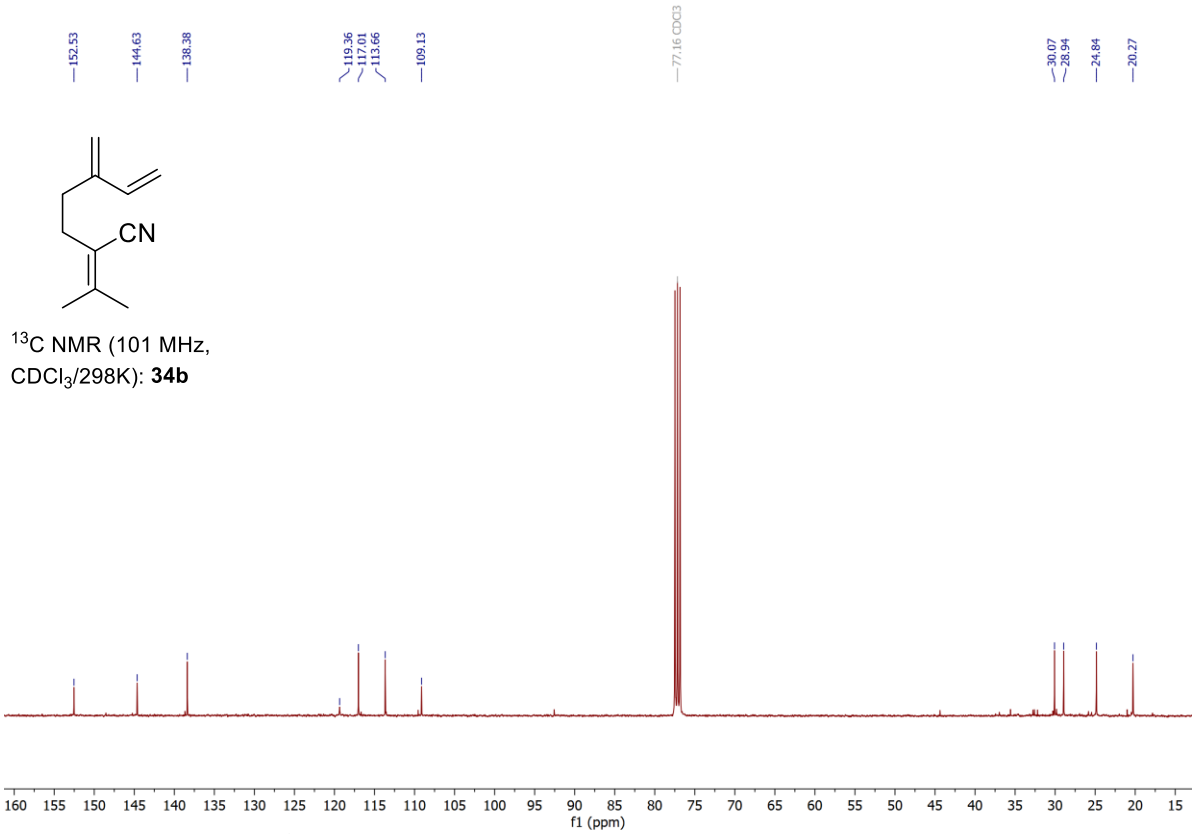

Figure 45. 101 MHz ^{13}C NMR spectrum of 5-methylene-2-(propan-2-ylidene)hept-6-enenitrile (**34b**).

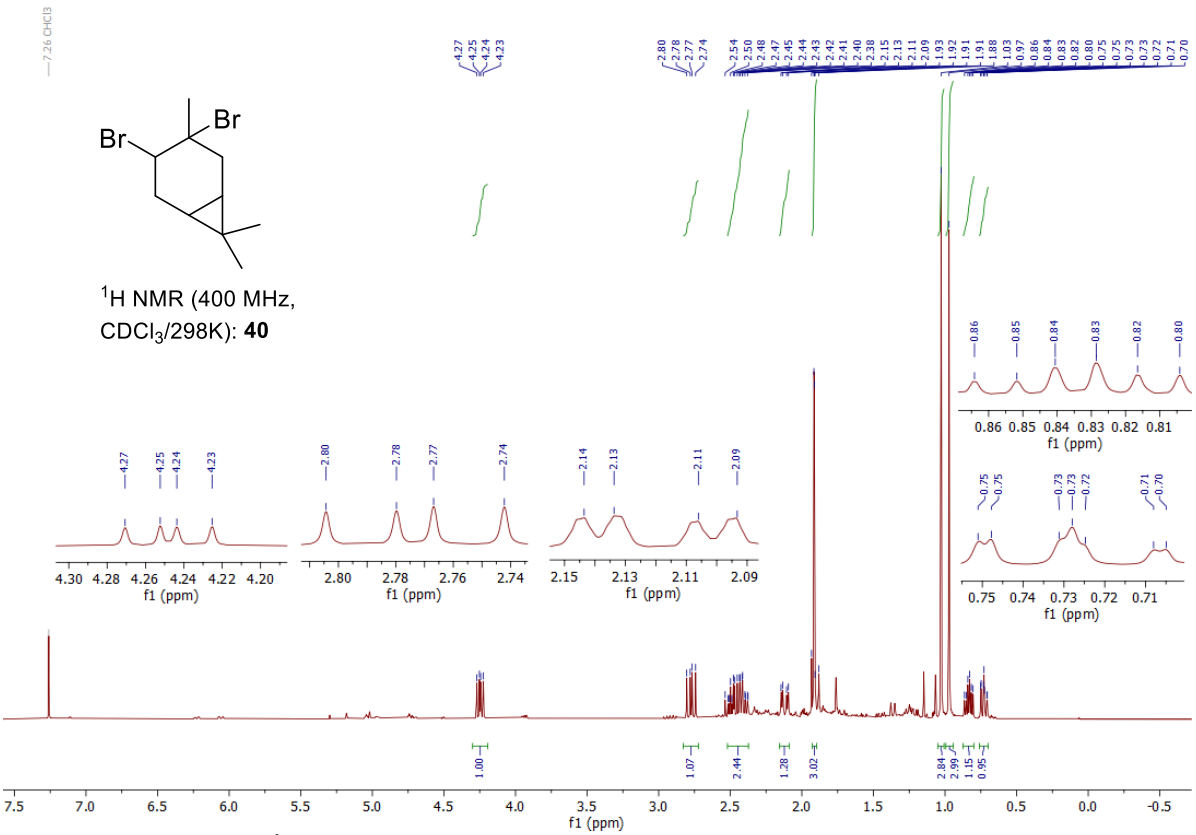

Figure 46. 400 MHz ^{1}H NMR spectrum of 3,4-dibromocarane (**40**).

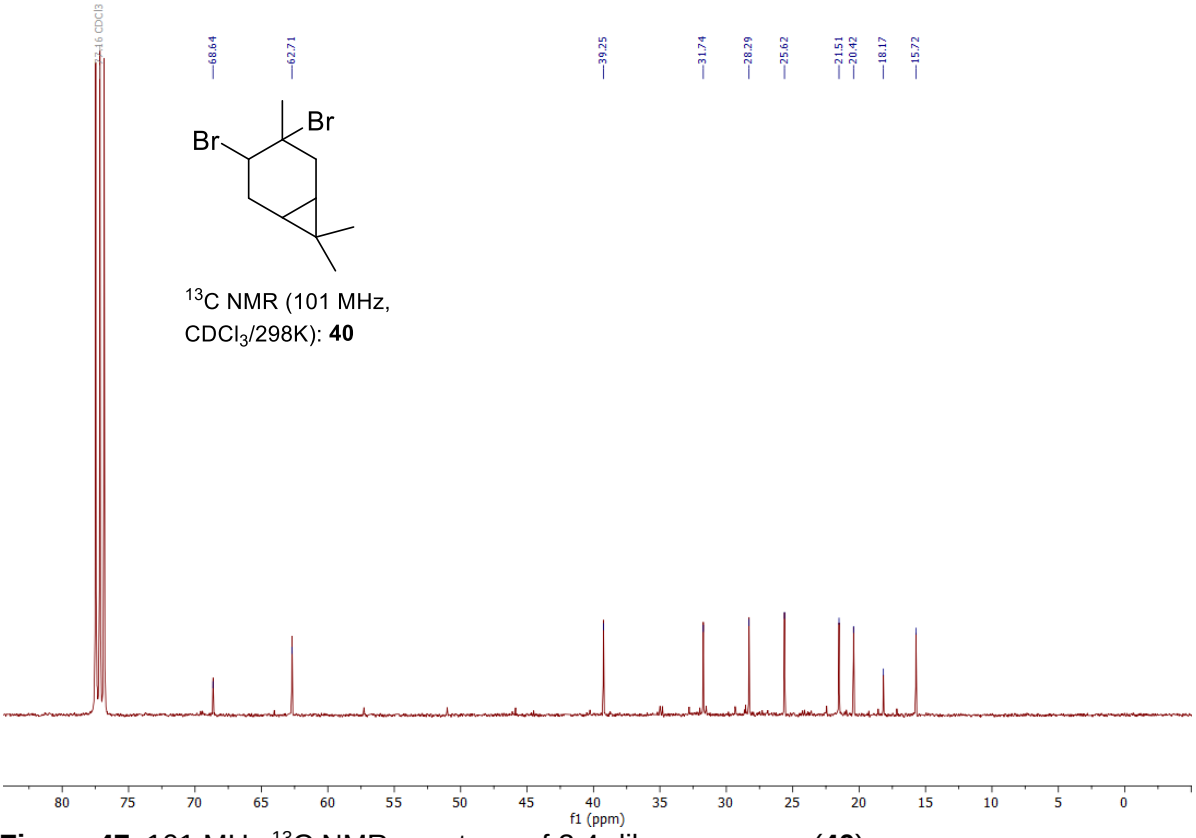

Figure 47. 101 MHz ^{13}C NMR spectrum of 3,4-dibromocarane (**40**).

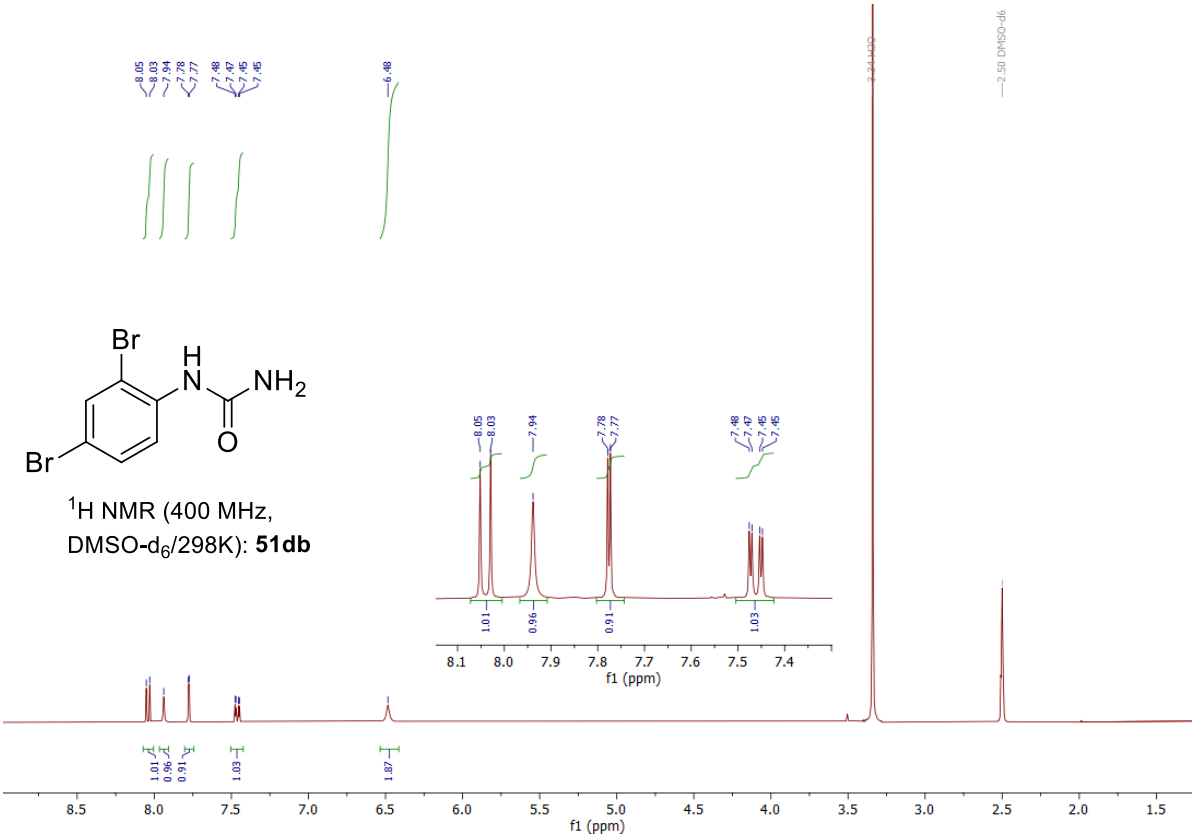

Figure 48. 400 MHz ^{1}H NMR spectrum of 1-(2,4-dibromophenyl)urea (**51db**).

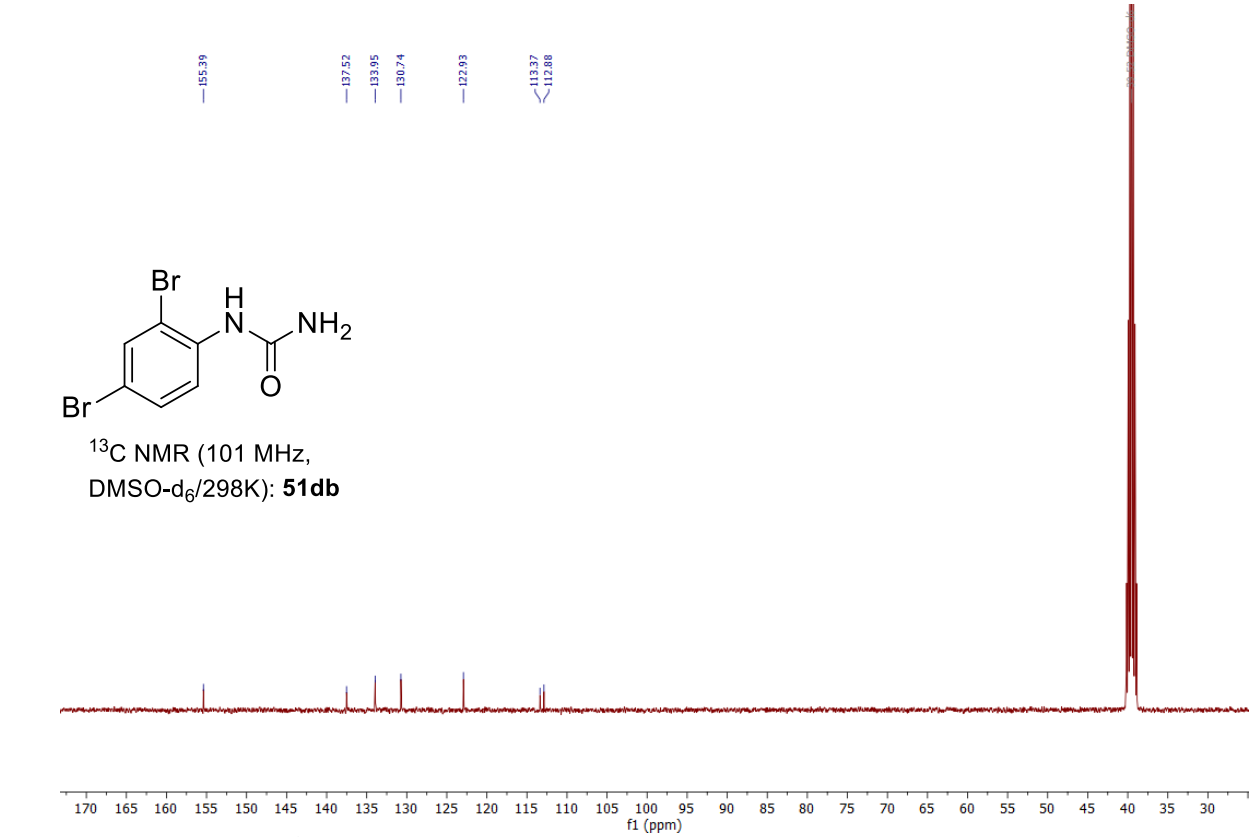

Figure 49. 101 MHz ^{13}C NMR spectrum of 1-(2,4-dibromophenyl)urea (**51db**).

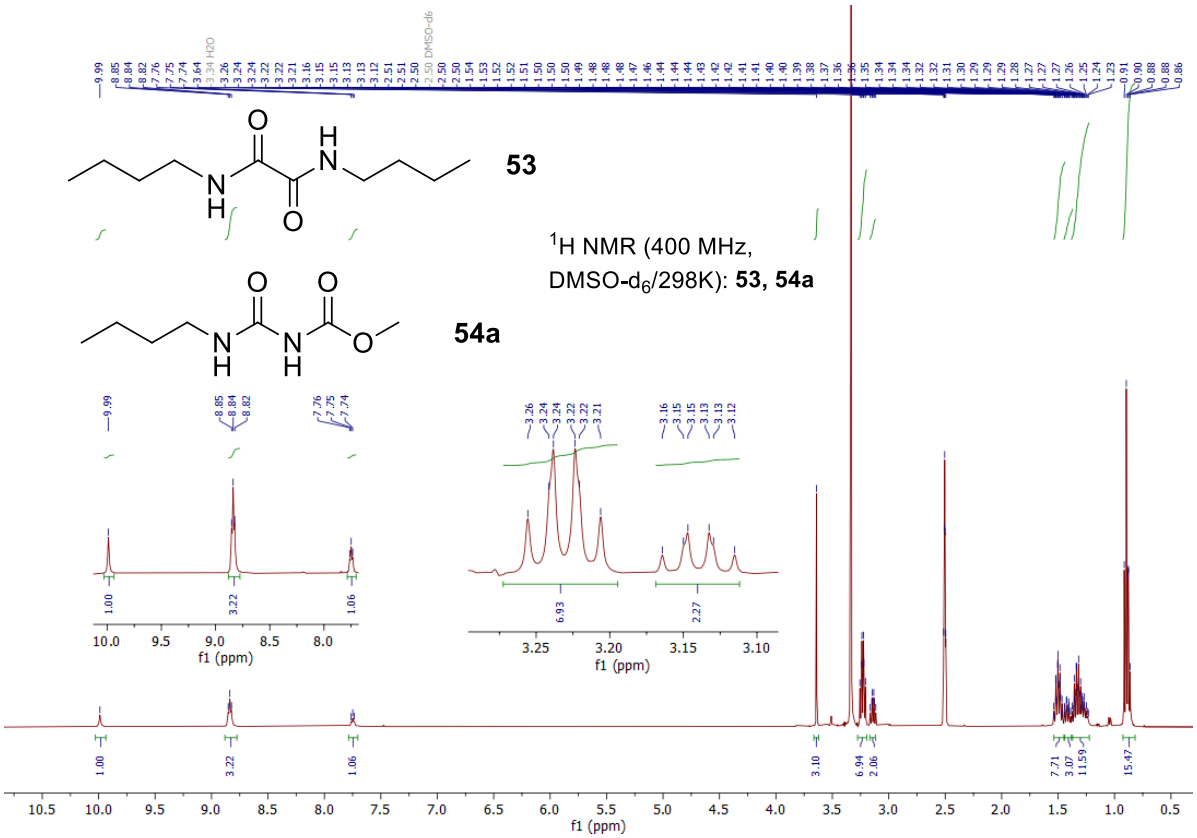

Figure 50. 400 MHz ^{1}H NMR spectrum of *N,N´*-dibutyloxalamide (**53**) and methyl *N*-(butylcarbamoyl)carbamate (**54a**).

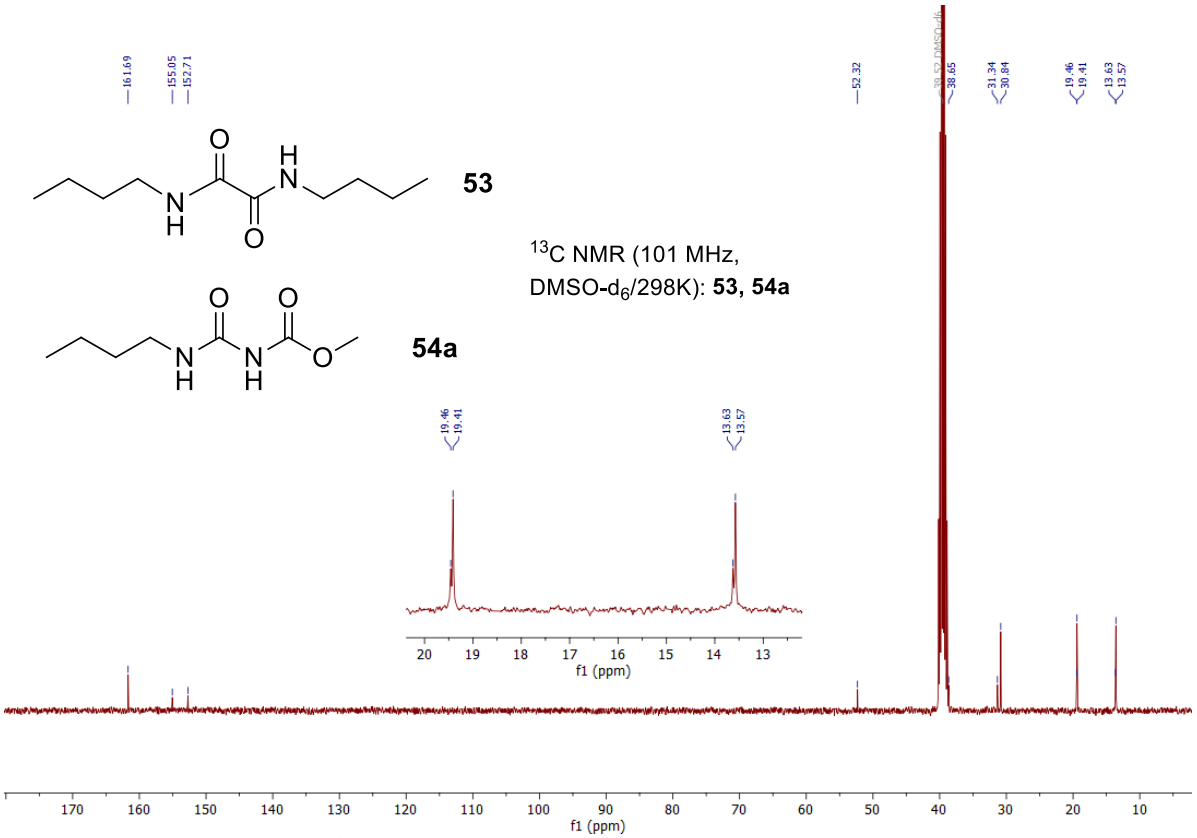

Figure 51. 101 MHz ^{13}C NMR spectrum of *N,N´*-dibutyloxalamide (**53**) and methyl *N*-(butylcarbamoyl)carbamate (**54a**).

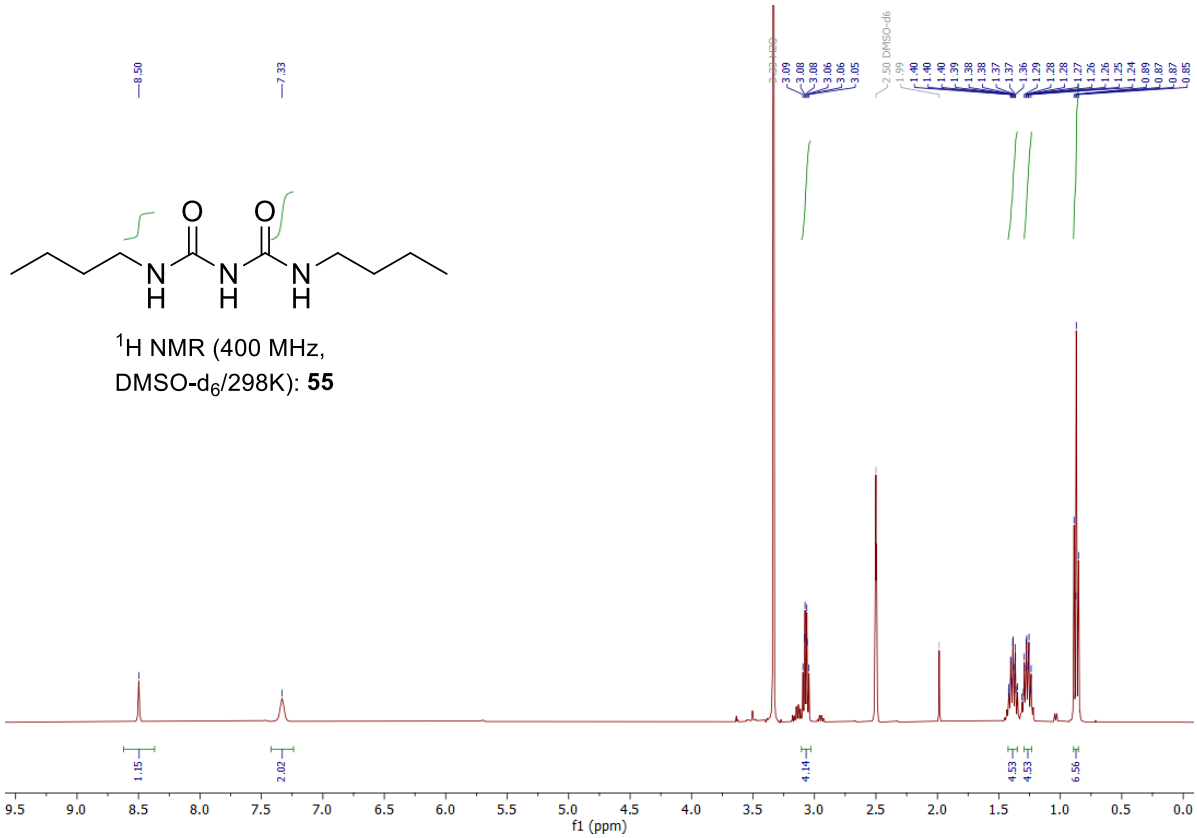

Figure 52. 400 MHz ^{1}H NMR spectrum of 1-butyl-3-(butylcarbamoyl)urea (**55**).

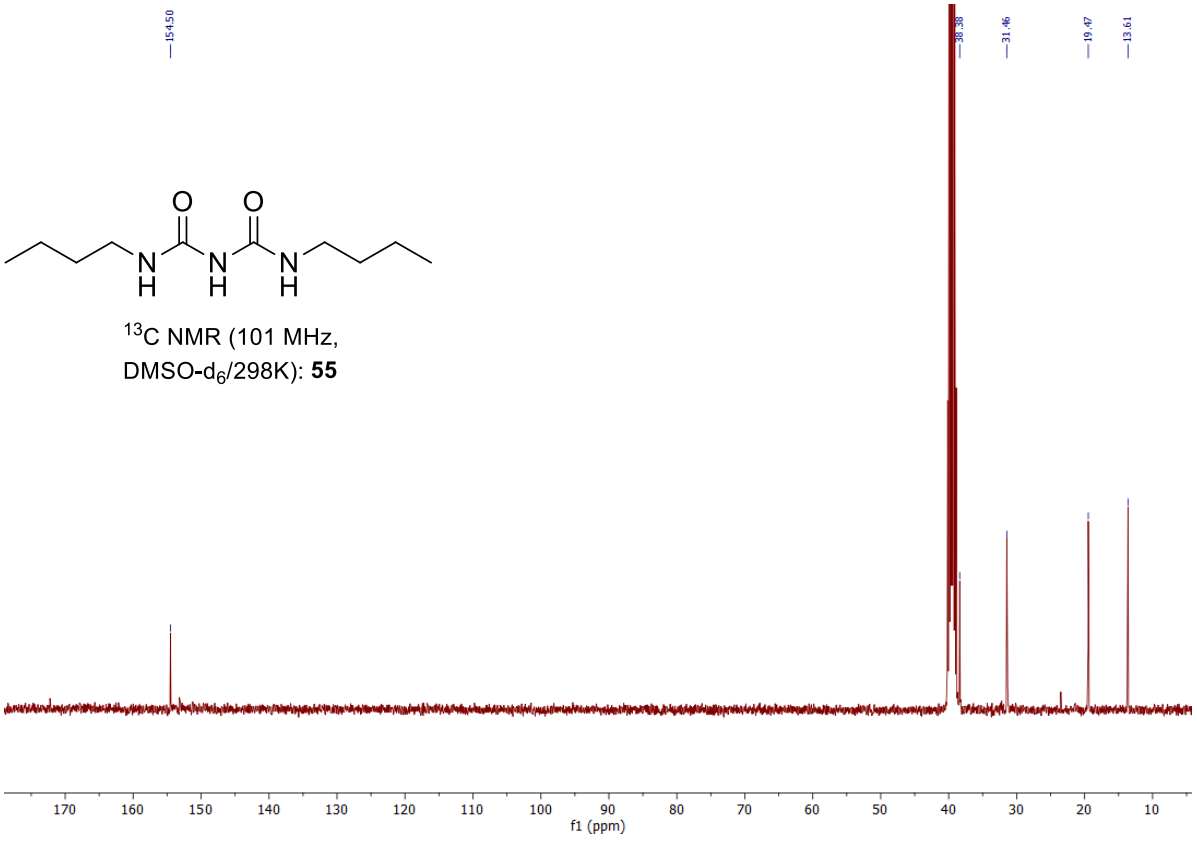

Figure 53. 101 MHz ^{13}C NMR spectrum of 1-butyl-3-(butylcarbamoyl)urea (**55**).

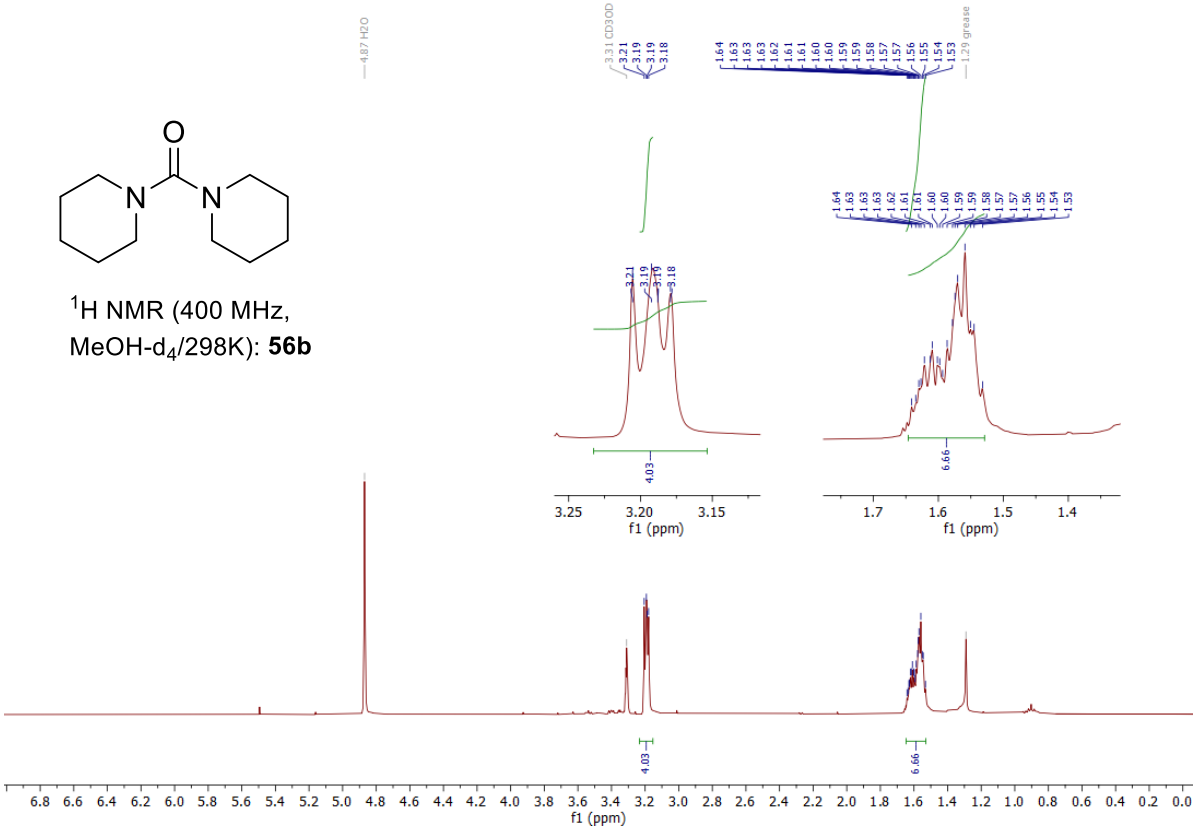

Figure 54. 400 MHz ^{1}H NMR spectrum of 1,1´-carbonyldipiperidine (**56b**).

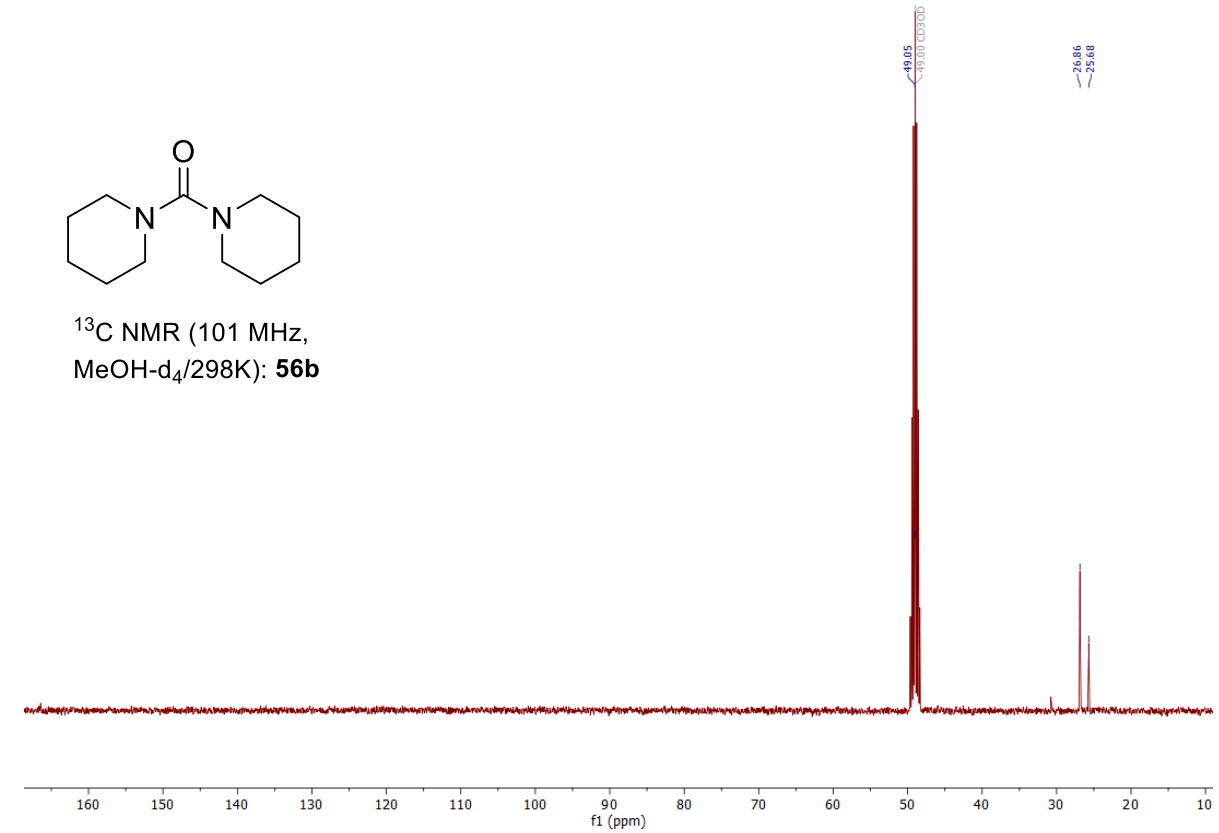

Figure 55. 101 MHz ^{13}C NMR spectrum of 1,1´-carbonyldipiperidine (**56b**).

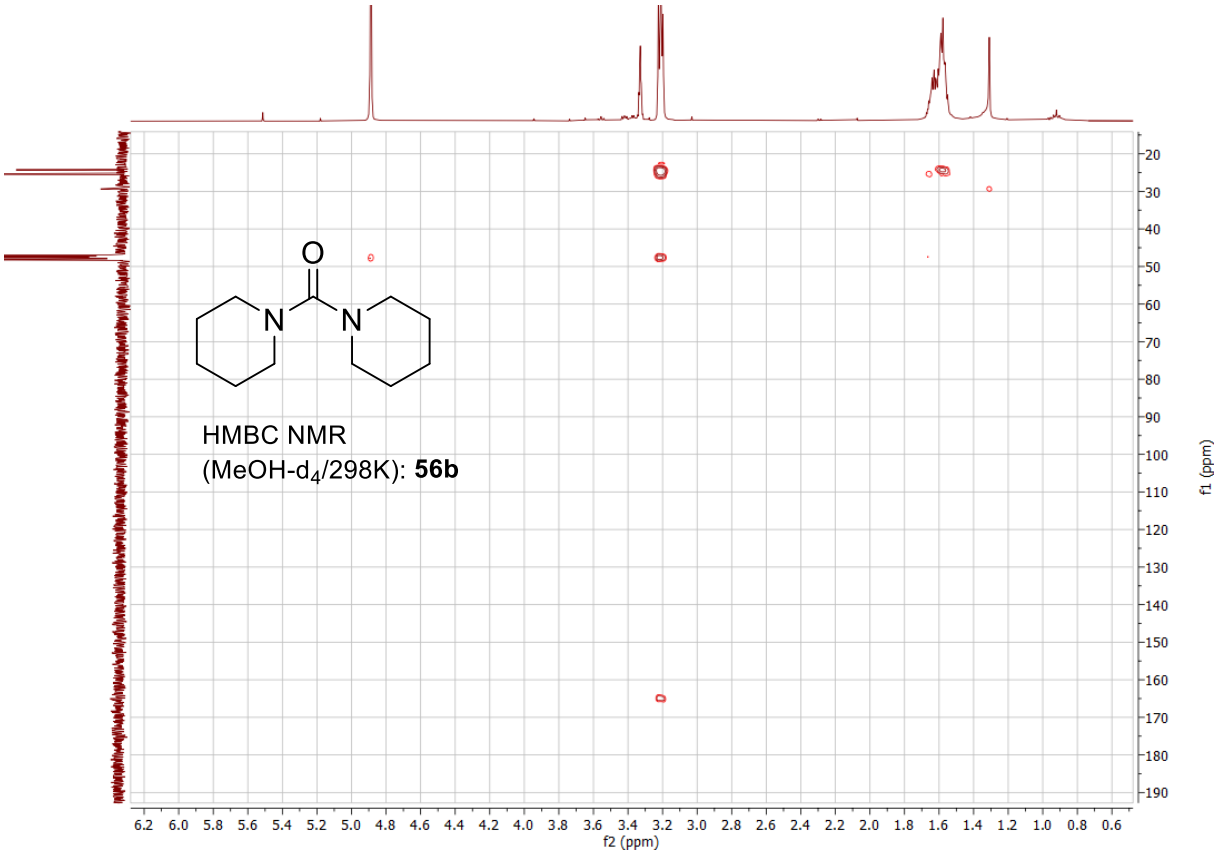

Figure 56. HMBC NMR spectrum of 1,1´-carbonyldipiperidine (**56b**).

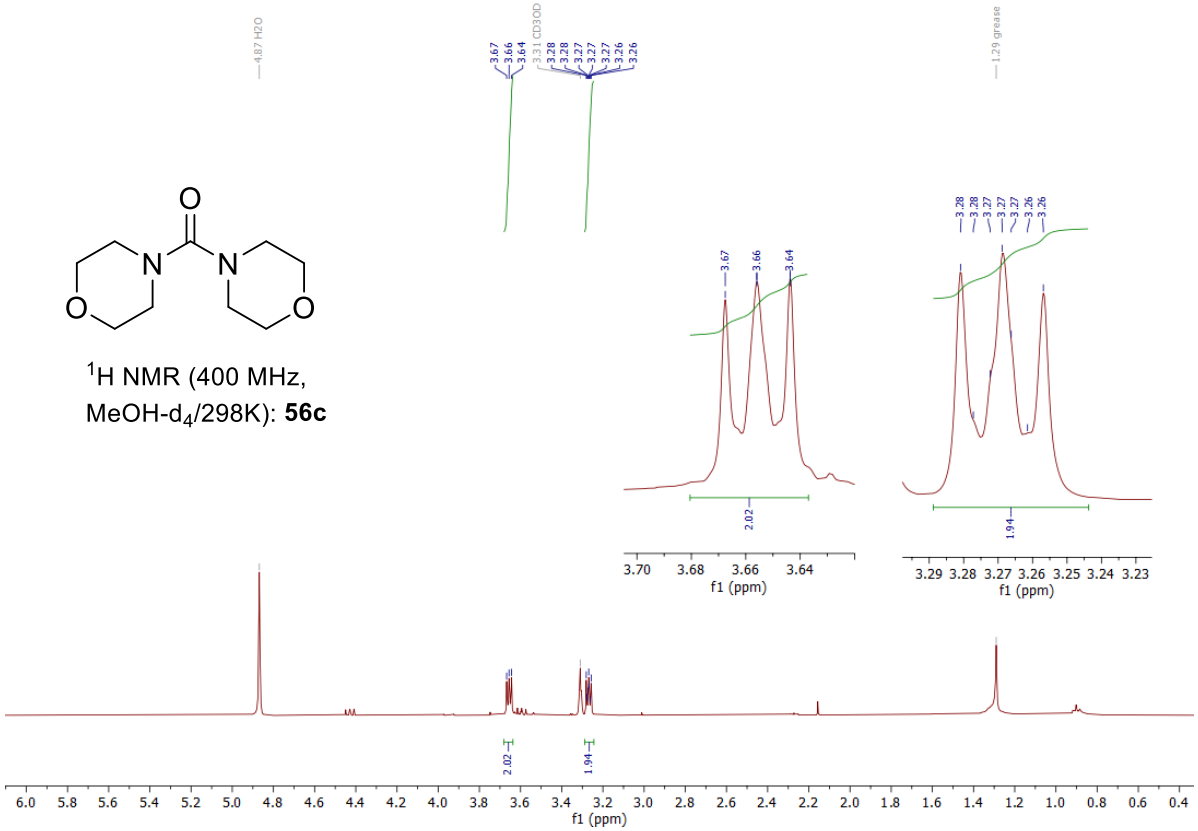

Figure 57. 400 MHz ^{1}H NMR spectrum of 4,4´-carbonyldimorpholine (**56c**).

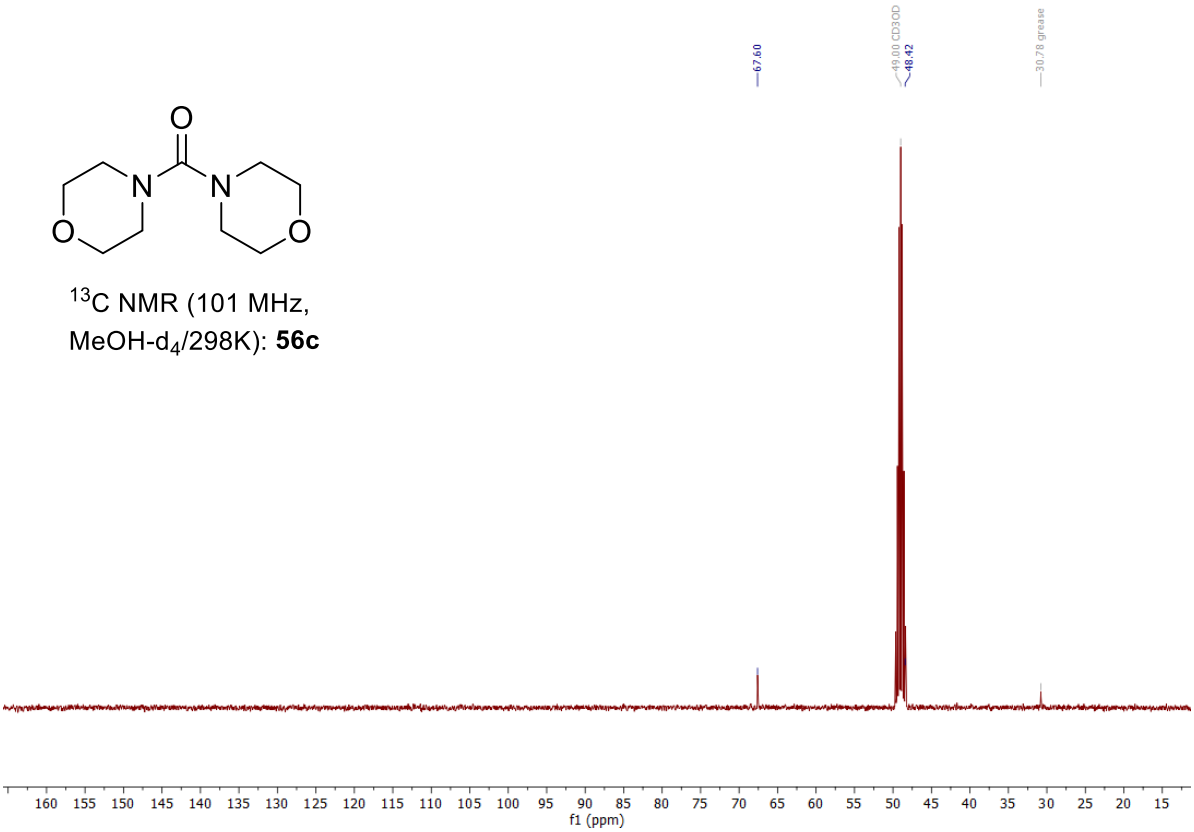

^{13}C NMR (101 MHz, MeOH-d_4/298K): **56c**

Figure 58. 101 MHz ^{13}C NMR spectrum 4,4´-carbonyldimorpholine (**56c**).

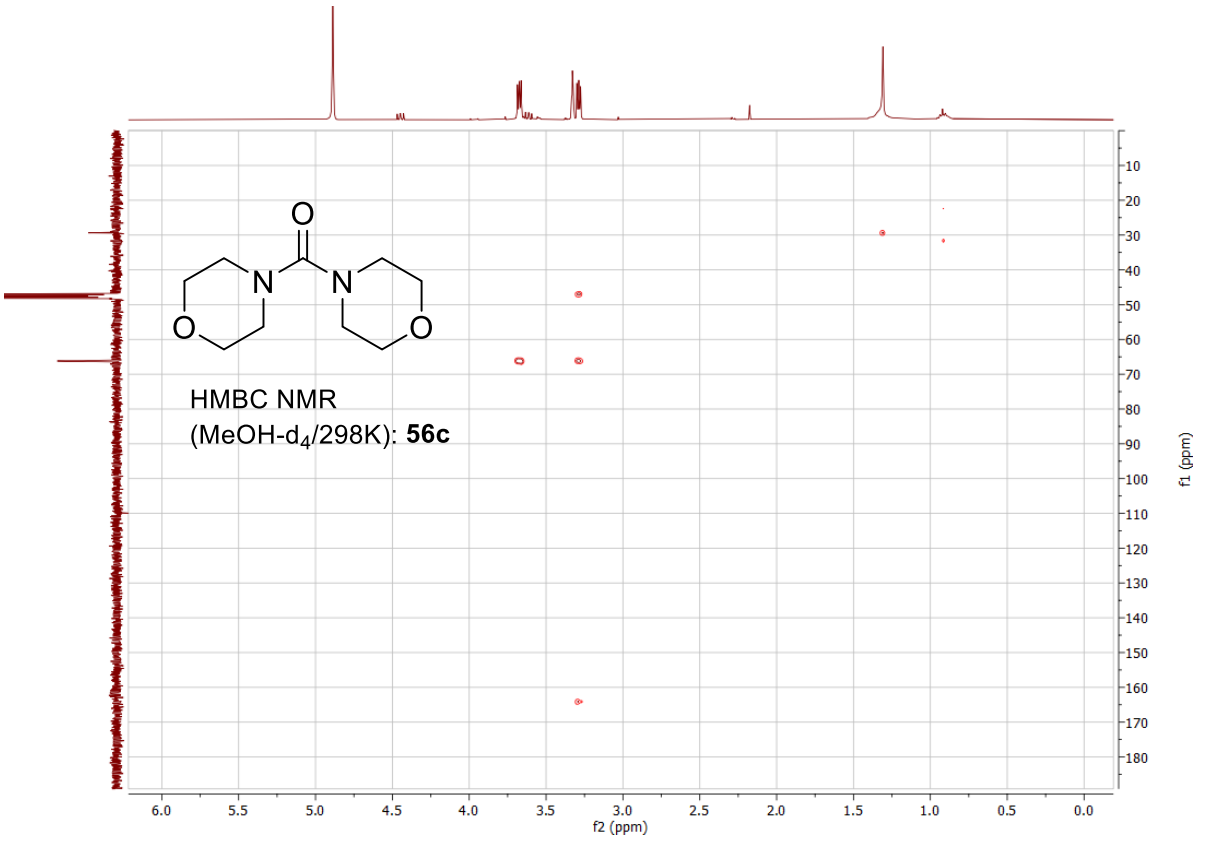

Figure 59. HMBC NMR spectrum of 4,4´-carbonyldimorpholine (**56c**).

sustainable chemistry

MDPI

Review

Electrochemical Bromofunctionalization of Alkenes and Alkynes—To Sustainability and beyond

Lilla G. Gombos and Siegfried R. Waldvogel *

Department of Chemistry, Johannes Gutenberg University of Mainz, D-55128 Mainz, Germany
* Correspondence: waldvogel@uni-mainz.de

Abstract: The electrochemical generation of highly reactive and hazardous bromine under controlled conditions as well as the reduction of surplus oxidizers and reagent waste has placed electrochemical synthesis in a highlighted position. In particular, the electrochemical dibromination and bromofunctionalization of alkenes and alkynes have received significant attention, as the forming of synthetically important derivatives can be generated from bench-stable and safe bromide sources under "green" conditions. Readily available and non-corrosive bromide salts have been utilized with a dual role as both a reagent and supporting electrolyte. However, this trend seems to change with the preparation of organobromine species. In this review, the electrochemical dibromination and bromofunctionalization of alkenes and alkynes was addressed in terms of their bromine sources and sustainability.

Keywords: anode; alkenes; alkynes; bromine; electrochemistry; oxidation; synthesis

Citation: Gombos, L.G.; Waldvogel, S.R. Electrochemical Bromofunctionalization of Alkenes and Alkynes—To Sustainability and beyond. *Sustain. Chem.* **2022**, *3*, 430–454. https://doi.org/10.3390/suschem3040027

Academic Editor: Matthew Jones

Received: 26 August 2022
Accepted: 11 October 2022
Published: 13 October 2022

1. Introduction

With the increasing amount of economic, environmental and political pressure, the chemical industry faces the challenge of providing the public and the scientific community a sustainable and greener alternative to conventional chemical methods [1]. Electro-organic synthesis has become one of the most attractive research topics in recent years, providing highly versatile synthetic methodologies [2–6]. Using electrons as "traceless" redox reagents allows the elimination of the excess use of harmful redox chemicals with a high atom efficiency [7]. The electro-generation of highly reactive species in-situ allows the utilization of inherently safe surrogates and provides a simplified approach [8]. These advantages, in combination with the valorization of renewable feedstock and "green electricity", makes electrochemical functionalization particularly attractive.

There have been many recent reviews discussing C–C [9–15], C–N [13,16–18], C–O [12,13,17], C–S [19,20] and C–P [12,21] bond formation under electrochemical conditions [22,23]. In parallel to this, the implementation of halogens in electro-organic synthesis has also received significant attention [24,25]. The highly versatile and valuable organohalides that serve as prevalent structural motifs in pharmaceuticals [26,27], natural products [28] and intermediates [29] have encouraged electrochemists to provide more sustainable methodologies for the installation of halo-substituents. The precise control of electron transfer at the electrode via constant electric current or potential without the addition of metal-catalysts or exogeneous oxidants overcomes the conventional halogenation methods that burden conventional synthetic protocols [30–32]. Furthermore, the use of inexpensive and bench-stable halides allows the controlled generation of halonium species, halogen radicals or halogens in-situ. In particular, the electrochemical generation of bromine has received significant attention. Bromine can be easily generated under electrochemical conditions and equally holds its place as a direct halogenating reagent as well as a mediator [24,33,34]. A great example of electrochemically generated bromine as a mediator in organic synthesis was demonstrated via the electrooxidation of alcohols [35], as well as via the Clauson–Kaas electro-alkoxylation of furanes in the presence of bromide

and methanol [36]. The latter was also demonstrated in the preparation of the natural product hispanolone [37].

In this review, the electrochemical dibromination and bromofunctionalization of alkenes and alkynes will be discussed in terms of their bromine source and sustainability.

2. Bromine and Bromination Agents

Bromine is a dark brown-red, volatile, noxious liquid at room temperature. Due to its high reactivity, it is mainly found as alkali bromides in brines, minerals and the Earth's crust. One of the richest sources is the Dead Sea, which has a bromide content of ca. 5 g/L [38]. However, these sources are diminishing, and their prices are increasing steadily. Currently, bromine is produced on a global scale at 390,000 t/year, and bromine demand has been increasing over the last 5 years and is predicted to rise dramatically [39].

In particular, vicinal 1,2-dibromides are prevalent motifs used in fine chemicals and flame retardants [29]. Almost half of the globally produced bromine is used to produce the latter, which can easily leach out, posing a persistent environmental problem [40,41]. As well as its environmental toxicity, bromine's storage and transportation equally pose hazards [42,43].

The most common bromination methods include the direct use of elemental bromine or HBr, which is toxic, corrosive and creates hazardous reagent waste. Alternatively, inorganic or organic bromide salts with an external oxidant allows the in-situ generation of bromine, however, above-stoichiometric amounts of exogenous oxidizers are required under harsh conditions [44]. The utilization of inherently safe bromine surrogates such as *N*-bromosuccinimide and pyridinium tribromide allows the controlled liberation of Br_2. Nevertheless, their preparation is difficult, wasteful and costly. Moreover, their recycling as well as their production requires elemental bromine, and therefore these agents are considered low-atom economic [45,46].

Oxidative electrochemistry provides a fundamentally greener alternative compared to the traditional strategies, as electricity replaces the usually harmful and surplus redox reagents. The relatively low oxidation potential of bromides has inspired extensive studies for the electro-generation of bromine in different solvent systems [47–49]. The oxidation of bromide to bromine or to its stable tribromide salt is described as a two-electron transfer process (Equation (1)), which has been extensively studied in aprotic media due to the stabilization effect of solvent, facilitating the formation of both brominating species simultaneously [47–49]. The first oxidation potential corresponds to the direct formation of bromine (0.82 V in acetonitrile at a platinum disk electrode), which simultaneously forms stable tribromide complexes in the presence of a high bromide concentration in aprotic media (Equation (2)) [47]. Via a second oxidation potential, bromine is generated from the aforementioned tribromide species (1.2 V in acetonitrile at a platinum disk electrode) (Equation (3)) [47].

$$2Br^- \rightarrow Br_2 + 2e^- \quad (1)$$

$$Br_2 + Br^- \rightleftarrows Br_3^- \quad (2)$$

$$2Br_3^- \rightarrow 3Br_2 + 2e^- \quad (3)$$

Moreover, as bromine can be generated easily from its salts under electrochemical conditions, the traditional production of bromine via the chlorine oxidation process can be completely avoided.

Bromides are popular alternatives due to their proportionate pricing compared to traditional brominating agents such as HBr and Br_2 (Table 1). In particular, NaBr and KBr provide an economically greener choice, as the abundance of sodium (2.36%) and potassium metal (2.09%) in the Earth´s crust is relatively high, with sodium being the sixth most abundant element [50]. In combination with their non-corrosive natures and long shelf-lives, they are desired substitutes for smaller research facilities that struggle with the burden of conventional brominating reagents and storage issues.

Table 1. Price comparison of bromide salts with classical brominating reagents [51].

Reagents [1]	Bulk Price [2]	Molar Price [3]
KBr	€95/kg	€11.31/mol
NaBr	€135/kg	€13.93/mol
LiBr	€294/kg	€25.53/mol
NH_4Br	€220/kg	€21.55/mol
NEt_4Br	€121/kg	€25.43/mol
NBu_4Br	€831/kg	€267.89/mol
N-Bromosuccinimide	€140/kg	€24.92/mol
Pyridinium tribromide	€362/kg	€115.77/mol
HBr (48%)	€151/L	€8.20/mol
Bromine	€264/L	€13.57/mol *

[1] Prices were obtained from Sigma Aldrich website: https://www.sigmaaldrich.com/DE/en (accessed on 14 September 2022). [2] Bulk prices are given in EUR per kg or L. [3] Molar prices are calculated from bulk, prices are given in EUR per mol. * Refers to molar price of Br_2.

Organic bromide salts bridge the obligatory protic additive issue that is associated with alkali bromide salts, providing a simpler setup. Nevertheless, these agents are more expensive, and their preparation is elaborate and therefore low-atom economic.

Via the conscious choice of bromine substitution and the precise amendment of the electrochemical parameters, an intrinsically green, efficient and viable approach can be provided [4,52,53]. In particular, careful consideration has to be made regarding the counter electrode reactions [54–57]. In combination with sustainable electro-organic chemistry and green chemistry principles, it is highly desired that bromine from a "green source" can be generated synergically, for example under linear paired electrolysis conditions [58–62].

3. Electrochemical Bromofunctionalization of Alkenes

The electrochemical bromination and bromofunctionalization of alkenes are well-researched areas, as their products serve as highly valuable synthetic intermediates and important chemicals. Vicinal dibromides, bromohydrins and bromoesters serve as useful intermediates for pharmaceuticals and fine chemicals [29,63]. Moreover, the halogenated species can be simply further functionalized resulting in a plethora of elaborated products. Therefore, the simultaneous and selective installation of one or two functionalities across the alkenes has been extensively researched as the desired products can be obtained under a simplified set-up and "green" conditions. The electrochemical bromofunctionalization of alkenes is mostly represented by the utilization of bromide salt with a dual role as both a reagent and supporting electrolyte in aprotic media accompanied by a protic additive such as water or short-chained alcohols. These agents do not only provide the respective hydroxyl or ether functionalities but also compliment the cathodic reaction liberating H_2, providing a "clean" by-product [54]. The employment of organobromines as halogenating agents has also become popular as it allows bromine to form as a result of an electrochemical redox process, excluding the need for the sacrificial half reaction. Nevertheless, these agents are usually harmful and therefore should be avoided.

3.1. HBr, MBr and Alkylammonium Bromides as Bromine Sources

Pioneering work in the field was demonstrated by Torii in the early 80s, reporting the bromofunctionalization of alkenes in the presence of aq. NaBr, which popularized the indirect electrochemical oxidation of olefins using stable and inexpensive metal halide salts [64–68]. This form of a bromine source has received particular attention due to its ability to tame hazardous and toxic molecular bromine in-situ under controlled conditions. It is worth mentioning that the complementary half-reaction´s electrode choice is usually a low-hydrogen-overpotential material such as platinum or nickel, which supports cathodic hydrogen evolution. Nevertheless, platinum group metals are depleting, costly and highly contaminating [69–71].

In 2019 Hu, Fang and Mei reported the electrochemical radical formyloxylation–bromination of various alkenes in a regio- and chemoselective fashion [72]. The implementation of stable NaBr as a radical bromine source makes this approach sustainable. DMF serves a dual role as both the solvent and the formyloxylation reagent, while acetic acid supports the cathodic reaction. *Para*-substituted electron-rich styrene derivatives afforded excellent yields, while electron-deficient and strongly electron-withdrawing groups prolonged the reaction time. The naturally derived safrole-type and estrone-type derivates also readily underwent electrochemical formyloxylation, proving the possibility for the late-stage functionalization of pharmaceutical scaffolds. In total, 30 examples were reported with excellent yields up to 97%. The scalability was proved via a gram-scale experiment (6.0 mmol) resulting in an isolated yield of 90%. The method was extended to the formyloxylation–chlorination and formyloxylation–trifluoromethylation of alkenes as well. The authors suggest that bromide is oxidized at the anode to bromo-radicals, which then rapidly combine with arylalkene **1** to form the benzyl radical **I**. Via a second oxidation, the forming benzylic carbocation **II** is subjected to nucleophilic attack by DMF to iminium intermediate **III**, which is subsequently hydrolyzed resulting in the formyloxylated brominated product **2** (Scheme 1).

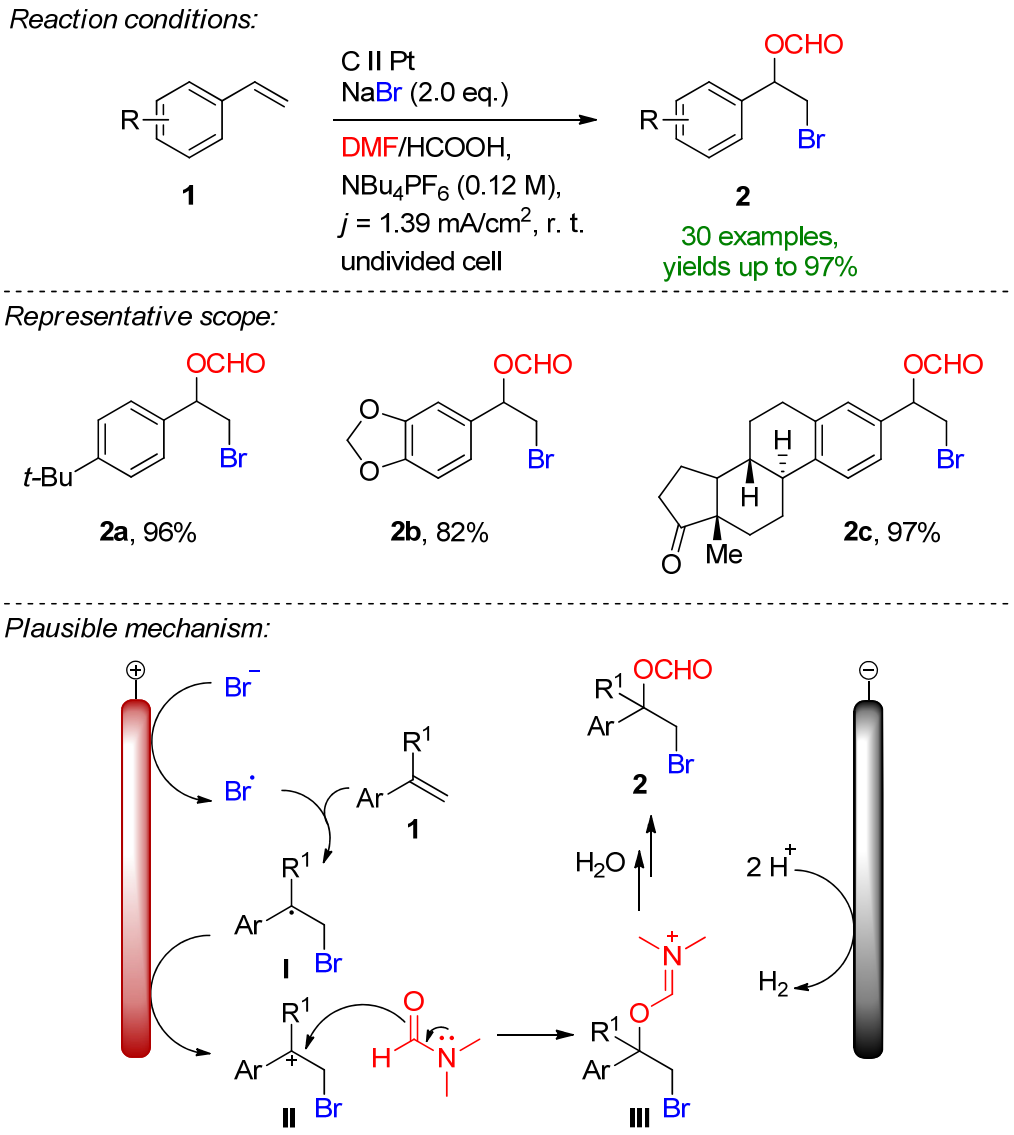

Scheme 1. Electrochemical radical formyloxylation bromination of alkenes [72].

The electrobiocatalytic bromolactonization was reported by Bormann and Holtmann on carbon-nanotube-modified gas-diffusion electrodes [73]. The paper reports the cathodic reduction of ambient oxygen to H_2O_2 at a reduced overpotential in a divided cell separated via a proton exchange membrane. *Curvularia inaequalis* (*Ci*VCPO), a vanadium-dependent chloroperoxidase enzyme converts the forming peroxide in the presence of potassium bromide into hypobromite, which leads to the bromolactonization of 5-pentenoic acid. The reaction is complimented via the oxidation of water at a platinum anode. The superiority of the reaction lies in the oxygen-enriched, modified-carbon-nanotube diffusion electrode that significantly lowers the overpotential for peroxide formation, which is a sensible factor for the enzymatic catalytic reactivity [74].

The electrochemical bromocyclization of tryptophol, tryptamine and tryptophan derivatives was recently reported by Wu and Vincent [75]. This efficient protocol features $MgBr_2$ with a dual role as a halogen source and supporting electrolyte. The reaction proceeds in an undivided cell under both constant current (CCE) and constant potential (CPE) conditions in the presence of 1 eq. $MgBr_2$. Magnesium bromide is oxidized at the carbon anode into bromine in an acetonitrile/water solution under ambient conditions. It is worth mentioning that under CPE, the constant potential window is maintained via measuring the potential against a reference electrode. Here, the constant terminal voltage of the cell was determined via measuring the constant terminal voltage between the electrodes, which is not an adequate parameter for CPE conditions. The dearomative reaction proceeds via the formation of bromonium intermediate **IV**, followed by intramolecular cyclization to form the corresponding brominated derivatives with excellent yields (Scheme 2). This simple and environmentally friendly set up featured 22 examples with up to 96% isolated yields and a broad scope of functional group tolerance.

The synthetic utility was demonstrated via the electrochemical bromocyclization and further functionalization of *L*-tryptophan-derived diketopiperazine (**5**) to (−)-*epi*-amauromine (**7a**) and (+)-novoamauromine (**7b**), which was reported to be superior to the conventional procedure using stoichiometric NBS (Scheme 3) [76].

Solvent stabilizing effects have been reported in electrochemical synthesis, for example using hexafluoroisopropanol (HFIP) [77–82]. Yoshida demonstrated the formation of α-bromocarbonyls and bromohydrins via a low-temperature DMSO-stabilized halogen cation pool method [83,84]. Based on these reports, a sophisticated technique for the electrochemical bromohydrin and bromohydrin ether formation was reported in a chemoselective fashion (Scheme 4) [85]. The anodic oxidation of potassium bromide on a glassy carbon electrode in the presence of 10 eq. acetic acid in DMSO/H_2O allowed the corresponding bromohydrins to be produced in excellent yields. By changing the solvent system to acetonitrile/alcohol, bromohydrin ethers were obtained. The key additive of this approach is the addition of acetic acid or trifluoroacetic acid. In the absence of the additive, the yield drops dramatically. The reaction is complemented with hydrogen evolution at a platinum cathode.

Sun and co-workers reported an elegant way of on-site bromination and hydrogenation in a simultaneous fashion [86]. The paired electrolysis takes place in a H-type cell setup divided by a Nafion membrane. This method demonstrates high halogenation flexibility and functional group tolerance, as the bromination reaction is spatially separated from the electrolysis event. The key principle is the use of bench-stable NaBr as a halogen source and the utilization of cathodic hydrogen evolution to achieve a high atom economy and energy efficiency. The anodically generated bromine gas from aqueous sodium bromide in acidic media is transferred into a separate compartment, where ideal conditions for the corresponding substrates can be set up. Likewise, cathodically generated hydrogen gas is used in the presence of Pt/C, demonstrating the synergic pairing of on-site bromination and hydrogenation. This is an excellent example for the utilization of the redox properties of the electrochemical cell.

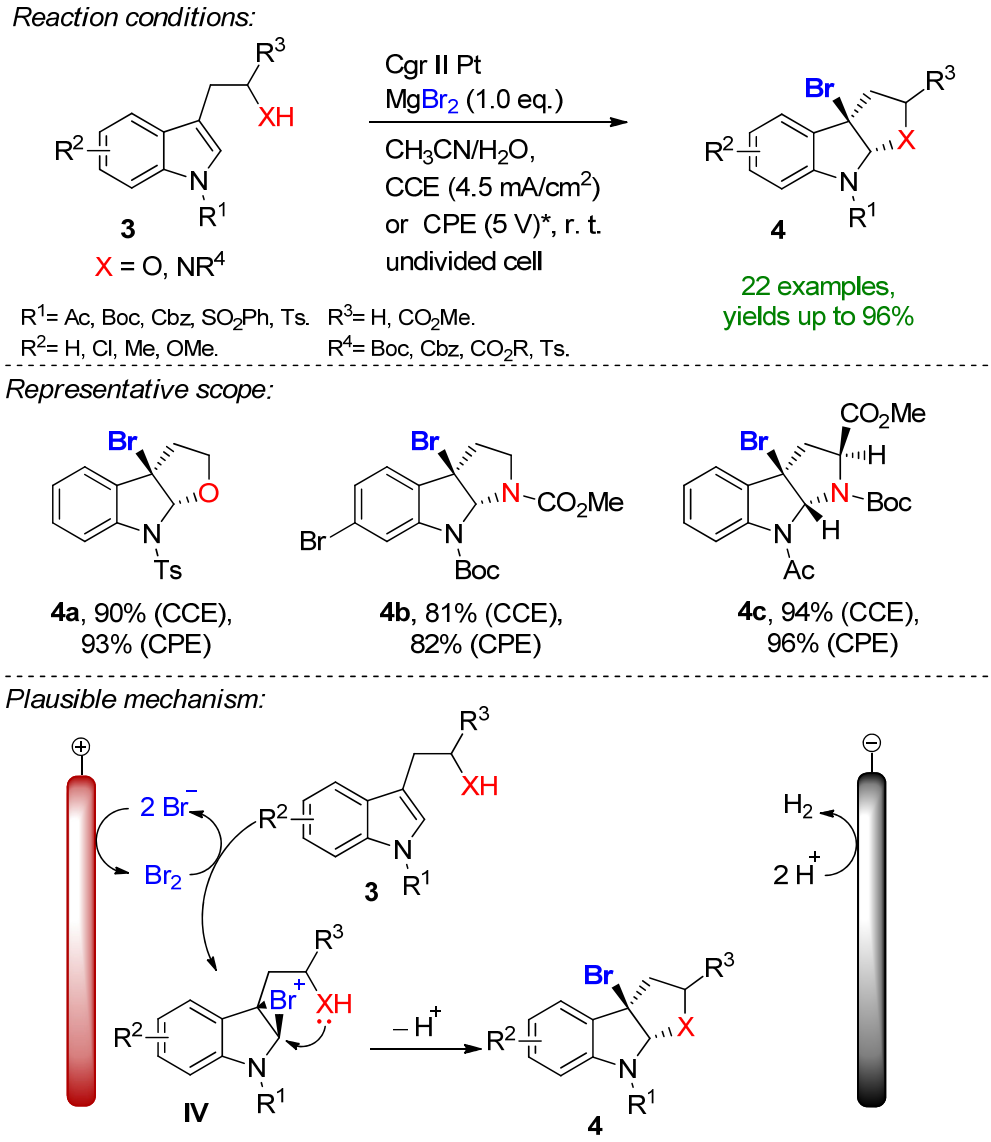

Scheme 2. The electrochemical bromocyclization of tryptophol, tryptamine and tryptophan derivates utilizing $MgBr_2$. * Constant terminal voltage of the cell was observed between a graphite anode and platinum plate cathode [75]. Cgr = graphite.

Similarly, Hilt and his group published a linear paired electrolysis for the electrochemical dibromination of alkenes with the realization of 200% current efficiency for stoichiometric transformations in the presence of oxygen [87]. The dual role supporting electrolyte and bromide source NBu_4Br is used as a brominating agent. Bromide undergoes direct oxidation at the anode to bromine and is produced mediated via reductively formed H_2O_2 determining the theoretical applied charge of 1 *F* (Scheme 5). The stable tribromide species are the results of the stabilizing effect of acetonitrile and the high concentration of bromide. Using this method, the authors reported 13 examples with good to excellent yields, providing **11c** quantitatively with a current efficiency of 200%. The reaction proved to have a good functional group tolerance via performing the Glorius-test [88,89]. The method could be adopted to the bromination of arenes and for the iodination of alkenes as well.

A highly regioselective electrochemical protocol for the synthesis of isoxazolines from β,γ-unsaturated ketoximes via cascade C–O and C–Br annulation was reported (Scheme 6) [90]. The stable inorganic potassium bromide has a dual role of serving as a bromine source as well as a supporting electrolyte. The key features of this method are the

generation of DMSO-stabilized bromine in-situ and the employment of a sodium acetate base under high current density conditions to form the desired bromoethyl-substituted isoxazolines. The method demonstrated excellent functional group tolerance and a high selectivity, and the isoxazoline derivatives could be obtained with up to 81% isolated yields. The presence of the base as well as the electrode material choice is crucial to the success of the reaction. The scalability in both batch-type and flow electrolysis were demonstrated.

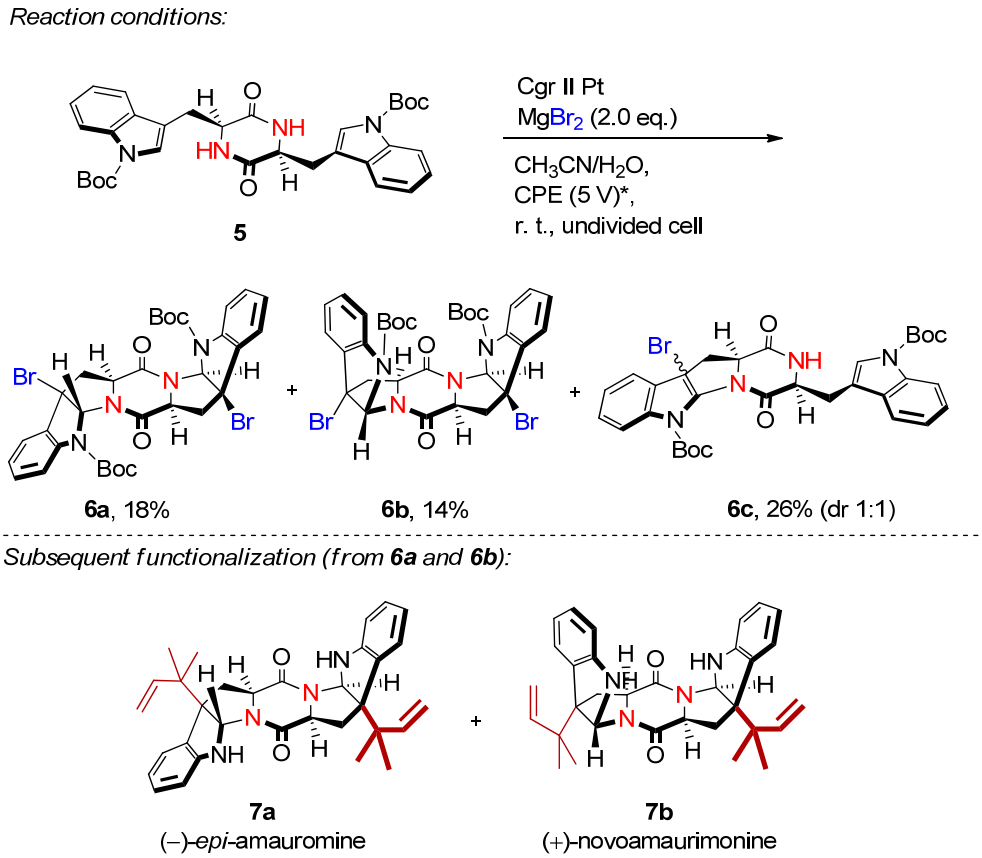

Scheme 3. Electrochemical formation and subsequent functionalization of **6a** and **6b** [76]. * Constant terminal voltage of the cell was observed between a graphite anode and a platinum cathode [75]. Cgr = graphite.

Yin and co-workers introduced an oxidant- and base-free electrochemical intramolecular halo-amination of unactivated alkenes to form diverse brominated *N*-heterocycles [91]. They provide a simple electrochemical protocol using bench-stable LiBr or LiI as a halide source and a supporting electrolyte furnishing a dual role. The reaction proceeded smoothly at room temperature, providing 26 examples combined with the iodo-cyclization in excellent yields. The reaction tolerates labile functional groups such as cyclopropyl, substituted aromatics and heterocycles. Moreover, in the presence of LiI, highly challenging *N*-heterocycles such as the three-membered aziridine or six-membered piperidine could be formed (Scheme 7).

Similarly, the electrochemical oxidative bromolactonization of unsaturated carboxylic acids was reported for the first time [92]. This environmentally friendly approach features sodium bromide as the halogen source in acetonitrile, which is oxidized at the carbon rod anode to give the corresponding bromine radical, which directly reacts with the alkene of the carboxylic acid to form intermediate **V** (Scheme 8). After subsequent oxidation to the stabilized cationic intermediate **VI** and cyclization, the corresponding bromoethylated γ-lactones could be formed with excellent yields. Control experiments also supported the proposed mechanism, as in the presence of radical scavengers or molecular bromine,

the yield dropped dramatically. The authors propose hydrogen evolution as a cathodic counter-reaction at a nickel electrode.

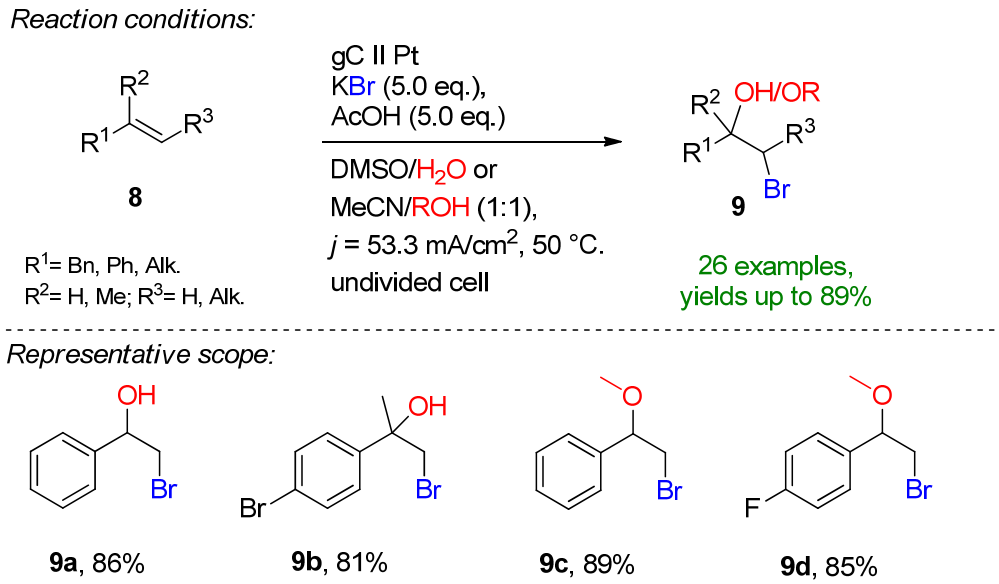

Scheme 4. Electrochemical bromohydrin and bromohydrin ether formation [85]. gC = glassy carbon.

The electrochemical bromination of electron-deficient alkenes in quinones, coumarins, quinoxalines and 1,3-diketones has also been reported [93]. The synthetically useful organohalides could be obtained using bromides on graphite felt in combination with a platinum cathode. The key feature of this bromination method is the in-situ formation of HBr from KBr and H_2SO_4, which is anodically oxidized to bromine. Control experiments with 2,6-di-*tert*-butyl-4-methylphenol suggest a radical pathway by the formation of the halogen.

Recently, Waldvogel et al. published the selective electrochemical bromination of terpenes and naturally derived alkenes [94]. The challenging halofunctionalization of renewable feedstock was demonstrated by the employment of inexpensive and bench-stable NaBr with a dual role of being both a bromine source and supporting electrolyte. The test substrate, limonene, could be brominated selectively under ambient conditions giving the brominated derivative in a 53% yield. The optimization procedure showed that the careful consideration of the MeCN/H_2O solvent system as well as the NaBr as a bromide source are important features of the method. Other inorganic or organic bromide salts resulted in a diminished yield or no conversion. The method could be successfully extended to linear and cyclic monoterpenes, terpenoids and phenylpropanoids to give 10 desired vicinal 1,2-dibromo derivatives, with the bromination of carvone representing the best yield of 82% (**20b**, Scheme 9). A slight change in the electrochemical parameters provided the tetrabrominated limonene derivative in a 74% isolated yield. The reaction proved to be scalable and a synthetic utility could be demonstrated via subsequent functionalization to the α,β-unsaturated nitrile derivative **21a** for the first time. Cyclic voltammetry studies support the oxidative bromine formation in-situ, which is complimented by the liberation of H_2 at the cathode.

Another form of metal-free in-situ bromine generation is the use of HBr as a bromine source. Lei et al. reported an electrochemical oxidative clean halogenation of alkenes using HBr on a carbon anode and platinum cathode, providing 23 examples with up to 89% isolated yields under constant current conditions [95]. The method provides a general halogenation system of HX/MX including the chlorination and bromination of various heteroarenes, arenes, alkenes, aliphatic hydrocarbons and alkynes as well. Under the optimal conditions, the gram-scale synthesis of the electrochemical dibromination of

dodecane (**22**) allowed the formation of 1,2-dibromododecane (**23**) with a yield of 86% and 50.9 g isolated clean product (Scheme 10).

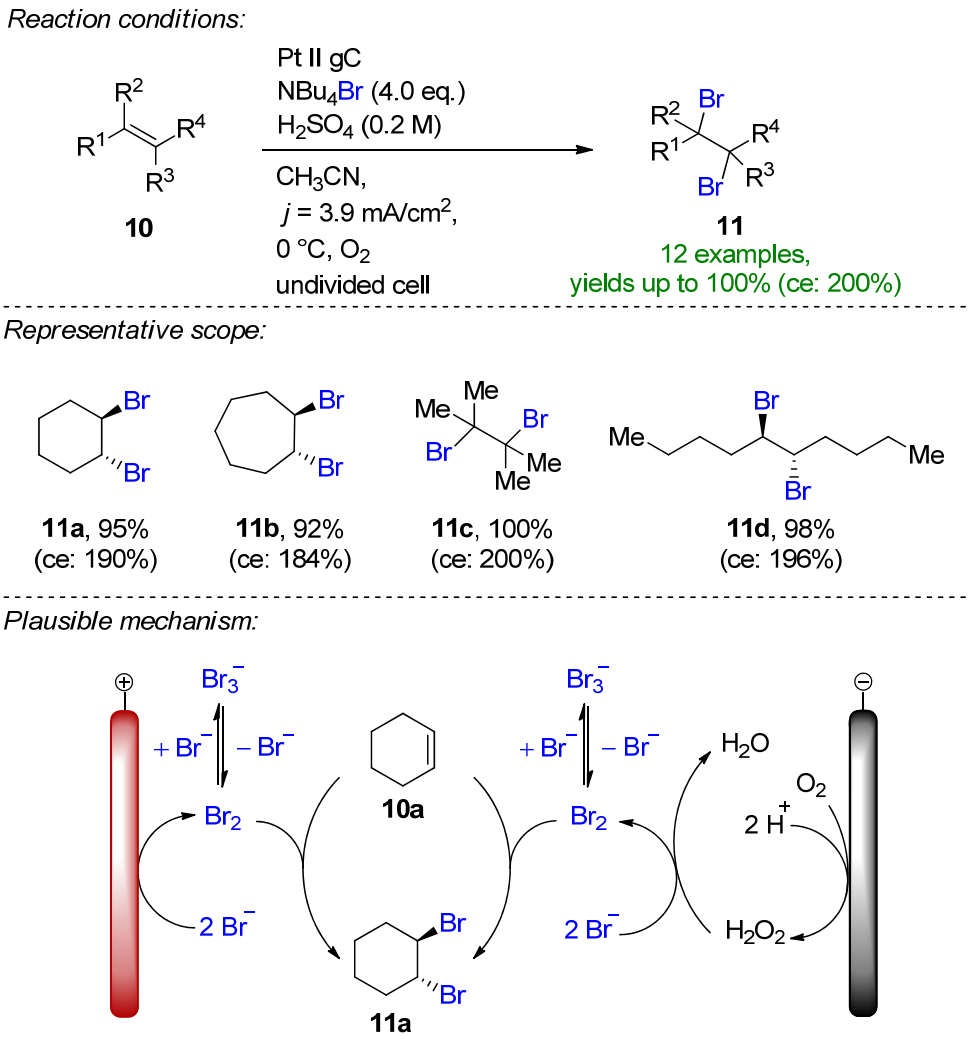

Scheme 5. Linear paired electrolysis for the dibromination of alkenes [87]. gC = glassy carbon.

Encouraged by these results, the Wirth group described the electrochemical bromination and bromofunctionalization of activated and unactivated alkenes in a flow reactor under single-pass conditions [96]. The 600 µL reactor was equipped with platinum foil electrodes separated by a 500 µM fluorinated ethylene propilene (FEP) spacer. The small interelectrode distance allowed the omission of the addition of water and supporting electrolyte, which was described in previous studies. The optimized conditions for the dibromination of styrene were found in the presence of 6 eq. HBr in pure acetonitrile. The combination of a 0.4 mL/min flow rate, 4 *F* applied charge and platinum electrodes allowed the formation of **25a** in a 79% isolated yield (Scheme 11). When the optimized conditions were applied using a platinum-coated titanium cathode, **25a** could be obtained in an excellent yield of 86%. Via switching the co-solvent, the electrochemical bromohydrin formation could be also targeted. The applicability of this method was demonstrated on several aromatic and aliphatic alkenes. In total, 33 examples were provided exhibiting the formation of dibrominated, tetrabrominated, hydrobrominated and alkoxybrominated products with good to excellent yields. The scalability of the flow-procedure was also demonstrated via applying the conditions for 9.5 h providing **25a** in an isolated yield of 65% and a productivity of 413 mg/h.

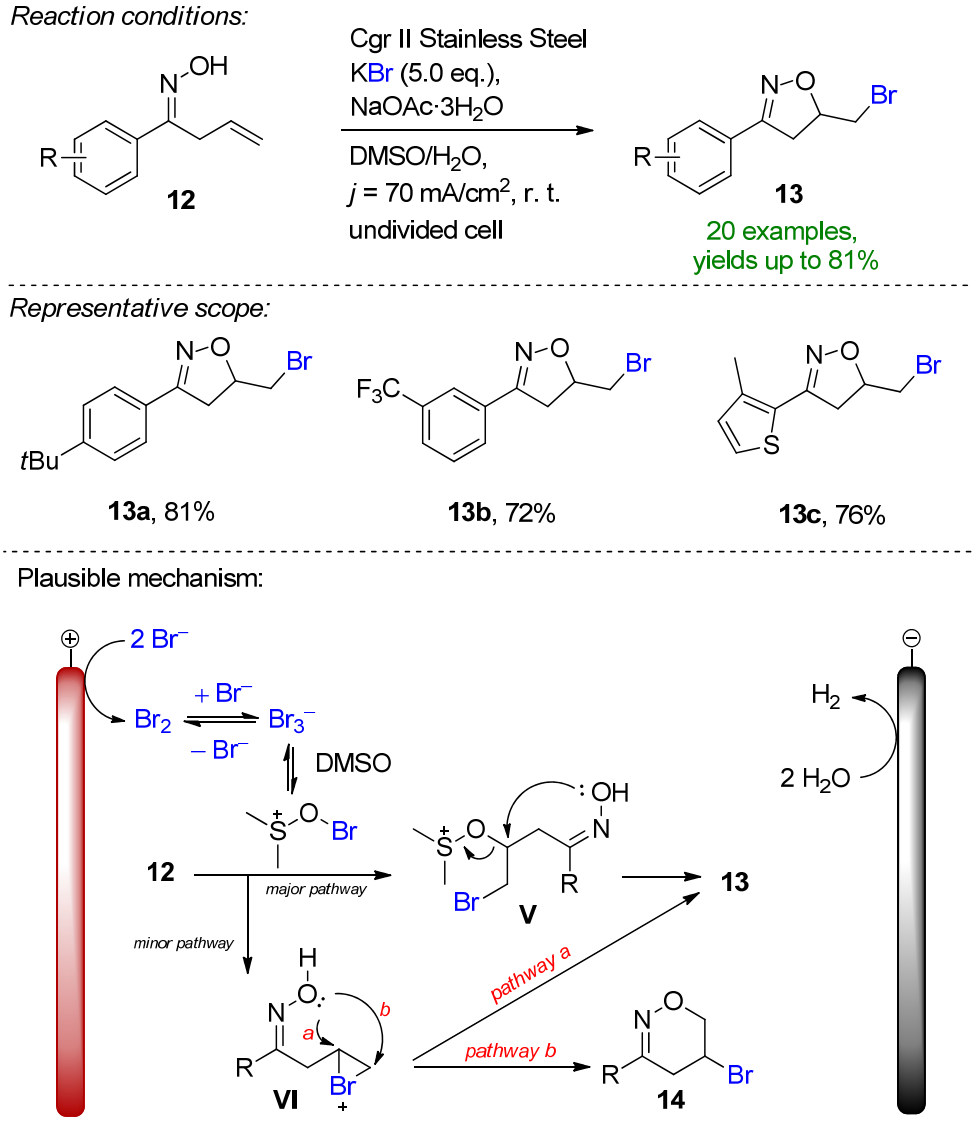

Scheme 6. Electrochemical formation of isoxazolines with the aid of KBr [90]. Cgr = graphite.

3.2. Organohalides as Bromine Sources

Li et al. reported a three-component, TEMPO-mediated 1,2-bromoesterification of alkenes with the aid of carboxylic acids and *N*-bromosuccinimide [97]. The method allows the simultaneous addition of a C–O and C–Br bond to form β-bromoalkyl esters, which are excellent intermediates for natural products and pharmaceutical agents [97,98]. The reaction proceeded well in the presence of 50 mol% TEMPO, 2 eq. of carboxylic acids and 2 eq. NBS to form **27b** in an 88% isolated yield (Scheme 12). The optimized conditions were extended to a variety of carboxylic acids and alkenes, and a total of 40 examples were provided with excellent yields. Even challenging substrates such as adamantane-1-carboxylic acid and amino acids were tolerated. The reaction is complemented via H_2 evolution at the cathode.

Paired electrolysis methods are generally preferred over a sacrificial approach [57]. Here, the same authors introduced electrochemical alkoxyhalogenation and organohalide dehalogenation within a convergent strategy [99]. Diethyl-2-bromomalonate (**29**) serves as the bromine source. The key promoters of this method are NBu_4OH and Cp_2Fe, as omitting one or both decreases the yield. The reaction mechanism was postulated via the mediated oxidation of alkene **28** by Cp_2Fe^+, which forms the radical cation **IX**. Intermediate **IX** is scavenged by the bromine radical or bromine that is either formed via the cathodic

reduction of bromomalonate to **XIII** or via the S_N2 reaction induced by the supporting electrolyte (Scheme 13).

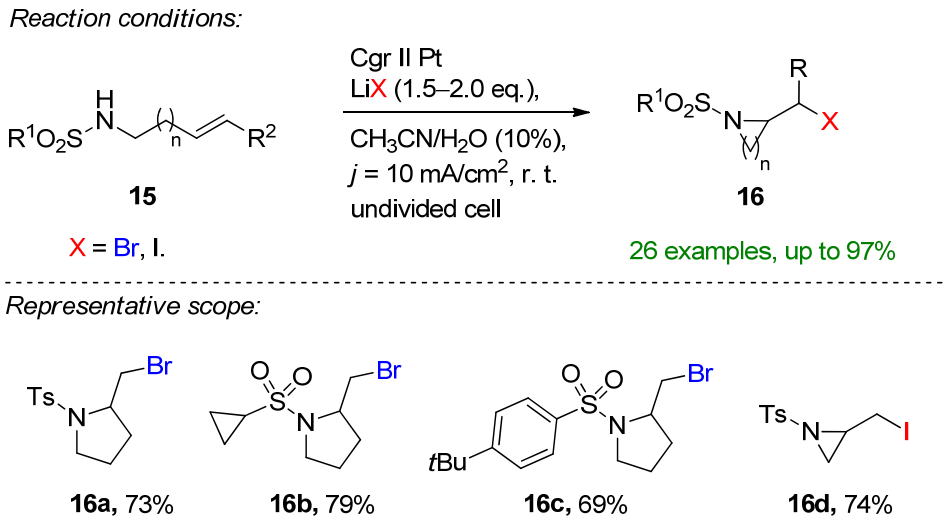

Scheme 7. Electrochemical intramolecular haloamination with the aid of LiBr and LiI [91]. Cgr = graphite.

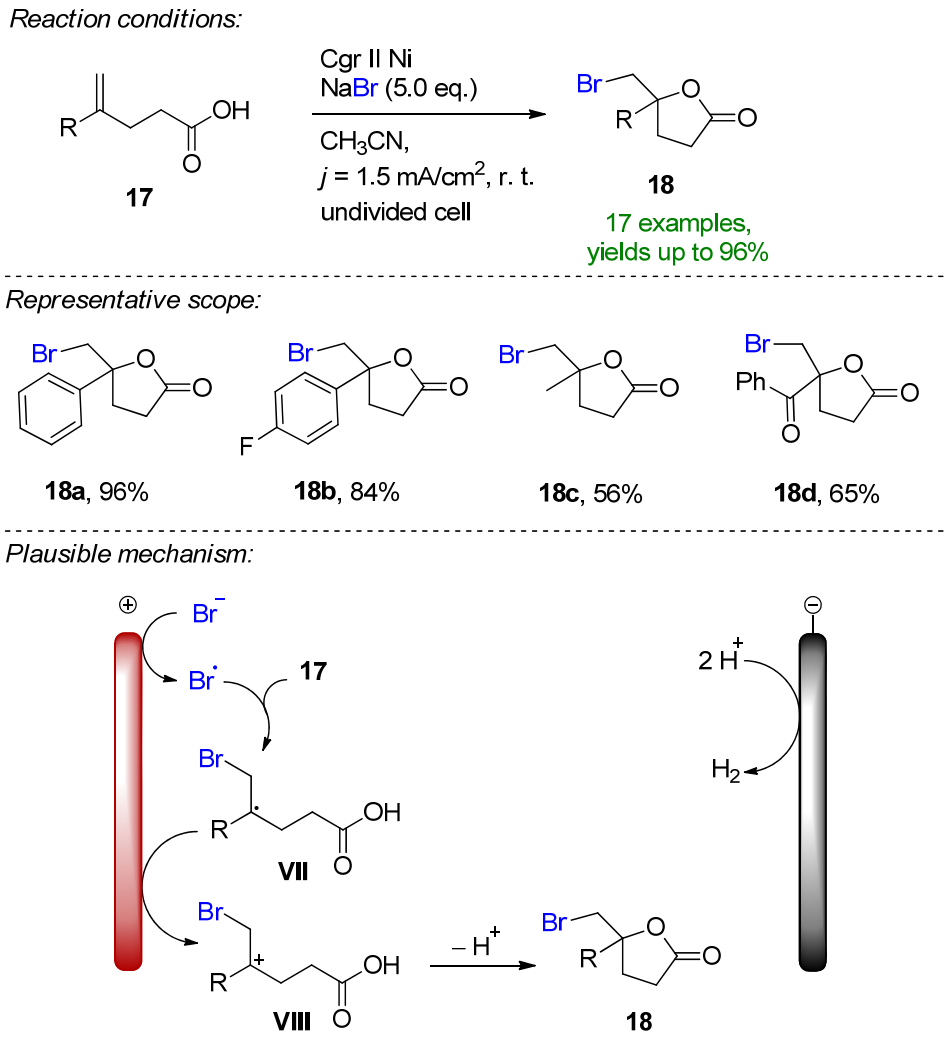

Scheme 8. Electrochemical bromolactonization of unsaturated carboxylic acids [92]. Cgr = graphite.

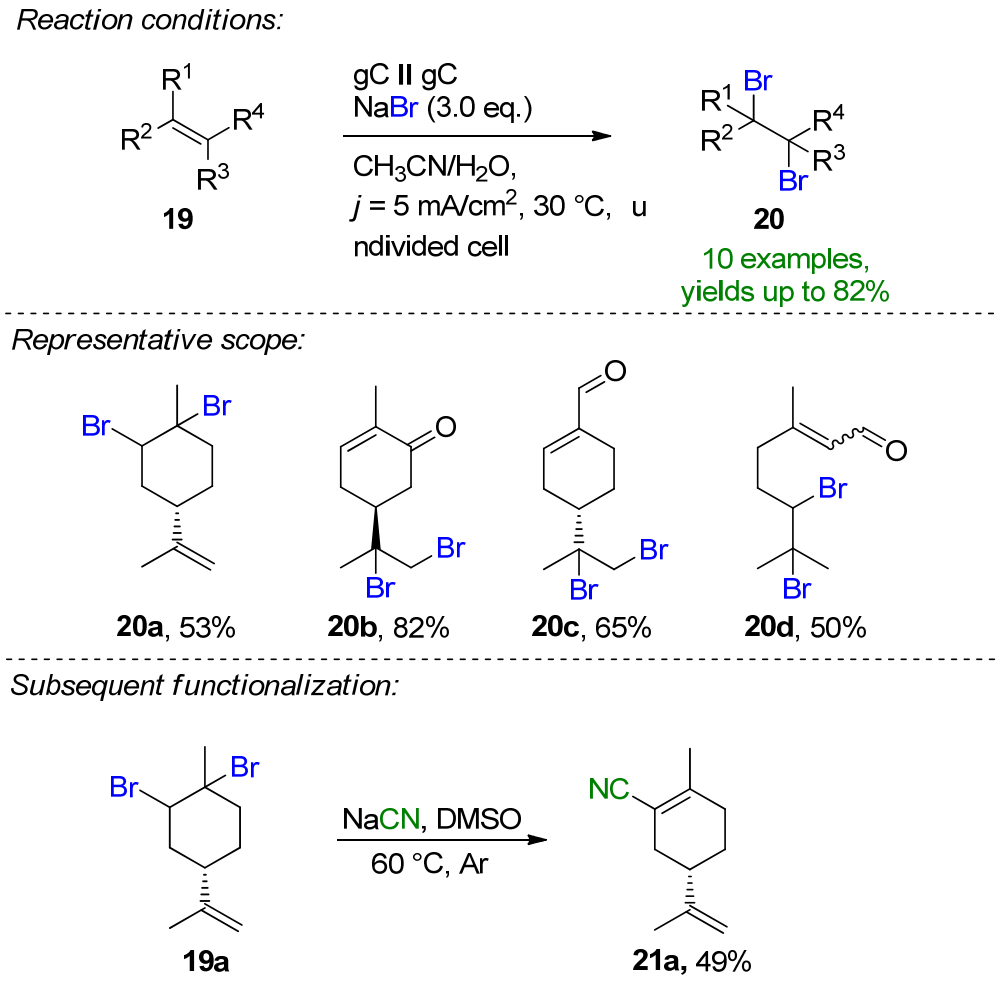

Scheme 9. Electrochemical dibromination of terpenes and terpenoids [94]. gC = glassy carbon.

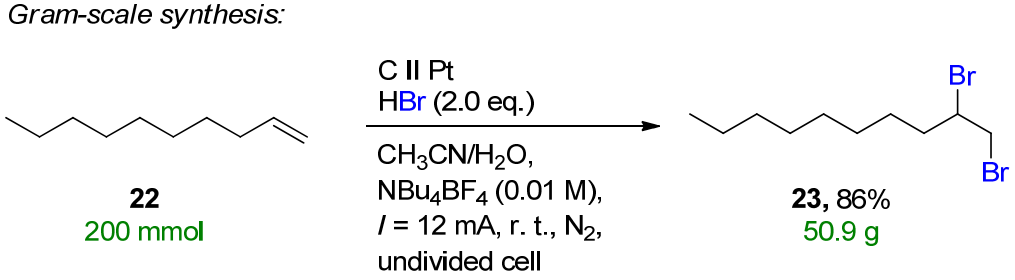

Scheme 10. Electrochemical dibromination of **22** on a gram scale [95]. CCE conditions were described with current (*I*), as the immersed electrode area was not specified.

The bromide could also be oxidized in-situ to form bromine. The formed alkyl cation **XI** is complemented via methanol to provide the desired product. The formation of malonic ester (**31**) is depicted via GC and GC-MS. The convergent strategy was demonstrated on various aryl alkenes bearing *para-*, *meta-* or both substituents and alkyl halides. The alkoxyhalogenation of bioactive molecules such as adamantene, estrone and ibuprofen derivatives were also demonstrated. In combination, 43 examples were provided with up to a 98% yield.

A merging e-shuttle reaction for the retro-dihalogenation reaction was developed by Waldvogel and Morandi, enhancing the already existing halogenation reactions (Scheme 14) [62].

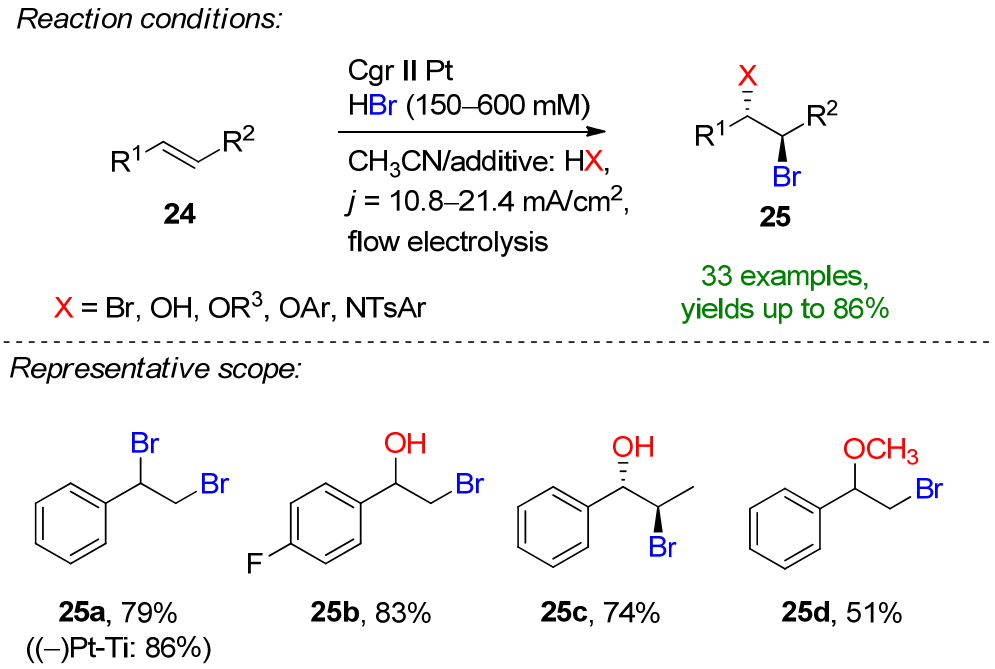

Scheme 11. Electrochemical bromination and bromofunctionalization of alkenes in flow electrolysis [96]. Cgr = graphite.

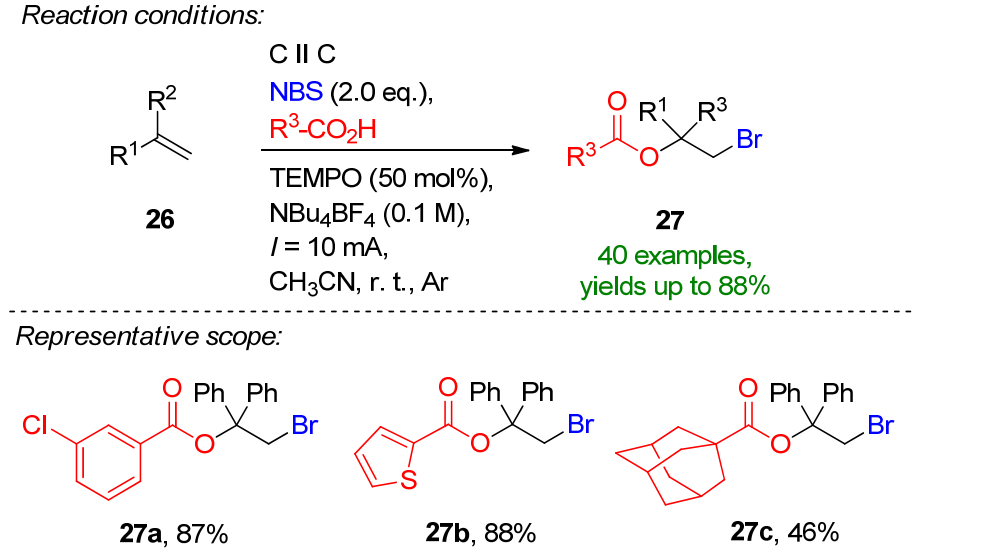

Scheme 12. The three-component, TEMPO-mediated 1,2-bromoesterification of alkenes [97]. CCE conditions were described with current (*I*), as the immersed electrode area was not specified.

The attraction of this elegant, electrochemically promoted shuttle reaction is the use of non-corrosive vicinal 1,2-organodihalides as halogen promoters, which eliminate the use of low-atom -efficient halogenating agents and surrogates. Readily available, inexpensive, non-oxidizing 1,2-dibromoethane serves as the bromine source. The aforementioned organohalide undergoes reductive dehalogenation at the cathode and is transferred to an acceptor alkene, providing a convergent application for the reductive dehalogenation and formation of fine chemicals in one step. The reaction proceeds readily on cheap graphite electrodes in the presence of 1 v/v% HFIP in acetonitrile. The additive suppresses the oxidation of alkene and promotes dehalogenation at the cathode. Via this method, the dibromination, dichlorination, thiobromination and thiochlorination of alkenes was facilitated. The method demonstrates an extensive functional group tolerance as alkenes

with alcohols, ethers, silylethers, sulfones, phosphones, aromatics and alkyne functional groups equally remained intact. Moreover, the electrochemical dehalogenation of persistent and toxic hexachlorocyclohexane (HCH) to benzene was also described. Various lindane-contaminated soil samples were subjected to the optimized conditions to yield the corresponding benzene and vicinal 1,2-dichloride in excellent yields.

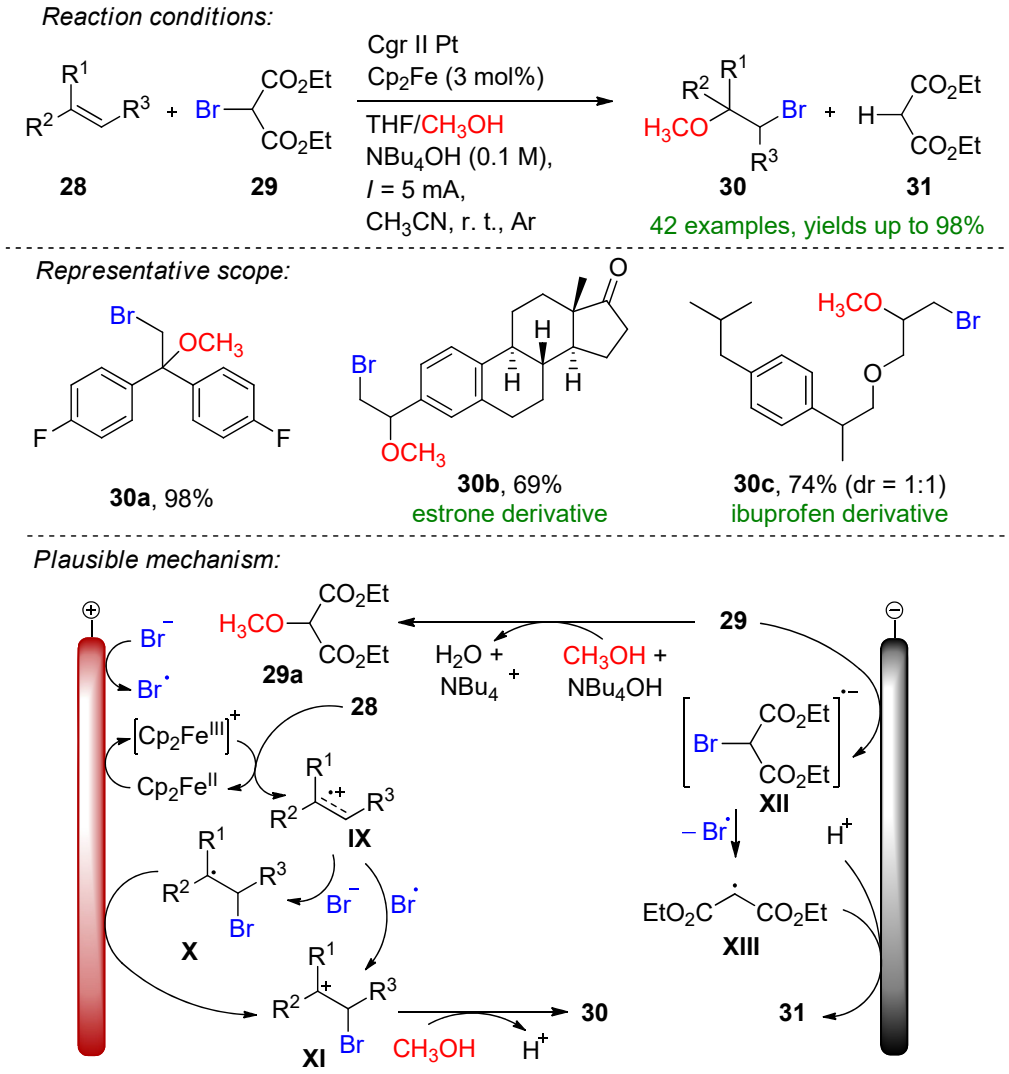

Scheme 13. The electrochemical alkoxyhalogenation of alkenes within a convergent paired electrolysis method [99]. CCE conditions were described with current (*I*), as the immersed electrode area was not specified. Cgr = graphite.

While the electrochemical dibromination and bromofunctionalization of alkenes are mainly characterized by the application of metal bromide salts as potential bromine sources, there are more and more methods that provide the electrochemical generation of bromine in a synergistic operation. The advantage of the former is the utilization of bench-stable and safe bromide salts. These, unfortunately, usually require an obligatory protic additive for solubility reasons and, except for organic salts, are not metal-free. Replacing the alkali bromide salts with usually toxic organobromine compounds overcomes the solubility issues, providing a simpler setup. These procedures allow the elimination or the utilization of the sacrificial half-reaction as bromine can be generated in a linear-paired fashion [62,87].

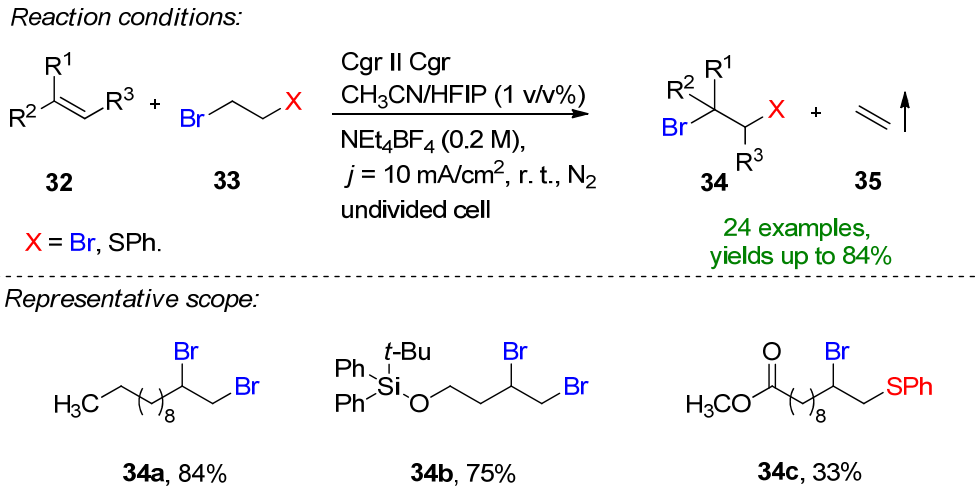

Scheme 14. Merging e-shuttle for the retro-dibromination and bromofunctionalization of alkenes [62]. Cgr = graphite.

4. Electrochemical Bromofunctionalization of Alkynes

Although there have been substantially less protocols reported, alkynes still represent a popular electrochemical target functionality [100]. In terms of halofunctionalization, they have also received significant attention, as the forming organohalides are excellent synthons for heterocyclic molecules and other synthetic intermediates [101,102].

4.1. HBr, MBr and Alkylammonium Bromides as Bromine Sources

Wang et al. reported the electrochemical oxyhalogenation of alkynes in the presence of KBr or HCl to form the corresponding α,α-dihaloacetoketone derivatives [103]. The reaction proceeds readily in a divided cell equipped with a cation exchange membrane to form the desired products in good to excellent yields. $LiClO_4$ serves as an additional supporting electrolyte and platinum electrodes promote the oxidation of halides at the anode and the liberation of hydrogen at the cathode. The authors suggest the in-situ formation of HOBr and HOCl as powerful halogenating agents.

An improved electrochemical method for the oxidative functionalization of arylalkynes was published under undivided cell conditions [104]. The desired α,α-dibro moacetophenone derivatives readily formed in the presence of 3 eq. LiBr and *p*-toluenesulfonic acid monohydrate in aqueous media including 10% methanol. H_2O (100%) as well as H_2O/MeOH (50%) resulted in reduced yields, suggesting that water had a significant role in the reaction and the co-solvent was beneficial as it promoted the solvation of phenylacetylene. The combination of LiBr and *p*-TsOH·H_2O was obligatory to the success of the reaction as switching either the bromide salt or the acid resulted in diminished yields. Under the optimized conditions, 16 different α,α-dibromoacetophenones were presented with yields up to 88%. The reaction proved to be scalable both in a batch and in-flow setup, and the synthetic applicability of the products were presented in the synthesis of three different heterocyclic compounds (Scheme 15).

A highly stereoselective, three-component annulation–sulfonylation method of 1,6-enynes to 1-indanones was reported in the presence of NaI or NaBr [105]. The test substrate, 1,6-enyne **39** was readily converted to the corresponding bromosulfonylated product **40** in the presence of 2 eq. of NaBr and 3 eq. of 4-methylbenzenesulfonylhydrazine as the sulfonyl donor (Scheme 16). The halide salts play a triple role of an electrolyte, redox catalysts and halogenating reagents. The reaction performed best at platinum electrodes in a solvent mixture consisting of THF/H_2O (1:1). The highly selective nature of the reaction was postulated to rise from the electrochemically formed arylsulfonyl halide intermediate, that undergoes homolytic fission to the arylsulfonyl radical and bromine radical. The latter is oxidized at the anode to a bromonium ion. The resulting arylsulfonyl radical is

scavenged by **39** to form intermediate **XIV,** which then, due to steric hindrance, selectively forms the *Z* isomer.

The direct halogenation of *o*-arylalkynylanilines to C3-halogenated indoles using NH_4Br both as electrolyte and the halogen source was reported [106]. The reaction proceeded smoothly on platinum electrodes in undivided cell conditions using ethanol as solvent. The reaction also proceeded to yield to corresponding 3-iodoindoles in the presence of ammonium iodide, providing access to skeletally diverse indole derivatives with yields up to 92%. Slightly changing the electrochemical parameters allowed the formation of unexpected indole derivatives. Changing the halide source to KI favored the generation of pentacyclic indole (**43**), while in the presence of NH_4I in acetone solvent, **44** was formed establishing the diverse applicability of the electrochemical method (Scheme 17).

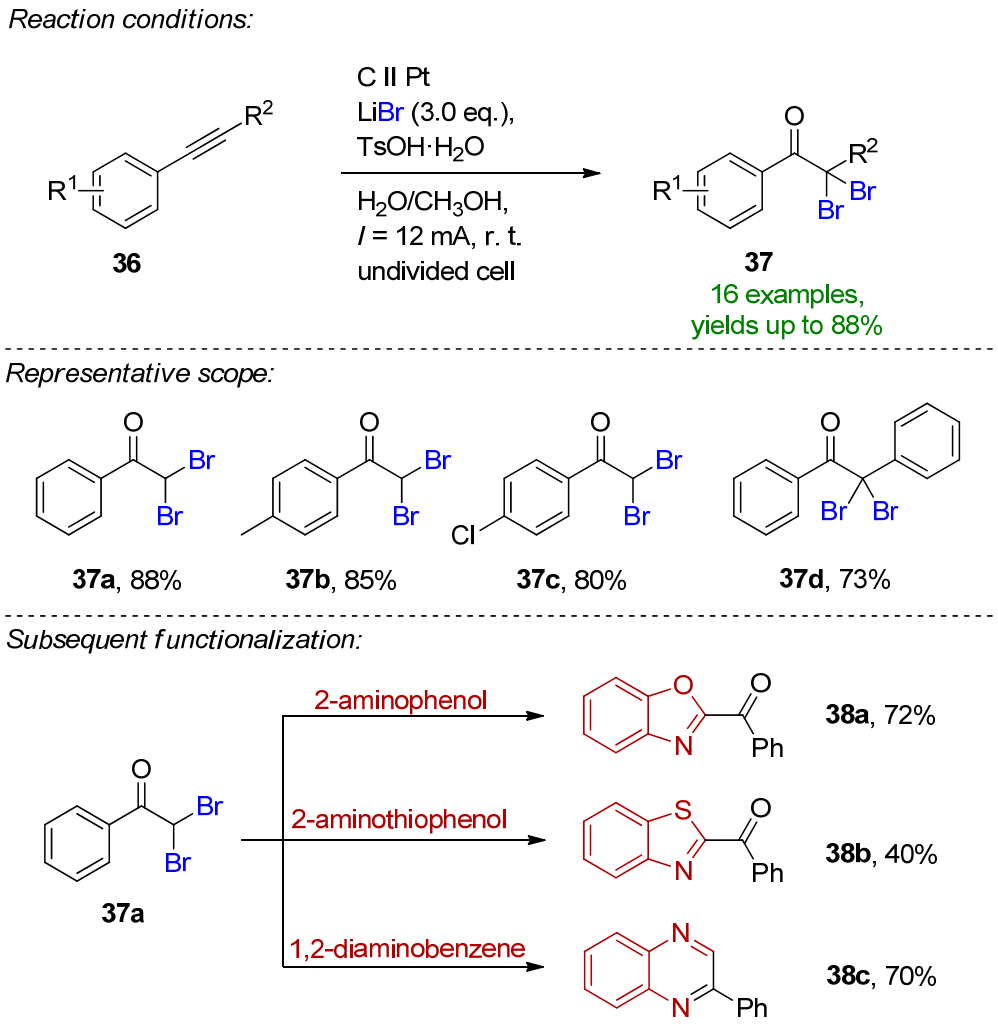

Scheme 15. Electrochemical α,α-dibromoacetophenone formation with the aid of LiBr in an undivided cell [104]. CCE conditions were described with current (*I*), as the immersed electrode area was not specified.

The oxidative *5-exo-dig-oxo*-cyclization of *o*-alkynylbenzamides for the synthesis of isobenzofuran-1-imines using NaBr was reported (Scheme 18) [107]. Using additional $LiClO_4$ as an electrolyte at platinum electrodes at room temperature gave the brominated derivatives with up to a 77% isolated yield. The choice of additional supporting electrolyte as well as the solvent were the key features of this electrochemical method. Changing $LiClO_4$ or the absence of the supporting electrolyte had detrimental effect on the reaction. Using 1.5 eq. NaI as a halogen source gave the corresponding 3-iodo-isobenzofuran-1-

imines with excellent yields. The combined halogenation process provided 33 examples with up to an 84% isolated yield.

The electrochemical dearomative spirocyclization of *N*-aryl alkynamides to the corresponding spiro[4,5]trienones was reported [108]. The highly selective reaction was catalyzed by inexpensive and bench-stable lithium halides on graphite electrodes. The model substrate showed high affinity in the presence of 2 eq. LiBr to form the 3-bromoderivative. Extension of the scope provided 20 different brominated examples with up to a 98% isolated yield. Substitutions both on the nitrogen as well as the aniline were tolerated with only noticeable changes in the yield in the presence of electron-withdrawing groups on the nitrogen. In absence of the methoxy group as well as the halogen, no formation of the desired product was detected. Similarly, the chloro- and iodo-derivatives could be also obtained with moderate to good yields. The synthetic utility was proved by a 32-fold scale-up to provide **48** with a yield of 80% (Scheme 19).

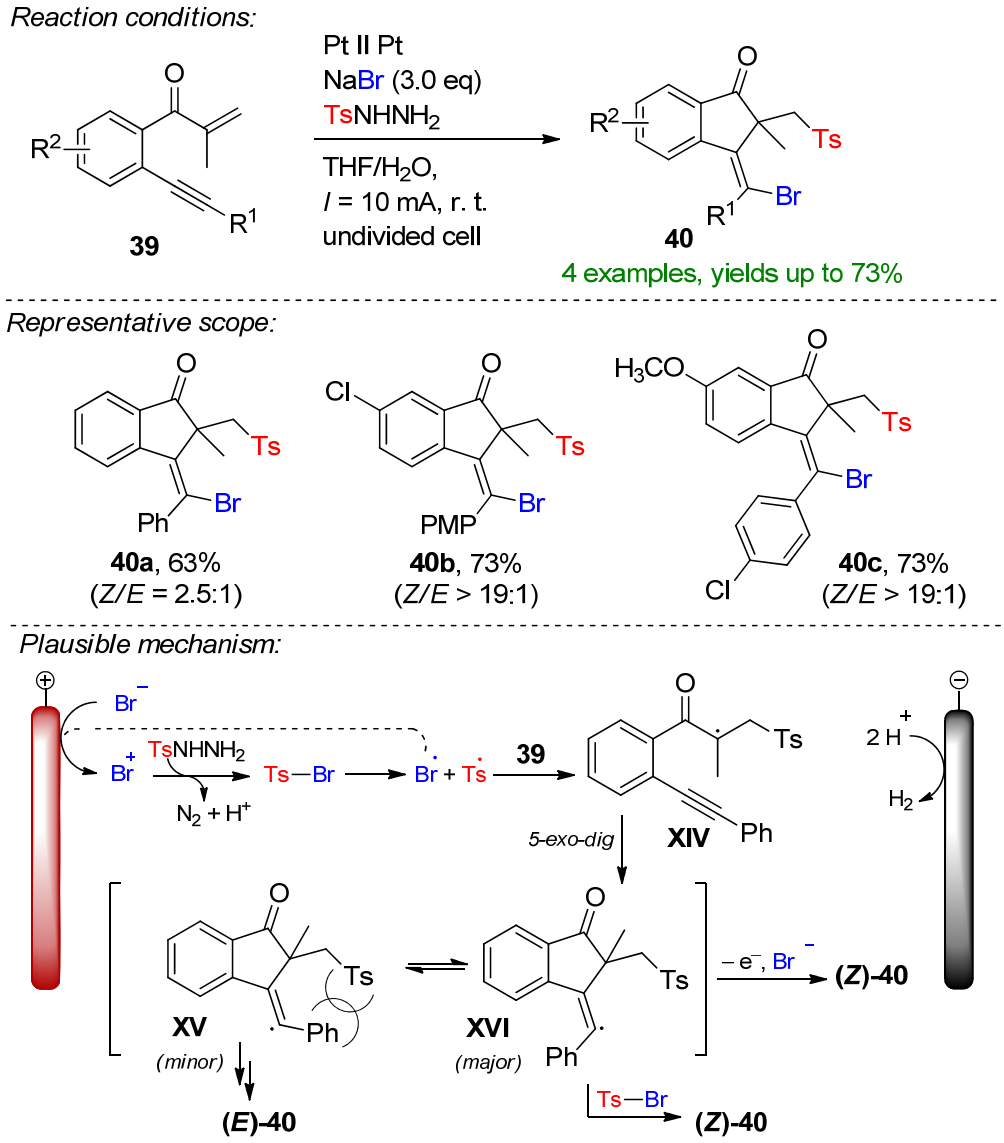

Scheme 16. Electrochemical three-component annulation–sulfonylation of 1,6-enynes to 1-indanones [105]. CCE conditions were described with current (*I*), as the immersed electrode area was not specified.

4.2. Organohalides as Bromine Sources

The first electrocatalytic oxydihalogenation of alkynes using organohalides (CH_2Br_2, $CHCl_3$, CH_2Cl_2, Cl–CH_2–CH_2–Cl) with water as an eco-friendly oxygen source and NBu_4I as a catalyst was reported [109]. The reaction also worked for the formation of dichloroacetophenone using different organochlorine sources. The mechanism was previsioned by the S_N2 substitution of the CH_2Br_2 by iodide, which then underwent oxidation at the anode to a bromine radical that was subsequently trapped by the alkene **49** (Scheme 20). The resulting intermediate **XVII** was oxidized to carbocation **XVIII,** which then, upon reaction with water, formed the corresponding enol, and further combination with bromoradical and subsequent oxidation resulted in the product **50**. The procedure could be extended to provide 13 examples with up to 84% isolated yields.

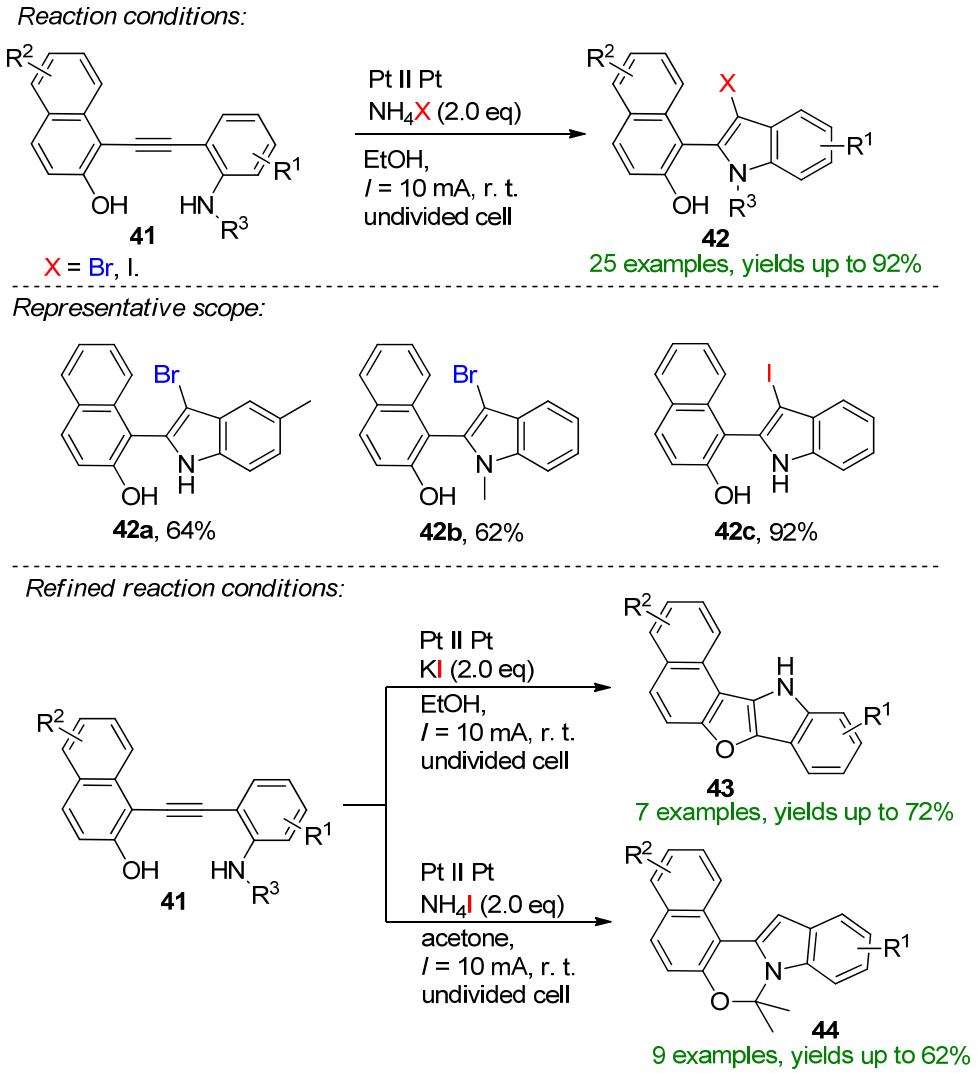

Scheme 17. Electrochemical halogenation of arylalkylanilines to C3-halogenated indoles [106]. CCE conditions were described with current (*I*), as the immersed electrode area was not specified.

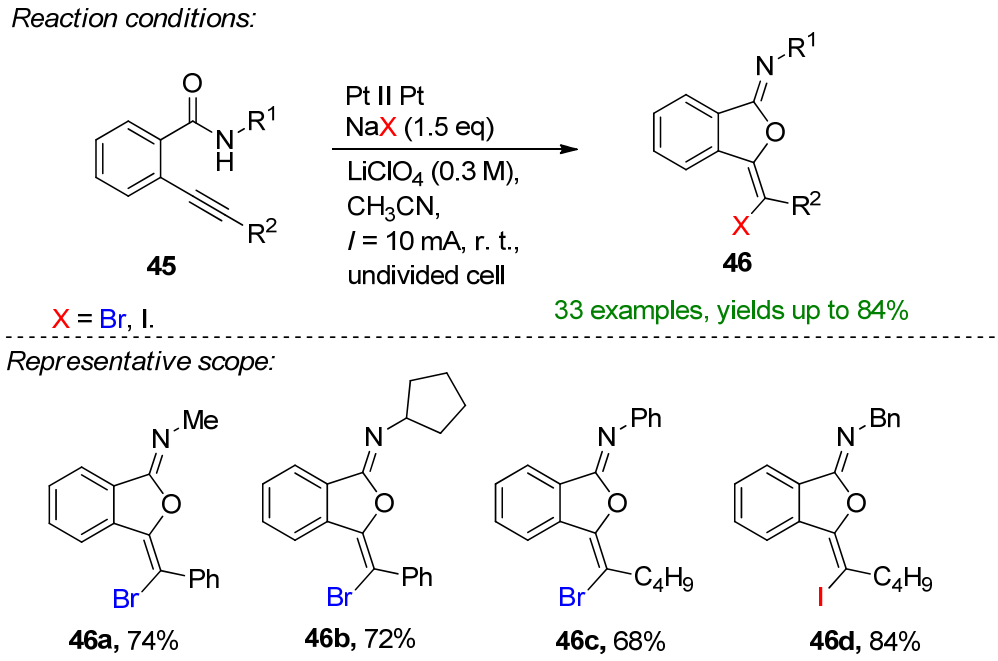

Scheme 18. The oxidative *5-exo-dig-oxo*-cyclization of *o*-alkynylbenzamides to isobenzofuran-1-imines using NaBr and NaI [107]. CCE conditions were described with current (*I*), as the immersed electrode area was not specified.

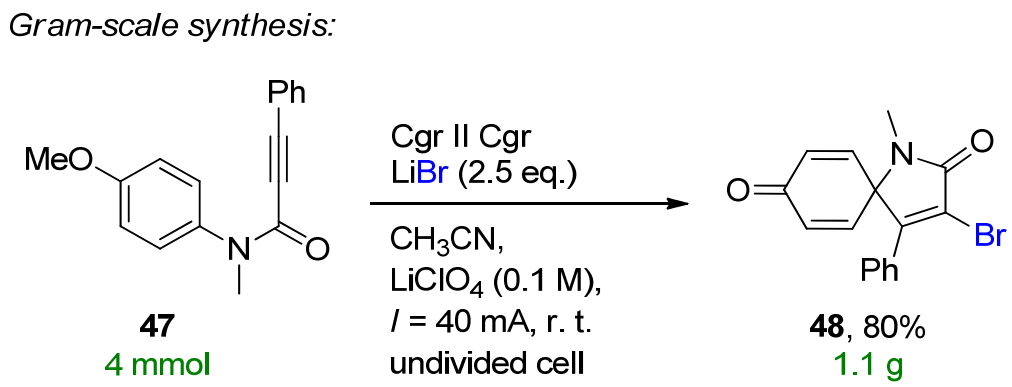

Scheme 19. Gram-scale synthesis of spiro[4,5]trienone **48** [108]. CCE conditions were described with current (*I*), as the immersed electrode area was not specified. Cgr = graphite.

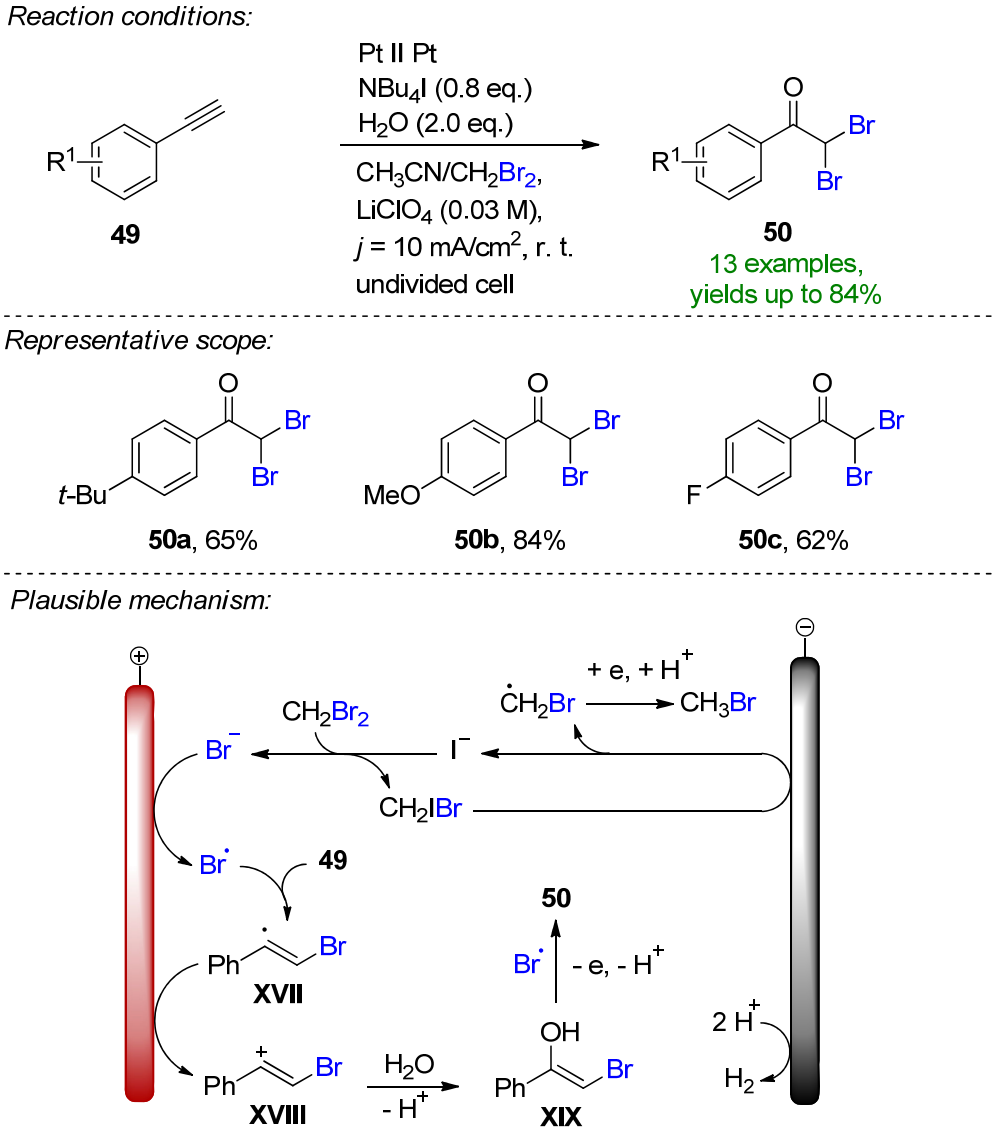

Scheme 20. Electrocatalytic oxydihalogenation of alkynes in the presence of dibromoethane [109].

5. Conclusions

The electrochemical bromination and bromofunctionalization of alkenes and alkynes have proved to be emerging hot topics in the last years. Via the anodic oxidation of readily available and bench-stable bromides, bromine can be generated under controlled parameters to form the desired brominated products and intermediates in a highly sustainable fashion without the use of catalysts or exogenous oxidants. The utilization of alkali bromide salts in a dual role as both a reagent and supporting electrolyte augments electrochemical bromination protocols over the traditional ones, providing a greener and accessible alternative for the scientific community. Furthermore, their non-toxic and non-corrosive nature provides a solution for the handling and storage issues that are indispensable requirements for Br_2 or HBr, thus opening a more sustainable and atomically economic way for the electrochemical generation of bromine and bromofunctionalization reactions.

While the electrochemical methods are represented via the utilization of metal bromide as brominating agents, there are more and more procedures that use organobromines in a paired electrolysis fashion, replacing the usual H_2 evolution as a cathodic counterpart. Although the exchange of bench-stable and safe bromide salts to organobromine compounds might raise questions, this approach could potentially open a field and draw interest for the elimination of persistent halogenated organic pollutants, such as hexachlorocyclohexane or

hexabromocyclododecane. Since the cathodic removal of bromo substituents is a common synthetic tool, which has even been applied to pharmaceutical intermediates, the basis for an electrically driven circular economy for bromine has been virtually established [110–112].

Author Contributions: L.G.G. and S.R.W. wrote the manuscript. All authors have read and agreed to the published version of the manuscript.

Funding: This research was funded by the Forschungsinitiative des Landes Rheinland-Pfalz in frame of SusInnoScience.

Institutional Review Board Statement: Not applicable.

Informed Consent Statement: Not applicable.

Data Availability Statement: Not applicable.

Acknowledgments: L.G.G. and S.R.W. highly appreciate the support from the Forschungsinitiative des Landes Rheinland-Pfalz in frame of SusInnoScience.

Conflicts of Interest: The authors declare no conflict of interest.

References

1. Hoegh-Guldberg, O.; Jacob, D.; Taylor, M. Global Warming of 1.5 °C. Available online: https://www.ipcc.ch/sr15/ (accessed on 25 August 2022).
2. Yan, M.; Kawamata, Y.; Baran, P.S. Synthetic organic electrochemical methods since 2000: On the verge of a renaissance. *Chem. Rev.* **2017**, *117*, 13230–13319. [CrossRef]
3. Shatskiy, A.; Lundberg, H.; Kärkäs, M.D. Organic electrosynthesis: Applications in complex molecule synthesis. *ChemElectroChem* **2019**, *6*, 4067–4092. [CrossRef]
4. Hilt, G. Basic strategies and types of applications in organic electrochemistry. *ChemElectroChem* **2020**, *7*, 395–405. [CrossRef]
5. Pollok, D.; Waldvogel, S.R. Electro-organic synthesis—A 21st century technique. *Chem. Sci.* **2020**, *11*, 12375–12592. [CrossRef]
6. Novaes, L.F.T.; Liu, J.; Shen, Y.; Lu, L.; Meinhardt, J.M.; Lin, S. Electrocatalysis as an enabling technology for organic synthesis. *Chem. Soc. Rev.* **2021**, *50*, 7941–8002. [CrossRef]
7. Beil, S.B.; Pollok, D.; Waldvogel, S.R. Reproducibility in electroorganic synthesis—Myths and misunderstandings. *Angew. Chem. Int. Ed.* **2021**, *60*, 14750–14759. [CrossRef]
8. Yoshida, J.; Shimizu, A.; Hayashi, R. Electrogenerated cationic reactive intermediates: The pool method and further advances. *Chem. Rev.* **2017**, *118*, 4702–4730. [CrossRef]
9. Röckl, J.L.; Pollok, D.; Franke, R.; Waldvogel, S.R. A decade of electrochemical dehydrogenative C,C-coupling of aryls. *Acc. Chem. Res.* **2020**, *53*, 45–61. [CrossRef]
10. Waldvogel, S.R.; Lips, S.; Selt, M.; Riehl, B.; Kampf, C.J. Electrochemical arylation reactions. *Chem. Rev.* **2018**, *118*, 6706–6765. [CrossRef]
11. Seidler, J.; Strugatchi, J.; Gärtner, T.; Waldvogel, S.R. Does electrifying organic synthesis pay off—The energy efficiency of electro-organic conversions. *MRS Energy Sustain.* **2020**, *7*, E42. [CrossRef]
12. Margarita, C.; Lundberg, H. Recent advances in asymmetric catalytic electrosynthesis. *Catalysts* **2020**, *10*, 982. [CrossRef]
13. Chicas-Baños, D.F.; Frontana-Uribe, B.A. Electrochemical generation and use in organic synthesis of *C*-,*O*-, and *N*-centered radicals. *Chem. Rec.* **2021**, *21*, 2538–2573. [CrossRef]
14. Klüh, D.; Waldmüller, W.; Gaderer, M. Kolbe electrolysis for the conversion of carboxylic acids to valuable products—A process design study. *Clean Technol.* **2021**, *3*, 1–18. [CrossRef]
15. Gleede, B.; Selt, M.; Franke, R.; Waldvogel, S.R. Developments in the dehydrogenative electrochemical synthesis of 3,3´,5,5´-tetramethyl-2,2´-biphenol. *Chem. Eur. J.* **2021**, *27*, 8252–8263. [CrossRef]
16. Zheng, Y.; Shao, X.; Ramadoss, V.; Tian, L.; Wang, Y. Recent developments in photochemical and electrochemical decarboxylative C(sp^3)-N bond formation. *Synthesis* **2020**, *52*, 1357–1368. [CrossRef]
17. Listratova, A.V.; Sbei, N.; Voskressensky, L.G. Catalytic electrosynthesis of *N*,*O*-heterocycles—Recent advances. *Eur. J. Org. Chem.* **2020**, *2020*, 2012–2027. [CrossRef]
18. Wirtanen, T.; Rodrigo, E.; Waldvogel, S.R. Recent advances in the electrochemical reduction of substrates involving N-O bonds. *Adv. Synth. Catal.* **2020**, *362*, 2088–2101. [CrossRef]
19. Mei, H.; Pajkert, R.; Wang, L.; Li, Z.; Röschenthaler, G.; Han, J. Chemistry of electrochemical oxidative reactions of sulfinate salts. *Green Chem.* **2020**, *22*, 3028–3059. [CrossRef]
20. Blum, S.P.; Hofman, K.; Manolikakes, G.; Waldvogel, S.R. Advances in photochemical and electrochemical incorporation of sulfur dioxide for the synthesis of value-added compounds. *Chem. Commun.* **2021**, *57*, 8236–8249. [CrossRef]
21. Sbei, N.; Martins, G.M.; Shirinfar, B.; Ahmed, N. Electrochemical phosphorylation of organic molecules. *Chem. Rec.* **2020**, *20*, 1530–1552. [CrossRef]

22. Thang, S.; Liu, Y.; Lei, A. Electrochemical oxidative cross-coupling with hydrogen evolution: A green and sustainable way for bond formation. *Chem* **2018**, *4*, 27–45. [CrossRef]
23. Yang, Q.; Fang, P.; Mei, T. Recent Advances in organic electrochemical C-H functionalization. *Chin. J. Chem.* **2018**, *36*, 338–352. [CrossRef]
24. Scheide, M.R.; Nicoleti, C.R.; Martins, G.M.; Braga, A.L. Electrohalogenation of organic compounds. *Org. Biomol. Chem.* **2021**, *19*, 2578–2602. [CrossRef]
25. Kisukuri, C.M.; Fernandes, V.A.; Delgado, J.A.C.; Häring, A.P.; Paixão, M.W.; Waldvogel, S.R. Electrochemical installation of CFH_2^-, CF_2H^-, CF_3^-, and perfluoroalkyl groups into small organic molecules. *Chem. Rec.* **2021**, *21*, 2502–2525. [CrossRef]
26. Wilcken, R.; Zimmermann, M.O.; Lange, A.; Joerger, A.C.; Boeckler, F.M. Principles and applications of halogen bonding in medicinal chemistry and chemical biology. *J. Med. Chem.* **2013**, *56*, 1363–1388. [CrossRef]
27. Tiz, D.B.; Bagnoli, L.; Rosati, O.; Marini, F.; Sancineto, L.; Santi, C. New halogen-containing drugs approved by FDA in 2021: An overview on their synthesis and pharmaceutical use. *Molecules* **2022**, *27*, 1643. [CrossRef]
28. Bidleman, T.F.; Andersson, A.; Jantunen, L.M.; Kucklick, J.R.; Kylin, H.; Letcher, R.J.; Tysklind, M.; Wong, F. A review of halogenated natural products in Arctic, Subarctic and Nordic ecosystems. *Emerg. Contam.* **2019**, *5*, 89–115. [CrossRef]
29. Häggblom, M.M.; Bossert, I.D. Halogenated organic compounds: A global perspective. In *Dehalogenation: Microbial Processes and Environmental Applications*; Springer: Boston, MA, USA, 2003; pp. 3–29. [CrossRef]
30. Yuan, Y.; Lei, A. Is electrosynthesis always green and advantageous compared to traditional methods? *Nat. Commun.* **2020**, *11*, 802. [CrossRef]
31. Möhle, S.; Zirbes, M.; Rodrigo, E.; Gieshoff, T.; Wiebe, A.; Waldvogel, S.R. Modern electrochemical aspects for the synthesis of value-added organic products. *Angew. Chem. Int. Ed.* **2018**, *57*, 6018–6041. [CrossRef]
32. Wiebe, A.; Gieshoff, T.; Möhle, S.; Rodrigo, E.; Zirbes, M.; Waldvogel, S.R. Electrifying organic synthesis. *Angew. Chem. Int. Ed.* **2018**, *57*, 5594–5619. [CrossRef]
33. Tang, H.; Jia, J.; Pan, Y. Halogen-mediated electrochemical organic synthesis. *Org. Biomol. Chem.* **2020**, *18*, 5315–5333. [CrossRef]
34. Lian, F.; Xu, K.; Zeng, C. Indirect electrosynthesis with halogen ions as mediators. *Chem. Rec.* **2021**, *21*, 2290–2305. [CrossRef]
35. Inokuchi, T.; Matsumoto, S.; Torii, S. Indirect electrooxidation of alcohols by a double mediatory system with two redox couples of $[R_2N^+{=}O]/R_2NO\cdot$ and $[Br\cdot$ or $Br^+]/Br^-$ in an organic-aqueous two-phase solution. *J. Org. Chem.* **1991**, *56*, 2416–2421. [CrossRef]
36. Limborg, F.; Clauson-Kaas, N. A small cell for electrolytic alkoxylation of furans. *Acta Chem. Scand.* **1953**, *7*, 234–235. [CrossRef]
37. Nieto-Mendoza, E.; Guevara-Salazar, J.A.; Ramírez-Apan, M.T.; Frontana-Ulribe, B.A.; Cogordan, B.A.; Cárnedas, J. Electro-oxidation of hispanolone and anti-inflammatory properties of the obtained derivates. *J. Org. Chem.* **2005**, *70*, 4538–4541. [CrossRef]
38. Salameh, E.; Tarawneh, A.; Al-Raggad, M. Origin of high bromide concentration in the water sources in Jordan and in the Dead Sea water. *Arab. J. Geosci.* **2016**, *9*, 414. [CrossRef]
39. Fernández, L. Market Volume of Bromine Worldwide from 2015 to 2021, with a Forecast for 2022 to 2029. Available online: https://www.statista.com/statistics/1245240/bromine-market-volume-worldwide/ (accessed on 25 August 2022).
40. Wu, N.; Herrmann, T.; Paepke, O.; Tickner, J.; Hale, R.; Harvey, E.; La Guardia, M.; McClean, M.D.; Webster, T.F. Human exposure to PBDEs: Association of PBDE body burdens with food consumption and house dust concentrations. *Environ. Sci. Technol.* **2007**, *41*, 1584–1589. [CrossRef]
41. Hales, B.F.; Robaire, B. Effects of brominated and organophospate ester flame retardants on male reproduction. *Andrology* **2020**, *8*, 915–923. [CrossRef]
42. Addis, D.R.; Molyvdas, A.; Ambalavanan, N.; Matalon, S.; Jilling, T. Halogen exposure injury in the developing lung. *Ann. N. Y. Acad. Sci.* **2020**, *1480*, 30–43. [CrossRef]
43. Addis, D.R.; Aggarwal, S.; Lazrak, A.; Jilling, T.; Matalon, S. Halogen-induced chemical injury to the mammalian cardiopulmonary systems. *Physiology* **2021**, *36*, 272–291. [CrossRef]
44. Saikira, I.; Borah, A.J.; Phukan, P. Use of bromine and bromo-organic compounds in organic synthesis. *Chem. Rev.* **2016**, *116*, 6837–7042. [CrossRef]
45. Eissen, M.; Lenoir, D. Electrophilic bromination of alkenes: Environmental, health and safety aspects of new alternative methods. *Chem. Eur. J.* **2008**, *14*, 9830–9841. [CrossRef]
46. Van Kerrebroeck, R.; Horsten, T.; Stevens, C.V. Bromide oxidation: A safe strategy for electrophilic brominations. *Eur. J. Org. Chem.* 2022, *in press*. [CrossRef]
47. Tariq, Z.M. Electrochemistry of Br−/Br2 Redox Couple in Acetonitrile, Methanol and Mix Media of Acetonitrile–Methanol: An Insight into Redox Behavior of Bromide on Platinum (Pt) and Gold (Au) Electrode. *Phys. Chem.* **2019**, *234*, 295–312. [CrossRef]
48. Halász, D.; Visy, C.; Szűcs, A.; Novák, M. Bromide ion oxidation of various Pt surfaces. *React. Kinet. Catal. Lett.* **1992**, *48*, 177–188. [CrossRef]
49. Vojinovic, V.; Mentus, S.; Komnenic, V.J. Bromide oxidation and bromine reduction in propylene carbonate. *Electroanal. Chem.* **2003**, *547*, 109–113. [CrossRef]
50. Haynes, W.M. Abundance of elements in the earth's crust and in the sea. In *CRC Handbook of Chemistry and Physics*; CRC Press: Boulder, CO, USA, 2016; pp. 14–17. ISBN 978-1-4822-0868-9.
51. Sigma Aldrich. Available online: https://www.sigmaaldrich.com/DE/en (accessed on 14 September 2022).

52. Kingston, C.; Palkowitz, M.D.; Takahira, Y.; Vantourout, J.C.; Peters, B.K.; Kawamata, Y.; Baran, P.S. A survival guide for the "Electro-curious". *Acc. Chem. Rev.* **2020**, *53*, 72–83. [CrossRef]
53. Schotten, C.; Nicholls, T.P.; Bourne, R.A.; Kapur, N.; Nguen, B.N.; Williams, C.E. Making electrochemistry easily accessible to the synthetic chemist. *Green Chem.* **2020**, *22*, 3358–3375. [CrossRef]
54. Wu, T.; Nguyen, B.H.; Daugherty, M.C.; Moeller, K.D. Paired electrochemical reactions and the on-site generation of a chemical reagent. *Angew. Chem. Int. Ed.* **2019**, *58*, 3562–3565. [CrossRef]
55. Wu, T.; Moeller, K.D. Organic electrochemistry: Expanding the scope of paired reactions. *Angew. Chem. Int. Ed.* **2021**, *60*, 12883–12890. [CrossRef]
56. Marken, F.; Cresswell, A.J.; Bull, S.T. Recent advances in paired electrosynthesis. *Chem. Rec.* **2021**, *21*, 2585–2600. [CrossRef]
57. Klein, M.; Waldvogel, S.R. Counter electrode reactions—Important stumbling blocks on the way to a working electro-organic synthesis. *Angew. Chem. Int. Ed.* **2022**. *accepted*. [CrossRef]
58. Clark, J.H. Green Chemistry: Challenges and opportunities. *Green Chem.* **1998**, *1*, 1–8. [CrossRef]
59. Anastas, P.; Eghbali, N. Green Chemistry: Principles and practice. *Chem. Soc. Rev.* **2010**, *39*, 301–312. [CrossRef]
60. Frontana-Ulribe, B.A.; Little, R.D.; Ibanez, J.G.; Palma, A.; Vasquez-Medrano, R. Organic electrosynthesis: A promising green methodology in organic synthesis. *Green Chem.* **2010**, *12*, 2099–2119. [CrossRef]
61. Prat, D.; Wells, A.; Hayler, J.; Sneddon, H.; McElroy, R.; Abou-Shehada, S.; Dunn, P.J. CHEM21 selection guide of classical- and less classical solvents. *Green Chem.* **2016**, *18*, 288–296. [CrossRef]
62. Dong, X.; Roeckl, J.L.; Waldvogel, S.R.; Morandi, B. Merging shuttle reactions and paired electrolysis for reversible vicinal dihalogenations. *Science* **2021**, *371*, 507–514. [CrossRef]
63. Salom-Rolg, X.; Bauder, C. Recent applications in the use of sulfoxides as chiral auxiliaries for the asymetric synhesis of natural and biologically active products. *Synthesis* **2020**, *52*, 964–978. [CrossRef]
64. Torii, S.; Uneyama, K.; Ueda, K. Electrochemical procedure for a practical preparation of piperonal from isosafrole. *J. Org. Chem.* **1984**, *49*, 1830–1832. [CrossRef]
65. Uneyama, K.; Masatsugu, Y.; Torii, S. Electrochemical epoxidation and carbon-carbon bond cleavage for the preparation of 3-methyl-4-oxo-2-phenyl-4*H*-1-benzopyran-8-carboxylic acid from 3-methyl-2-phenyl-8-(1-prophenyl)-4*H*-1-benzopyran-4-one. *Bull. Chem. Soc. Jpn.* **1985**, *58*, 2361–2365. [CrossRef]
66. Inokuchi, T.; Matsumoto, S.; Tsuji, M.; Torii, S. Electrohalogenation of propargyl acetates and amides to form the 1,1-dibromo-2-oxo functionality and a facile synthesis of furaneol. *J. Org. Chem.* **1992**, *57*, 5023–5027. [CrossRef]
67. Inês, M.; Mendonça, A.J.; Esteves, A.P.; Mendonça, D.I.; Medeiros, M.J. Electroepoxidation of natural and synthetic alkenes mediated by sodium bromide. *Comptes Rendus Chim.* **2009**, *12*, 841–849. [CrossRef]
68. Kulangiappar, K.; Ramaprakash, M.; Vasudevan, D.; Raju, T. Electrochemical bromination of cyclic and acyclic enes using biphasic electrolysis. *Synth. Commun.* **2016**, *46*, 145–153. [CrossRef]
69. Yang, C. An impending platinum crisis and its implications for the future of the automobile. *Energy Policy* **2009**, *37*, 1805–1808. [CrossRef]
70. Das, K.K.; Reddy, R.C.; Bagoji, I.B.; Das, S.; Bagali, S.; Mullur, L.; Khodnapur, J.P.; Biradar, M.S. Primary concept of nickel toxicity—An overview. *J. Basic Clin. Physiol. Pharmacol.* **2019**, *30*, 141–152. [CrossRef]
71. Savignan, L.; Faucher, S.; Chéry, P.; Lespes, G. Platinum group elements contamination in soils: Review of the current state. *Chemosphere* **2021**, *271*, 129517. [CrossRef]
72. Sun, X.; Ma, H.; Mei, T.; Fang, P.; Hu, Y. Electrochemical radical formyloxylation-bromination, -chlorination, and -trifluoromethylation of alkenes. *Org. Lett.* **2019**, *21*, 3167–3171. [CrossRef]
73. Bormann, S.; Van Schie, M.M.C.H.; De Almeida, T.P.; Zhang, W.; Stöckl, M.; Ulber, R.; Hollman, F.; Holtmann, D. H_2O_2 production at low overpotential for electroenzymatic halogenation reactions. *ChemSusChem* **2019**, *12*, 4759–4763. [CrossRef]
74. Wever, R.; Renirie, R.; Hollmann, F. Vanadium chloroperoxidases as versatile biocatalysts. In *Vanadium Catalysis*; Sudradhar, M., Pombeiro, A.J.L., da Silva, J.A.L., Eds.; Royal Society of Chemistry: London, UK, 2021; Chapter 24; ISBN 978-1-78801-857-9.
75. Wu, J.; Abou-Hamdan, H.; Guillot, R.; Kouklovsky, C.; Vincent, G. Electrochemical synthesis of 3a-bromofuranoindolines and 3a-bromopyrroloindolines mediated by $MgBr_2$. *Chem. Commun.* **2020**, *56*, 1713–1716. [CrossRef]
76. Hakamata, H.; Sato, S.; Ueda, H.; Tokuyama, H. $AgNTf_2$-Mediated Allylation with Allylsilanes at C3a-Position of Hexahydropyrroloindoles: Application to Total Syntheses of Amauromine Alkaloids. *Org. Lett.* **2017**, *19*, 5308–5311. [CrossRef]
77. Ramos-Villaseñor, J.M.; Rodríguez-Cárdenas, E.; Díaz, C.E.B.; Frontana-Uribe, B.A. Review—Use of 1,1,1,3,3,3–hexafluoro–2–propanol (HFIP) Co-Solvent Mixtures in Organic Electrosynthesis. *J. Electrochem. Soc.* **2020**, *167*, 155509. [CrossRef]
78. Eberson, L.; Hartshorn, M.P.; Persson, O. 1,1,1,3,3,3-Hexafluoropropan-2-ol as a solvent for the generation of highly persistent radical cations. *J. Chem. Soc. Perkin Trans. 2* **1995**, 1735–1744. [CrossRef]
79. Eberson, L.; Hartshorn, M.P.; Persson, O. Generation of solutions of highly persistent radical cations by 4-tolylthallium(III) bis(trifluoroacetate) in 1,1,1,3,3,3-hexafluoropropan-2-ol. *J. Chem. Soc. Chem. Commun.* **1995**, 1131–1132. [CrossRef]
80. Eberson, L.; Persson, O.; Hartshorn, M.P. Detection and Reactions of Radical Cations Generated by Photolysis of Aromatic Compounds with Tetranitromethane in 1,1,1,3,3,3-Hexafluoro-2-propanol at Room Temperature. *Angew. Chem. Int. Ed.* **1995**, *34*, 2268–2269. [CrossRef]
81. Schulz, L.; Waldvogel, S.R. Solvent control in electro-organic synthesis. *Synlett* **2018**, *30*, 275–286. [CrossRef]

82. Röckl, J.L.; Dörr, M.; Waldvogel, S.R. Electrosynthesis 2.0 in 1,1,1,3,3,3-Hexafluoroisopropanol/Amine Mixtures. *ChemElectroChem* **2020**, *7*, 3686–3694. [CrossRef]
83. Ashikari, Y.; Shimizu, A.; Nokami, T.; Yoshida, J. Halogen and Chalcogen Cation Pools Stabilized by DMSO. Versatile Reagents for Alkene Difunctionalization. *J. Am. Chem. Soc.* **2013**, *135*, 16070–16073. [CrossRef]
84. Shimizu, A.; Hayashi, R.; Ashikari, Y.; Nokami, T.; Yoshida, J. Switching the reaction pathways of electrochemically generated β-haloalkoxysulfonium ions—Synthesis of halohydrins and epoxides. *Beilstein J. Org. Chem.* **2015**, *11*, 242–248. [CrossRef]
85. Bityukov, O.V.; Vil', V.A.; Nikishin, G.I.; Terent'ev, A.O. Alkene, Bromide, and ROH—How To Achieve Selectivity? Electrochemical Synthesis of Bromohydrins and Their Ethers. *Adv. Synth. Catal.* **2021**, *363*, 3070–3078. [CrossRef]
86. Shang, X.; Liu, X.; Sun, Y. Flexible on-site halogenation paired with hydrogenation using halide electrolysis. *Green Chem.* **2021**, *23*, 2037–2043. [CrossRef]
87. Strehl, J.; Abraham, M.L.; Hilt, G. Linear Paired Electrolysis—Realising 200 % Current Efficiency for Stoichiometric Transformations—The Electrochemical Bromination of Alkenes. *Angew. Chem. Int. Ed.* **2021**, *60*, 9996–10000. [CrossRef] [PubMed]
88. Pitzer, L.; Schäfers, F.; Glorius, F. Rapid Assessment of the Reaction-Condition-Based Sensitivity of Chemical Transformations. *Angew. Chem. Int. Ed.* **2019**, *58*, 8572–8576. [CrossRef] [PubMed]
89. Ye, J.H.; Quach, L.; Paulisch, T.; Glorius, F. Visible-light-induced, metal-free carbene insertion into B-H bonds between acylsilanes and pinacolborane. *J. Am. Chem. Soc.* **2019**, *141*, 16227–16231. [CrossRef]
90. Kale, A.P.; Nikolaienko, P.; Smirnova, K.; Rueping, M. Intramolecular Electrochemical Oxybromination of Olefins for the Synthesis of Isoxazolines in Batch and Continuous Flow. *Eur. J. Org. Chem.* **2021**, *2021*, 3496–3500. [CrossRef]
91. He, Y.; Qin, X.; He, X.; Wu, X.; Yin, Z. Practical Synthesis of Halogenated *N*-Heterocycles via Electrochemical Anodic Oxidation of Unactivated Alkenes. *Eur. J. Org. Chem.* **2021**, *2021*, 5831–5834. [CrossRef]
92. Kim, R.; Ha, J.; Woo, J.; Kim, D.Y. Electrochemical oxidative bromolactonization of unsaturated carboxylic acids with sodium bromide: Synthesis of bromomethylated γ-lactones. *Tetrahedron Lett.* **2022**, *88*, 153567. [CrossRef]
93. Yu, D.; Ji, R.; Sun, Z.; Li, W.; Liu, Z. Electrochemical chlorination and bromination of electron-deficient C-H bonds in quinones, coumarins, quinoxalines and 1,3-diketones. *Tetrahedron Lett.* **2021**, *86*, 153514. [CrossRef]
94. Gombos, L.G.; Werner, L.; Schollmeyer, D.; Martínez-Huitle, C.A.; Waldvogel, S.R. Selective Electrochemical Dibromination of Terpenes and Naturally Derived Olefins. *Eur. J. Org. Chem.* **2022**. *accepted*. [CrossRef]
95. Yuan, Y.; Yao, A.; Zheng, Y.; Gao, M.; Zhou, Z.; Qiao, J.; Hu, J.; Ye, B.; Zhao, J.; Wen, H.; et al. Electrochemical Oxidative Clean Halogenation Using HX/NaX with Hydrogen Evolution. *iScience* **2019**, *12*, 293–303. [CrossRef]
96. Seitz, J.; Wirth, T. Electrochemical bromofunctionalization of alkenes in a flow reactor. *Org. Biomol. Chem.* **2021**, *19*, 6892–6896. [CrossRef]
97. Wan, C.; Song, R.; Li, J.H. Electrooxidative 1,2-Bromoesterification of Alkenes with Acids and *N*-Bromosuccinimide. *J. Org. Lett.* **2019**, *21*, 2800–2803. [CrossRef] [PubMed]
98. Pan, G.; Ouyang, X.; Hu, M.; Xie, Y.; Li, J. Copper-Catalyzed Intermolecular Aminoalkylation of Alkenes with α-Bromoalkyl Esters and Amines toward Pyrrolidin-2-ones. *Adv. Synth. Catal.* **2017**, *359*, 2564–2570. [CrossRef]
99. Zhang, T.; Luo, M.; Li, Y.; Song, R.; Li, J. Electrochemical Alkoxyhalogenation of Alkenes with Organohalides as the Halide Sources via Dehalogenation. *Org. Lett.* **2020**, *22*, 7250–7254. [CrossRef] [PubMed]
100. Bortolami, M.; Petrucci, R.; Rocco, D.; Scarano, V.; Chiarotto, I. Alkynes as Building Blocks, Intermediates and Products in the Electrochemical Procedures Since 2000. *ChemElectroChem* **2021**, *8*, 3604–3613. [CrossRef]
101. Chung, W.; Vanderwal, C.D. Stereoselective Halogenation in Natural Product Synthesis. *Angew. Chem. Int. Ed.* **2016**, *55*, 4365–4434. [CrossRef]
102. Sadhukhan, S.; Santhi, J.; Baire, B. The α,α-Dihalocarbonyl Building Blocks: An Avenue for New Reaction Development in Organic Synthesis. *Chem. Eur. J.* **2020**, *26*, 7145–7175. [CrossRef]
103. Li, Z.; Sun, Q.; Qian, P.; Hu, K.; Zha, Z.; Wang, Z. Electrochemical synthesis of α,α-dihaloacetophenones from terminal alkyne derivatives. *Chin. Chem. Lett.* **2020**, *31*, 1855–1858. [CrossRef]
104. Wang, D.; Wan, Z.; Zhang, H.; Lei, A. Electrochemical Oxidative Functionalization of Arylalkynes: Access to α,α-Dibromo Aryl Ketones. *Adv. Synth. Catal.* **2021**, *363*, 1022–1027. [CrossRef]
105. Zhang, T.; Hao, W.; Wang, R.; Wang, S.; Tu, S.; Jiang, B. Electrocatalytic three-component annulation-halosulfonylation of 1,6-enynes toward 1-indanones using sodium halides as both halogen sources and electrolytes. *Green Chem.* **2020**, *22*, 4259–4269. [CrossRef]
106. Zhang, J.; Shi, S.; Hao, W.; Dong, G.; Tu, S.; Jiang, B. Tunable Electrocatalytic Annulations of o-Arylalkynylanilines: Green and Switchable Syntheses of Skeletally Diverse Indoles. *J. Org. Chem.* **2021**, *86*, 15886–15896. [CrossRef]
107. Reddy, M.B.; Peri, R.; Bhagavathiachari, M.; Anandhan, R. Electrochemical synthesis of isobenzofuran-1-imines using oxidative halocyclization of o-alkynylbenzamides. *Org. Biomol. Chem.* **2021**, *19*, 6792–6796. [CrossRef] [PubMed]
108. Yu, K.; Kong, X.; Yang, J.; Li, G.; Xu, B.; Chen, Q. Electrochemical Oxidative Halogenation of *N*-Aryl Alkynamides for the Synthesis of Spiro[4.5]trienones. *J. Org. Chem.* **2021**, *86*, 917–928. [CrossRef] [PubMed]
109. Meng, X.; Zhang, Y.; Luo, J.; Wang, F.; Cao, X.; Huang, S. Electrochemical Oxidative Oxydihalogenation of Alkynes for the Synthesis of α,α-Dihaloketones. *Org. Lett.* **2020**, *22*, 1169–1174. [CrossRef] [PubMed]

110. Gütz, C.; Selt, M.; Bäzinger, M.; Bucher, C.; Römelt, C.; Hecken, N.; Gallou, F.; Galvão, T.R.; Waldvogel, S.R. Novel cathode material for cathodic dehalogenation of 1,1,-dibromo cyclopropane derivatives. *Chem. Eur. J.* **2015**, *21*, 13878–13882. [CrossRef] [PubMed]
111. Gütz, C.; Bäzinger, M.; Bucher, C.; Galvão, T.R.; Waldvogel, S.R. Development and scale-up of electrochemical dehalogenation for the synthesis of a key intermediate for NS5A inhibitors. *Org. Process Res. Dev.* **2015**, *19*, 1428–1433. [CrossRef]
112. Gütz, C.; Grimaudo, V.; Holtkamp, M.; Hartmer, M.; Werra, J.; Frensemeier, L.; Kehl, A.; Karst, U.; Broekmann, P.; Waldvogel, S.R. Leaded Bronze—An Innovative Lead Substitute for Cathodic Electrosynthesis. *ChemElectroChem* **2018**, *5*, 247–252. [CrossRef]

EurJOC
European Journal of Organic Chemistry

Research Article
doi.org/10.1002/ejoc.202200857

Chemistry Europe
European Chemical Societies Publishing

www.eurjoc.org

VIP *Very Important Paper*

Selective Electrochemical Dibromination of Terpenes and Naturally Derived Olefins

Lilla G. Gombos,[a] Leo Werner,[a] Dieter Schollmeyer,[a] Carlos A. Martínez-Huitle,[a, b] and Siegfried R. Waldvogel*[a]

A simple electrochemical protocol is established for the selective alkene dibromination of naturally derived olefins, such as terpenes. The use of hazardous Br_2 or its analogues have been elegantly avoided by employing readily available, inexpensive, and harmless sodium bromide with a dual role as reagent and supporting electrolyte in combination with sustainable carbon-based electrodes. This electrochemical protocol provides the desired products with good to excellent yields up to 82% with 10 examples. Scalability has been proved by a 5-fold scale-up. Notably, higher yields and selectivity were achieved in comparison to conventional bromination by Br_2 and DMSO/HBr system and the dibrominated compound was eligible for further functionalization, such as cyanation according to the Kolbe nitrile synthesis protocol.

Introduction

Converting renewable resources to biologically active molecules and functional materials are one of the hot topics among sustainable research fields.[1–2] Terpenes are considered as one of the largest class of natural compounds with more than 50,000 different molecules identified, isolated and readily utilized by the pharmaceutical, agricultural and chemical industry.[3–5] Multiple reports demonstrate antifungal,[6–7] antiparasitic,[8] antibacterial[7,9] and anticancer[10–12] properties of modified or even natural terpenes, like the naturally occurring brominated sesquiterpenoid, (−)-dactylone. The plant and fungi synthesized terpenes and terpenoids represent a valuable and inexpensive biomass resource and they are readily available in large scale from essential oils or as industrial by-products.[13–14] For example, limonene, which is produced on 60,000 ton/year scale as the by-product of citrus juice industry.[15–16] Their unique structural features enable versatile functionalization possibilities, hence it became a major spotlight in polymer chemistry in recent years.[17–22] For these versatile application methods, terpenes represent one of the biggest renewable sources for conversion into valuable products. Nevertheless, the current functionalization methods are accompanied with several difficulties. Chemical transformations such as isomerization, hydrolyzation, condensation and oxidation reactions are often accompanied with the formation of undesired by-products, reduced chemoselectivity and requires the utilization of several metal catalysts, such as Ru, Rh, Mn or Ni.[2,23–24] Hence, to this date, selective transformation of such delicate molecules is still highly challenging.

The introduction of bromine groups for the functionalization of molecules is a well-known method, however it is not readily established for terpenes.[25] Conventional methods for the dibromination of olefins usually employ hazardous and corrosive bromine,[26–29] as well as the application of HBr or metal bromides in the presence of an external oxidant (Scheme 1).[30–33] The utilization of next generation agents such as *N*-bromosuccinimide, pyridinium tribromide or hypervalent iodine reagents have also gained attention.[34–36] While these agents enable simpler handling, their preparation is difficult and due to cost and atom economy aspects, a greener alternative is highly desired.

Oxidative electrochemistry provides a superior and "green" alternative to the traditional strategies. The use of electricity as a clean and inexpensive reagent diminishes waste generation and replaces the usually harmful redox reagents.[37–41] Furthermore, constant current conditions in combination with carbon-based electrodes allow an easy and safe operation by simply switching on or off the electrochemical current.[39,42–43] The electrochemical bromofunctionalization of alkenes including the generation of 1,2-vicinal dihalides have attracted special attention.[44–50] Many great protocols have been reported recently for the electrochemical bromination of alkenes featuring direct electrochemical bromination,[44–45] electrocatalytic bromination[48] and bromination via linear paired electrosynthesis.[46,49] Recently, the electrochemical bromofunctionalization of alkenes in a flow reactor was also reported.[47] While these methods are widely applicable and provide good to excellent yields, they often utilize dangerous bromine sources, such as HBr,[45,47] and depleting metal electrodes.[44–48]

[a] *L. G. Gombos, L. Werner, D. Schollmeyer, Prof. Dr. C. A. Martínez-Huitle, Prof. Dr. S. R. Waldvogel*
Department of Chemistry
Johannes Gutenberg University Mainz
Duesbergweg 10–14, 55128, Mainz, Germany
E-mail: waldvogel@uni-mainz.de
https://www.aksw.uni-mainz.de/
[b] *Prof. Dr. C. A. Martínez-Huitle*
Institute of Chemistry
Federal University of Rio Grande do Norte
Lagoa Nova, CEP 59078-970, Natal, RN, Brazil

Supporting information for this article is available on the WWW under https://doi.org/10.1002/ejoc.202200857

Research Article
doi.org/10.1002/ejoc.202200857

Chemistry Europe
European Chemical Societies Publishing

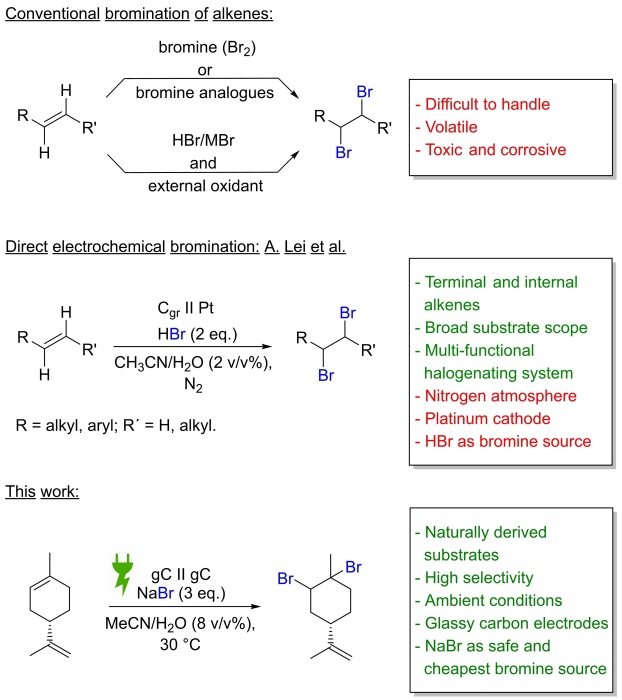

Scheme 1. Synthetic strategies for the bromination of olefins, M = alkali metal, Cgr = graphite, gC = glassy carbon.

Table 1. Optimization of electrochemical dibromination of (4*S*)-(−)-limonene in 5 mL PTFE electrolysis cells, PTFE = polytetrafluoroethylene.

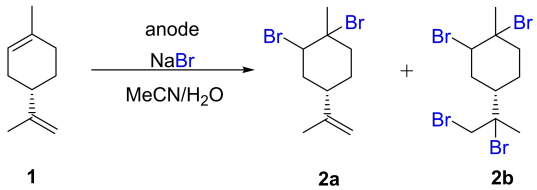

1 **2a** **2b**

Entry	Deviation from standard conditions[a]	**2a** [%][b]	**2b** [%][b]
1	NBu_4Br	0	0
2	NEt_4Br	2	0
3	None	30	4
4	LiBr	32	6
5	divided cell	32	8
6	acetone/H_2O (8 v/v%)	52	4
7	HFIP/H_2O (8 v/v%)	0	0
8	MeCN/H_2O (20 v/v%)	9	0
9	gC II gC	46	5
10	gC II gC, 2.2 *F*	44	0
11	gC II gC, 3.0 *F*	35	1
12	gC II gC, $j = 5$ mA/cm^2	54	0

[a] Standard conditions: **1** (0.7 mmol), NaBr (2.1 mmol), MeCN/H_2O (5 mL, 8 v/v%), graphite electrodes, undivided cell, constant current, $j = 20$ mA/cm^2, 1.5 *F* (ref. terpene), 30 °C. [b] Yields determined by ^{1}H NMR (internal standard: CH_2Br_2). gC = glassy carbon.

To overcome these drawbacks, a novel method for the trans-halogenation of numerous alkenes via an electron shuttle reaction was recently reported by our group.[49] Nevertheless, while the electrochemical bromination of simple alkenes was extensively researched, the functionalization of naturally derived compounds and especially the dibromination of terpenes and terpenoids casts only very few examples.[50]

This work presents a simple and sustainable electrochemical alternative to the already existing bromination methods extending the protocol to renewable resources in a selective manner. The implementation of naturally occurring terpenes and terpenoids facilitates a wide variety of brominated derivatives that can act as appropriate intermediates for further functionalization purposes. Employing inexpensive carbon-based electrodes such as graphite or glassy carbon instead of expensive platinum contributes to the principles of green chemistry.[51–53] Sodium bromide acts both as the supporting electrolyte and a safe, bench-stable bromide source that can in-situ oxidised into bromine under ambient conditions. Moreover, to the best of our knowledge this method features the first electrochemical bromination of structurally challenging terpenes and terpenoids.

Results and Discussion

Initial optimization reactions were carried out in a PTFE undivided cell (see Supporting Information) according to Table 1. Readily available (4*S*)-(−)-limonene (**1**) was chosen as a test substrate as the presence of multiple functionalizable double bonds offers regioselectivity issues. The first screening experiments revealed that **1** only tolerates NaBr (Table 1, Entry 1–4) which determines the composition of the solvent system obliging the presence of an additive. The utilization of LiBr as bromide salt provided equally great results, however, heavy cathode corrosion was observed. Under multiple solvent systems especially acetone/H_2O performed well with 52% of **2a**. However, due to the volatility of acetone solvent, further optimizations were carried on with MeCN/H_2O (see Supporting Information). The solvent/additive ratio also plays an important role in the outcome of the reaction. With increasing water content, the selectivity of the reaction decreases dramatically (Table 1, Entry 8). The reaction is highly selective towards the formation of **2a**, even after an increased amount of applied charge, there was no significant change in the yield of **2b** (see Supporting Information). When applying 1.5 *F* charge, **2a** was obtained in 46%. Increasing the charge did not lead to higher yields (Table 1, Entry 10–11). Surprisingly, the yield with the application of a current density of 5 mA/cm^2 in MeCN/H_2O (8 v/v%) media turned out to be superior compared to the standard conditions (Table 1, Entry 12). Interestingly, different electrode materials did not have a significant effect on the outcome of the reaction (see Supporting Information).

Based on our findings, the scope was further extended with both mono- und polyunsaturated monoterpenes with the presence of different functional groups (Scheme 2). Structurally challenging cyclic, linear monoterpenes, terpenoids and phenylpropanoids were subjected to the optimized conditions by varying the amount of charge to obtain their dibrominated derivatives. Among all the terpenes tested, the cyclic monoterpenoid, carvone went readily under electrochemical bromination to **3** with an isolated yield of 82%. Similarly, peril-

Research Article
doi.org/10.1002/ejoc.202200857

Chemistry Europe
European Chemical Societies Publishing

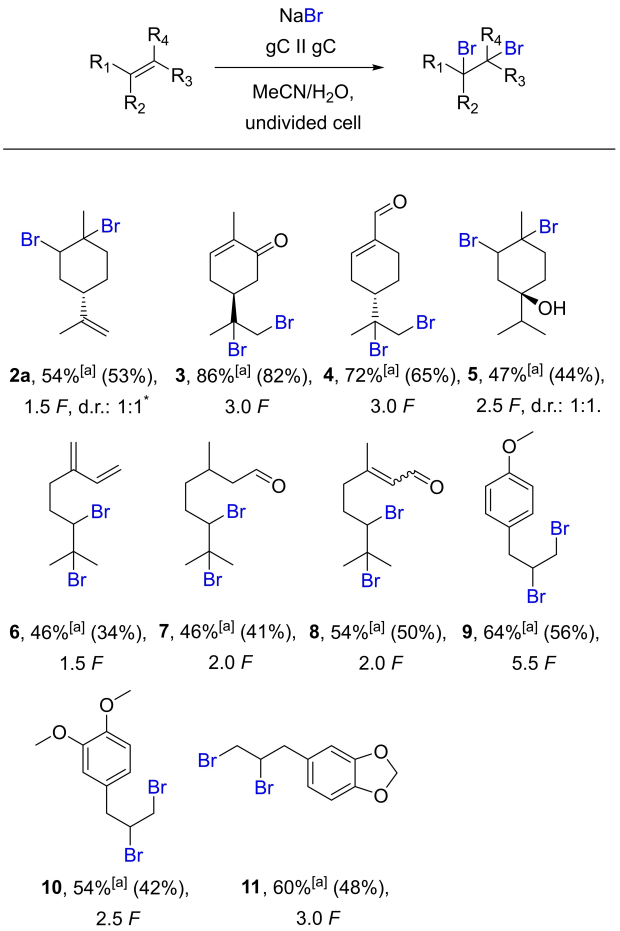

Scheme 2. Scope for the synthesis of dibrominated derivatives. Reaction conditions: Substrate (0.7 mmol), NaBr (2.1 mmol), MeCN/H_2O (5 mL, 8 v/v%), glassy carbon electrodes, undivided cell, constant current, $j = 5$ mA/cm^2, 1.5–5.5 *F*, 30 °C. [a] Yields determined by ^{1}H NMR (internal standard: CH_2Br_2). Isolated yields are in brackets. gC = glassy carbon. [*] Diastereomeric ratio was postulated from the crystallographic data and d.r. of **2b**.

laldehyde and 4-allylanisole showed great selectivity to give **4** and **9** with an isolated yield of 65% and 56% respectively. In the presence of an electron-withdrawing group the yields were generally higher. This could be attributed to the fact that electron-withdrawing groups in the vinylic position reduces the nucleophilicity of the given alkene and it is less susceptible to side reactions. The effect was also observed, that in the case of such terpenes and terpenoids (e.g. carvone and perillaldehyde) bromination was observed on the terminal alkene which is less nucleophilic by electronic means. The method proved to be applicable for a wide range of natural terpenes and terpenoids including various functional groups such as ketones, aldehydes and alcohols with good to high yields and great selectivity.

Subsequently, the scalability of the reaction was studied. To demonstrate, the synthesis of **3** was scaled up from 0.7 mmol to 3.5 mmol (5-fold scale-up) in a 25 mL PTFE undivided cell (Figure 1). However, the reaction showed a slightly decreased yield of 72%.

By adjusting the reaction parameters and the cell geometry, the reaction selectivity could be inversed to favor the formation

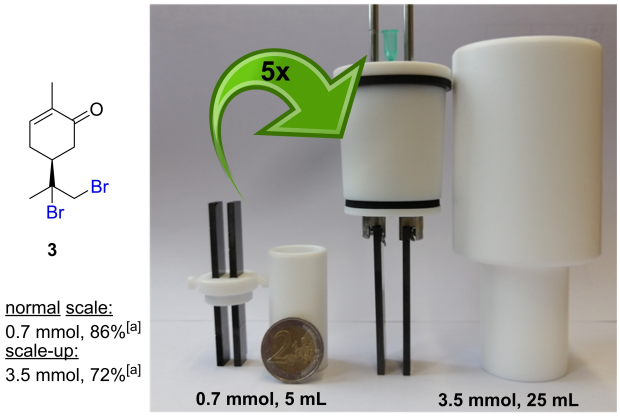

Figure 1. Scale-up reaction. Comparison between screening cell and scale-up cell. A two-euro coin is included for size comparison. [a] ^{1}H NMR yields (internal standard: CH_2Br_2).

of **2b**. As carbon-halogen bonds are prone to cathodic lability, a PTFE divided cell with glass frit membrane was employed.[54] Via applying an increased amount of charge, **2b** were obtained with an isolated yield of 74%. Upon crystallization of **2b** only crystals from (1*R*,2*R*,4*S*,8*S*)-diastereomer were obtained (Scheme 3) (see Supporting Information).

To exhibit the utility of our procedure over the conventionally available methods, dibromination of (4*S*)-(−)-limonene was carried out in the presence of elemental bromine and via a DMSO/HBr system (Table 2).[55,56] In both cases, the desired products were obtained in diminished yields. In terms of the DMSO/HBr system, **2a** was obtained in 39% yield, however, the selectivity of the reaction was dramatically decreased (See SI for more information). The high selectivity of the electrochemical bromination method could be attributed to the slower and controlled in-situ generation of bromine during the electrolysis.

The reaction mechanism was postulated according to Scheme 4. Cyclic voltammetry studies revealed that the generation of bromine is a 2-electron-oxidation process in which bromide anions undergo oxidation to form bromine that are in equilibria with the relatively stable tribromide species. The second oxidation is accounted to the oxidation of these

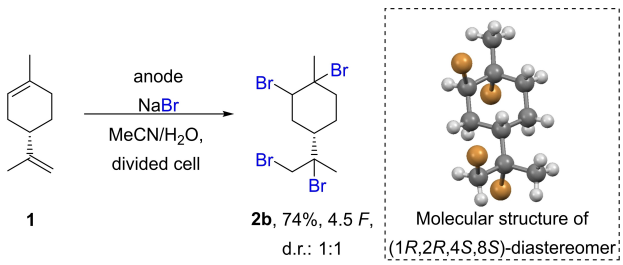

Scheme 3. Electrochemical tetrabromination of **1**. Reaction conditions: Anodic compartment: **1** (0.7 mmol), NaBr (2.1 mmol), MeCN/H_2O (5 mL, 8 v/v %). Cathodic compartment: NaBr (2.1 mmol), MeCN/H_2O (5 mL, 8 v/v%), glass frit membrane, glassy carbon electrodes, divided cell, constant current, $j = 5$ mA/cm^2, 4.5 *F*, 30 °C. Isolated yield. Molecular structure of (1*R*,2*R*,4*S*,8*S*)-diastereomer of **2b** was obtained by crystallographic X-ray analysis.

Research Article
doi.org/10.1002/ejoc.202200857

Table 2. Control experiments of the dibromination of (4*S*)-(−)-limonene.

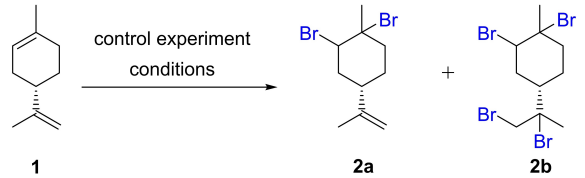

1		2a	2b
Conditions[a]		2a [%][b]	2b [%][b]
a) Br_2[55]		22	13
b) DMSO/HBr[56]		39	10
c) Electrochemical method		54	0

[a] Control experiments. Reaction conditions: a) Terpene (0.7 mmol), Br_2 (99.6%, 0.7 mmol), DCM (2.0 mL), 0 °C, 30 minutes. b) Terpene (0.7 mmol), DMSO (0.8 mmol), HBr (48 w/w% aq., 1.6 mmol), EtOAc (2.8 mL), 60 °C, 30 minutes. c) terpene (0.7 mmol), NaBr (2.1 mmol), MeCN/H_2O (5 mL, 8 v/v %), glassy carbon electrodes, undivided cell, constant current, $j = 5$ mA/cm^2, 1.5–5.5 *F*, 30 °C. [b] Yield determined by ^{1}H NMR (internal standard: CH_2Br_2).

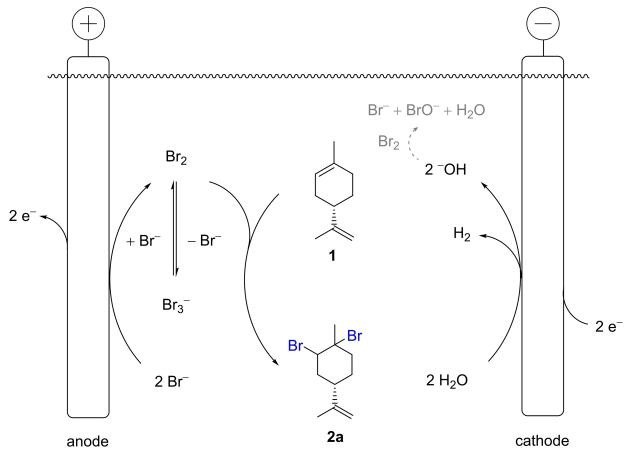

Scheme 4. Postulated reaction mechanism for the electrochemical bromination of **1**.

tribromide species to bromine, which was in accordance with previous reports.[57–60] The electrochemical bromination is assumed to occur via the formation of the reactive bromonium ion intermediates which then undergo nucleophilic ring opening by the free bromide anions resulting in the desired products. The reaction is complemented by the cathodic reduction of water to generate hydrogen gas. This was further supported by the visual observation of gas evolution at the cathode as well as an increase of the pH value from 6 to 14 in the cathodic chamber of divided cells. In undivided cells the pH value remained constant, suggesting the formation of hypobromite.[61]

To exhibit the multipurpose application of 1,2-vicinal dibromides as intermediates, **2a** was subjected to the well-known Kolbe nitrile method (Scheme 5).[62] Nitrile groups are vital building blocks in organic synthesis due to their ability to be converted into multiple functional groups. Via a nucleophilic substitution and a subsequent elimination in one-pot, the α,β-unsaturated nitrile derivative **12** could be synthesized for the first time with an isolated yield of 49%.

Scheme 5. Functionalization of **2a**. Conditions: **2a** (1.0 mmol), NaCN (4.0 mmol), dimethylsulfoxide (DMSO), argon atmosphere, 60 °C, isolated yield.

Conclusion

To conclude, a safe, selective, and sustainable electrochemical bromination protocol of terpenes was established. The highlights of this approach are the utilization of NaBr that serves both as a reagent and supporting electrolyte, the use of inexpensive electricity as "green" oxidant as well as the application of sustainable carbon electrodes. This method facilitates the selective functionalization of both mono- and polyunsaturated molecules demonstrated in 10 examples with yields up to 82%. The electrochemical bromination of structurally delicate compounds has been proven to be superior towards the already existing methods. Scalability as well as further functionalization has been demonstrated.

Experimental Section

General procedure for the reactions in 5 mL undivided PTFE cells

A solution of sodium bromide (2.1 mmol) in 5.0 mL of solvent mixture constructed of acetonitrile (4.6 mL) and deionized water (0.4 mL, 8 v/v%) was transferred into an undivided 5 mL PTFE cell and warmed to 30 °C. Once the electrolysis temperature was reached, terpene (0.7 mmol) was added via a 100 µL Hamilton syringe and electrolyzed at glassy carbon electrodes with a current density of 5 mA/cm^2 at 30 °C. After applying 1.5–5.5 *F*, the reaction solution was extracted with 15 mL ethyl acetate and 15 mL deionized water. After phase separation, the organic layer was washed two times with deionized water (15 mL), with brine, dried over magnesium sulfate and concentrated under vacuo. The product was quantified via ^{1}H NMR using CH_2Br_2 as internal standard. In most cases, the crude product was spectroscopically pure.

General procedure for the reactions in 5 mL divided PTFE cells

A solution of sodium bromide (2.1 mmol) in 5 mL of solvent mixture constructed of acetonitrile (4.6 mL) and deionized water (0.4 mL, 8 v/v%) was transferred into the anodic compartment of PTFE cell. The same step was repeated for the cathodic compartment. The cell is warmed to 30 °C. Once the electrolysis temperature was reached, **terpene** (0.7 mmol) was added to the anodic compartment via a 100 µL Hamilton syringe and electrolyzed at glassy carbon electrodes. A constant current electrolysis with a current density of 5 mA/cm^2 was performed at 30 °C. After applying 4.5 *F*, the reaction solution was extracted with 15 mL ethyl acetate and

15 mL deionized water. After phase separation, the organic layer was washed two times with deionized water (15 mL), with brine, dried over magnesium sulfate and concentrated under vacuo to give the spectroscopically pure product.

General procedure for the reaction in 25 mL divided PTFE cell

A solution of sodium bromide (10.5 mmol) in 25 mL solvent mixture constructed of acetonitrile (23.0 mL) and deionized water (2.0 mL, 8 v/v%) was transferred into an undivided 25.0 mL PTFE cell warmed to 30 °C. Once the electrolysis temperature was reached, terpene (3.5 mmol) was added via a 500 µL Hamilton syringe and electrolyzed at glassy carbon electrodes. A constant current electrolysis with a current density of 5 mA/cm^2 was performed at 30 °C. After applying 3.0 *F*, the reaction solution was extracted with 80 mL ethyl acetate and 80 mL deionized water. After phase separation, the organic layer was washed two times with deionized water (80 mL), with brine, dried over magnesium sulfate and concentrated under vacuo. The product was quantified by ^{1}H NMR using CH_2Br_2 as internal standard.

Acknowledgements

Support from the Forschungsinitiative des Landes Rheinland-Pfalz in frame of SusInnoScience is highly appreciated. L.G. thanks Nicole Ehler and Christopher Kampf for analytical support. Carlos A. Martínez-Huitle acknowledges the funding provided by the Alexander von Humboldt Foundation (Germany) and CAPES (Brazil) as a Humboldt fellowship for Experienced Researcher (88881.136108/2017-01) at the Johannes Gutenberg-Universität Mainz, Germany. Open Access funding enabled and organized by Projekt DEAL.

Conflict of Interest

The authors declare no conflict of interest.

Data Availability Statement

The data that support the findings of this study are available in the supplementary material of this article.

Keywords: Alkenes · Bromine · Electrochemistry · Halogenation · Renewable resources

[1] T. Kim, B. Song, K. S. Cho, I. Lee, *Int. J. Mol. Sci.* **2020**, *21*, 2187–2218.
[2] M. E. G. Mosquera, G. Jiménez, V. Tabernero, J. Vinueza-Vaca, C. García-Estrada, K. Kosalková, A. Sola-Landa, B. Monje, C. Acosta, R. Alonso, M. Á. Valera, *Sustain. Chem.* **2021**, *2*, 467–492.
[3] Y. Yamada, T. Kuzuyama, M. Komatsu, K. Shin-Ya, S. Omura, D. E. Cane, H. Ikeda, *Proc. Natl. Acad. Sci. USA* **2015**, *112*, 857–862.
[4] E. J. N. Helfrich, G. Lin, C. A. Voigt, J. Clardy, *Beilstein J. Org. Chem.* **2019**, *15*, 2889–2906.
[5] S. Zwenger, C. Basu, *Biotechnol. Mol. Biol. Rev.* **2008**, *3*, 1–7.
[6] E. Pinto, C. Pina-Vaz, L. Salgueiro, M. J. Gonçalves, S. Costa-de-Oliveira, C. Cavaleiro, A. Palmeira, A. Rodrigues, J. Martinez-de-Oliveira, *J. Med. Microbiol.* **2006**, *55*, 1367–1373.
[7] K. Knobloch, A. Pauli, B. Iberl, H. Weigand, N. Weis, *J. Essent. Oil Res.* **1989**, *1*, 119–128.
[8] R. Paduch, M. Kandefer-Szerszeń, M. Trytek, J. Fiedurek, *Arch. Immunol. Ther. Exp.* **2007**, *55*, 315–327.
[9] A. C. Guimarães, L. M. Meireles, M. F. Lemos, M. C. C. Guimarães, D. C. Endringer, M. Fronza, R. Scherer, *Molecules* **2019**, *24*, 2471–2483.
[10] S. M. Kupchan, M. A. Eakin, A. M. Thomas, *J. Med. Chem.* **1971**, *14*, 1147–1152.
[11] J. S. Raut, S. M. Karuppayil, *Ind. Crops Prod.* **2014**, *62*, 250–264.
[12] S. N. Fedorov, L. K. Shubina, A. M. Bode, V. A. Stonik, Z. Dong, *Cancer Res.* **2007**, *67*, 5914–5920.
[13] A. Corma, S. Iborra, A. Velty, *Chem. Rev.* **2007**, *107*, 2411–2502.
[14] F. R. Marín, C. Soler-Rivas, O. Benavente-García, J. Castillo, J. A. Pérez-Alvarez, *Food Chem.* **2007**, *100*, 736–741.
[15] E. Jongedijk, K. Cankar, M. Buchhaupt, J. Schrader, H. Bouwmeester, J. Beekwilder, *Appl. Microbiol. Biotechnol.* **2016**, *100*, 2927–2938.
[16] B. M. Lange, *Advances in Biochemical Engineering/Biotechnology: Biosynthesis and Biotechnology of High-Value p-Menthane Monoterpenes, Including Menthol, Carvone and Limonene*, Springer Cham., **2015**, Vol. 148.
[17] A. Llevot, P. Dannecker, M. von Czapiewski, L. C. Over, Z. Söyler, M. A. R. Meier, *Chem. Eur. J.* **2016**, *22*, 11510–11521.
[18] Y. Zhu, C. Romain, C. K. Williams, *Nature* **2016**, *540*, 354–362.
[19] B. M. Stadler, C. Wulf, T. Werner, S. Tin, J. G. de Vries, *ACS Catal.* **2019**, *9*, 8012–8067.
[20] M. Winnacker, B. Rieger, *ChemSusChem* **2015**, *8*, 2455–2471.
[21] F. D. Monica, A. W. Kleij, *Polym. Chem.* **2020**, *11*, 5109–5127.
[22] F. Parrino, A. Fidalgo, L. Palmisano, L. M. Ilharco, M. Pagliaro, R. Ciriminna, *ACS Omega* **2018**, *3*, 4884–4890.
[23] W. Schwab, C. Fuchs, F. Huang, *Eur. J. Lipid Sci. Technol.* **2013**, *115*, 3–8.
[24] K. A. D. Swift, *Top. Catal.* **2004**, *27*, 143–155.
[25] D. Yoffe, R. Frim, S. D. Ukeles, M. J. Dagani, H. J. Barda, T. J. Benya, D. C. Sanders, *Ullmann's Encyclopedia of Industrial Chemistry: Bromine Compounds*, Wiley-VCH, Weinheim, Germany, **2013**.
[26] G. Bellucci, R. Bianchini, S. Vecchiani, *J. Org. Chem.* **1986**, *51*, 4224–4232.
[27] R. M. Carman, B. N. Venzke, *Aust. J. Chem.* **1973**, *26*, 2235–2256.
[28] P. R. R. Costa, J. A. Rabi, *Tetrahedron Lett.* **1975**, *51*, 4535–4538.
[29] S. Lochyński, B. Jarosz, M. Walkowicz, K. Piątrowski, *J. Prakt. Chem.* **1988**, *2*, 284–288.
[30] T. Ying, W. Bao, Y. Zhang, *J. Chem. Res.* **2004**, *12*, 806–807.
[31] R. R. Tang, N. H. Gong, *B. Korean Chem. Soc.* **2009**, *30*, 1832–1834.
[32] U. Husstedt, H. J. Schäfer, *Synthesis* **1979**, *12*, 966–968.
[33] R. Mestres, J. Palenzuela, *Green Chem.* **2002**, *4*, 314–316.
[34] D. G. Vassão, D. R. Gang, T. Koeduka, B. Jackson, E. Pichersky, L. B. Davina, N. G. Lewis, *Org. Biomol. Chem.* **2006**, *4*, 2733–2744.
[35] M. Zhu, S. Lin, G. Zhao, J. Sun, A. Córdova, *Tetrahedron Lett.* **2010**, *51*, 2708–2712.
[36] L. Peilleron, T. D. Grayfer, J. Dubois, R. H. Dodd, K. Cariou, *Beilstein J. Org. Chem.* **2018**, *14*, 1103–1111.
[37] M. D. Kärkäs, *Chem. Soc. Rev.* **2018**, *47*, 5786–5865.
[38] S. R. Waldvogel, B. Janza, *Angew. Chem. Int. Ed.* **2014**, *53*, 7122–7123.
[39] S. R. Waldvogel, S. Lips, M. Selt, B. Riehl, C. J. Kampf, *Chem. Rev.* **2018**, *118*, 6706–6765.
[40] D. Pollok, S. R. Waldvogel, *Chem. Sci.* **2020**, *11*, 12386–12400.
[41] S. B. Beil, D. Pollok, S. R. Waldvogel, *Angew. Chem. Int. Ed.* **2021**, *60*, 14750–14759.
[42] A. Wiebe, T. Gieshoff, S. Möhle, E. Rodrigo, M. Zirbes, S. R. Waldvogel, *Angew. Chem. Int. Ed.* **2018**, *57*, 5594–5619.
[43] S. Möhle, M. Zirbes, E. Rodrigo, T. Gieshoff, A. Wiebe, S. R. Waldvogel, *Angew. Chem. Int. Ed.* **2018**, *57*, 6018–6041.
[44] K. Kulangiappar, M. Ramaprakash, D. Vasudevan, T. Raju, *Synth. Commun.* **2015**, *46*, 145–153.
[45] Y. Yuan, A. Yao, Y. Zheng, M. Gao, Z. Zhou, J. Qiao, J. Hu, B. Ye, J. Zhao, H. Wen, A. Lei, *iScience* **2019**, *12*, 293–303.
[46] J. Strehl, M. L. Abraham, G. Hilt, *Angew. Chem. Int. Ed.* **2021**, *60*, 9996–10000.
[47] J. Steitz, T. Wirth, *Org. Biomol. Chem.* **2021**, *19*, 6892–6896.
[48] J. C. Siu, N. Fu, S. Lin, *Acc. Chem. Res.* **2020**, *53*, 547–560.
[49] X. Dong, J. L. Röckl, S. R. Waldvogel, B. Morandi, *Science* **2021**, *371*, 507–514.
[50] S. S. Milisavljević, K. Wurst, G. Laus, M. D. Vukićević, R. D. Vukićević, *Steroids* **2005**, *70*, 867–872.
[51] J. H. Clark, *Green Chem.* **1998**, *1*, 1–8.
[52] P. Anastas, N. Eghbali, *Chem. Soc. Rev.* **2010**, *39*, 301–312.

[53] A. Frontana-Ulribe, R. D. Little, J. G. Ibanez, A. Palma, R. Vasquez-Medrano, *Green Chem.* **2010**, *12*, 2099–2119.
[54] C. Gütz, M. Selt, M. Bäzinger, C. Bucher, C. Römelt, N. Hecken, F. Gallou, T. R. Galvão, S. R. Waldvogel, *Chem. Eur. J.* **2015**, *21*, 13878–13882.
[55] G. S. Buchanan, K. P. Cole, G. Li, Y. Tang, L. You, R. P. Hsung, *Tetrahedron* **2011**, *67*, 10105–10118.
[56] S. Song, X. Li, X. Sun, Y. Yuan, N. Jiao, *Green Chem.* **2015**, *17*, 3285–3289.
[57] M. Tariq, *Z. Phys. Chem.* **2019**, *234*, 295–312.
[58] D. Halász, Cs. Visy, A. Szűcs, M. Novák, *React. Kinet. Catal. Lett.* **1992**, *48*, 177–188.
[59] V. Vojinovic, S. Mentus, V. Komnenic, *J. Electroanal. Chem.* **2003**, *547*, 109–113.
[60] J. G. Bell, J. Wang, *J. Electroanal. Chem.* **2015**, *754*, 133–137.
[61] B. N. Grgur, *J. Electrochem. Soc.* **2019**, *166*, E50–E61.
[62] E. Dinca, P. Hartmann, J. Smrćek, I. Dix, P. G. Jones, U. Jahn, *Eur. J. Org. Chem.* **2012**, *24*, 4461–4482.

Manuscript received: July 15, 2022
Revised manuscript received: August 12, 2022
Accepted manuscript online: August 12, 2022

European Journal of Organic Chemistry

Supporting Information

Selective Electrochemical Dibromination of Terpenes and Naturally Derived Olefins

Lilla G. Gombos, Leo Werner, Dieter Schollmeyer, Carlos A. Martínez-Huitle, and Siegfried R. Waldvogel*

Table of contents

1. General information

All reagents were used in analytical grades. Solvents were purified by standard methods.[1] Electrochemical reactions were perfomed at isostatic graphite, glassy carbon or boron-doped diamond (BDD) electrodes. Highly isostatic graphite electrodes, Sigrafine™ V2100 were obtained from SGL Carbon, Bonn, Germany. Glassy carbon electrodes, SIGRADUR® G, were obtained from HTW Hochtemperatur Werkstoffe GmbH, Thierhaupten, Germany. BDD electrodes, DIACHEM®, 15 µm boron-doped diamond layer on 3 mm silicon support/wafer were purchased from CONDIAS GmbH, Itzehoe, Germany. The electrolysis was carried out with a two-electrode set-up under galvanostatic conditions. ^{1}H and ^{13}C NMR spectra were recorded at 25 °C, using a Bruker Avance III HD 400 (400 MHz, Analytische Messtechnik, Karlsruhe, Germany). Chemical shifts (δ) are reported in parts per million (ppm) relative to traces of non-deuterated solvent in the corresponding deuterated solvent. Dibromomethane served as internal standard for ^{1}H NMR (δ = 4.947 ppm).[2] Gas chromatography was performed on a Shimadzu GC-2025 (Shimadzu, Japan) using a HP-5 column (Agilent Technologies, Santa Clara, California; length: 30 m, inner diameter: 0.25 mm, film: 0.25 µm, carrier gas: hydrogen). GC-MS measurements were carried out on a Shimadzu GC-2010 (Shimadzu, Japan) using a HP-1 column (Agilent Technologies, Santa Clara, California; length: 30 m, inner diameter: 0.25 mm, film: 0.25 µm, carrier gas: helium). The chromatograph was coupled to a mass spectrometer Shimadzu GC-MS-QP2010. Column chromatography was performed on silica gel 60 M (0.040–0.063 mm, MachereyNagel GmbH & Co, Düren, Germany) using a mixture of cyclohexane and ethyl acetate as eluent. Silica gel 60 sheets on aluminium (F254, Merck KGaA, Darmstadt, Germany) were used for thin layer chromatography. High performance liquid chromatography (HPLC) was performed on a Shimadzu HPLC–MS system using an autosampler SIL-20AHT, a column oven CTO-20AC, two pump modules LC-20AD for adjusting the solvent mixtures, a diode array detector SPD-M20A, a communication BUS module CBM-20A, and an Eurospher II 100-5 C18 column 150 x 4 mm (Knauer, Berlin, Germany). Mass spectra and high-resolution mass spectra were obtained by using a QTof Ultima 3 (Waters, Milford, Massachusetts) apparatus employing ESI± and APCI±. In some cases, $AgNO_3$ was added to the analyte solution for better ionization of the compounds. X-ray analysis data were collected on a STOE IPDS-2T diffractometer (STOE & Cie GmbH, Darmstadt, Germany) using graphite monochromated Mo-Kα radiation (λ= 0.71073 Å). Intensities were measured using fine-slicing ω and corrected for background, polarization and Lorentz effects. The structures were solved by direct methods and refined anisotropically by the least-squares procedure implemented in the SHELX program system. The supplementary crystallographic data for this paper can be obtained free of charge from the Cambridge Crystallographic Data Center via www.ccdc.cam.ac.uk/data_request/cif. Deposition numbers and further details are given with the individual characterization data.

Infrared spectra were recorded on an ATR IR device of the type ALPHA from Bruker. Cyclic voltammetry was conducted on an Autolab PGSTAT101 from Metrohm AG, Herisau, Switzerland.

For all unknown compounds and compounds with predicted spectra ^{1}H and ^{13}C NMR, HRMS and IR analytical data were provided.

2. Experimental considerations

Due to the volatile nature of the starting material (4*S*)-(–)-limonene **1**, quantification after electrolysis is limited. For reliable quantitative measurements, a combination of external standard calibration method with regards to the starting material and NMR quantification method with regards to the products were carried out.

2.1. External standard calibration

5.0 mL solutions of (4*S*)-(–)-limonene in acetonitrile/deionized water (8 v/v%) with known concentrations (5.2 mmol/cm^3; 8.7 mmol/cm^3; 19.2 mmol/cm^3; 50.6 mmol/cm^3, 68.1 mmol/cm^3) were prepared in 25.0 mL round-bottom flasks. Three samples of 1.5 mL were prepared of each solution in GC vials via taking an aliquant of 50 µL from the round-bottom flasks and filtered via approx. 245 mg silica gel 60M, using ethyl acetate as eluent. The resulting 15 samples were analyzed via GC and the response was plotted in the diagram giving the straight-line equation (Equation 1) below:

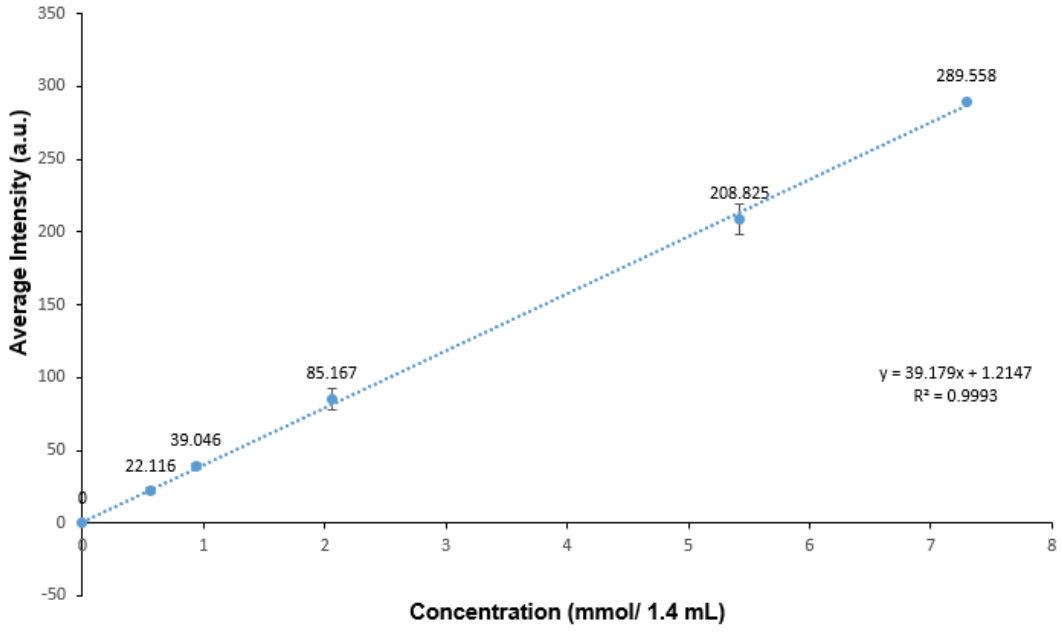

Figure 1. External standard calibration of the starting material **1**.

$$y = b_0 + b_1 c \qquad \textbf{(1)}$$

The straight-line equation (Equation 1) is used to calculate the analysis function (Equation 2), that is used to determine the concentration of an unknown sample, hence conversion of **1** can be determined.

$$c = \frac{y - b_0}{b_1} \qquad \textbf{(2)}$$

3. Electrochemical set-up and synthesis protocols

3.1. Experimental set-up for the synthesis of brominated terpene derivatives in undivided cells

The electrochemical reactions were conducted in undivided PTFE (polytetrafluoroethylene) 5.0 mL cells are homemade by the university's own mechanical workshop and detailed information of their set-up have already been described.[3] However, the complete setup with screening blocks is also available commercially as IKA Screening System (8 cells), IKA-Werke GmbH & Co. KG, Staufen, Germany. It is operated with isostatic graphite, glassy carbon or BDD electrodes (dimensions of both type of electrodes: 0.3 x 1.0 x 7.0 cm).

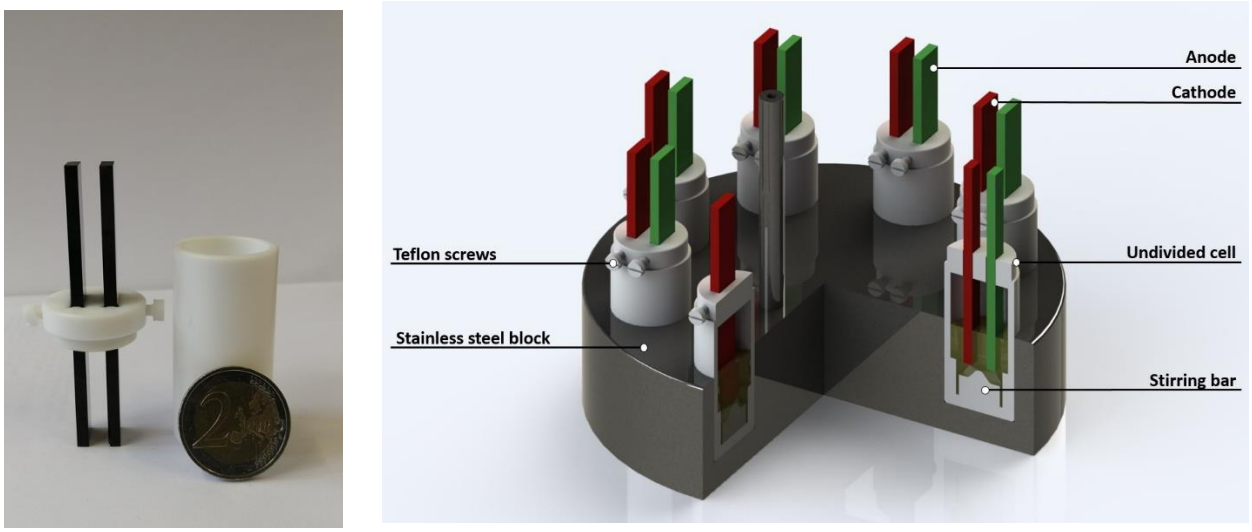

Figure 2. 5 mL undivided screening cell (left) and schematic visualization of 5 mL screening cells with screening block (right). A two-euro coin is included for size comparison.

3.2. Experimental set-up for the synthesis of brominated terpene derivatives in divided cells:

The electrochemical bromination was also conducted in PTFE divided cells according to Figure 2. A porous glass frit (type: P4) served as a membrane between the cathodic and anodic compartment, sealed by an EPDM ring. The complete setup with screening blocks can be obtained commercially as IKA Screening System package (6 cells), IKA-Werke GmbH & Co. KG, Staufen, Germany. It is operated with isostatic graphite and glassy carbon electrodes (dimensions of both type of electrodes: 0.3 x 1.0 x 7.0 cm).

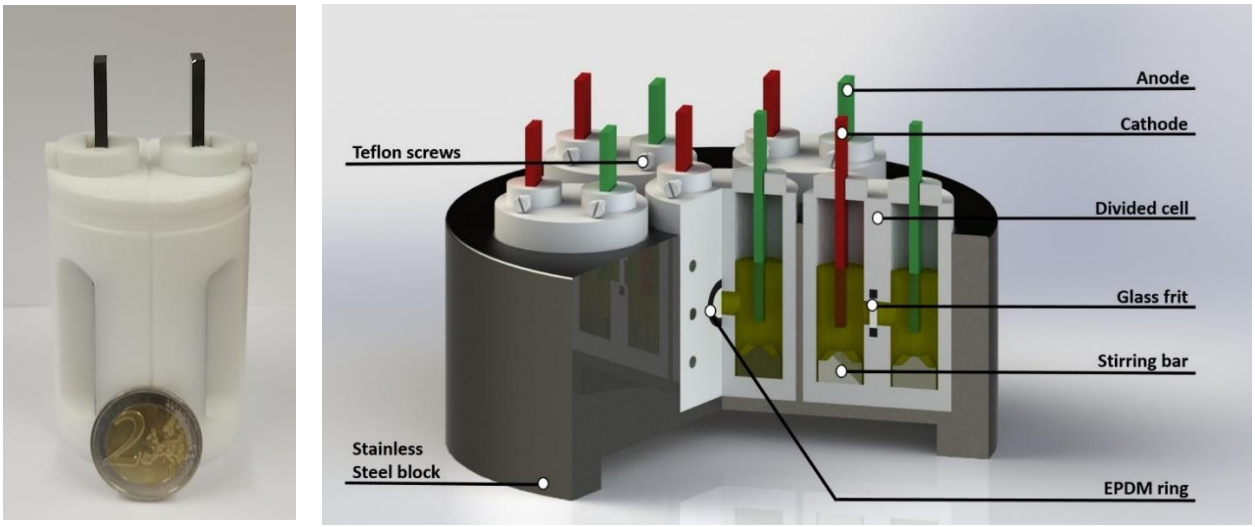

Figure 3. 5 mL divided screening cell (left) and schematic visualization of the PTFE divided cells with screening block (right). A two-euro coin is included for size comparison.

3.3. Experimental set-up for a 5-fold scale-up reaction

The scale-up reaction was conducted in a PTFE undivided beaker-type cell according to Figure 4. The cell (25.0 mL) consists of a PTFE beaker and is closed by a PTFE plug. This cap allows precise arrangement of the electrodes in a distance of 10.0 mm. Dimensions of the glassy carbon electrodes used were 0.6 x 6.0 x 2.0 cm. The immersed part of the glassy carbon anode had a dimension of 0.6 x 4.2 x 2.0 cm. A current of 42 mA was applied, resulting in a geometrical current density of 5 mA/cm². Terminal voltage in 25 mL beaker-type cells typically was in the range of 4–5 V.

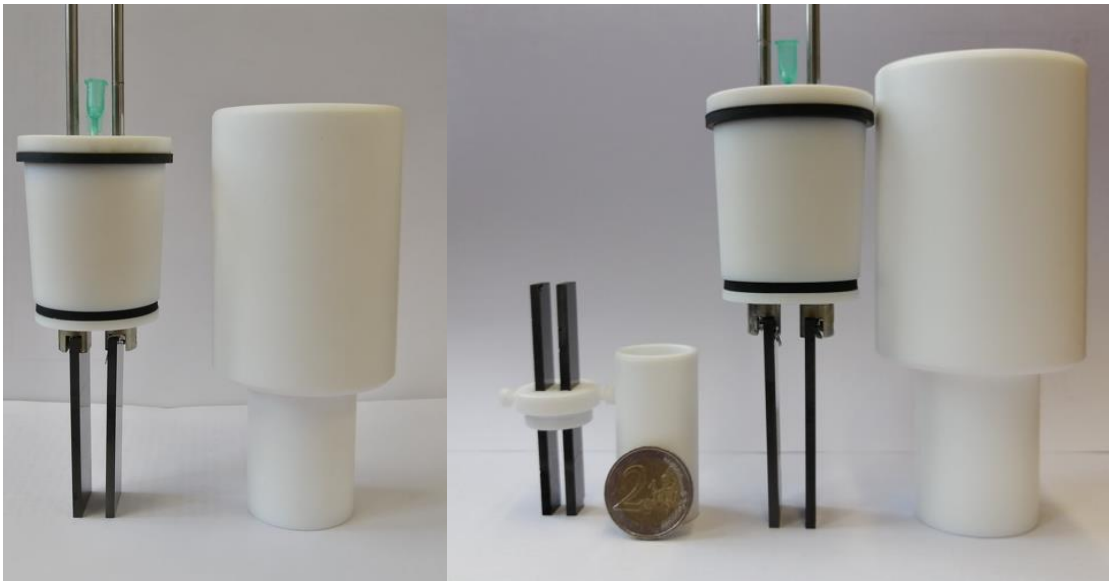

Figure 4. 25 mL PTFE beaker-type cell (left) and comparison of 5 mL undivided screening cell and 25 mL beaker-type cell (right).

3.4. General procedure for the optimization reactions in undivided screening cells (GP1)

A solution of **sodium bromide** (2.1 mmol) in 5.0 mL of solvent mixture constructed of acetonitrile (4.6 mL) and deionized water (0.4 mL, 8 v/v%) was transferred into an undivided 5 mL PTFE cell and warmed to 30 °C. Once the electrolysis temperature was reached, **terpene** (0.7 mmol) was added via a 100 µL Hamilton syringe and electrolyzed at isostatic graphite, glassy carbon or BDD electrodes. The immersed part of the electrodes had dimensions of 0.3 x 1.0 x 1.8 cm. A constant current electrolysis with current densities of 5–28 mA/cm^2 was performed at 30 °C. After applying 1.5–5.5 *F*, an aliquant of approx. 50 µL was taken from the reaction solution and filtered via approx. 245 mg silica gel 60M, whereby 1.5 mL ethyl acetate was used as eluent. The filtrate was examined via GC and GC–MS analysis. The reaction solution was then transferred into a 100 mL separatory funnel followed by the addition of 15.0 mL ethyl acetate and 15.0 mL deionized water. After phase separation, the organic layer was further washed two times with deionized water (15.0 mL). The organic layer was washed with brine, dried over magnesium sulfate and concentrated under *vacuo*. The product was quantified *via* ^{1}H NMR using CH_2Br_2 as internal standard. In most cases, the crude product was spectroscopically pure.

3.5. General procedure for the optimization reactions in divided screening cells (GP2)

A solution of **sodium bromide** (2.1 mmol) in 5 mL of solvent mixture constructed of acetonitrile (4.6 mL) and deionized water (0.4 mL, 8 v/v%) was transferred into the anodic compartment of PTFE cell. The same step was repeated for the cathodic compartment. The cell is warmed to 30 °C. Once the electrolysis temperature was reached, **terpene** (0.7 mmol) was added to the anodic compartment via a 100 µL Hamilton syringe and electrolyzed at glassy carbon electrodes. A constant current electrolysis with a current density of 5 mA/cm^2 was performed at 30 °C. After applying 4.5 *F*, an aliquant of approx. 50 µL was taken from the reaction solution and filtered via approx. 245 mg silica gel 60M, whereby 1.5 mL ethyl acetate was used as eluent. The filtrate was examined via GC and GC-MS analysis. The reaction solution was then transferred into a 100 mL separatory funnel followed by the addition of 15 mL ethyl acetate and 15 mL deionized water. After phase separation, the organic layer was further washed two times with deionized water (15.0 mL). The organic layer was washed with brine, dried over magnesium sulfate and concentrated under *vacuo*.

3.6. General procedure for a 5-fold scale-up reaction (GP3)

A solution of sodium bromide (10.5 mmol) in 25.0 mL solvent mixture constructed of acetonitrile (23.0 mL) and deionized water (2.0 mL, 8 v/v%) was transferred into an undivided 25.0 mL PTFE cell warmed to 30 °C. Once the electrolysis temperature was reached, **terpene** (3.5 mmol) was added via a 500 µL Hamilton syringe and electrolyzed at glassy carbon electrodes. A constant current electrolysis with a current density of 5 mA/cm^2 was performed

at 30 °C. After applying 3.0 *F*, an aliquant of approx. 50 µL was taken from the reaction solution and filtered via approx. 245 mg silica gel 60M, whereby 1.5 mL ethyl acetate was used as eluent. The filtrate was examined via GC and GC-MS analysis. The reaction solution was then transferred into a 250.0 mL separatory funnel followed by the addition of 80 mL ethyl acetate and 80 mL deionized water. After phase separation, the organic layer was washed two times with deionized water (80 mL). The organic layer was washed with brine, dried over magnesium sulfate and concentrated under *vacuo*. The product was quantified by ^{1}H NMR using CH_2Br_2 as internal standard.

3.7. Procedure for the conventional bromination of (4*S*)-(-)-limonene using Br_2

(4*S*)-(–)-limonene was subjected to dibromination method using elemental bromine.[4]

Bromine (99.6%, 0.7 mmol) was added dropwise to the continuously stirring solution of (4*S*)-(–)-limonene (0.7 mmol) and dichloromethane (2.0 mL) at 0 °C. The solution remained transparent. After 30 minutes, the solution was left to warm to room temperature and it was quenched with 2mM aqueous metabisulfate solution. The organic layer was washed with brine, drived over $MgSO_4$ and concentrated under vacuo. The product was quantified by ^{1}H NMR using CH_2Br_2 as internal standard.

3.8. Procedure for the conventional bromination of (4*S*)-(–)-limonene using DMSO/HBr

(4*S*)-(–)-limonene was subjected to dibromination method published by Jiao *et al*.[5]

HBr (aq. 48 w/w%, 1.6 mmol) was added to a continuously stirring solution of (4*S*)-(–)-limonene (0.7 mmol), DMSO (0.8 mmol) and ethyl acetate at 60 °C. The solution turned from transparent to bright orange. After 30 minutes, the solution was left to cool down to room temperature and it was concentrated under *vacuo*. The product was quantified by ^{1}H NMR using CH_2Br_2 as internal standard.

3.8. Important considerations

The solvation of metal bromide salt in the solvent system is crucial to the success of the reaction. After reaching reaction temperature, a waiting time of 30 minutes is highly recommended before the addition of terpene to the solution.

4. Cyclic voltammetry studies

Cyclic voltammetry (CV) studies were carried out in a 10 mL glass vial fitter with a glassy carbon disk working electrode (3 mm in diameter), an $Ag/AgCl^{+}$ reference electrode and a glassy carbon rod counter electrode. The solution of interest was purged with argon for 5 min before collection of data. The elucidation of the reaction mechanism was supported via cyclic voltammetry experiments. The red voltammogram postulates a quasi-reversible process. The first oxidation potential corresponds to the oxidation of bromide to bromine (Equation 3). The excess of bromide concentration facilitates the formation of stable tribromide complexes which is in equilibria with the electrochemically generated bromine (Equation 4). The second oxidation potential corresponds to the oxidation of tribromide complexes to bromine, which is in accordance with literature.[6–9]

$$2\ Br^{-} \longrightarrow Br_2 + 2\ e^{-} \quad \textbf{(3)}$$

$$Br_2 + Br^{-} \rightleftharpoons Br_3^{-} \quad \textbf{(4)}$$

$$Br_3^{-} \longrightarrow 2\ Br_2 + 2\ e^{-} \quad \textbf{(5)}$$

In the presence of the substrate (blue voltammogram) the first oxidation potential is slightly shifted (from 0.49 V to 0.58 V) and the second oxidation potential is reduced indicating that the electrochemically generated bromine is reacting immediately with the olefin, reducing the formation of Br_3^{-}. The absence of reduction potential of the blue voltammogram also indicates that bromine is consumed by the olefin in the solution.

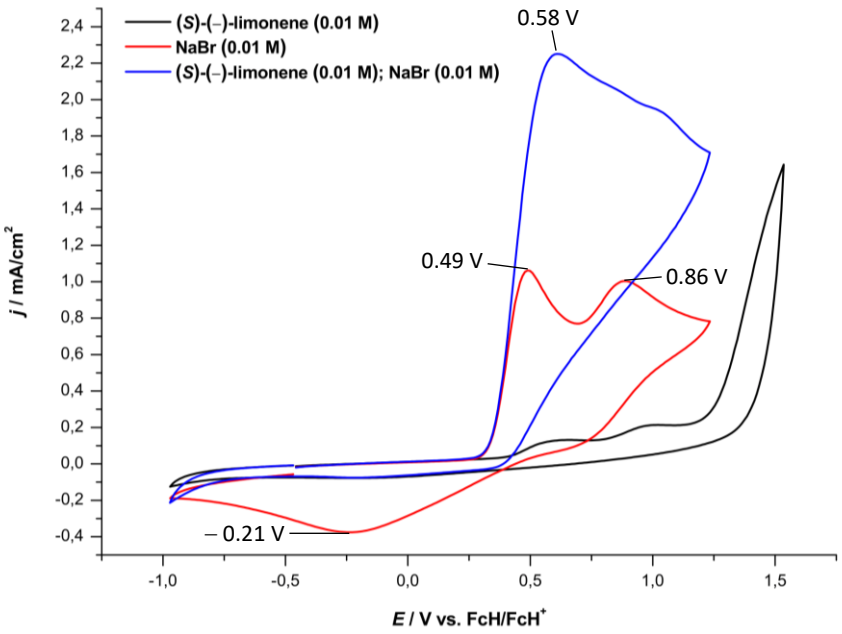

Figure 5. Cyclic voltammetry measurements.

5. Optimization of reaction conditions

The reaction conditions were subjected to One-Variation-At-Time (OVAT) approach (GP1) to maximize product formation and achieve high reaction selectivity. The bromide source, cell geometry, solvent system, electrode materials, current density (*j*), applied charge (*Q*), bromide concentration and reaction temperature were screened.

5.1. Optimization of bromide source

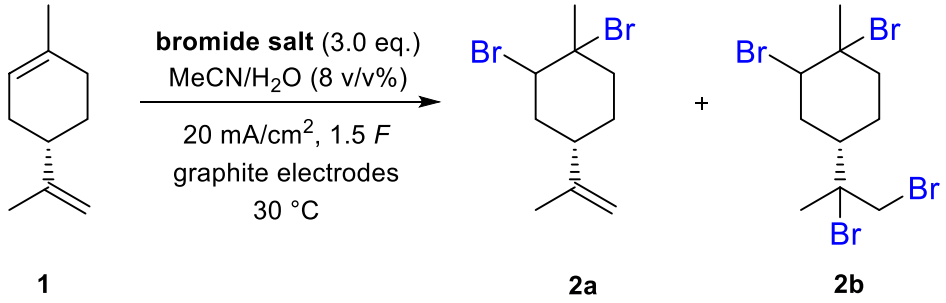

Scheme 1. Optimization of reaction conditions by varying bromide salts.

To determine the composition of the electrolyte, different types of bromide salts were tested with both organic- and metal counterions (Table 1).

Table 1. Screening of different type of bromide salts for the electrochemical bromination of (4*S*)-(–)-limonene **1**.

Entry	Bromide salt	Yield 2a[a] (%)	Yield 2b[a] (%)	Conversion 1 (%)
1	NBu_4Br	0	0	47
2	NEt_4Br	2	0	64
3	NaBr	30	4	57
4	LiBr	32	6	83

[a] Yield determined via internal NMR standard (dibromomethane, CH_2Br_2). Conversion was determined via external GC calibration of **1**.

Highest yields were observed with the utilization of metal bromide salts. While LiBr provided the highest NMR yield of 32% of product **2a** (Entry 4), excessive cathode amortization was observed. Therefore, further optimization reactions were concentrated on the employment of NaBr as bromide source.

5.2. Screening of cell geometry

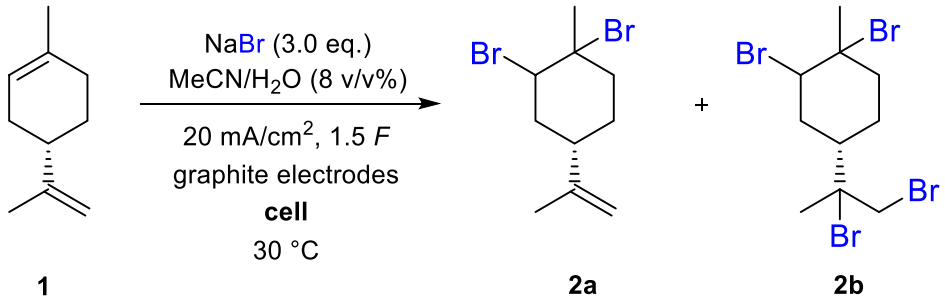

Scheme 2. Comparison of cell geometry.

To investigate the effect of cell geometry on the yield of **2a**, the reaction was carried out in a screening divided cell separated by a glass frit membrane. While in the formation of the desired product was no significant difference, the polybrominated derivative **2b** was increased to 8% under these conditions.

Table 2. Screening of cell geometry.

Entry	Cell geometry	Yield 2a[a] (%)	Yield 2b[a] (%)	Conversion 1 (%)
5	undivided	30	4	57
6	divided	32	8	-

[a] Yield determined via internal NMR standard (dibromomethane, CH_2Br_2), conversion was determined via external GC calibration of **1**.

5.3. Optimization of solvent system and additive ratio

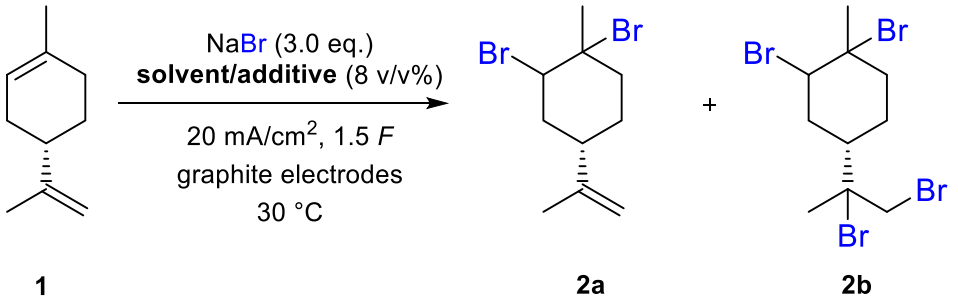

Scheme 3. Optimization of solvent systems in the presence of 8 v/v% additive

Initially, to determine the most suitable solvent system for the reaction, different set of solvents and additives (8 v/v%) were tested (Table 3).

Table 3. Screening of different solvents in the presence of 8 v/v% additive.

Entry	Solvent/Additive (8v/v%)	Yield 2a[a] (%)	Yield 2b[a] (%)	Conversion 1 (%)
7	MeCN/H_2O	30	4	57
8	acetone/H_2O	52	4	57
9	acetone/AcOH	0	0	42
10	HFIP/acetone	0	0	42
11	pyridine/H_2O	12	6	43

[a] Yield determined via internal NMR standard (dibromomethane, CH_2Br_2), conversion was determined via external GC calibration of **1**, AcOH = acetic acid, HFIP = 1,1,1,3,3,3-Hexafluoro-2-propanol.

The highest NMR yield was detected when acetone in the presence of 8 v/v% water was employed, which can be attributed to the good solubility of the terpene in the solvent. Therefore, further optimization was carried out parallel on the MeCN/H_2O (8 v/v%) and acetone/H_2O (8 v/v%) systems. It is worth to note, that when other additives were tested than water, product formation was not observed. Moreover, less than 8 v/v% water does not facilitate the solution of the salt in the reaction media. To understand the role of water, a higher additive ratio was tested in acetonitrile, acetone and pyridine solvents (Table 4).

Table 4: Screening of water content (20 v/v%) in different solvents.

Entry	Solvent/Additive (20 v/v%)	Yield 2a[a](%)	Yield 2b[a](%)	Conversion 1 (%)
12	MeCN/H_2O	9	0	63
13	acetone/H_2O	8	4	38
14	pyridine/H_2O	4	4	76

[a] Yield determined via internal NMR standard (dibromomethane, CH_2Br_2), conversion was determined via external GC calibration of **1**.

With an increased water content, the formation of the desired compound **2a** was capped at 9% (Entry 12) and reaction selectivity was lost resulting in a complex mixture of products. Therefore, the additive ratio was set to 8 v/v%.

5.4. Optimization of electrode materials

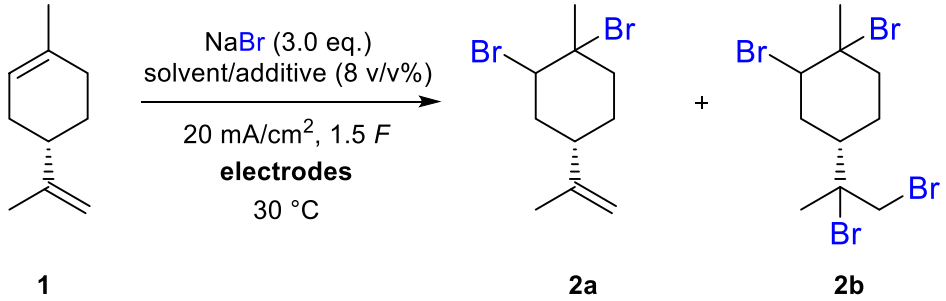

Scheme 4. Optimization of reaction conditions on different electrode materials.

The reaction conditions were tested with both glassy carbon and boron-doped diamond (BDD) electrodes.

Table 5. Screening of different electrode materials.

Entry	Solvent/ H_2O (8 v/v%)	Electrode	Yield 2a[a] (%)	Yield 2b[a] (%)	Conversion 1 (%)
15	MeCN/H_2O	gC II gC	46	5	59
16	MeCN/H_2O	BDD II BDD	32	0	69
17	acetone/H_2O	gC II gC	24	0	53
18	acetone/H_2O	BDD II BDD	30	0	59

[a] Yield determined via internal NMR standard (dibromomethane, CH_2Br_2), conversion was determined via external GC calibration of **1**, gC = glassy carbon, BDD = boron-doped diamond.

An increase of product formation **2a** was observed when glassy carbon was applied as electrode material in the presence of MeCN/H_2O (8 v/v%) as solvent system (Entry 15). In case

of acetone/H_2O system, graphite still remained superior compared to the other conditions. However, graphite electrodes showed a tendency towards cathodic amortization which affected reproducibility of the reactions.

5.5. Optimization of current density

In the next step different current densities were tested on both MeCN/H_2O (8 v/v%, system A) and acetone/H_2O (8 v/v%, system B) conditions. In both cases, a range of current density values between 5 and 28 mA/cm^2 were applied.

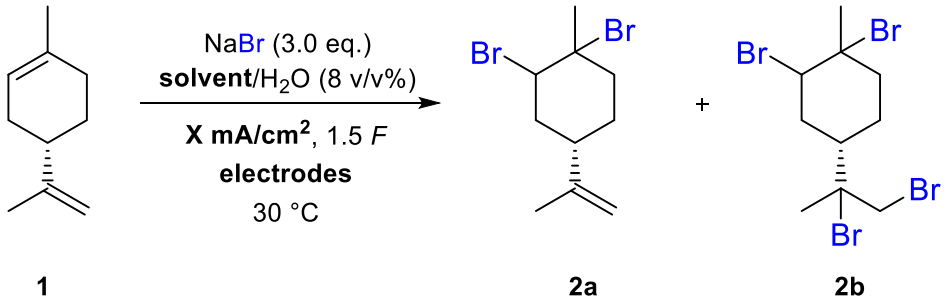

Scheme 5. Screening of different current densities.

Table 6. Application of different current density values.

Entry	System	*j* (mA/cm^2)	Yield 2a[a] (%)	Yield 2b[a] (%)	Conversion 1 (%)
19	A	5	54	0	74
20	A	10	24	0	87
21	A	28	25	0	85
22	B	5	34	0	74
23	B	10	22	0	60
24	B	28	20	0	53

[a] Yield determined via internal NMR standard (dibromomethane, CH_2Br_2), conversion was determined via external GC calibration of **1**, *j* = current density, A: MeCN/H_2O (8 v/v%), glassy carbon electrodes; B: Acetone/H_2O (8 v/v%), graphite electrodes.

The application of 5 mA/cm^2 increased the product formation of **2a** to 54% (Entry 19). At this point, acetonitrile/water system proved superior towards the acetone/water solvent system. Therefore, further investigations were continued on system A.

5.6. Optimization of the amount of applied charge

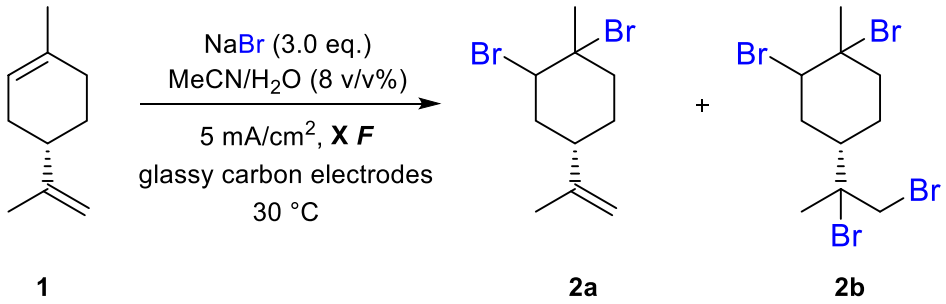

Scheme 6. Reaction conditions for the optimization of amount of charge.

The amount of applied charge referred to the substrate was varied. Due to the presence of starting material after electrolysis, higher charge quantities were applied from 0 *F* up to 3.0 *F* (referring **1**, Table 7). Without electricity, no formation of **2a** and **2b** was observed.

Table 7. Optimization of amount of applied charge (*Q*).

Entry	Solvent/Additive (8 v/v%)	*Q* (*F*)	Yield 2a[a] (%)	Yield 2b[a] (%)	Conversion 1(%)
25	MeCN/H_2O	2.2	44	4	83
26	MeCN/H_2O	3.0	35	8	98
27	MeCN/H_2O	0	0	0	2

[a] Yield determined via internal NMR standard dibromomethane, CH_2Br_2, conversion was determined via external GC calibration of **1**.

With increasing charge quantity, the formation of **2a** decreased, while the starting material was diminished. Therefore, the optimal charge quantity was fixed on 1.5 *F*.

5.7. Optimization of bromide salt concentration

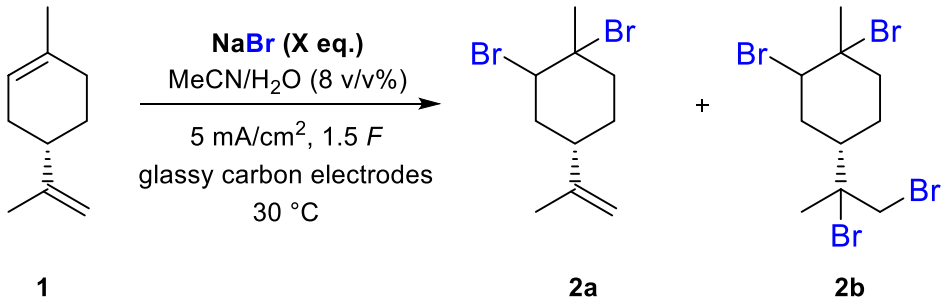

Scheme 7. Variation of bromide salt equivalents.

According to Scheme 7, the reaction conditions were subjected to different amount of bromide equivalents. At this stage, 1, 2 and 4 equivalents (0.14 M, 0.28 M and 0.56 M) of sodium bromide were tested.

Table 8: Optimization of amount of bromide quantity.

Entry	Equivalent of NaBr	*c* (NaBr)	Yield 2a[b] (%)	Yield 2b[b] (%)	Conversion 1 (%)
28	1 eq.	0.14	21	0	57
29	2 eq.	0.28	36	0	74
30	4 eq.	0.56	42	1	67

[a] Yield determined via internal NMR standard (dibromomethane, CH_2Br_2), conversion was determined via external GC calibration **1**.

Both lower and higher quantities of NaBr decreased the formation of desired product **2a**. This can be attributed to the fact, that NaBr is the limiting reagent in the reaction (Entries 28 and 29). Interestingly, an increased NaBr content also decreased the yields from 54% (Entry 19) to 42% (Entry 30).

5.8. Optimization of reaction temperature

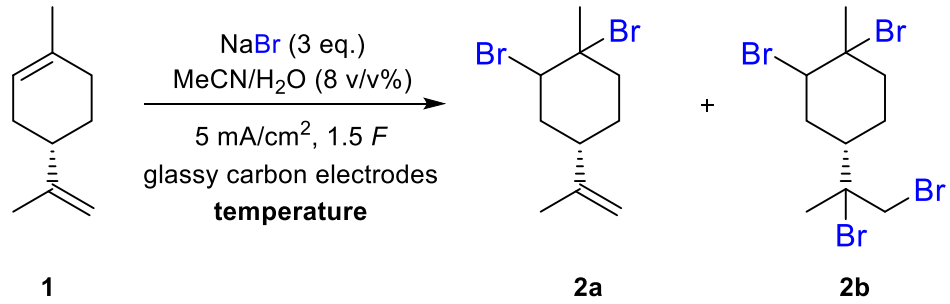

1 **2a** **2b**

Scheme 8. Optimization of reaction temperature.

To understand the effect of temperature on the reaction outcome, the now optimized conditions were run on different temperatures. Interestingly, both lower and higher temperature ranges diminished the formation of the desired product **2a**.

Table 9. Variation of reaction temperature.

Entry	Temperature (°C)	Yield 2a[a] (%)	Yield 2b[a] (%)	Conversion 1 (%)
31	20	31	0	68
32	40	16	0	44

[a] Yield determined via internal NMR standard (dibromomethane, CH_2Br_2), conversion was determined via external GC calibration of **1**.

5.9. Control experiments

To prove superiority of our conditions over the already existing procedures, (4S)-(-)-limonene was subjected to the dibromination procedure with elemental bromine and via an DMSO/HBr system (See procedure **3.7** and **3.8**).[4,5]

Table 10. Comparison of reaction selectivity of conventional bromination methods and our method.

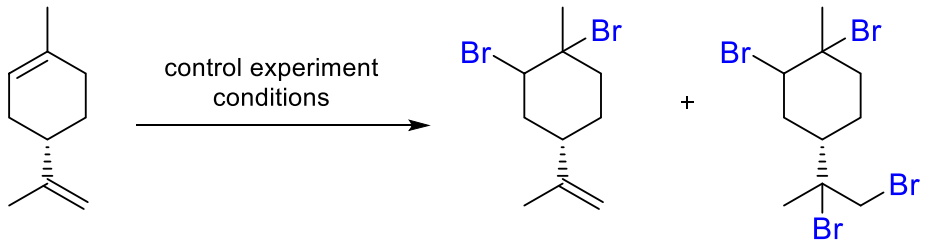

1 **2a** **2b**

Entry	Reaction conditions	Yield 2a[a] (%)	Yield 2b[a] (%)
33	Br_2 [4]	22	13
34	DMSO/HBr [5]	39	10
35	Electrochemical method	54	0

[a] Yield determined via internal NMR standard (dibromomethane, CH_2Br_2)

The reaction carried out in the presence of elemental bromine proved to be unselective, accompanied with one main by-product (7.125 mins, chromatogram **A**, Figure 6) and many

unidentified by-products. The signal is depicted as a monobrominated limonene derivative according to GCMS measurements. The system reported by Jiao et al. proved to be more selective, providing **2a** in 39% and **2b** in 13% NMR yield (Entry 34). Our method proved to be superior compared to the already existing ones providing the desired product in 54% NMR yield (Entry 35).

For clearer visualization of the selectivity, GC chromatograms of the previously mentioned reactions were included in Figure 6.

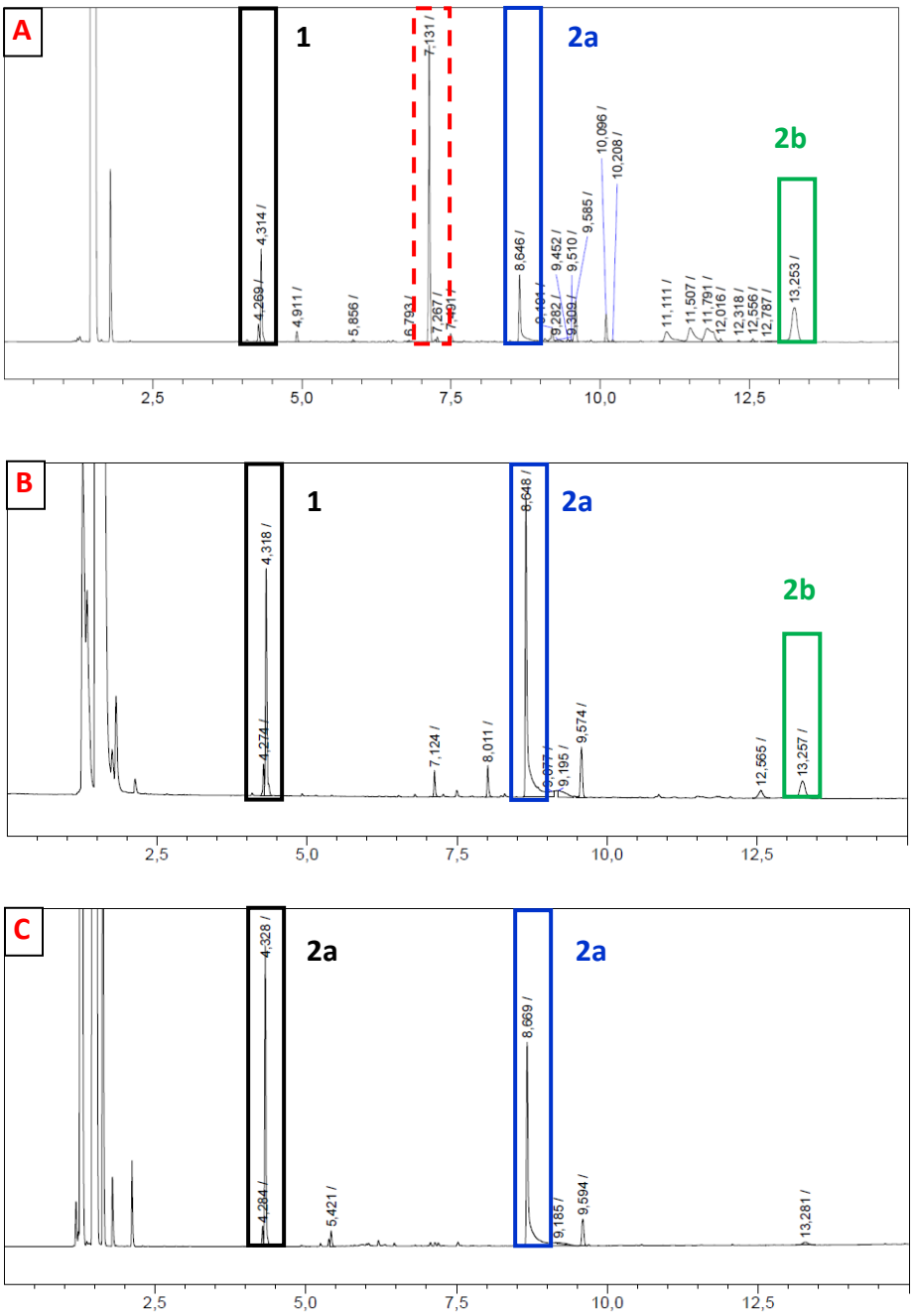

Figure 6: GC chromatograms of Entry 33 (A), Entry 34 (B) and Entry 35 (C) for qualitative visualization of reaction selectivity. Signals of **1**, **2a** and **2b** were identified via GC, GCMS and NMR measurements.

6. Product characterization

6.1. (4*S*)-1,2-Dibromo-*p*-menth-8-ene (2a)

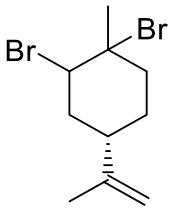

According to the general protocol (GP1), (4*S*)-(–)-limonene (95 mg, 0.70 mmol, 1.00 eq.) was used as terpene. The reaction solution was electrolyzed until 1.5 *F* (101 C) were applied at 5 mA/cm^2 (9 mA/1.8 cm^2). After the extraction procedure, 116 mg of crude product were obtained. NMR quantification with internal standard gave a yield of 54% **2a**. Minor impurities were removed under *vacuo* to yield **2a** (110 mg, 0.37 mmol, 53%) as a yellow oil.

Diastereomeric ratio 1:1[*]

The crude product was used for the formation of **12** without further purification.

^{1}H NMR (400 MHz, $CDCl_3$): δ [ppm] = 4.78–4.74 (m, 3H), 2.60–2.51 (m, 2H), 2.13–2.03 (m, 2H), 2.01–1.94 (m, 1H), 2.00 (s, 3H), 1.88–1.72 (m, 2H), 1.74 (s, 3H).

^{13}C NMR (101 MHz, $CDCl_3$): δ [ppm] = 148.5, 109.8, 70.7, 61.4, 38.1, 36.9, 36.5, 35.5, 28.0, 21.1.

HRMS for $C_{10}H_{16}{}^{79}Br_2$ (ESI+, APCI±): No ionization could be observed for this compound.

IR (cm^{-1}): 3083, 2970, 2930, 2865, 2177, 2155, 1645, 1448, 1431, 1379, 1170, 1086, 979, 947, 888, 533.

The spectroscopic data are in accordance with literature.[10]

[*] Diastereomeric ratio was postulated as 1:1 from the crystallographic data and d.r. of **2b**.

6.2. (4*S*)-1,2,8,9-Tetrabromo-*p*-menthane (2b)

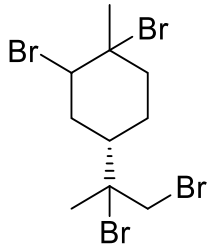

According to the general protocol (GP2), (4*S*)-(–)-limonene (95 mg, 0.70 mmol, 1.00 eq.) was used as terpene. The reaction solution was electrolyzed until 4.5 *F* (304 C) were applied at 5 mA/cm^2 (9 mA/1.8 cm^2). After the extraction procedure, minor impurities were removed under *vacuo* to yield **2b** (236 mg, 0.52 mmol, 74%) as highly viscous oil.

Diastereomeric ratio 1:1 (NMR data refer to both diastereomers).

^{1}H NMR (400 MHz, $CDCl_3$): δ [ppm] = 4.77–4.73 (m, 2H), 4.02 (d, *J* = 10.1 Hz, 1H), 3.95 (d, *J* = 10.1 Hz, 1H), 3.84 (d, *J* = 10.1 Hz, 1H), 3.83 (d, *J* = 10.1 Hz, 1H), 2.76 (ddd, *J* = 14.5 Hz, 11.5 Hz, 3.1 Hz, 1H), 2.65 (ddd, *J* = 14.5 Hz, 11.5 Hz, 3.1 Hz, 1H), 2.30–2.22 (m, 2H), 2.21–2.11 (m, 4H), 2.04–1.98 (m, 3H), 2.00 (s, 3H), 2.00 (s, 3H), 1.91 (s, 3H), 1.87 (s, 3H), 1.87–1.83 (m, 3H).

^{13}C NMR (101 MHz, $CDCl_3$): δ [ppm] = 71.6, 71.6, 69.5, 69.4, 60.7, 60.3, 41.7, 41.4, 38.8, 38.6, 35.9, 35.7, 35.2, 35.2, 34.9, 34.1, 29.4, 29.3, 25.1, 24.8.

HRMS for $C_{10}H_{16}{}^{79}Br_4$ (ESI+, APCI±): no ionization could be observed for this compound.

IR (cm^{-1}): 2972, 2928, 1448, 1429, 1376, 1084, 565, 528.

The spectroscopic data are in accordance with literature.[10]

Crystallization was performed by dissolving **2b** (50 mg) in dichloromethane (1 mL) and cyclohexane (2 mL) at room temperature, whereby crystals of one diastereomer were obtained. Crystal structure determination of (1*R*,2*R*,4*S*,8*S*)-1,2,8,9-tetrabromo-*p*-menthane (also see Figure 6): $C_{10}H_{16}Br_4$, M = 455.87 g/mol; colorless plate (0.050 x 0.300 x 0.420 mm^3), T = 120 K, λ(Mo-Kα) = 0.71073 Å, space group $P2_12_12_1$, a = 7.9502(2) Å, b = 18.5812(6) Å, c = 18.7339(4) Å, α = 90(2)°, ß = 90(6)°, γ = 90(4)°, V = 2767.45(13) Å^3 , z = 8, ρ_{xray} = 2.188 mg/m^3 , $2\theta_{max}$ = 56,9°, μ = 11.599 mm^{-1}, F(000) = 1728, 27602 reflections, 6601 unique reflections (R_{int} = 0.0293), final R-values [I > 2σ(I)]: R_1 = 0.0339, *w*R_2 = 0.0728, R-values (all data): R_1 = 0.0406, *w*R_2 = 0.0767, CCDC-2123110.

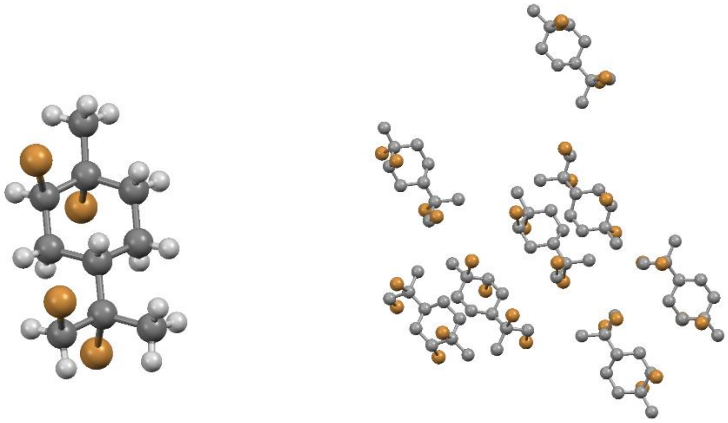

Figure 7. Molecular structure of (1*R*,2*R*,4*S*,8*S*)-1,2,8,9-tetrabromo-*p*-menthane of the unit cell (left) and in packing (right) determined by X-ray analysis. Hydrogen atoms are omitted for better visualization (right).

6.3. (4*S*)-8,9-Dibromo-*p*-menth-6-en-2-one (3)

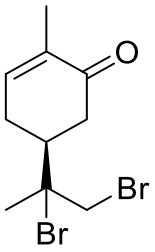

According to general protocol (GP1), (4*S*)-(+)-carvone (105 mg, 0.70 mmol, 1.00 eq.) was used as terpenoid. The reaction solution was electrolyzed until 3.0 *F* (202 C) were applied at 5 mA/cm^2 (9 mA/1.8 cm^2). After the extraction procedure, 178 mg of crude product were obtained. NMR quantification with internal standard gave a yield of 86% **3.** Minor impurities were removed under *vacuo* to yield **3** (178 mg, 0.57 mmol, 82%) as a yellow oil.

Diastereomeric ratio 1:1 (NMR data refer to both diastereomers).

^{1}H NMR (400 MHz, $CDCl_3$): δ [ppm] = 6.78–6.73 (m, 2H), 3.96 (d, *J* = 10.6 Hz, 1H), 3.94 (d, *J* = 10.6 Hz, 1H), 3.86 (d, *J* = 10.6 Hz, 1H), 3.82 (d, *J* = 10.6 Hz, 1H), 2.68–2.35 (m, 10H), 1.89 (s, 3H), 1.88 (s, 3H), 1.80 (s, 6H).

^{13}C NMR (101 MHz, $CDCl_3$): δ [ppm] = 198.7, 198.2, 143.8, 143.6, 135.5, 135.5, 71.2, 71.1, 42.4, 42.1, 40.8, 40.7, 40.7, 40.1, 28.9, 28.5, 28.0, 15.8, 15.7.

HRMS for $C_{10}H_{15}{}^{79}Br_2O$ (ESI+) $[M+H]^+$: calc.: 308.9484, found: 308.9483.

IR (cm^{-1}): 3030, 2975, 2924, 2892, 1722, 1669, 1435, 1380, 1368, 1085, 639, 568, 540.

The spectroscopic data are in accordance with literature.[11]

6.4. (4*S*)-8,9-Dibromo-*p*-menth-1-en-7-al (4)

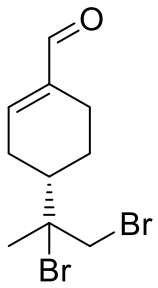

According to general protocol (GP1), (4*S*)-(–)-perillaldehyde (105 mg, 0.7 mmol, 1.00 eq.) was used as terpenoid. The reaction solution was electrolyzed until 3.0 *F* (202 C) were applied at 5 mA/cm^2. (9 mA/1.8 cm^2). After the extraction procedure, 175 mg of crude product were obtained. NMR quantification with internal standard gave a yield of 72% **4**. Minor impurities were removed under *vacuo* to yield **4** (140 mg, 0.45 mmol, 65%) as a yellow oil.

Diastereomeric ratio 1:1 (NMR data refer to both diastereomers).

^{1}H NMR (400 MHz, $CDCl_3$): δ [ppm] = 9.46 (s, 2H), 6.82–6.80 (m, 2H), 4.13 (d, *J* = 10.3 Hz, 1H), 3.97 (d, *J* = 10.3 Hz, 1H), 3.87 (d, *J* = 10.3 Hz, 1H), 3.85 (d, *J* = 10.3 Hz, 1H), 2.61–2.46 (m, 5H), 2.41–2.32 (m, 1H), 2.14–1.93 (m, 6H), 1.95 (s, 3H), 1.89 (s, 3H), 1.88–1.82 (m, 1H), 1.52–1.31 (m, 2H).

^{13}C NMR (101 MHz, $CDCl_3$): δ [ppm] = 193.6, 193.5, 149.3, 149.1, 141.3, 72.0, 71.8, 41.6, 41.5, 41.3, 41.1, 29.3, 29.3, 29.2, 28.7, 24.3, 23.7, 21.7, 21.5.

HRMS for $C_{10}H_{15}{}^{79}Br_2O$ (ESI+) $[M+H]^+$: calc.: 308.9484, found: 308.9483.

IR (cm^{-1}): 3347, 2929, 2722, 1679, 1646, 1434, 1420, 1396, 1379, 1168, 774, 700, 567.

6.5. (4*R*)-1,2-Dibromo-*p*-menthan-4-ol (5)

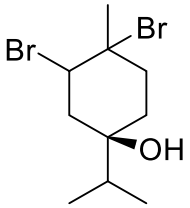

According to general protocol (GP1), (4*R*)-(–)-terpinen-4-ol (108 mg, 0.70 mmol, 1.00 eq.) was used as terpenoid. The reaction solution was electrolyzed until 2.5 *F* (169 C) were applied at 5 mA/cm^2 (9 mA/1.8 cm^2). After the extraction procedure, 112 mg of crude product were obtained. NMR quantification with internal standard gave a yield of 46% **5**. Minor impurities were removed under *vacuo* to yield **5** (96 mg, 0.31 mmol, 44%) as a yellow oil.

Diastereomeric ratio 1:1 (NMR data refer to both diastereomers).

^{1}H NMR (400 MHz, $CDCl_3$): δ [ppm] = 4.87 (dd, *J* = 12.5, 4.6 Hz, 1H), 4.73–4.70 (m, 1H), 2.76 (ddd, *J* = 13.5, 13.5, 4.6 Hz, 1H), 2.72 (dd, *J* = 16.0, 4.4 Hz, 1H), 2.38 (ddd, *J* = 13.6, 4.1, 3.0 Hz, 1H), 2.38–2.37 (m, 1H), 2.24–2.14 (m, 3H), 2.04 (s, 3H), 2.00–1.87 (m, 3H), 1.86 (s, 3H), 1.78–1.72 (m, 1H), 1.66–1.53 (m, 5H), 1.52–1.44 (m, 1H), 0.96 (s, 3H), 0.94 (s, 3H), 0.92 (s, 3H), 0.90 (s, 3H).

^{13}C NMR (101 MHz, $CDCl_3$): δ [ppm] = 75.3, 72.4, 70.8, 68.0, 61.7, 58.4, 43.6, 39.7, 38.9, 38.4, 38.3, 35.0, 33.0, 32.4, 31.7, 24.8, 16.8, 16.8, 16.7, 16.6.

HRMS for $C_{20}H_{36}{}^{107}Ag^{79,81}Br_4O_2$ (ESI+) $[2M+Ag]^+$: calc.: 734.8459, found: 734.8446.

HRMS for $C_{20}H_{36}{}^{109}Ag^{79,81}Br_4O_2$ (ESI+) $[2M+Ag]^+$: calc.: 736.8455, found: 736.8444.

IR (cm^{-1}): 3460, 2963, 2877, 1450, 1430, 1379, 1024, 1003, 991, 952, 696, 537, 517.

6.6. 6,7-Dibromo-7-methyl-3-methyleneoct-1-ene (6)

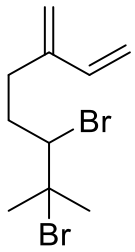

According to general protocol (GP1), myrcene (95 mg, 0.70 mmol, 1.00 eq.) was used as terpene. The reaction solution was electrolyzed until 1.5 *F* (101 C) were applied at 5 mA/cm^2 (9 mA/1.8 cm^2). After the extraction procedure, 131 mg of crude product were obtained. NMR quantification with internal standard gave a yield of 46% **6**. The crude residue was subjected to flash column chromatography (cyclohexane, 100%) to yield **6** (70 mg, 0.24 mmol, 34%).

Caution is to be taken due to the volatile nature of this product.

^{1}H NMR (400 MHz, $CDCl_3$): δ [ppm] = 6.38 (dd, *J* = 17.5, 11.1 Hz, 1H), 5.30 (d, *J* = 17.5 Hz, 1H), 5.12–5.08 (m, 3H), 4.20 (dd, *J* = 10.7, 1.5 Hz, 1H), 2.71–2.57 (m, 3H), 2.38–2.31 (m, 1H), 1.98 (s, 3H), 1.81 (s, 3H).

^{13}C NMR (101 MHz, $CDCl_3$): δ [ppm] = 144.8, 138.5, 117.1, 114.0, 68.6, 66.5, 35.4, 34.7, 3.2, 28.4.

HRMS for $C_{20}H_{32}{}^{107}Ag^{79}Br_2$ (ESI+) $[2M+Ag-2Br]^{2\bullet+}$: calc.: 536.9922, found: 536.9903.

IR (cm^{-1}): 3087, 2977, 2931, 1595, 1455, 1386, 1371, 1223, 1097, 990, 896, 534.

The analytical data are in accordance with literature.[11,12]

6.7. 6,7-Dibromo-3,7-dimethyloctan-1-al (7)

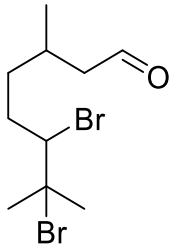

According to general protocol (GP1), citronellal (105 mg, 0.70 mmol, 1.00 eq.) was used as terpenoid. The reaction solution was electrolyzed until 2.0 *F* (135 C) were applied at 5 mA/cm^2 (9 mA/1.8 cm^2). After the extraction procedure, 116 mg of crude product were obtained. NMR quantification with internal standard gave a yield of 46% **7**. Minor impurities were removed under *vacuo* to yield **7** (90 mg, 0.29 mmol, 41%) as a transparent oil.

Diastereomeric ratio 1:1 (NMR data refer to both diastereomers).

^{1}H NMR (400 MHz, $CDCl_3$): δ [ppm] = 9.77 (dd, *J* = 1.7, 1.7 Hz, 2H), 4.16 (dd, *J* = 9.4, 1.7 Hz, 1H), 4.14 (dd, *J* = 9.4, 1.7 Hz, 1H), 2.50–2.40 (m, 4H), 2.43–2.32 (m, 2H), 2.16–2.08 (m, 2H), 1.97 (s, 3H), 1.97 (s, 3H), 1.80 (s, 3H), 1.79 (s, 3H), 1.64–1.57 (m, 2H), 1.53–1.47 (m, 2H), 1,39–1.31 (m, 2H), 1.01 (d, *J* = 7.0 Hz, 3H), 1.00 (d, *J* = 7.0 Hz, 3H).

^{13}C NMR (101 MHz, $CDCl_3$): δ [ppm] = 202.6, 202.5, 69.0, 68.9, 66.8, 66.5, 51.4, 50.6, 35.7, 35.6, 35.5, 33.7, 33.4, 28.1, 28.1, 27.8, 27.3, 20.4, 19.6.

HRMS for $C_{20}H_{34}{}^{107}Ag^{79,81}Br_2O_2$ (ESI+) $[2M+Ag-2HBr]^+$: calc.: 572.9951, found: 572.9917.

HRMS for $C_{20}H_{34}{}^{109}Ag^{79,81}Br_2O_2$ (ESI+) $[2M+Ag-2HBr]^+$: calc.: 574.9948, found: 574.9938.

IR (cm^{-1}): 2957, 2929, 1723, 1456, 1371, 1096, 541.

6.8. 6,7-Dibromo-3,7-dimethyloct-2-en-1-al (8)

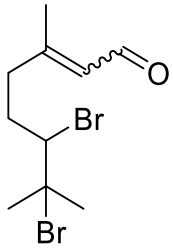

According to general protocol (GP1), citral (E/Z: 2:3) (107 mg, 0.70 mmol, 1.00 eq.) was used as terpenoid. The reaction solution was electrolyzed until 2.0 *F* (135 C) were applied at 5 mA/cm^2 (9 mA/1.8 cm^2). After the extraction procedure, 141 mg of crude product were obtained. NMR quantification with internal standard gave a yield of 54% **8**. Minor impurities were removed under vacuo to yield **8** (110 mg, 0.35 mmol, 50%) as a transparent oil.

Diastereomeric ratio (E/Z) 2:3 (NMR data refer to both diastereomers).

^{1}H NMR (400 MHz, $CDCl_3$): δ [ppm] = 10.05 (d, *J* = 8.0 Hz, 1H), 10.01 (d, *J* = 8.0 Hz, 1H), 5.97–5.95 (m, 2H), 4.11 (dd, *J* = 11.3, 1.4 Hz, 1H), 4.10 (dd, *J* = 11.3, 1.4 Hz, 1H), 3.02–2.92 (m, 1H), 2.80–2.57 (m, 5H), 2.44–2.35 (m, 1H), 2.21 (s, 3H), 2.03 (s, 3H), 2.02 (s, 6H), 1.98 (s, 3H), 1.81 (s, 3H), 1.80 (s, 3H).

^{13}C NMR (101 MHz, $CDCl_3$): δ [ppm] = 191.3, 190.9, 161.6, 161.5, 130.2, 128.3, 68.4, 68.2, 65.0, 64.8, 40.0, 35.6, 34.4, 33.3, 31.0, 28.0, 27.9, 24.8, 17.7.

HRMS for $C_{10}H_{17}{}^{79}Br_2O$ (APCI+) $[M+H]^+$: calc.: 310.9641, found: 310.9628.

IR (cm^{-1}): 2976, 2931, 1672, 1454, 1386, 1371, 1196, 1096, 848, 539.

6.9. 4-(2,3-Dibromopropyl)anisole (9)

According to general protocol (GP1), 4-allylanisole (104 mg, 0.70 mmol, 1.00 eq.) was used as substrate. The reaction solution was electrolyzed until 5.5 *F* (371 C) were applied at 5 mA/cm^2 (9 mA/1.8 cm^2). After the extraction procedure, 165 mg of crude product were obtained. NMR quantification with internal standard gave a yield of 64% **9**. The crude product was subjected to high performance liquid chromatography due to the presence of regioisomer (acetonitrile/H_2O 1:1 → 4:1) to yield **9** as a colorless oil (119 mg, 0.34 mmol, 56%).

^{1}H NMR (400 MHz, $CDCl_3$): δ [ppm] = 7.26–7.20 (m, 2H), 6.89–6.86 (m, 2H), 4.33 (dddd, *J* = 8.9, 7.6, 4.9, 4.2 Hz, 1H), 3.81 (dd, *J* = 10.5, 4.2 Hz, 1H), 3.81 (s, 3H), 3.62 (dd, *J* = 10.5, 8.9 Hz, 1H) 3.42 (dd, *J* = 14.7, 4.9 Hz, 1H), 3.11 (dd, *J* = 14.7, 7.6 Hz, 1H).

^{13}C NMR (101 MHz, $CDCl_3$): δ [ppm] =158.9, 130.7, 128.9, 114.0, 55.4, 53.0, 41.4, 36.1.

HRMS for $C_{10}H_{12}{}^{79}Br_2O$ (APCI+) $[M]^{\bullet+}$: calc.: 307.9234, found: 307.9230.

IR (cm^{-1}): 2954, 2834, 1611, 1584, 1510, 1463, 1431,1244, 1177, 1032, 830, 807, 555, 520.

The analytical data are in accordance with literature.[13,14]

6.10. 4-(2,3-Dibromopropyl)-1,2-dimethoxybenzene (10)

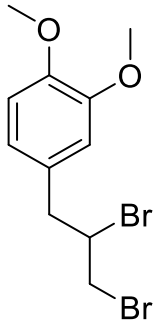

According to general protocol (GP1), 4-allyl-1,2-dimethoxybenzene (125 mg, 0.07 mmol, 1.00 eq.) was used as substrate. The reaction solution was electrolyzed until 4.0 *F* (270 C) were applied at 5 mA/cm^2 (9 mA/1.8 cm^2). After the extraction procedure, 204 mg of the crude product were obtained. NMR quantification with internal standard gave a yield of 57% **10**. The crude product was subjected to high performance liquid chromatography due to the presence of regioisomer (acetonitrile/H_2O 1:1 → 4:1) to yield **10** as a pale, yellow oil (99 mg, 0.29 mmol, 42%).

^{1}H NMR (400 MHz, $CDCl_3$): δ [ppm] = 6.84–6.82 (m, 3H), 4.35 (dddd, *J* = 8.9, 7.6, 5.0, 4.2 Hz, 1H), 3.89 (s, 3H), 3.88 (s, 3H), 3.81 (dd, *J* = 10.5, 4.2 Hz, 1H), 3.61 (dd, *J* = 10.5, 8.9 Hz, 1H) 3.41 (dd, *J* = 14.7, 4.9 Hz, 1H), 3.12 (dd, *J* = 14.7, 7.6 Hz, 1H).

^{13}C NMR (101 MHz, $CDCl_3$): δ [ppm] = 149.0, 148.3, 129.3, 121.9, 112.9, 111.2, 56.1, 52.8, 41.6, 36.2.

HRMS for $C_{11}H_{14}{}^{79}Br_2O_2$ (APCI+) $[M]^{\bullet+}$: calc.: 335.9356, found: 335.9359.

IR (cm^{-1}): 2933, 2833, 1591, 1514, 1462, 1418, 1261, 1235, 1142, 1025, 805, 765, 639, 570, 545.

6.11. 5-(2,3-Dibromopropyl)-1,3-benzodioxole (11)

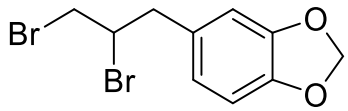

According to general protocol (GP1), 5-allyl-1,3-benzodioxole (113 mg, 0.70 mmol, 1.00 eq.) was used as substrate. The reaction solution was electrolyzed until 3.0 *F* (203 C) were applied at 5 mA/cm^2 (9 mA/1.8 cm^2). After the extraction procedure, 187 mg of the crude product were obtained. NMR quantification with internal standard gave a yield of 60% **11**. The crude product was subjected to high performance liquid chromatography due to the presence of regioisomer (acetonitrile/H_2O 1:1 → 4:1) to **11** as a pale, yellow oil (109 mg, 0.34 mmol, 48%).

^{1}H NMR (400 MHz, $CDCl_3$): δ [ppm] = 6.79–6.73 (m, 3H), 5.96 (s, 2H), 4.30 (dddd, *J* = 8.9, 7.6, 4.9, 4.2 Hz, 1H), 3.82 (dd, *J* = 10.5, 4.2 Hz, 1H), 3.62 (dd, *J* = 10.5, 9.0 Hz, 1H), 3.40 (dd, *J* = 14.7, 4.9 Hz, 1H), 3.06 (dd, *J* = 14.7, 7.6 Hz, 1H).

^{13}C NMR (101 MHz, $CDCl_3$): δ [ppm] = 147.8, 146.9, 130.6, 122.9, 110.0, 108.4, 101.2, 52.8, 41.8, 36.0.

HRMS for $C_{10}H_{10}{}^{79}Br_2O_2$ (APCI+) $[M]^{\bullet+}$: calc.: 319.9043, found: 319.9053.

IR (cm^{-1}): 2890, 1608, 1501, 1487, 1441, 1363, 1238, 1189, 1121, 1098, 1035, 926, 870, 806, 769, 565.

6.12. (4*S*)-*p*-Mentha-1,8-diene-2-carbonitrile (12)

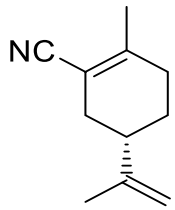

12 was prepared according to a modified protocol adopted from U. Jahn *et al*.[15]

2a (295 mg, 1.00 mmol) in 2 mL DMSO was added via a syringe pump (0.2 mL/min) to a continuously stirring solution of NaCN (196 mg, 4.00 mmol) in 8 mL DMSO at 60 °C under argon atmosphere. After addition, the reaction was left to stir for 30 mins at 60 °C. The reaction was monitored via TLC, GC. Once the reaction was complete, the mixture was left to cool to room temperature. It was partitioned with 50 mL Et_2O and 50 mL water. The organic phase was washed with water (4 x 50 mL). The organic layer was washed with brine (50 mL), dried over $MgSO_4$ and concentrated under *vacuo*. The residue was subjected to flash column chromatography (cyclohexane/ethyl acetate, 10:0 → 9:1) to yield **12** (79 mg, 0.49 mmol, 49%) as a transparent oil.

^{1}H NMR (400 MHz, $CDCl_3$): δ [ppm] = 4.78–4.78 (m, 1H), 4.72–4.71 (m, 1H), 2.38–2.28 (m, 1H), 2.23–2.11 (m, 4H), 2.00 (s, 3H), 1.87–1.81 (m, 1H), 1.73 (s, 3H), 1.53–1.43 (m, 1H).

^{13}C NMR (101 MHz, $CDCl_3$): δ [ppm] = 153.3, 147.7, 119.2, 110.0, 106.0, 40.0, 32.2, 32.0, 26.7, 22.7, 20.9.

HRMS for $C_{11}H_{16}N$ (APCI+) $[M+H]^{\bullet-}$: calc.: 162.1177, found: 162.1189.

IR (cm^{-1}): 3082, 2926, 2210, 1716, 1688, 1646, 1440, 1378, 1105, 893, 736, 422.

7. Spectral data

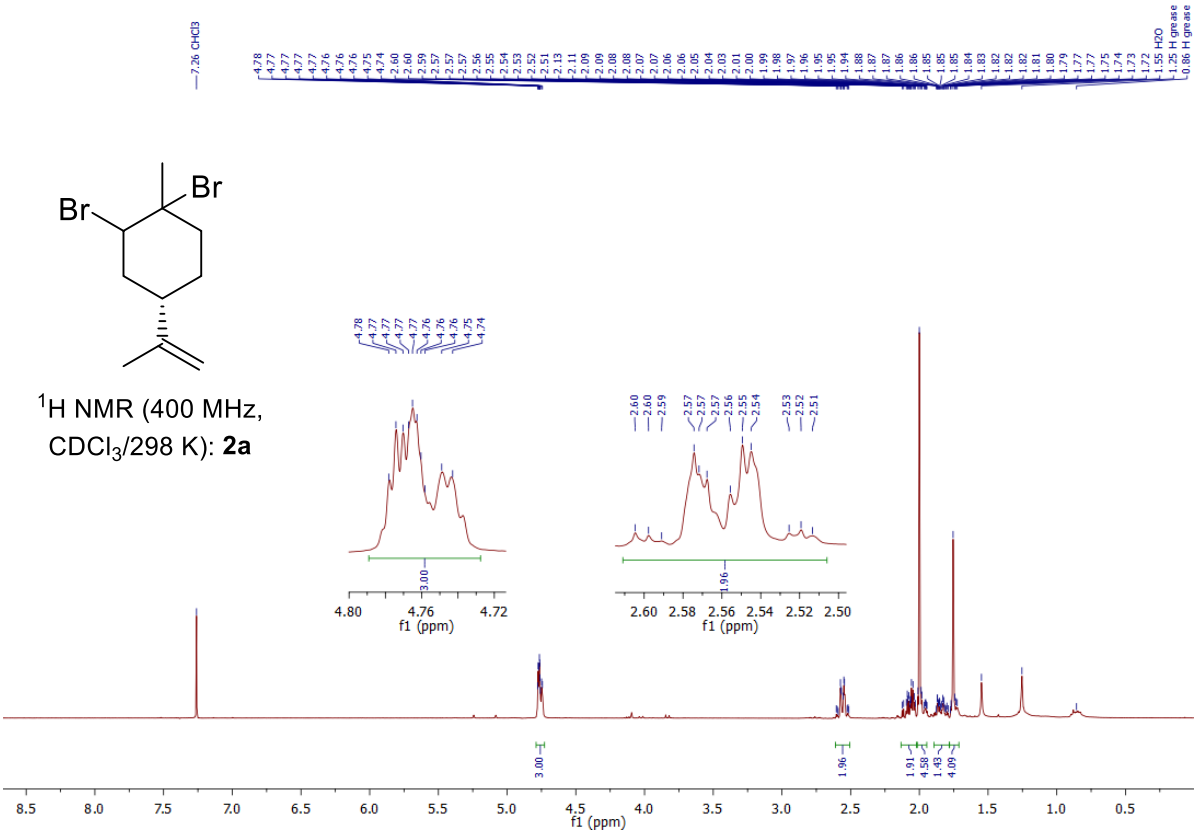

Figure 8. 400 MHz ^{1}H NMR spectrum of (4*S*)-1,2-dibromo-*p*-menth-8-ene (**2a**).

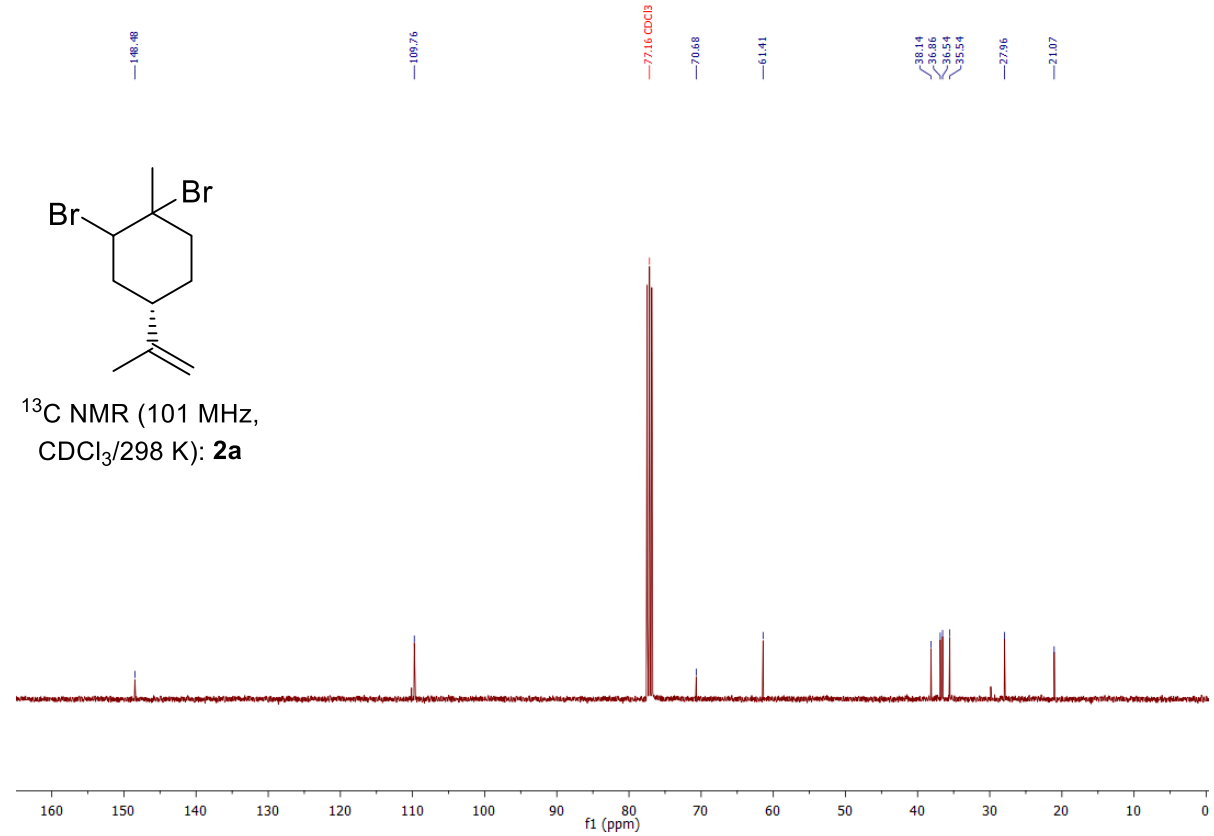

Figure 9. 101 MHz ^{13}C NMR spectrum of (4*S*)-1,2-dibromo-*p*-menth-8-ene (**2a**).

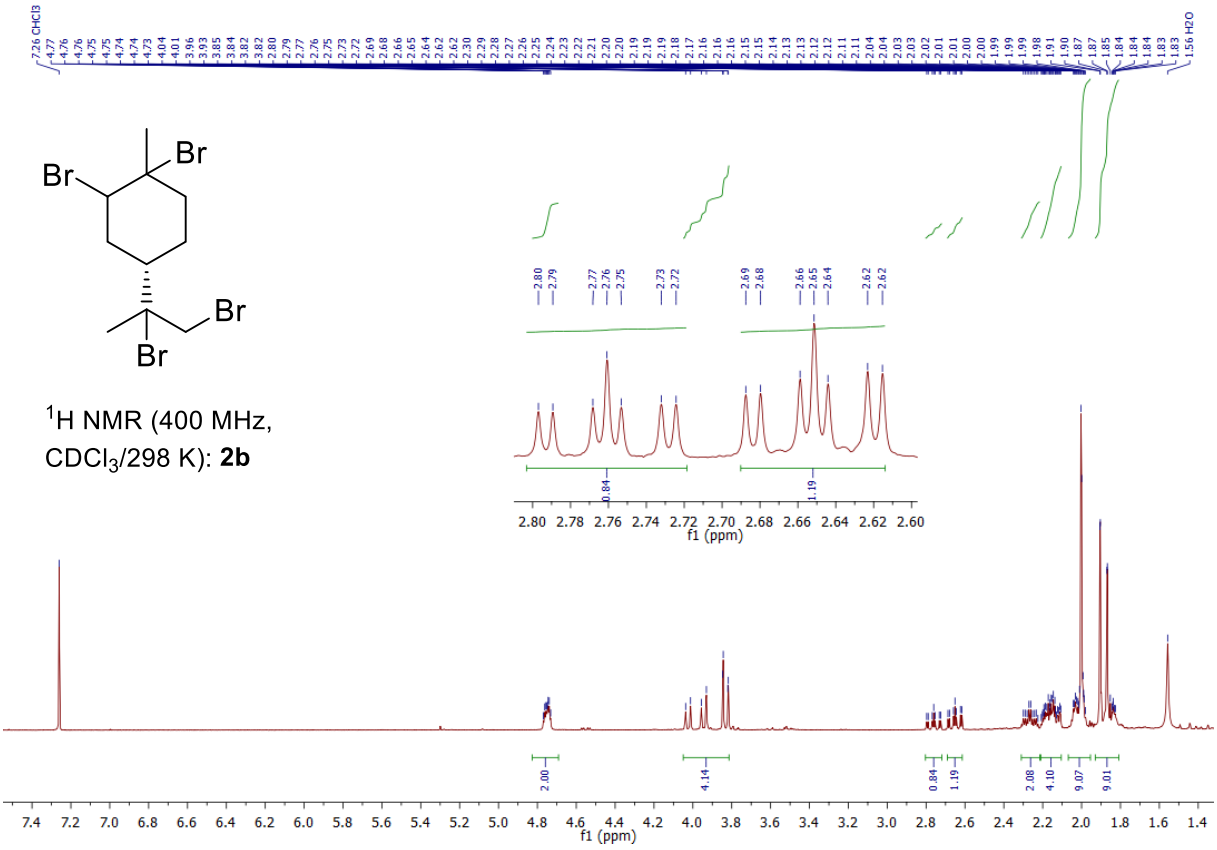

Figure 10. 400 MHz ^{1}H NMR spectrum of (4*S*)-1,2,8,9-tetrabromo-*p*-menthan (**2b**).

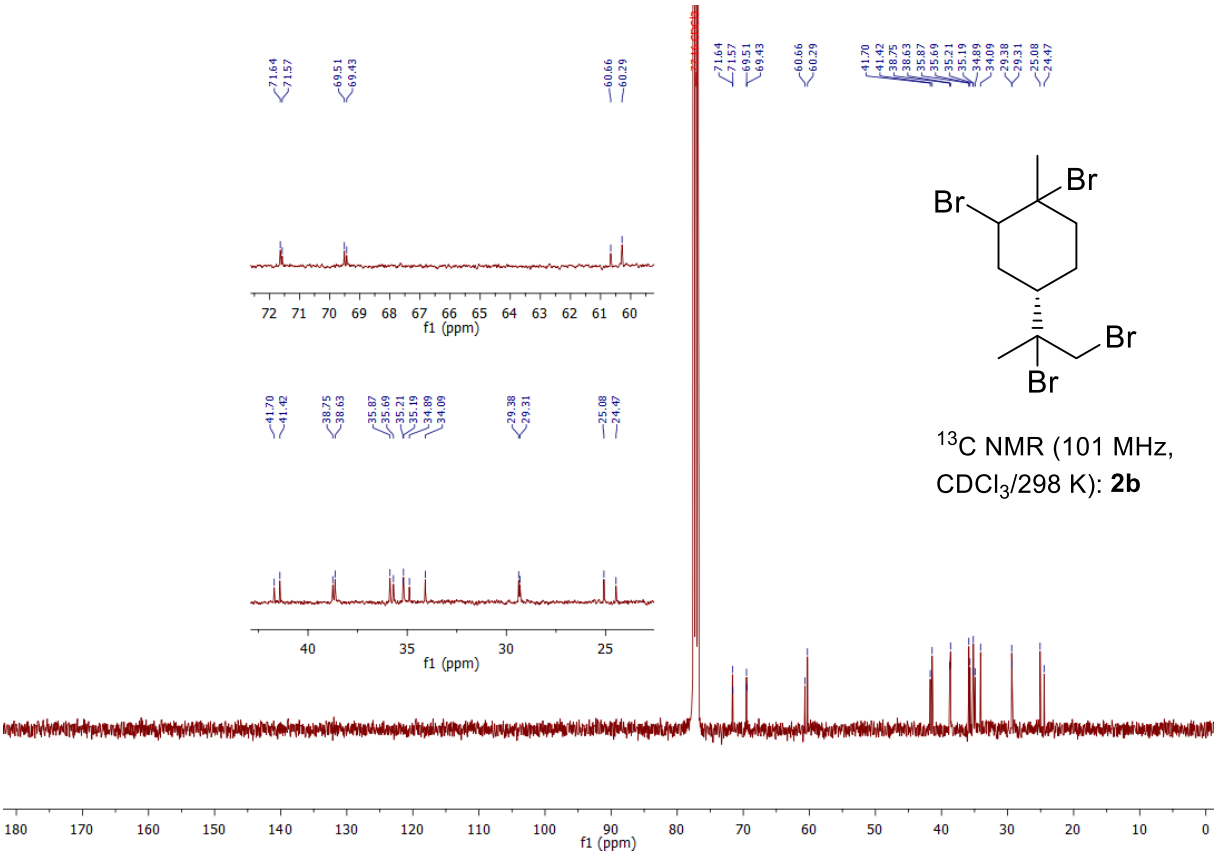

Figure 11. 101 MHz ^{13}C NMR spectrum of (4*S*)-1,2,8,9-tetrabromo-*p*-menthan (**2b**).

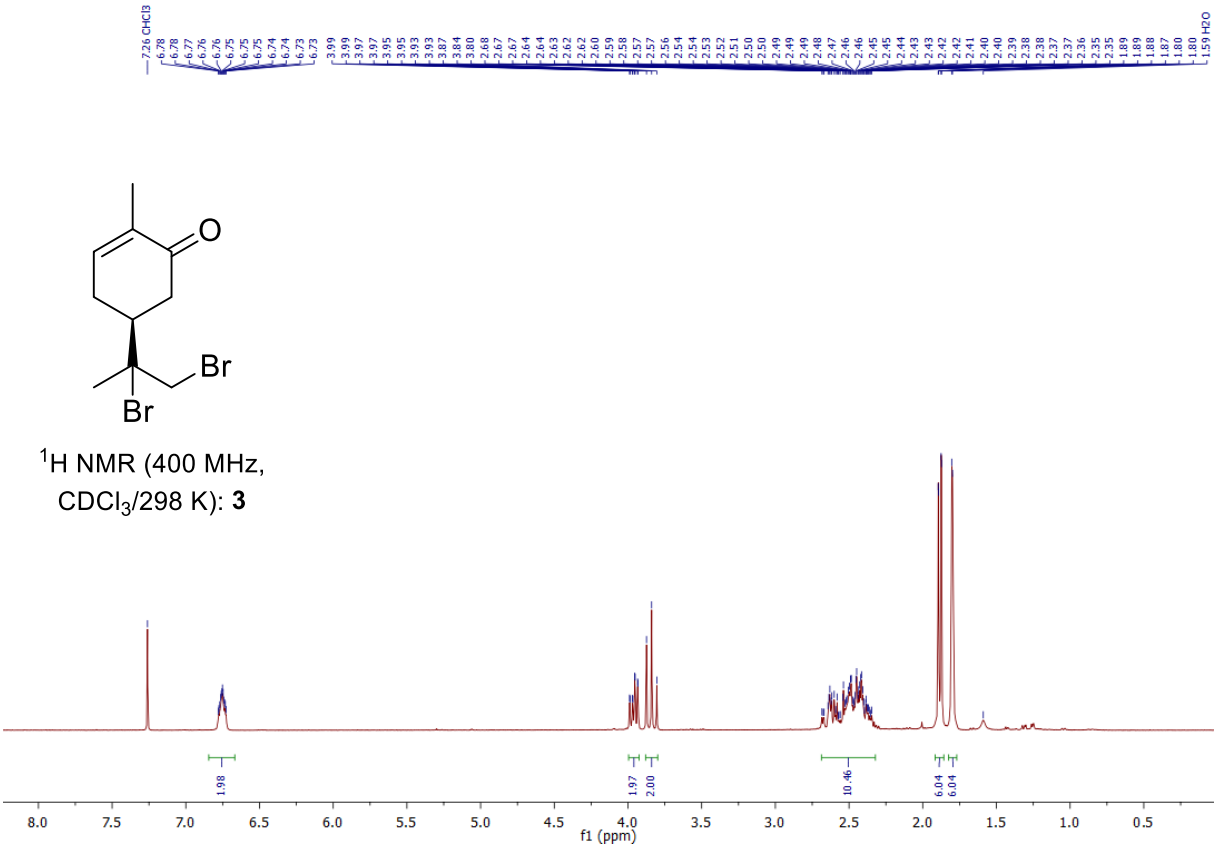

Figure 12. 400 MHz ^{1}H NMR spectrum of (4*S*)-8,9-dibromo-*p*-menth-6-en-2-one (**3**)

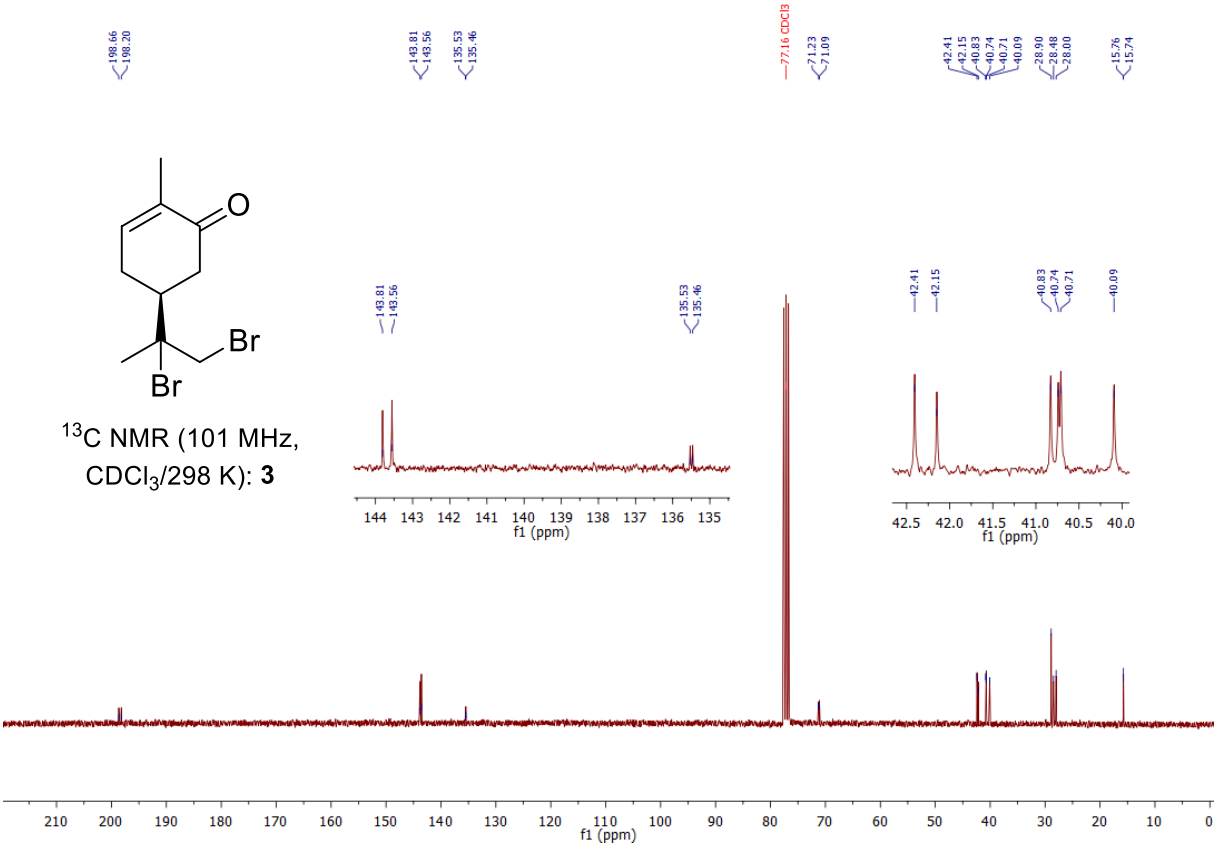

Figure 13. 101 MHz ^{13}C NMR spectrum of (4*S*)-8,9-dibromo-*p*-menth-6-en-2-one (**3**).

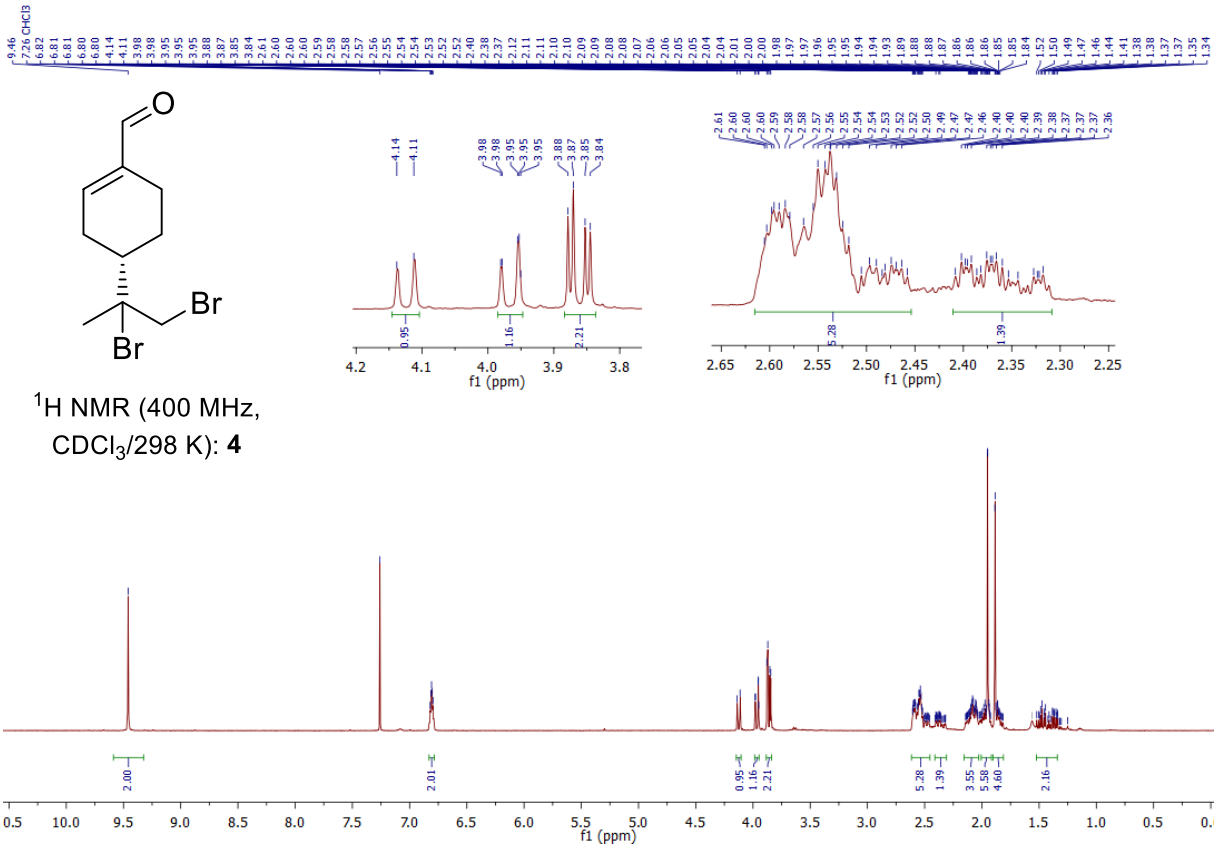

Figure 14. 400 MHz ^{1}H NMR spectrum of (4*S*)-8,9-dibromo-*p*-menth-1-en-7-al (**4**).

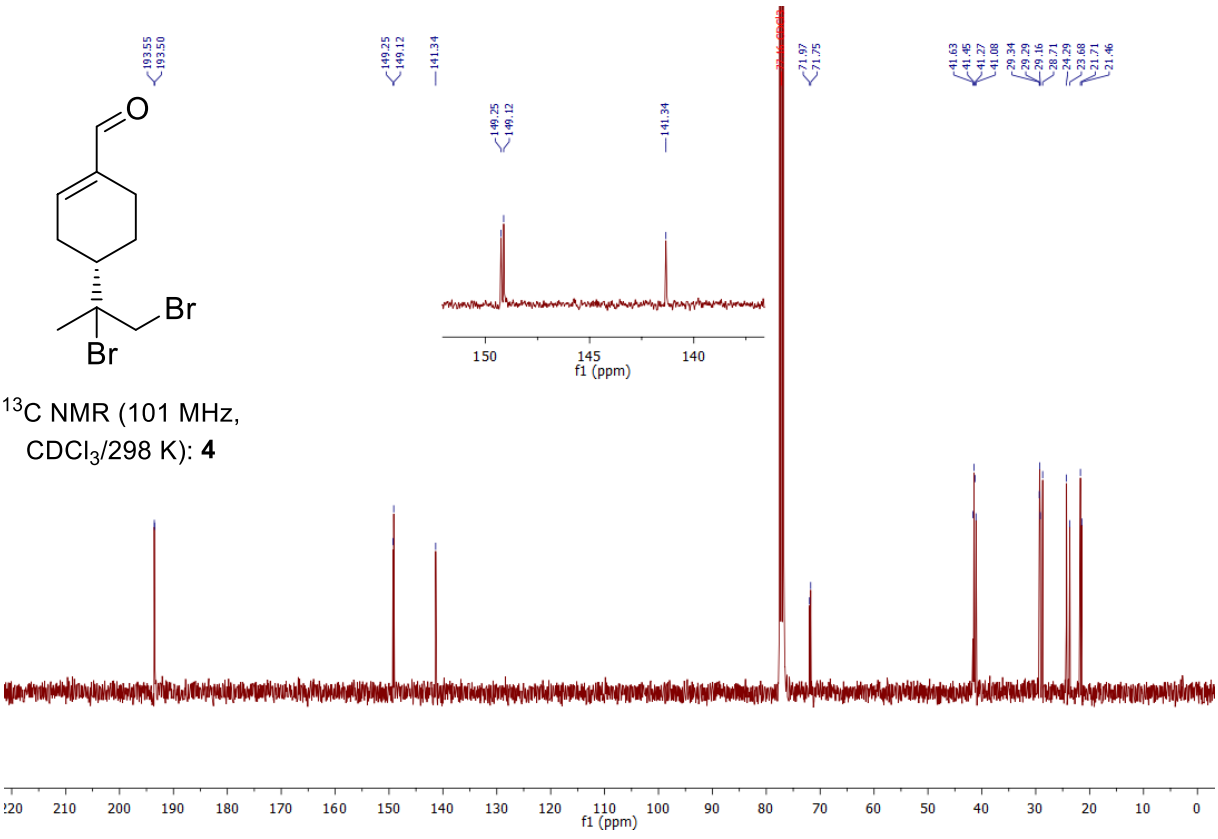

Figure 15. 101 MHz ^{13}C NMR spectrum of (4*S*)-8,9-dibromo-*p*-menth-1-en-7-al (**4**).

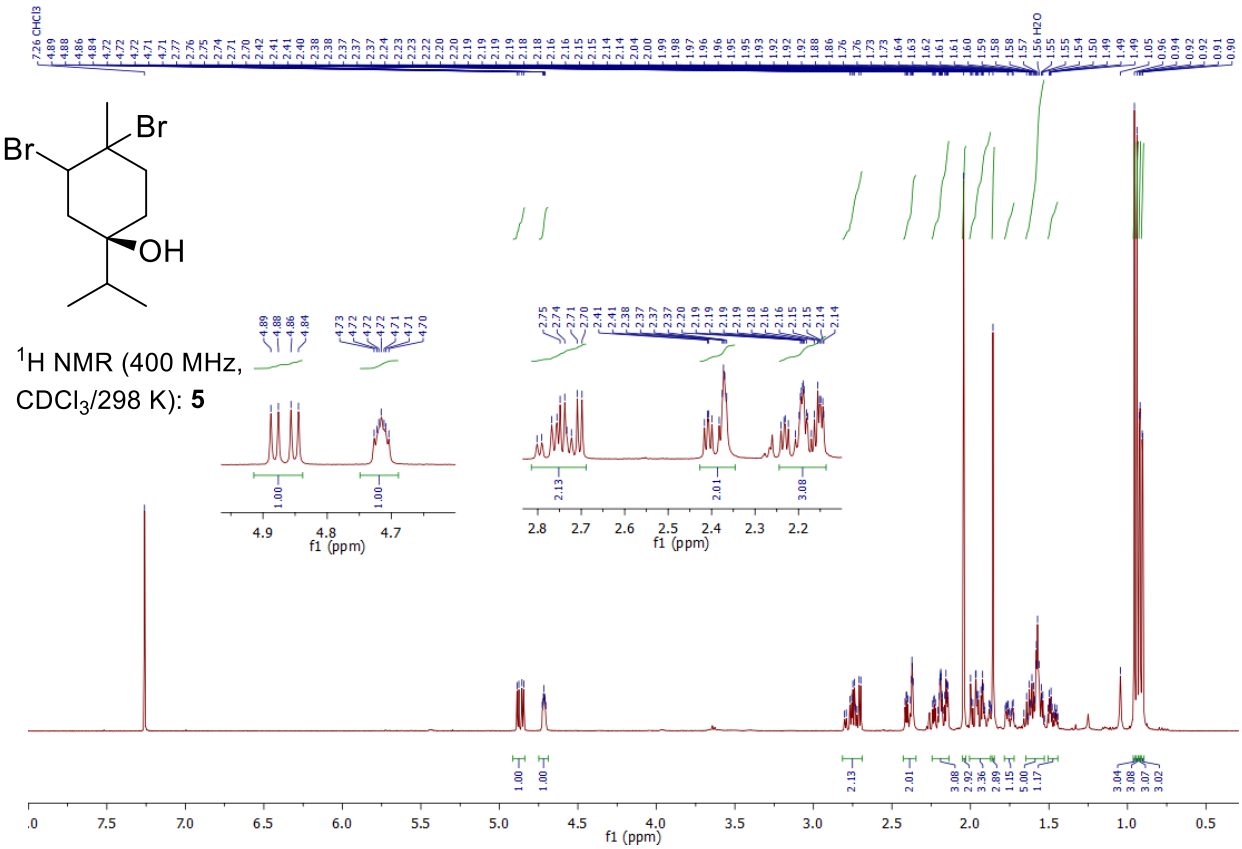

Figure 16. 400 MHz ^{1}H NMR spectrum of (4*R*)-1,2-dibromo-*p*-menthan-4-ol (**5**).

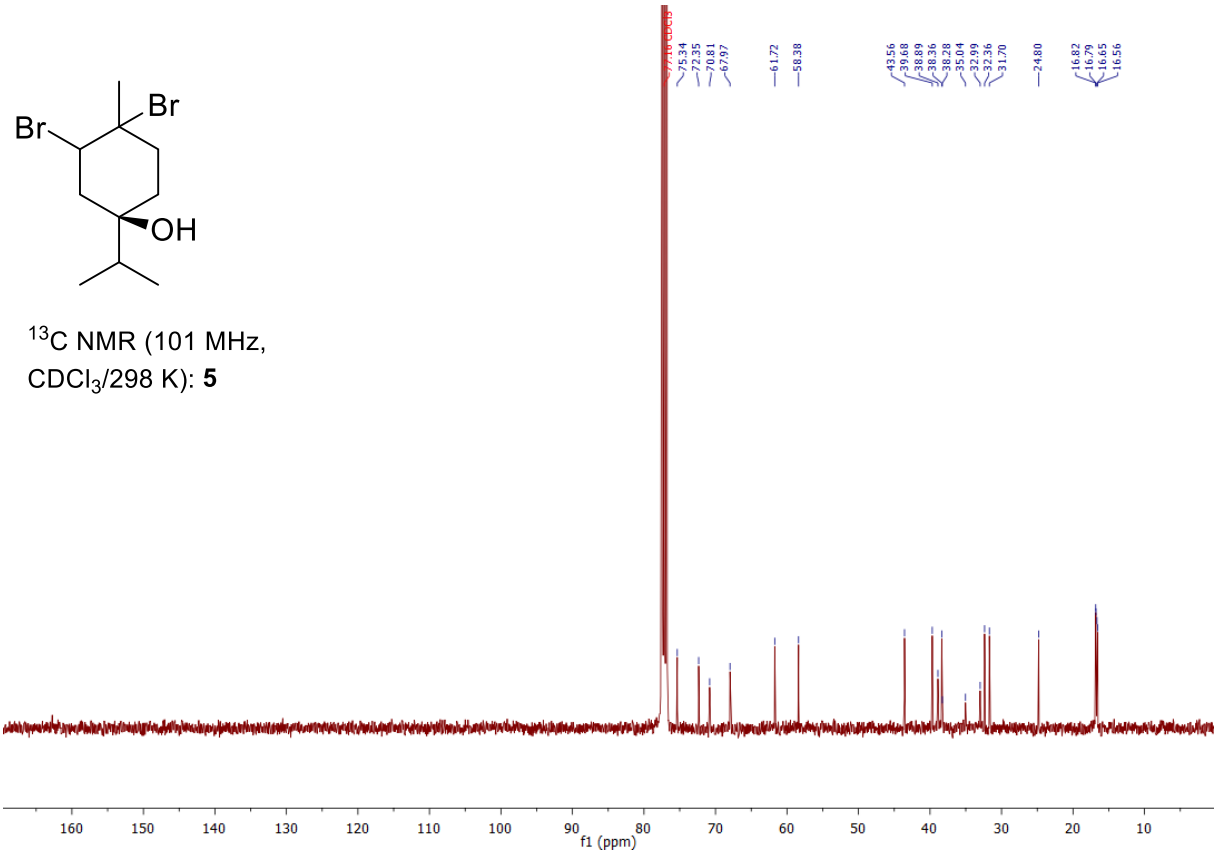

Figure 17. 101 MHz ^{13}C NMR spectrum of (4*R*)-1,2-dibromo-*p*-menthan-4-ol (**5**).

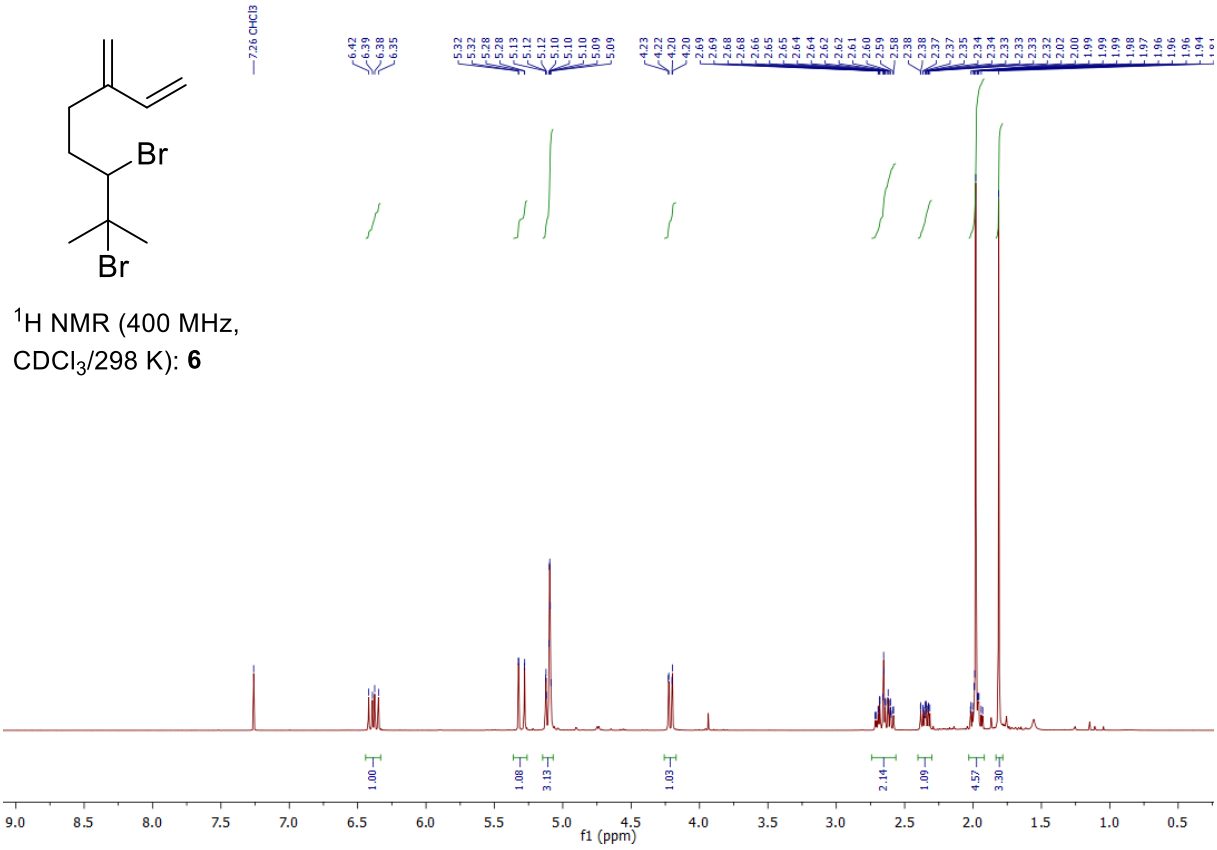

^{1}H NMR (400 MHz, $CDCl_3$/298 K): **6**

Figure 18. 400 MHz ^{1}H NMR spectrum of 6,7-dibromo-7-methyl-3-methyleneoct-1-ene (**6**)

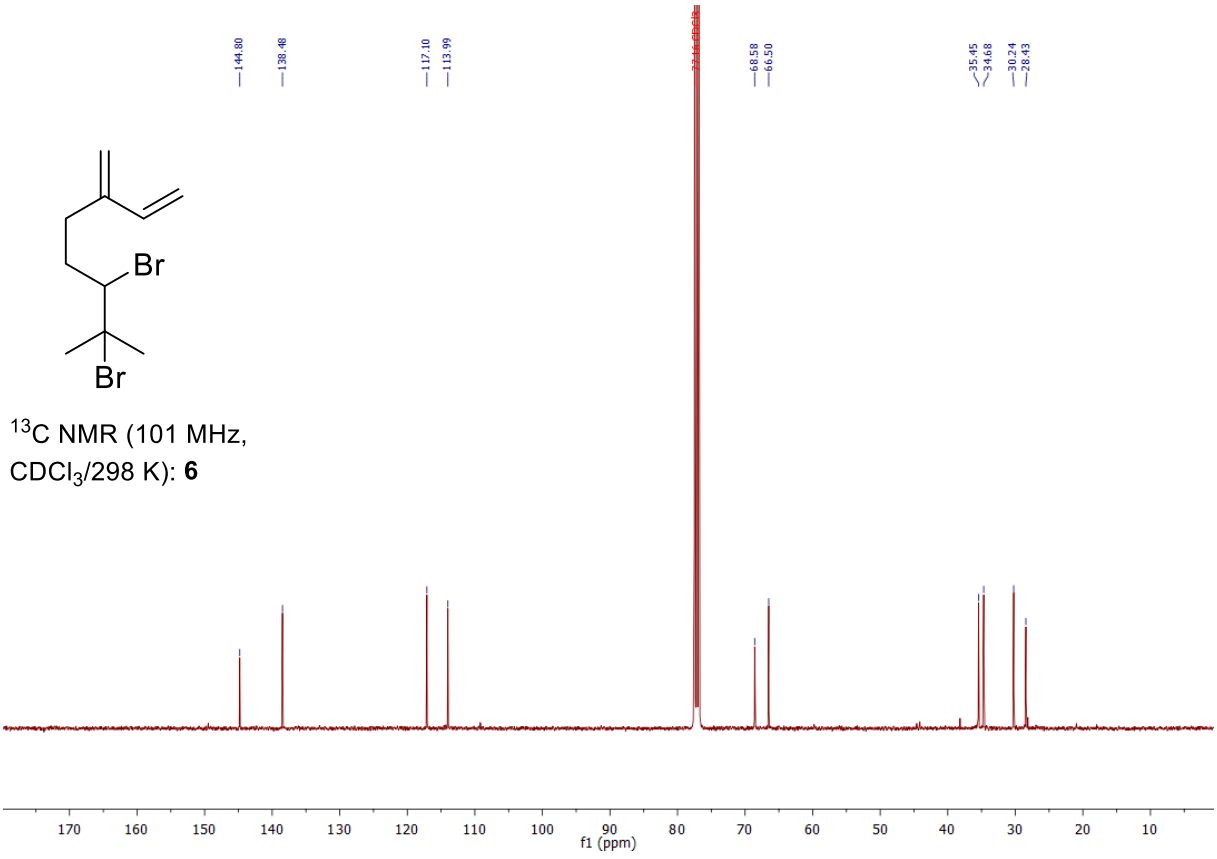

^{13}C NMR (101 MHz, $CDCl_3$/298 K): **6**

Figure 19. 101 MHz ^{13}C NMR spectrum of 6,7-dibromo-7-methyl-3-methyleneoct-1-ene (**6**).

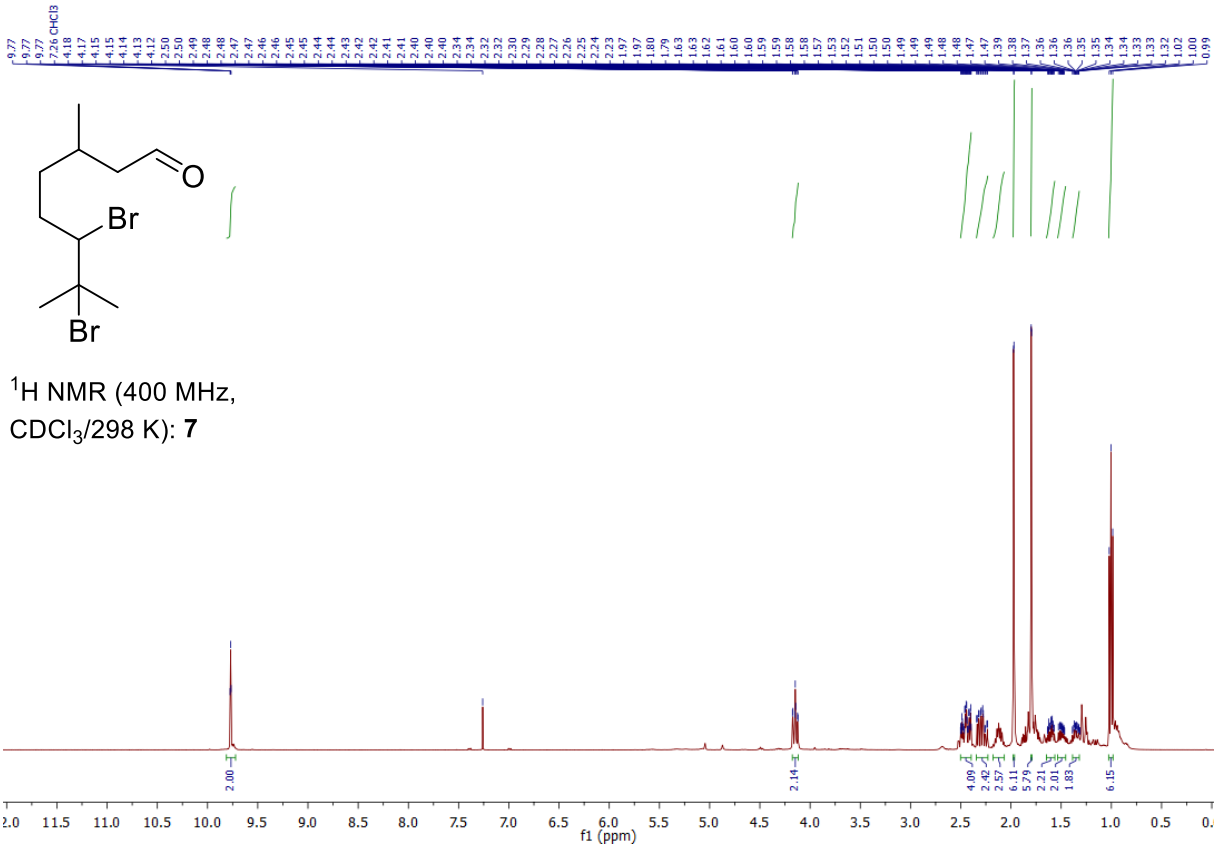

^{1}H NMR (400 MHz, $CDCl_3$/298 K): **7**

Figure 20. 400 MHz ^{1}H NMR spectrum of 6,7-dibromo-3,7-dimethyloctan-1-al (**7**).

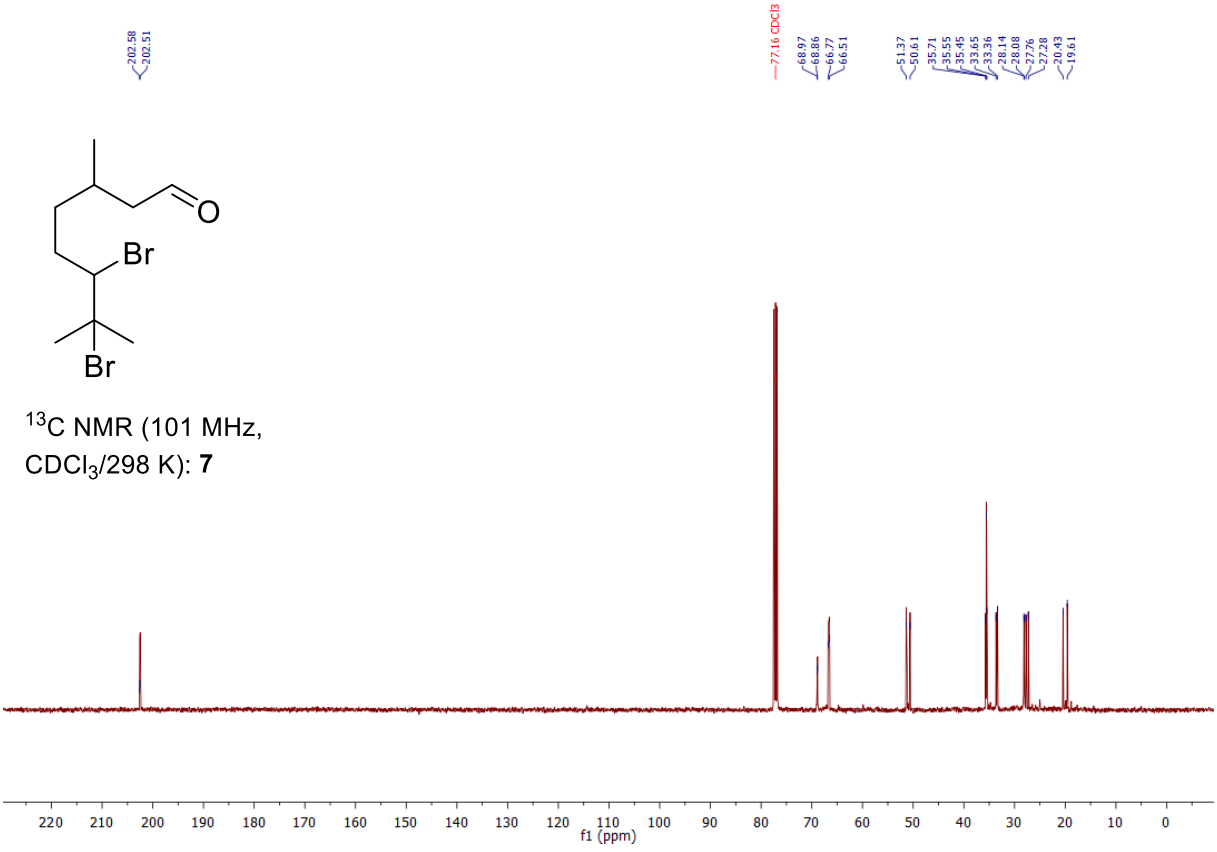

^{13}C NMR (101 MHz, $CDCl_3$/298 K): **7**

Figure 21. 101 MHz ^{13}C NMR spectrum of 6,7-dibromo-3,7-dimethyloctan-1-al (**7**).

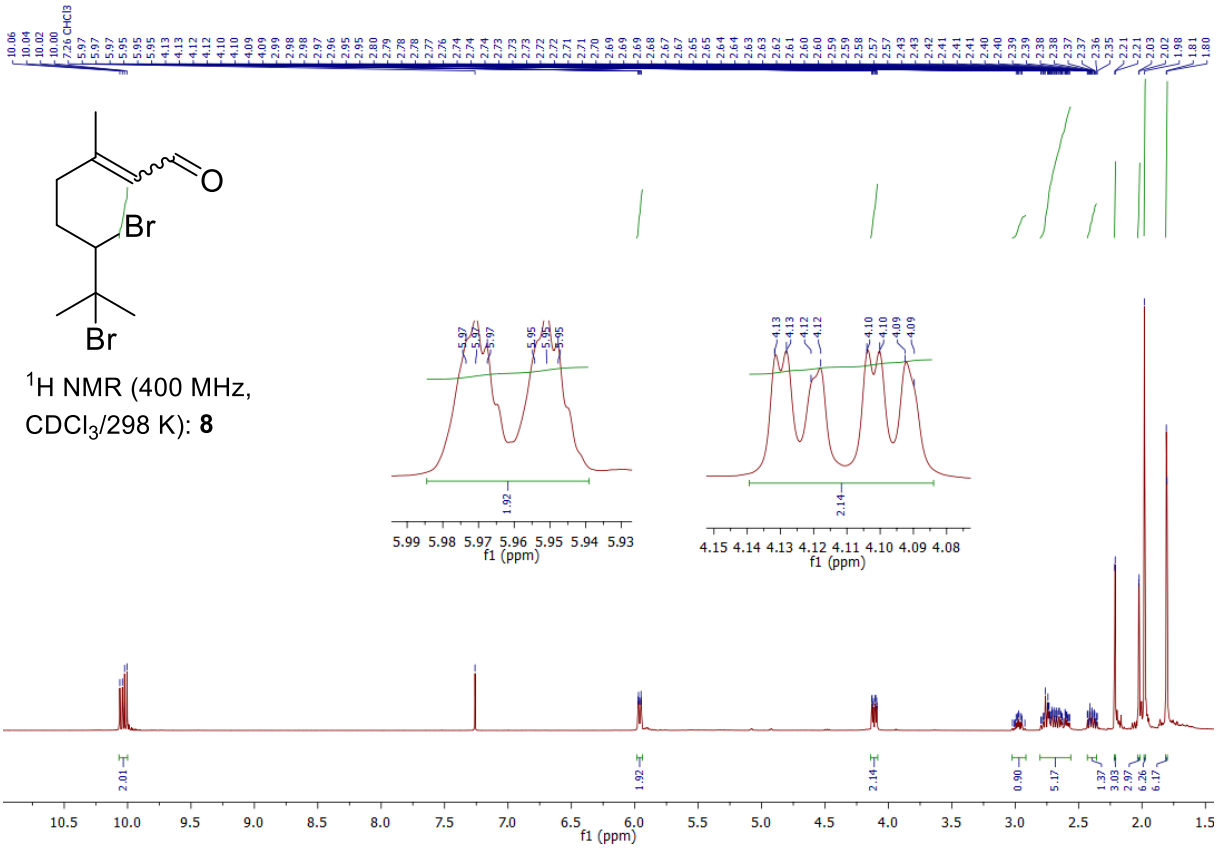

Figure 22: 400 MHz ^{1}H NMR spectrum of 6,7-dibromo-3,7-dimethyloct-2-en-1-al (**8**).

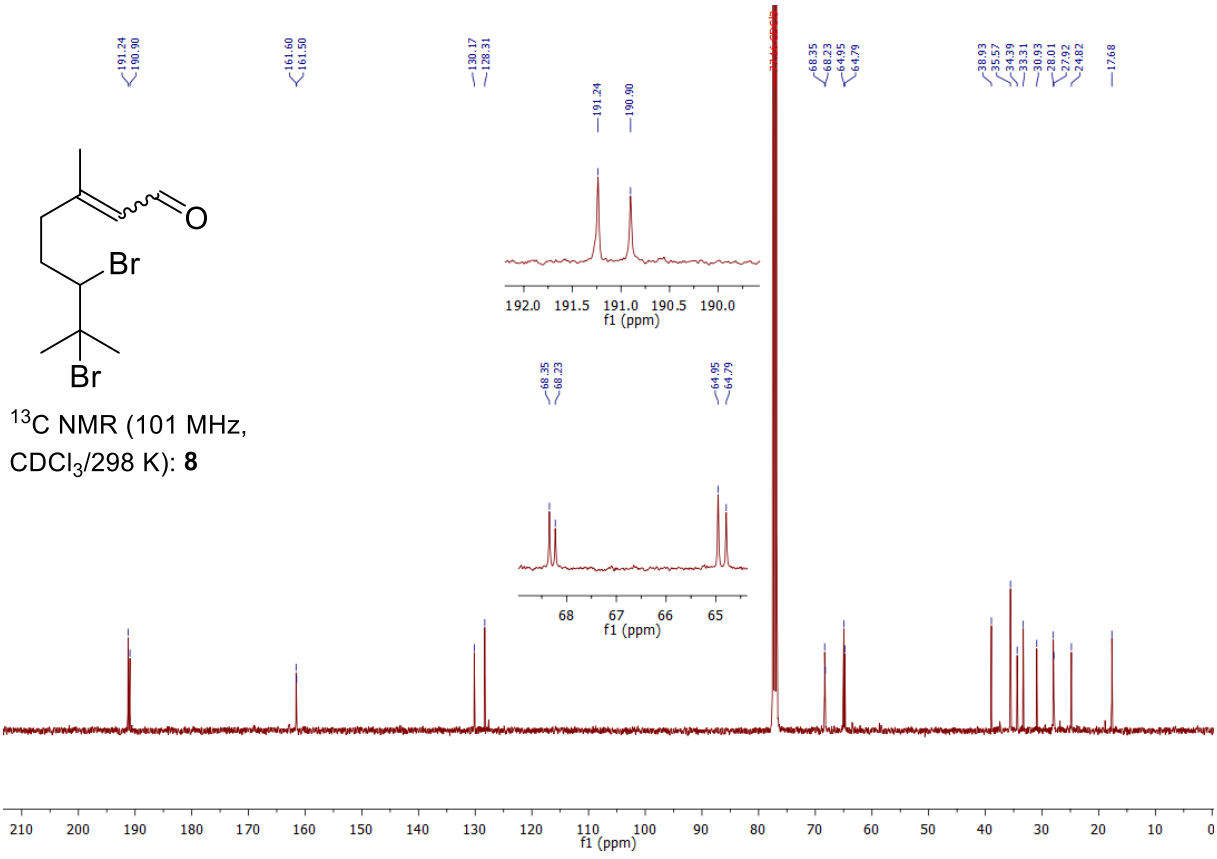

Figure 23: 101 MHz ^{13}C NMR spectrum of 6,7-dibromo-3,7-dimethyloct-2-en-1-al (**8**).

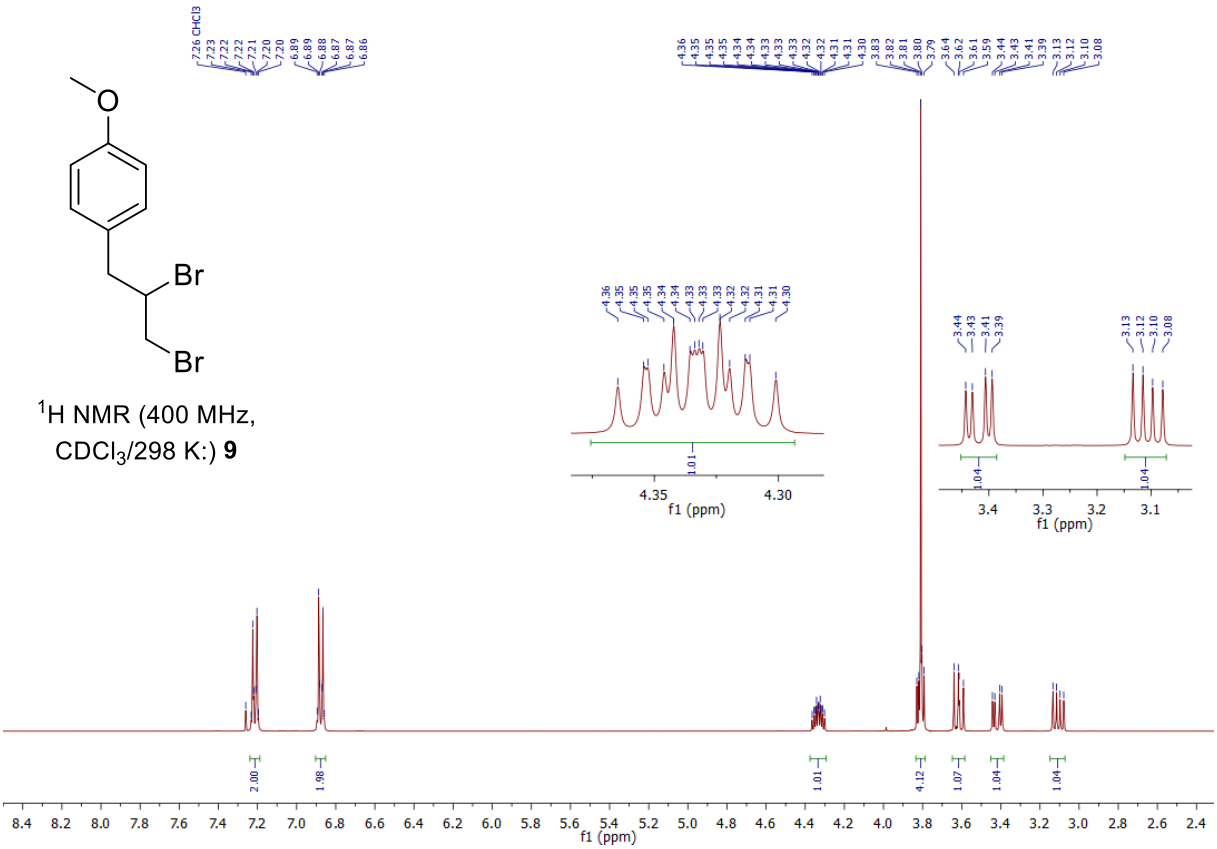

Figure 24. 400 MHz ^{1}H NMR spectrum of 4-(2,3-dibromopropyl)anisole (**9**).

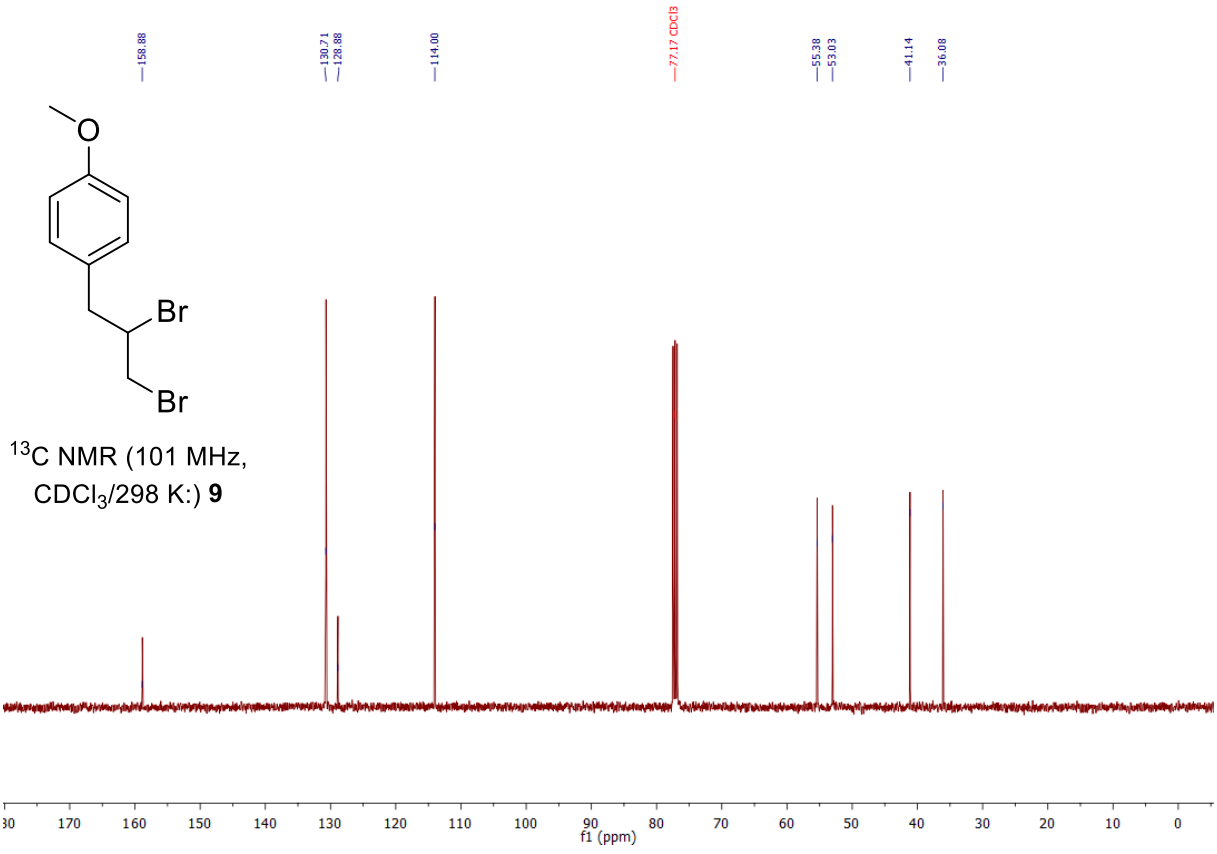

Figure 25: 101 MHz ^{13}C NMR spectrum of 4-(2,3-dibromopropyl)anisole (**9**).

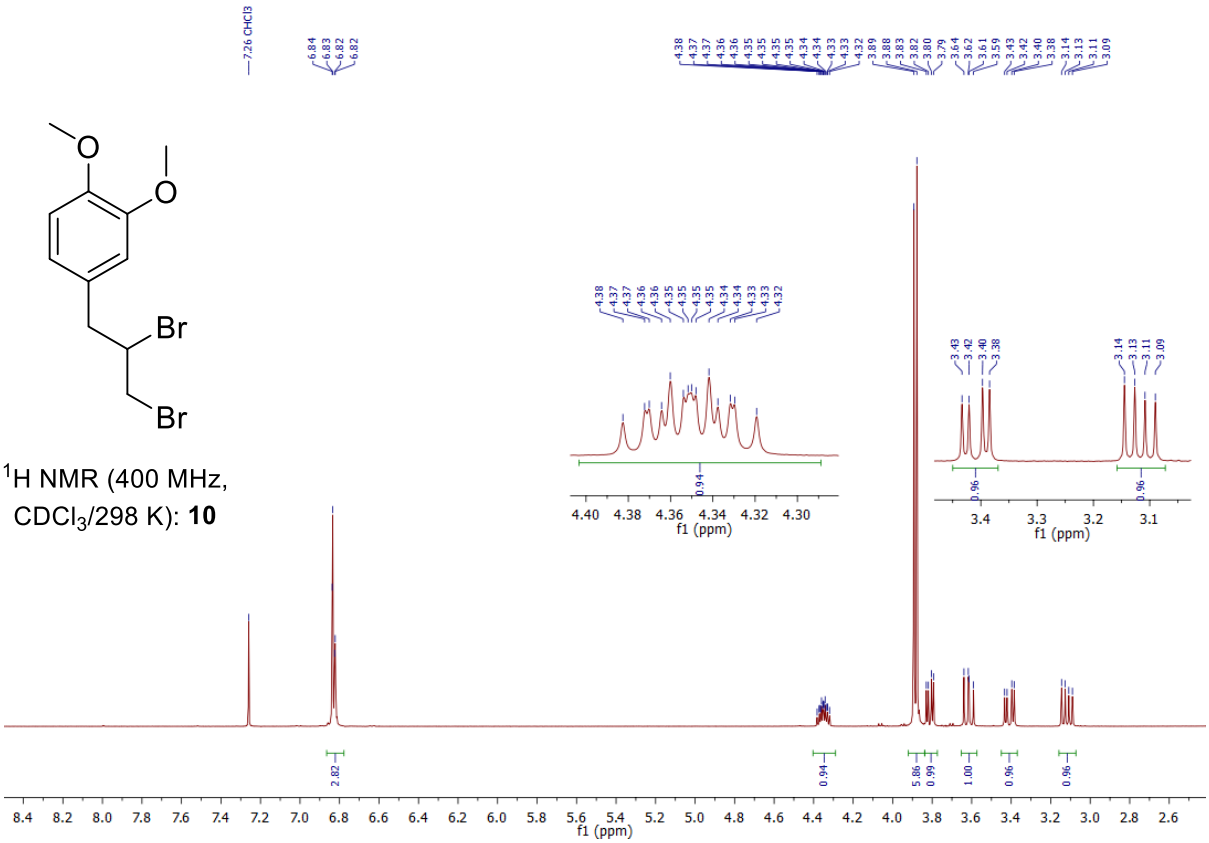

Figure 26. 400 MHz ^{1}H NMR spectrum of 4-(2,3-dibromo)-1,2-dimethoxybenzene (**10**).

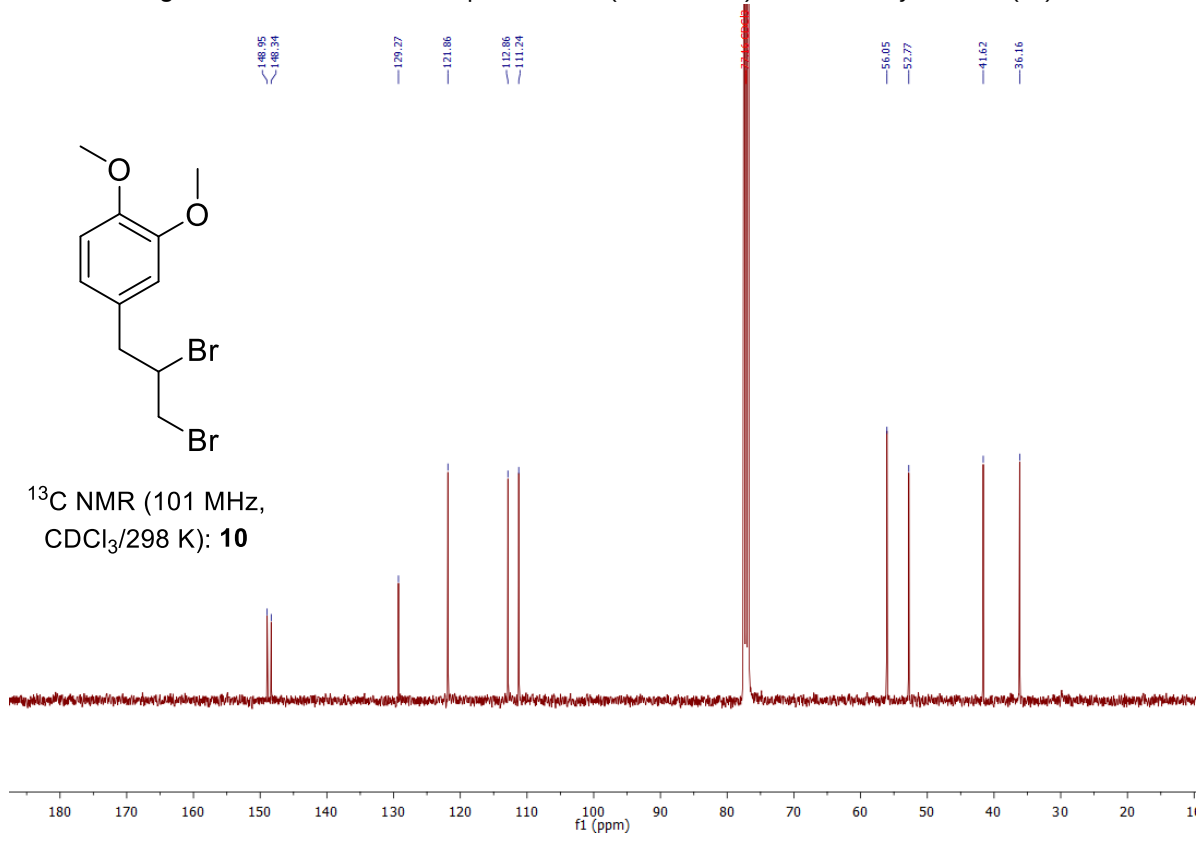

Figure 27. 101 MHz ^{13}C NMR spectrum of 4-(2,3-dibromopropyl)-dimethoxybenzene (**10**).

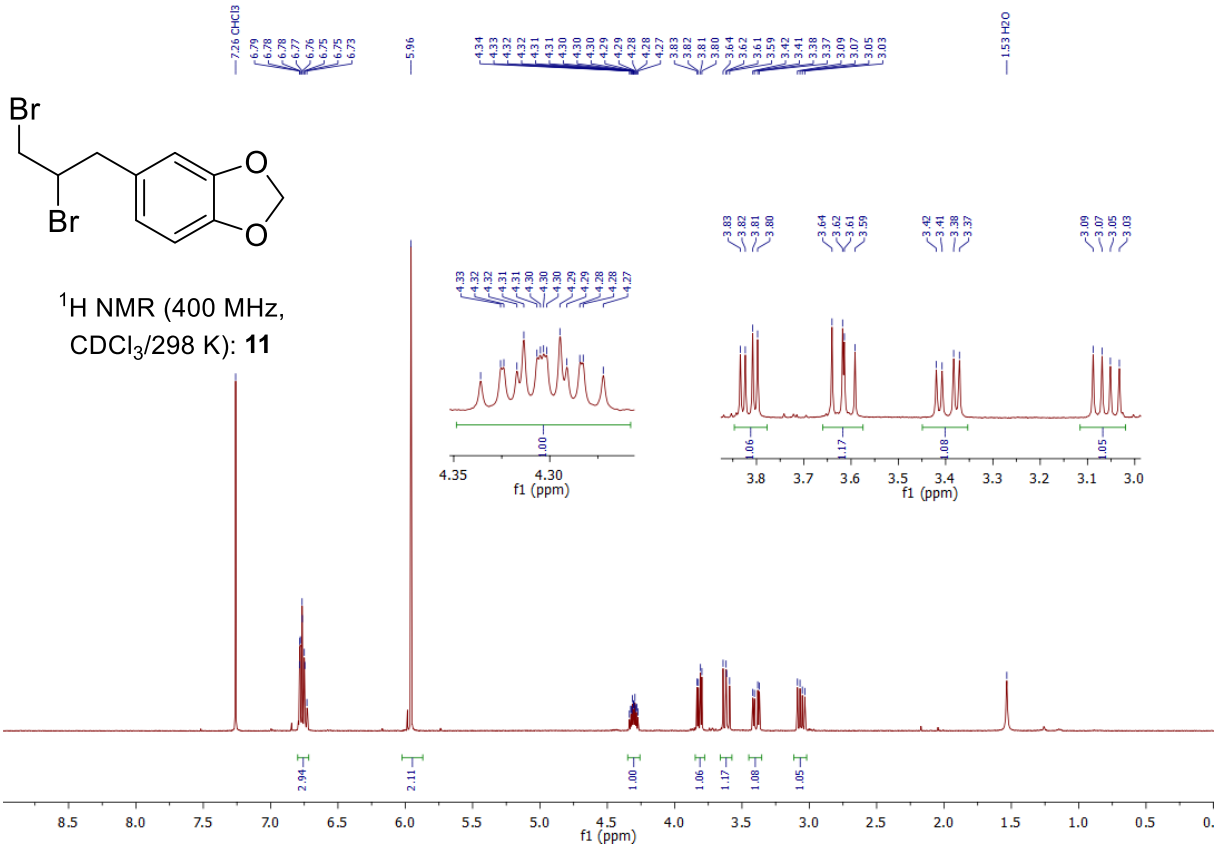

Figure 28. 400 MHz ^{1}H NMR spectrum of 5-(2,3-dibromopropyl)-1,3-benzodioxole (**11**).

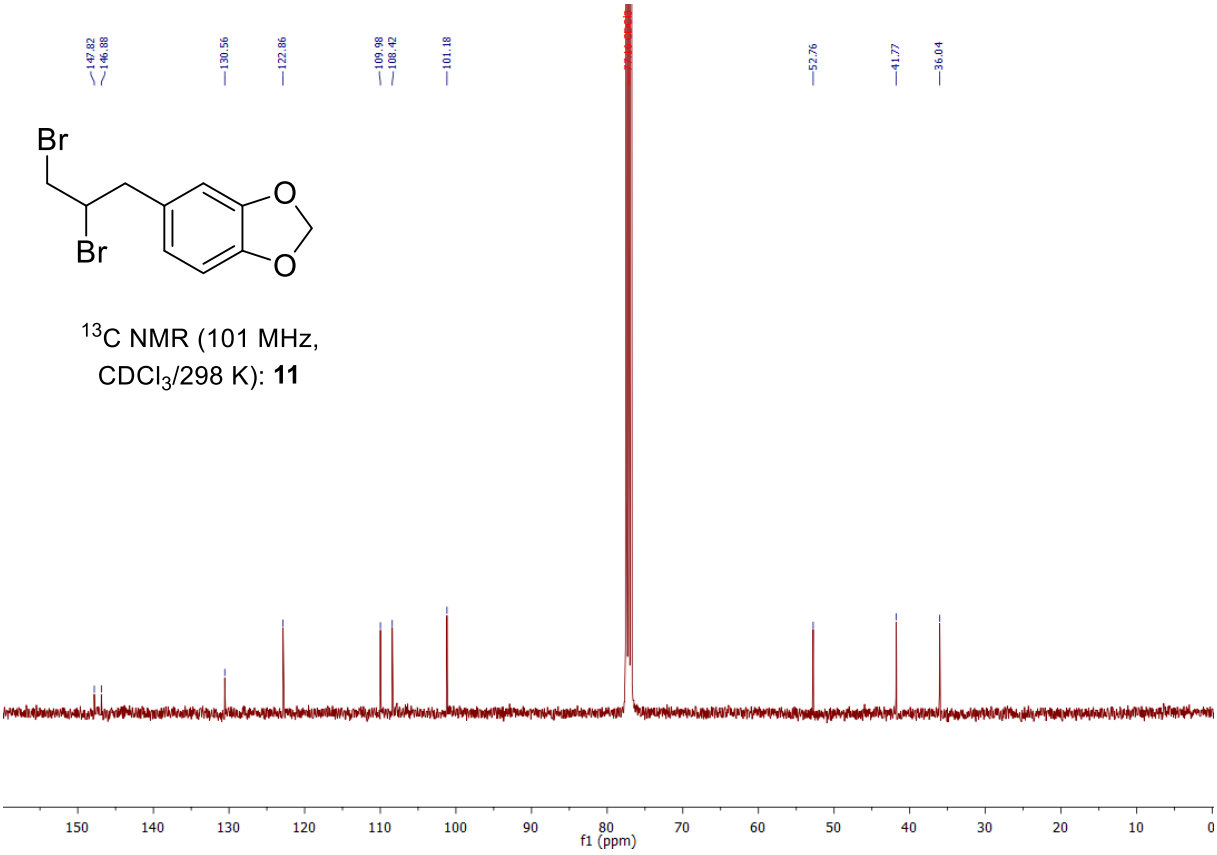

Figure 29. 101 MHz ^{13}C NMR spectrum of 5-(2,3-dibromopropyl)-1,3-benzodioxole (**11**).

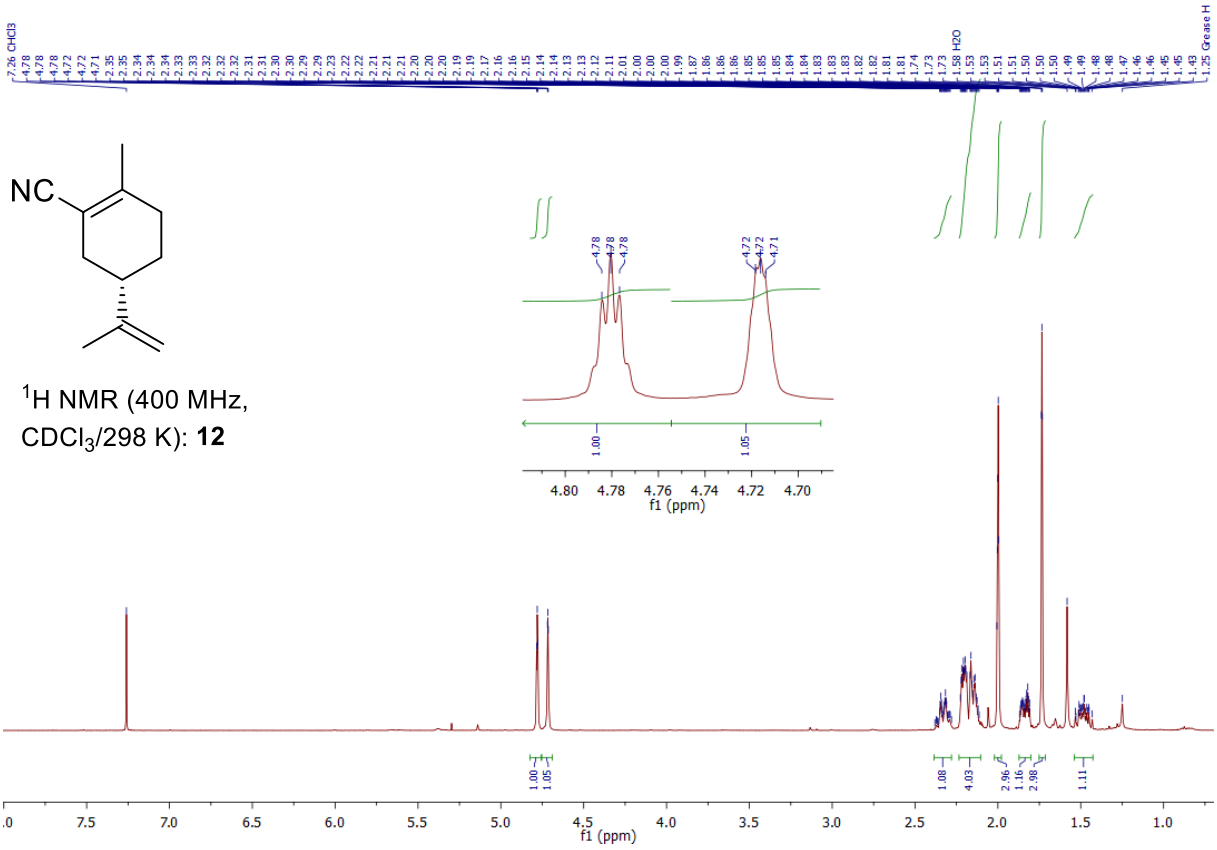

Figure 30. 400 MHz ^{1}H NMR spectrum of (4*S*)-*p*-mentha-1,8-diene-2-carbonitrile (**12**).

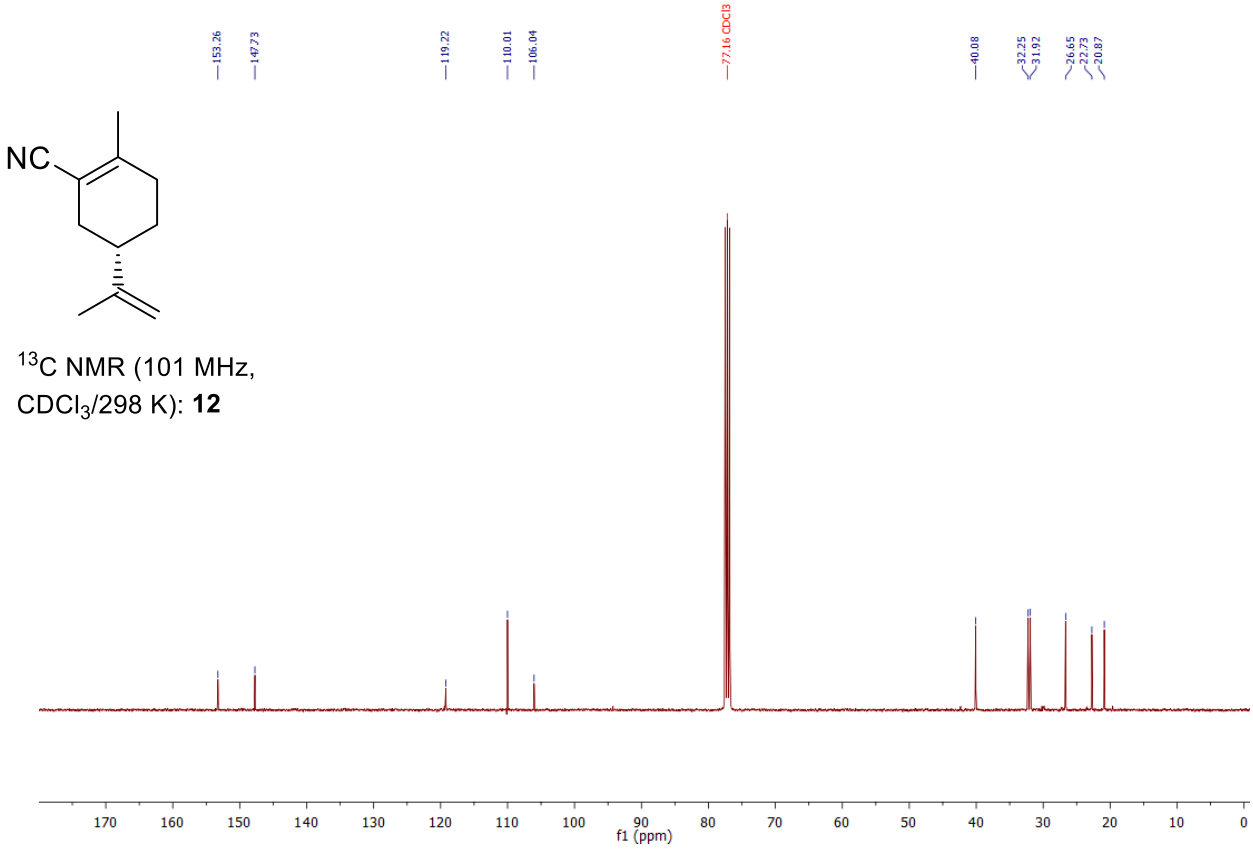

Figure 31. 101 MHz ^{13}C NMR spectrum of (4*S*)-*p*-mentha-1,8-diene-2-carbonitrile (**12**).

8. References

1. W. L.F. Armarego, C. Chai, Eds, *Purification of Laboratory Chemicals* (Seventh Edition); ButterworthHeinemann, Boston, **2013**.
2. R. K. Harris, E. D. Becker, Cabral de Menezes, Sonia M, R. Goodfellow, P. Granger, *Solid State Nucl. Magn. Reson.* **2002**, *22*, 458–483.
3. C. Gütz, B. Klöckner, S. R. Waldvogel, *Org. Process Res. Dev*. **2016**, *20*, 26–32.
4. G. S. Buchanan, K. P. Cole, G. Li, Y. Tang, L. You, R. P. Hsung, Tetrahedron, **2011**, *67*, 10105–10118.
5. S. Song, X. Li, X. Sun, Y. Yuan and N. Jiao, *Green Chem*. **2015**, *17*, 3285–3289.
6. M. Tariq, Z. *Phys. Chem*. **2019**, *234*, 295–312.
7. D. Halász, Cs. Visy, A. Szűcs and M. Novák, *React. Kinet. Catal. Lett*. **1992**, *48*, 177–188.
8. V. Vojinovic, S. Mentus, V. Komnenic, *J. Electroanal. Chem.* **2003**, *547*, 109–113.
9. J. G. Bell, J. Wang, *J. Electroanal Chem*. **2015**, *754*, 133–137.
10. U. Husstedt, H. J. Schäfer, *Synthesis*,**1979**, *12*, 966–968.
11. T. Kato, I. Ichinose, *J. Chem. Soc., Perkin Trans. 1*, **1980**, 1051–1056.
12. L. Peilleron, T. D. Grayfer, J. Dubois, R. H. Dodd and K. Cariou, *Beilstein J. Org. Chem.* **2018**, *14*, 1103–1111.
13. T. Ying, W. Bao, Y. Zhang, *J. Chem. Res*. **2004**, 806–807.
14. D. G. Vassão, D. R. Gang, T. Koeduka, B. Jackson, E. Pichersky, L. B. Davina, N. G. Lewis, *Org. Biomol. Chem*. **2006**, *4*, 2733–2744.
15. E. Dinca, P. Hartmann, J. Smrćek, I. Dix, P. G. Jones and U. Jahn, *Eur. J. Org. Chem*. 2012, 4461–4482.

Personal data